UNIVERSITY OF SOUTHAMPTON

TWO DIMENSIONAL LANGMUIR-BLODGETT MAGNETS

by

David Ian Head

DEPARTMENT OF PHYSICS

FACULTY OF SCIENCE

Submitted for the degree of Doctor of Philosophy

December 1988

CONTENTS

UNIVERSITY OF SOUTHAMPTON

ABSTRACT

FACULTY OF SCIENCE

PHYSICS

Doctor of Philosophy

TWO DIMENSIONAL LANGMUIR BLODGETT MAGNETS

by David Ian Head

The susceptibility of quasi-two-dimensional magnets formed by the Langmuir-Blodgett deposition of manganese stearate on aluminium foil has been measured at several points between 20 K and 0.4 K. Large area samples of 101 and 11 layers were detected by a SQUID magnetometer. With the magnetic field parallel to the film we deduced an equivalent volume susceptibility of 6.4×10^{-3} at 4.2 K. The signals from the multilayers were paramagnetic in nature and no evidence for a transition was found. Unfortunately the signal from a bilayer and monolayer were masked by contaminants on the substrate.

The magnetometer used a cold finger to which the sample was attached. This was then moved into the pick-up coil, which was a second order gradiometer capable of cancelling out the signal from the long (150 mm) substrates. The magnetometer was usefully capable of detecting a sample with a moment down to 5×10^{-11} Am^2 but vibration noise restricted the magnetic field to below 10 mT.

New equations were developed to describe the magnetic signals from a cylindrical magnetised sample within a superconducting shield. They were developed for use on a micro-computer making it possible to simulate the signal from the sample.

The π-A curves for Manganese stearate were also studied. The uncertainty in the measurement of π using filter papers was studied and estimated to be 2%. The manganese stearate was observed to transfer by Y and forced-Z type dipping.

ACKNOWLEDGEMENTS

I would like to thank Drs Blott and Melville for supervising my work, and to acknowledge the Physics Department of Southampton University for providing the facilities needed to carry out an experimental project. This included the technical assistance from members of the electronics and mechanical workshop, especially Brian Heath and Alf Gardiner who helped in so many ways. I would also like to thank Colin Miles for his hard work in providing an almost 100% secure supply of liquid helium and nitrogen as well as Ian Mears and Robert Igra (of the Institute of Cryogenics) for their help on various occasions. I also appreciated the advice and computational help of Dr Chris Cornelius, particularly the production of a new thermometer interpolation table. Also I would like to acknowledge Dr Geoff Daniell for his assistance in deriving an alternative solution to the shield problem which enabled the simulation work described to in chapter six. Finally I must thank God, because knowing Him helped me to keep on going to get this thesis finished.

CHAPTER ONE - TWO DIMENSIONAL MAGNETS

1.1 GENERAL INTRODUCTION

This thesis describes the search for magnetic ordering in magnetically doped Langmuir Blodgett films using a SQUID magnetometer. A Langmuir Blodgett film is an experimental approximation to an idealised two dimensional material. Experiments on two dimensional substances are of interest because they could be of use in:

i) measuring the characteristics of materials with lower dimensionality and comparing experimental data with theoretical models of two dimensional systems.

ii) making very small, low temperature, magnets - which might be used within a superconducting electronics system as an information storage medium.

In this chapter some basic theoretical results for two dimensions are outlined and relevant examples of quasi two dimensional experimental systems are described. In chapters two and three the Langmuir Blodgett technique and the preparation of samples are explained. The cryostat, the magnet, the thermometry and the sample detector are described in chapter four as well as some of the problems which arose. This is followed in chapter five by a description of the SQUID detector along with the design and construction of the sample substrate and the sample holder.

To check whether the results were sensible we calculated the sample signal using computer simulations which are described in chapter six. This is followed by the experimental results so calculation and experiment can be compared. Chapter seven summarises the results and conclusions as well as describing possible future directions for this research.

1.2 THEORETICAL BACKGROUND TO 2-D

1.2.1 Phase transitions

For some time there has been a considerable theoretical and experimental interest in phase transitions. A phase transition occurs when a substance changes its internal arrangement from one form to another in response to a change in its environment. For example, on cooling, a paramagnet might order to a ferromagnetic state.

On an atomic scale, the different particles all "see" each other through different interactions, of varying strengths. Some are long ranged e.g. electrostatic, while others are short ranged and can only directly affect close neighbours. Even if only short range interactions are present a phase transition may still be possible.

Short range interactions may produce short range order; for example two or three atoms with magnetic dipoles (or spins) may be locally aligned. Above the critical temperature any further ordering is overcome by the disordering effect of random thermal motions. When averaged over large distances, the sum of any alignments has no gross effect. However, at the critical point (say as the temperature falls) the short range interactions are able to "transmit" the effect at one point over long distances via the intervening atoms. Then long range order sets in, causing a net alignment of atoms over large areas.

The spatial dimensionality of the material has an important bearing on when and how a transition occurs (Pomerantz 1980).

1.2.2 Dimensionality

The different theoretical models can be conveniently classified according to their spatial dimensionality (denoted by d or D) and the degrees of freedom the interacting elements have (denoted by n). There has been a lot of theoretical work done on idealised two and one dimensional (2-D & 1-D) systems, some of which has been reviewed by Fisher (1967 & 1974). Why this interest when we live in a three dimensional world? Several reasons:

i) Two (or one) dimensional systems are easier to visualise and are often easier to calculate (Kosterlitz 1980). Some 2-D systems have been exactly solved but no realistic three dimensional one has (Wilson 1979).

ii) Two dimensional systems can be used to test approximate mathematical techniques, which might be generalisable to three dimensions. Two dimensions is much better than 1-D for this, as 1-D systems have some special properties of their own.
iii) There are also some real materials which, due to their microscopic construction, are well described as 2-D or 1-D materials; for example K_2NiF_4 (see deJongh & Miedema 1974).

When the number of degrees of freedom, n, is ≥ 2 then two dimensions is also a "lower critical dimension" (l.c.d.). The l.c.d. has been defined (Young 1980) as that dimensionality where the system is unstable with respect to the creation of a sufficiently large number of low energy excitations (e.g. spin waves) that an ordered ground state breaks up at finite temperature. Hence a system can be on the borderline of having a transition so other influences would be very important in modifying transition behaviour.

Henceforth we will consider these models in terms of magnetic systems. Then each individual unit is a "spin" which may be resolvable into 1, 2, 3 or more directions. Names have been given to models with the same value of n, e.g. n=1 is conventionally called the "Ising" model. Theoretical calculations attempt to predict whether or not a system has a phase transition, and if so to evaluate when and how the transition occurs.

1.2.3 The Theoretical Models

Some of the earliest theories were based on a mean field, i.e. all the interactions are replaced by an average background field. This implies infinite range interactions and gives the result that a phase transition to an ordered state always occurs. However mean field theories usually do not give the right answers. Since then theorists have developed many techniques which can be used to calculate the system parameters. The quantities often calculated, and hence those addressed by experimentalists, are the critical point exponents of a system. Having found the critical temperature, the variable under study is plotted against the reduced temperature-offset from the critical point.

e.g. if $\epsilon=(T-T_c)/T_c$ where T = varying temp.

T_c = critical temp.

we find that the zero field magnetisation M:

$$M \propto -\epsilon^{\beta}$$

where β is the critical point exponent. (Strictly the value is that which applies as $\epsilon \rightarrow 0$). There are many such exponents, a list of which can be found in Stanley (1971). Theoretical values naturally depend on d and n.

A famous exact solution to one problem was produced by Onsager (1944). He showed that an Ising system (n=1) in two dimensions would order to a state of finite magnetisation at a low (but non-zero) temperature. Subsequently Mermin and Wagner (1966) along with Fisher and Jasnow (1971) showed that for an isotropic two dimensional system with n>1 there can be no transition to long range order at a non-zero temperature (assuming no anisotropy). The spontaneous magnetisation is zero. (An ideal classical Heisenberg system (n=3) actually has a critical point at T=0 (Kosterlitz & Santos 1978). However such an ideal system can not be realised). But using extrapolation techniques (high temperature series) Stanley and Kaplan (1966) have shown that there was a non-zero value for the critical temperature (T_c). At this temperature an infinite susceptibility was found, implying that ordering might occur. This "contradiction" appears to have been resolved by Kosterlitz and Thouless (1973) in their "XY model" (n=2) where they have postulated a "topological" form of long range order. The net magnetisation is zero, and any spin correlations tend to zero at a finite temperature. But the spins can be thought of as being arranged in bound pairs of vortices.

Navarro and deJongh (1979) have developed a two dimensional spinwave theory for thin films of only a few molecular layers thick. Using a quadratic lattice they calculated the magnetisation of samples with varying number of layers (from one upwards), for both the ferromagnetic (FM) and anti-ferromagnetic (AFM) cases. They found that twenty layers of material gave answers which were close to bulk 3-D values. Since their derivation was in terms of number of layers, they suggest that their theory might be applicable to LB magnetic films (if they ordered FM or AFM). However for more than one layer they use a

simple cubic model which would overestimate inter-layer interactions because it ignores the long length of LB hydrocarbon chains.

1.2.4 Anisotropy

It was realised that the Mermin & Wagner results only apply to isotropic systems. With anisotropy 2-D Heisenberg systems can order (Malyshev 1975, Robinson 1969). Stoll & Schneider (1978) state that anisotropy would destroy the Kosterlitz and Thouless vortex picture. Another factor which will cause transitions to occur in real systems is their three dimensional environment. As the temperature drops any three dimensional interaction will become increasingly important. This can then lead to three dimensional ordering in a quasi 2-D system (Liu & Stanley 1973). An example of theoretical work on lattice dimensionality crossover which can be fitted to experimental data is found in a paper by deJongh and Stanley (1976). Nagaev (1986) has also considered the transition from 2-D to 3-D behaviour for a Heisenberg ferromagnet. He calculated how T_c varied with film thickness and suggested that the transition from 2-D to 3-D should be regarded as the appearance of a non-zero T_c. A summary of whether a transition occurs is given in table 1.1. From this table we can see that experimentally, two dimensional systems are the most interesting because there may or may not be a transition depending on the environment. Finally one needs to be aware that the application of a magnetic field can actually broaden some transitions, perhaps making them difficult to see (Stanley 1971).

1.3 TWO DIMENSIONAL SYSTEMS

1.3.1 Non-Magnetic Examples

There are several non-magnetic systems which can be used to approximate a two dimensional model. A review has been produced by Kosterlitz and Thouless (1978). Two examples are:

i) Adsorption of gas molecules onto a solid substrate:
Substrates are usually chosen for a large surface to volume ratio and their homogeneity. The strength of the molecular binding to the substrate must be stronger than the molecule-molecule binding in the liquid; e.g. argon on graphite. The temperature and pressure on the

INTERACTION & SPIN DIMENSION (n) / SPATIAL DIMENSION (D)	ISING 1	XY 2	HEISENBERG 3	MEAN FIELD ∞
1	NONE	NONE	NONE	YES
2 ISOTROPIC	YES T=2.3J/K	NONE but KT	NONE	YES
2 ANISOTROPIC	YES	YES	YES	YES
3	YES	YES	YES	YES

Table 1.1 Occurrence of a Phase Transition

surface film can be varied and hence, via measurements of specific heat capacity, neutron and X-ray diffraction, the phase diagram and monolayer structure can be deduced. These can then be compared with theory. Much of this work has been summarised by Heiney et al (1983a) and Dimon et al (1985).

ii) Two dimensional electron gas:
Instead of having atoms or molecules on a surface, it is possible to hold electrons on the surface of helium. (The helium provides a clean surface whilst the image effect holds the electrons on). However there are effects due to the substrate which need accounting for. It is also possible to trap electrons in an "inversion layer" at a semiconductor surface which has been coated with an insulating oxide layer. An applied "gate voltage" can be used to confine the electrons to move in the two dimensions parallel to the surface only.

There are a few other types of two dimensional systems which we would like to review below in greater detail.

1.3.2 Layered Compounds

There are very many solid, magnetic, compounds which have a layer structure within them, and which can provide approximations to ideal two dimensional systems. Many of them have been described in a review by deJongh and Miedema (1974). Below we will mention a small selection

of them.

The most studied material is K_2NiF_4. Its neighbouring planes are shifted by half a unit cell distance from each other. As it orders anti-ferromagnetically each spin sees an equal number of up and down spins. Hence there is no net interaction for static properties at T = 0 K. Together with a small superexchange interaction this means that it makes a good 2-D approximation. It shows nearly pure 2-D behaviour within $|T-T_n|/T_n < 10^{-4}$ (where T_n is the ordering temperature). Experimentally it is found that anti-ferromagnetic correlations appear around 200 K and that the susceptibility becomes anisotropic around 100 K. The compound has an ordering temperature of 97.1 K and a sub-lattice magnetisation exponent (β) of 0.138±0.004 in a reduced temperature range $|T-Tn|/T_n$ between $3x10^{-4}$ and 0.2 (c.f. 2-D Ising β = 0.125). Below T_n 3-D long range order sets in. The intra-layer exchange interaction has a value of J/k = -60±5 K for nearest neighbours (where J is the exchange energy and k is Boltzmann's constant). For next nearest neighbours J/k = 0.5 K (approx.) while the relative inter/intra-layer exchange J'/J is < $2x10^{-4}$. The anisotropy is $2x10^{-3}J$ and is mainly due to single ion anisotropy. K_2NiF_4 is classed as a 2-D Heisenberg anti-ferromagnet. However using "high resolution" specific heat measurements Hatta and Ikeda (1980) have shown that the critical behaviour is better described by the Ising model. They cite neutron scattering results on the critical indices γ and ν which after correction for some unwanted diffuse scattering give values consistent with those of the 2-D Ising model (Birgeneau 1977).

There have been few examples of an XY type magnetic system. However recently there have been results which indicate that the theories of Kosterlitz and Thouless can be applied to K_2CuF_4 (Hirakawa 1982). The system is dominantly of the Heisenberg type with a small XY like anisotropy. Using static magnetisation and neutron scattering Hirakawa has shown that the transition to a 2-D planar ferromagnet is basically Kosterlitz-Thouless like (though with some 3-D interaction).

One other reported system with 2-D XY nature is $BaNi_2(PO_4)_2$ (Regnault et al 1983). This material has a transition temperature of 23.5±0.5 K and is supposed to be a much closer realisation of a 2-D planar magnet than K_2CuF_4.

An example of a 2-D Ising compound is K_2CoF_4. The nature of the cobalt atom leads to a large anisotropy (A). It can be valued at 0.9 in K_2CoF_4, where A=1 means pure Ising and A=0 means pure Heisenberg. This large anisotropy favours the c-axis. It is possible to fit the theoretical S=1/2 quadratic exchange Ising curve to the susceptibility data with reasonable agreement. It orders anti-ferromagnetically at 107 K with an exchange value J/k = -97 K.

1.3.3 Magnetic Thin Films

In the last few years it has become possible to produce very thin films of magnetic atoms, e.g. iron, directly. This is done, using UHV, by evaporating the magnetic atoms onto a substrate such as gold, copper or silicon. The films are usually ferro- or near ferro-magnetic but sometimes enhanced paramagnetism is displayed. These films have been investigated by a variety of methods including electron diffraction techniques, Mössbauer spectroscopy and SQUID magnetometry. References to these methods along with a summary of results can be found in reviews given by Bayreuther (1983) and Gradmann et al (1985). It has also been possible to study multiple film sandwiches with polarised neutron scattering. SQUID magnetometers have been used (but at higher temperatures than the Southampton machine) to detect single layers of iron. However at this low level it is not possible to measure how much material is actually there. At present the experimental materials do not approach the idealised structures required for comparision with fundamental theories. But it has been possible to fit spin wave theory; e.g. the results of magnetisation against film thickness. There is a decrease in Curie temperature and the spontaneous magnetisation as the number of layers decrease.

1.3.4 Graphite Intercalation Compounds

Graphite Intercalation Compounds (G.I.C.s) are made by depositing transition metal chlorides, from the vapour phase, onto the carbon layers formed by the graphite lattice. Some of the metals used have been cobalt, manganese, nickel and iron. By varying the amount of material it is possible to prepare samples with different numbers of adjacent magnetic layers (or stages), which are attached to the graphite layers. For single stage compounds the graphite layers separate the magnetic ions in the third dimension, giving a quasi 2-D

material. The graphite layers can provide a separation of just under a nanometre (much less than in LB films), while nearest neighbours in, for example, $MnCl_2$-G.I.C. are separated by 0.37 nm. Most of these transition metal G.I.C.s show a transition, but the nature of the transition has not always been established. When using cobalt, incommensurate with the graphite layer, susceptibility measurements have indicated two phase transitions at 9 & 8 K. The atoms progress from a disordered state, through a Kosterlitz-Thouless XY state with short range order, to one with long range order (Elahy & Dresselhaus 1984). More theoretical work using high temperature series expansions (Szeto et al 1985) fitted the results to a classical 2-D XY model with an effective exchange J_{eff} = 7.1 K.

In $MnCl_2$-G.I.C., the atoms seem to interact in an anti-ferromagnetic manner, though with some weak ferromagnetism. The ordering being of a Heisenberg type, forming an incommensurate triangular lattice on the graphite (Kimishima et al 1985). More recently Ibrahim and Zimmerman (1987) have reported that the $FeCl_3$-G.I.C. will produce a useful 2-D magnet system, where the electronic structure of the intercalatant is only affected by the contacting graphite layer.

1.3.5 Oxygen

One of the better approximations to a two dimensional magnet is molecular oxygen adsorbed on graphite. This provided the first observation of a magnetically ordered phase in a monolayer (McTague & Nielson 1976). Using neutron diffraction from incommensurate O_2 monolayers on oriented graphite (Grafoil) they found that below 10 K the O_2 molecules formed a distorted triangular network with frustrated anti-ferromagnetic coupling. It was believed to be a second order transition to a 2-D Heisenberg magnet. They likened this to the similar α phase of bulk oxygen and a phase diagram based on coverage and temperature was proposed. Since then several workers have added to this work. (See Heiney et al (1983a) for a summary).

At a coverage of just over one monolayer, as one lowers the temperature one passes through the paramagnetic δ and η phases to reach the ζ phase (originally named β after a phase in bulk oxygen). The ζ phase is assumed to be paramagnetic. Following X-ray experiments it was suggested that this phase is a centred rectangle structure rather than that of an equilateral triangle as originally suggested

(Stephens et al 1980). The actual transition to the ordered ϵ phase (originally denoted α) occurs between 11.7 and 11.3 K (Marx & Christoffer 1983). This result was obtained by specific heat measurements.

Apparently more than one layer is needed in order to get a transition. It is assumed that a partial second layer provides extra surface pressure. The transition temperature remains constant as the second layer is added (Stoltenberg & Vilches 1980). But between two and three layers there is a three dimensional signal as well (Awschalom et al 1983), presumed due to aggregation while it is three dimensional above three layers (Gregory 1978). No transition has been detected for one monolayer or partial coverage. This could be due to a lack of anisotropy which means the Mermin and Wagner theorem is applicable (Gregory 1978), hence no ordering.

The first theoretical interpretation was in terms of a Heisenberg transition with cubic anisotropy (Domany and Riedel 1978). This is now doubtful. Diep-The-Hung and Motchane (1982) said that the cubic anisotropy is unnecessary (and unphysical). A more realistic dipole-dipole interaction could be used instead. These both assume a triangular η phase as does Marx and Christoffer. Only Marx and Christoffer have applied magnetic fields to the oxygen system, both parallel and perpendicular to the plane. Fields (of 1.1 T) parallel to the plane cause a loss of the lower specific heat peak while a perpendicular field has little effect. Marx and Christoffer suggest a three state Potts structural transition at 11.7 K followed by an Ising transition at 11.3 K. They say that the response to this anisotropic application of a magnetic field supports their model, and invalidates the cubic anisotropy idea. (The perpendicular field would not affect the Ising transition, except for a field dependent temperature shift). But a sufficiently strong parallel field would eventually cause a spin flop phase. This would mean the system looks XY like, reducing a transition peak to a flat cusp, in accord with their data. Stephens et al (1980), when previously proposing the centred rectangle ζ phase, have suggested that there could be a second order transition to a non-collinear three sub-lattice system, which was either followed or pre-empted by a first order transition to a two lattice system.

Mochrie & Birgeneau (1984) also discounted the triangle lattice in the ζ phase, and suggested a two phase region at the ζ-ϵ transition.

However until recently the original, anti-ferromagnetically ordered, distorted triangles of McTague and Nielsen have been confirmed for the ϵ phase. Then Etters and Hardouin Dupar (1985) while confirming anti-ferromagnetism in both the ϵ and δ phases, have suggested that the magnetic interaction is found to break the triangular symmetry. Although a lot of work has been carried out on oxygen there still remains much about the actual transitions to these phases that is not understood.

1.3.6 Manganese Formate Dihydrate

Coming to a structure more akin to manganese stearate, we have the quasi 2-D compound manganese formate dihydrate ($Mn(HCOO)_2.2H_2O$). Work on this compound has been reviewed by DeJongh and Miedema (1974) up to that year. It is made up of two different planes of manganese atoms. At 3.68 K (T_N) the "A" planes order anti-ferromagnetically while the "B" planes (which intersperse the A) remain paramagnetic. There is also a weak ferromagnetic moment on the A plane, as the spins are not exactly anti-parallel. The specific heat shows 2-D Heisenberg characteristics, while 2-D magnetic correlations are seen up to $2xT_N$ by neutron scattering. One would expect Heisenberg nature as manganese atoms usually have a low anisotropy. In fact the overall anisotropy in this compound is lower than calculated. Looking at the susceptibility one finds a paramagnetic nature with two peaks (due to the weak ferromagnetism) occurring at T_N and 1.7 K. (At 1.7 K there is also a very sharp peak in the specific heat curve). This is a first order transition due to re-orientation of the anti-ferromagnetic axis.

Yamamoto et al (1977) successfully fitted a high temperature expansion for an ideal S=5/2 Heisenberg anti-ferromagnet to the magnetic heat capacity data. (There is no exact theoretical prediction for this). They deduced an exchange constant of $J/k = -0.34\pm0.01$ K (slightly smaller than the value quoted by deJongh and Miedema (1974)). An external field was applied by Takeda and Koyama (1983a) and they produced a magnetic phase diagram via measurements of heat capacity and susceptibility. The field was applied along the hard and easy axes while a method was devised to subtract the paramagnetic contributions from the B planes. They found that as the field was increased along the easy axis the Néel temperature dropped. However above 0.6 T another heat capacity peak was detected at a temperature (T_p) above T_N. T_p increased as the field was raised reaching 3.95 K in 2 T, but

then T_p began to decrease above 4 T. When the field was applied along the hard axis an increase in $T_N(H)$ occurred with larger field. This was interpreted in a later paper (Takeda and Koyama 1983b) as evidence for a crossover in spin dimensionality from Heisenberg to XY type. The heat capacity results at 2 T were compared with a Monte-Carlo 2-D planar rotator model. There was agreement for $kT/J_{xy} > 1$, i.e. above the heat capacity peak, but no evidence for a divergence in staggered susceptibility was found below this temperature. (Theory indicates that there might be such a divergence).

In more recent work Ishizuka, Tohi and Haseda (1983) claimed to have detected critical fluctuations in the spontaneous magnetisation using a SQUID. These only occurred as the temperature was dropped through T_N (=3.686 K) with a polarising field of less than 1 mT. They named it the "Temperature Barkhausen Effect" from its similarity of curve shape to the Barkhausen effect in ferromagnets.

1.3.7 Manganese Stearate

In their search for compounds which approximate to two dimensional magnets, researchers have turned to transition metal salts of fatty acids. These salts allow one to vary which metal is incorporated and the inter-planar distance by altering the length of the hydrocarbon chain. The general formula is $M^{v+}[OOC\text{-}(CH_2)_n\text{-}CH_3]_v^-$ where M is a metal of valence v. For n=16 we have a stearic acid salt, with a single chain length of 2.4 nm (Von Sydow 1955). X-ray diffraction has shown that divalent salts of stearic acid have lattice spacings of 5 nm (Vold & Hattiangdi 1949). A diagram of the stearic acid molecule and the substitution of a manganese ion is shown in fig 1.1.

1.3.8 Powder Samples

Some early magnetic work was done by Aranaz and Lomer (1969) on powdered manganese salts with varying chain lengths where n=1,2,14 & 16. Between 300 and 2 K they observed Curie Weiss behaviour indicating anti-ferromagnetism with a negative Curie Weiss temperature of some tens of kelvin. But at lower temperatures they detected an increase in susceptibility (perhaps indicating some ferromagnetism); the actual "ordering" temperatures went down as the chain length was increased.

Since then Melvin Pomerantz has been the key worker in developing the work on two dimensional manganese stearate ($MnSt_2$). Firstly using

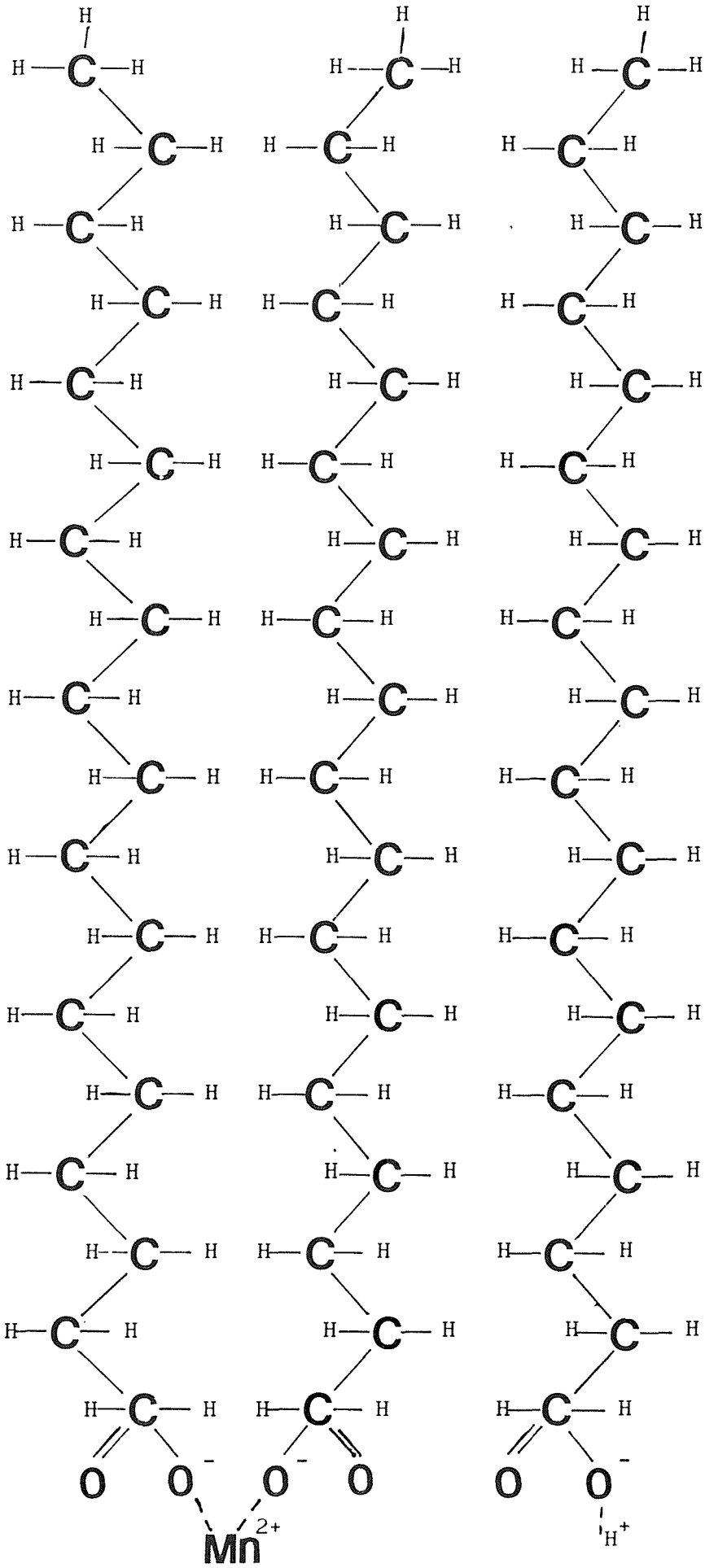

Fig 1.1 Stearic Acid Chains and Manganese Substitution

powdered manganese stearate, X-ray diffraction showed an inter-planar spacing of 4.94 nm (Pomerantz & Aviram 1976). This indicated that the unit cell was made up of two stearate chains, one on top of the other. Using a Faraday balance the magnetisation of the powder was measured between 56 K and 2 K. Below approximately 5 K, the high field values of the magnetisation did not extrapolate to M=0 as H tended to zero. The line width derived from electron spin resonance (E.S.R.) broadened as the temperature was lowered and then below 10 K the line centre shifted to lower fields and the shape became asymmetric. This was interpreted as evidence for weak ferromagnetism. Haseda et al (1977) have also measured the susceptibility of $MnSt_2$ powder between 0.05 K and 80 K by a.c. susceptibility. They found no transition at 5 K but did detect one at 0.5 K. Other measurements of susceptibility by a SQUID also suggested the appearance of spontaneous magnetisation below this temperature. They again believed it to be anti-ferromagnetism accompanied by a weak ferromagnetic moment. Since then however, Pomerantz and co-workers, using a modified synthesis procedure could only detect evidence for anti-ferromagnetism, with a Néel temperature at 10±1 K. Also the X-ray scattering on this new powder indicated that there might be a different side by side chain spacing than previously measured (Aviram & Pomerantz 1982).

1.3.9 Langmuir Blodgett Samples

Using the "Langmuir Blodgett" (LB) process it is possible to produce ordered mono- or multi- layers of long chain fatty acids and certain of their salts (see chs 2 & 3). Pomerantz was able to prepare samples of $MnSt_2$ or manganese arachidate ($MnAr_2$ where n=18) in which there were layers of Mn^{2+} ions separated by long hydrocarbon chains (giving a 5 nm spacing between the ionic layers). They were deposited on substrates such as glass, quartz, silicon or graphite. Using E.S.C.A., X-ray photon spectroscopy and electron microprobe analysis he showed that the manganese ion was in an S=5/2 spin state, in correct stoichiometric amounts, and attached to the carboxyl group of the fatty acid (Pomerantz & Pollack 1975). Later using I.R. absorption the position of the manganese ion was confirmed. Then Pomerantz et al (1978) used X-ray diffraction, which was capable of resolving one layer, to determine the unit cell dimensions, and to check for 3-D manganese contaminants. A molecular model could be fitted to the data. They also investigated these samples by electron spin resonance (E.S.R.) at 80 K. The results were in agreement with two dimensional

paramagnetic E.S.R. theory. These first X-ray results were later followed up with more detailed measurements on films varying from one to eleven layers. A more quantitative model of the atomic distribution within the $MnSt_2$ molecule was derived (Pomerantz & Segmüller 1980). Later these ideas were carried over to neutron scattering (Nicklow et al 1981). They obtained diffraction from as few as three layers at room temperature. Pomerantz has indicated that an attempt to see the magnetic transition with neutrons was not successful (1982).

To look for magnetic ordering as the temperature was lowered E.S.R. was again used as it had the necessary sensitivity (Pomerantz 1978). The experiment was carried out on a magnetic bilayer deposited on top of a non-magnetic monolayer, on both sides of the plates. This is known as a "Type II" sample. As the temperature was dropped the line width showed behaviour similar to other quasi 2-D anti-ferromagnetic compounds. Below 10 K there was a rapid increase in line width and a shift in position of the resonant field. Then at 2 K a sudden shift of 0.1 T occurred within a temperature range of 0.2 K. This indicated the presence of magnetic order. The results could be explained in terms of weak ferromagnetism, (like powdered $MnSt_2$) and it was possible to fit weak ferromagnetic theory to the data. Experiments on substrates with only one monolayer of $MnSt_2$ deposited on them did not find a transition at temperatures ≥ 1.3 K. (These samples are known as "Type I").

The only other magnetic work done on LB films of $MnSt_2$ at low temperatures was briefly reported by Haseda et al (1977). Preliminary SQUID measurements on a monolayer system (equivalent to a Pomerantz Type I film?) gave a susceptibility maximum around 0.3 K.

The new preparation method used for the $MnSt_2$ powder (see 1.3.8) has not been applied to LB samples. Pomerantz et al have also looked at the effect of diluting Mn with Cd by E.S.R. at room temperature (Ferrieu & Pomerantz 1980) and at the magnetic properties of other transition metals incorporated into fatty acids. Only ferric stearate has been seen to produce any magnetic signal (Pomerantz et al 1982). However problems occurred in producing these samples using normal LB methods. A procedural modification by Prakash et al (1987) seems to have overcome some of these. Pomerantz has produced several reviews of his work (1980, 1982, 1983).

We decided to make films of $MnSt_2$ as Pomerantz had done. Instead of measuring them via E.S.R. we planned to directly measure their magnetisation using a SQUID magnetometer. In the next two chapters we will survey some of the history and discuss the details of the Langmuir Blodgett process particularly as it applied to our project.

CHAPTER TWO - THE LANGMUIR TROUGH

2.1 HISTORICAL BACKGROUND

For a long time people have known that small quantities of oily liquids, when placed on water, are capable of spreading out over large surface areas. The earliest known reference to oil on water is reported to come from the eighteenth century B.C. However the experiments of Benjamin Franklin are often referred to as the first time anyone "scientifically" studied this spreading effect. He gave a report to the Royal Society in 1774. But it is believed that Lord Raleigh, at the end of the nineteenth century, was the first to suspect that these layers spread out until they were only a molecule thick.

The first attempt to manipulate these films is attributed to Agnes Pockels in the late nineteenth century. Pockels also investigated the effect of these films on the surface tension of water. She communicated with Lord Raleigh who made more accurate measurements of the effect of these films on the surface tension of water.

The person who is most associated with these films is Irwin Langmuir. During the early part of this century he did a considerable amount of work on monolayers spread in water troughs which have now been named after him. From Pockels he developed the barriers used to manipulate the film and made many studies on the relationships between surface tension, surface area and the amount of material present. Langmuir was joined by Katherine Blodgett and during the 1930s they improved the process by which monolayers could be transferred from the water surface onto a solid substrate. This was achieved by dipping the substrate up and down through the monolayer under controlled conditions. The process has become known as the Langmuir Blodgett (LB) technique and the coatings formed are called LB films. After their work there was a dormant period until interest was regained in W. Germany in the 1960s. LB films were used for fundamental work on energy transfer in monolayer assemblies. This was followed up in Britain and France, where attempts to apply LB films to the field of electronics has caused an upsurge in interest.

A more detailed account of the history of LB films is given by Tredgold (1987) and Roberts (1985) including references to the original papers. Some other historical references are found in Grunfeld (1983) and Gaines (1983 & 1966).

2.2 THE TROUGH

2.2.1 What is a Langmuir Trough?

A Langmuir trough is a piece of apparatus for defining and constraining an area of liquid surface. It consists of a shallow container full of a liquid which is usually water. The essential feature is the air/liquid interface although the interface between two liquids can sometimes be used. The denser liquid is known as the subphase and the air (or a lighter liquid) is the superphase. A fraction of the surface is constrained by a barrier, or enclosing tape, which is usually made of, or coated in, teflon (Du Pont Ltd). The size of area enclosed can be varied by moving the barrier/tape. A diagram of an idealised trough showing a change in the enclosed area is given in fig 2.1.

Within the expanded area the monolayer material is spread on the water surface. For a suitable monolayer material the constituent molecules must be non-volatile, water insoluble and amphipathic i.e. one end of the molecule is hydrophilic, (binding the molecules to the water) while the other is hydrophobic (inhibiting solution into the water). To deposit the monolayer material it is first dissolved in an organic solvent e.g. chloroform. Then using a microsyringe a few microlitres are deposited, a drop at a time, onto the subphase. The drops spread out over the surface and the solvent evaporates leaving a monolayer.

A thin oblong plate known as the "Wilhelmy plate" (Wilhelmy 1863) is suspended through the surface to measure the change in surface tension as the monolayer area is altered. This change is called the surface pressure.

2.2.2 The Monolayer

If the area of the trough is known as a function of the barrier position and there is a Wilhelmy plate to measure the surface

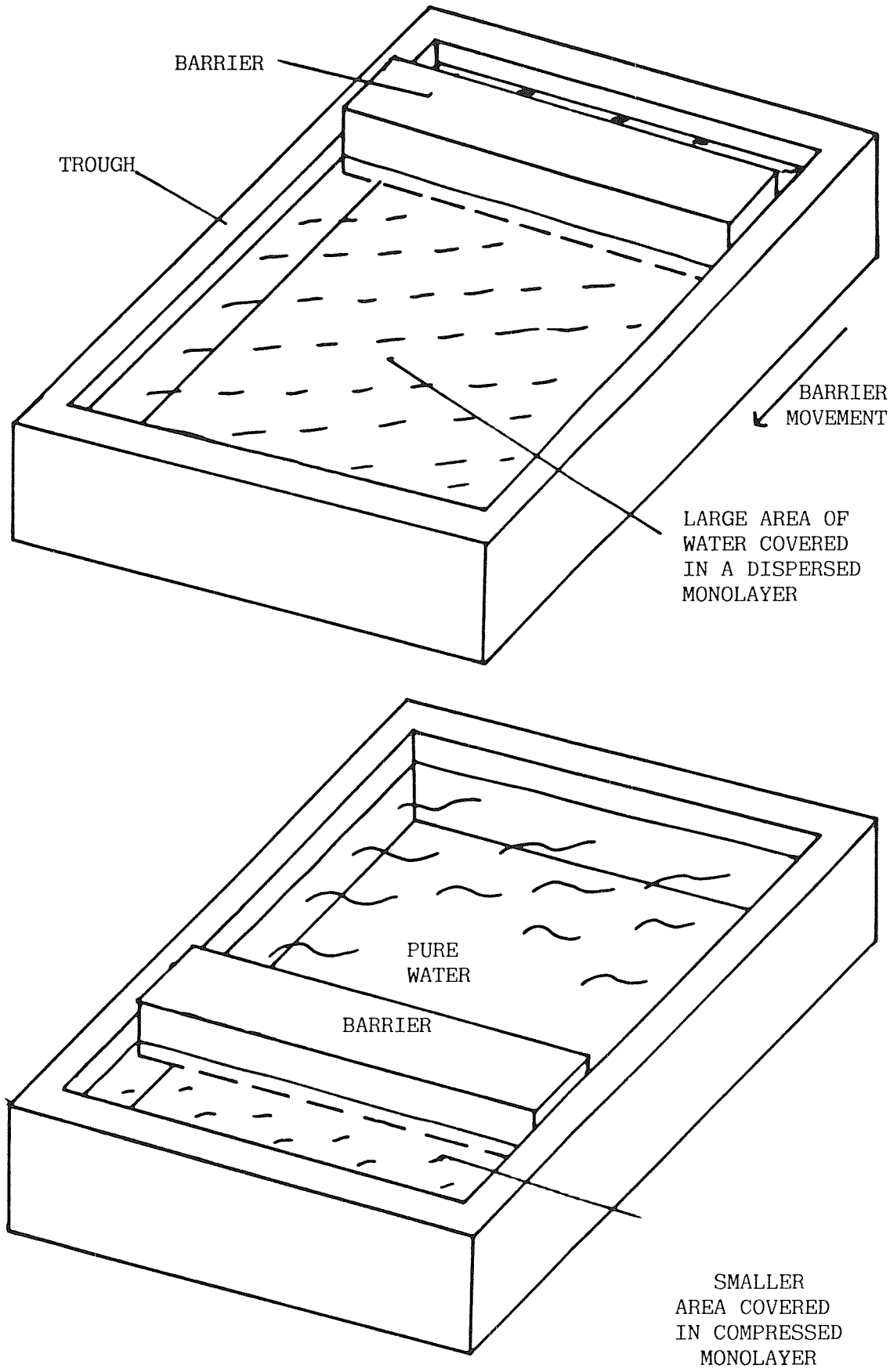

Fig 2.1 The Area Change On An Idealised Trough

pressure, then it is possible to characterise each monolayer by a surface pressure against area isotherm (a π-A isotherm, where π is the symbol used to denote surface pressure and is conventionally measured in mN/m). As the monolayer is compressed it will exhibit a series of phases, as the molecules reorient themselves, due to the pressure from their neighbours. (The π-A plot is analogous to a p-V isotherm in three dimensions). An idealised example is given, as well as a sketch of how the molecules might arrange themselves, in fig 2.2.

The different parts of the curve have been given names, similar to the usual three phases of matter. They are:

G gaseous
LE liquid expanded
LC liquid condensed
SC solid condensed

Note the sub-division of the "liquid" phase. (Some authors vary in their classification of phases).

A π-A curve depends on many factors, such as:
i) The chemical nature of the monolayer material
ii) The temperature
iii) The rate of compression/expansion of the monolayer
iv) The subphase pH
v) The presence of other monolayer material.

Commonly used monolayer materials are the series of fatty acids (or alkanoic acids) which have the general formula $CH_3(CH_2)_nCOOH$. They consist of hydrocarbon chains with an acidic COOH group at one end. This series allows some choice of the chain length and hence layer thickness, but keeping the same terminal group. The acidic end, usually referred to as the head group, is hydrophilic. The dissociation of this carboxyl group makes it possible to substitute the ionised hydrogen by a metal which can be obtained by dissolving salts, e.g. metal chlorides, in the subphase. The fraction of ions substituting for the 'H^+' ions depends on the subphase pH. At high pH the acid ionises and allows the substitution to take place. The pH also affects the stability of the monolayer, e.g. a more alkaline subphase usually means that an acidic monolayer is more stable. Monolayers are also more stable if the subphase is cooled from 20^oC down to 10^oC say. It is usual to control the temperature during experiments.

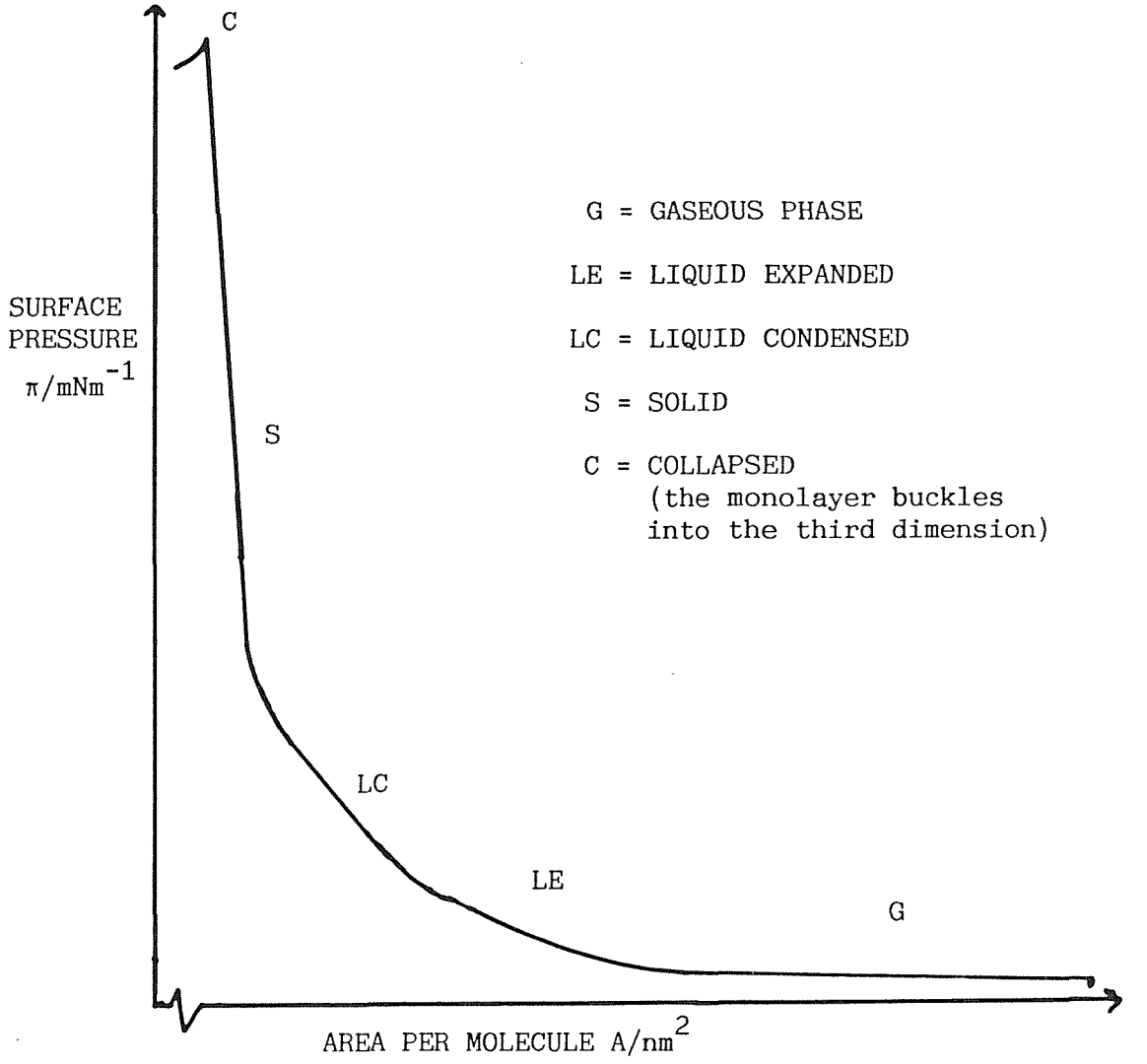

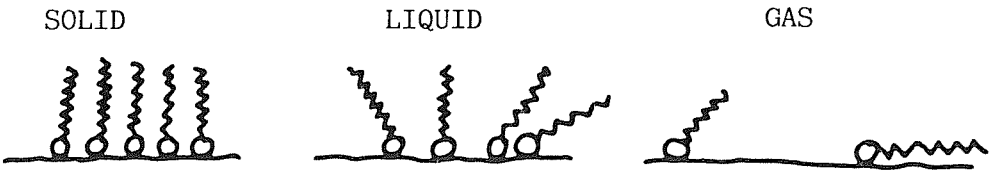

Possible Molecular Arrangements

Fig 2.2 An Idealised π-A Curve

All the experimental materials and the Langmuir trough have to be scrupulously cleaned. As a monolayer contains so little material (about 10^{17} molecules) results are easily affected by any contamination.

2.2.3 The Southampton Trough

The trough system at Southampton was originally built at ICI Corporate Laboratories and based on the design of Blight, Cumper and Kyte (1965). The trough was fabricated from soda glass to dimensions of 920x230x70 mm. Its maximum capacity was ten litres. Compared to many other troughs this is quite large, but it was necessary for the size of samples we prepared.

The monolayer was compressed by a continuous glass fibre tape, coated in teflon (Fothergill Tygaflor). The tape's position was controlled by two sets of twin teflon posts rigidly suspended from two movable trolleys. The trolleys were supported on a lacquered brass framework. A third set of posts provided a means of tensioning the tape; see fig 2.3.

To reduce the area the trolleys were driven towards each other, hence the two end walls of the constant perimeter tape approached each other. A potentiometer, attached to the tape drive mechanism, was used to give a calibrated voltage output proportional to the area enclosed by the tape. Because this was a constant perimeter system, and the tape was kept taut, it should be insensitive to differences in surface tension on either side of it. Boundary effects should also remain constant to a first approximation, e.g. the amount of water held above or below the main surface level due to meniscus effects at the tape. (More details of the construction of the trough, and the automatic control system for the trough area can be found in the PhD thesis of Asaolu (1983)).

The Wilhelmy plate used to measure the surface pressure was cut from a filter paper. This was then suspended from a Microforce electrobalance manufactured by C.I. Electronics Ltd; see fig 2.4. The force on the filter paper was balanced via a current in a coil attached to the balance arm. Changes in the force required to keep the balance in a fixed position gave a direct measure of changes in the surface pressure. As a further advantage the depth of immersion of the Wilhelmy plate was kept fixed, hence there were no changes in bouyancy

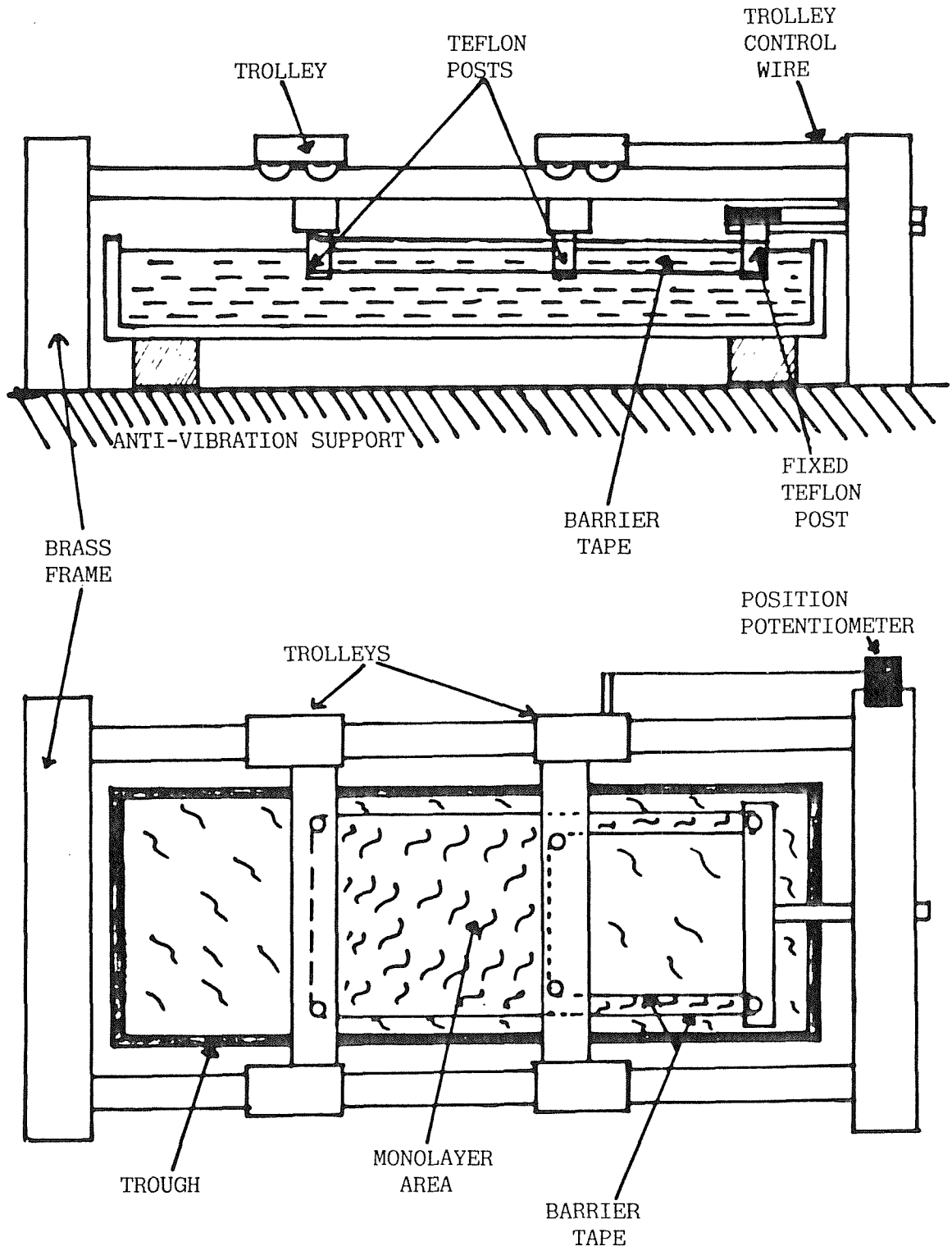

Fig 2.3 The Trolley, Tape and Posts

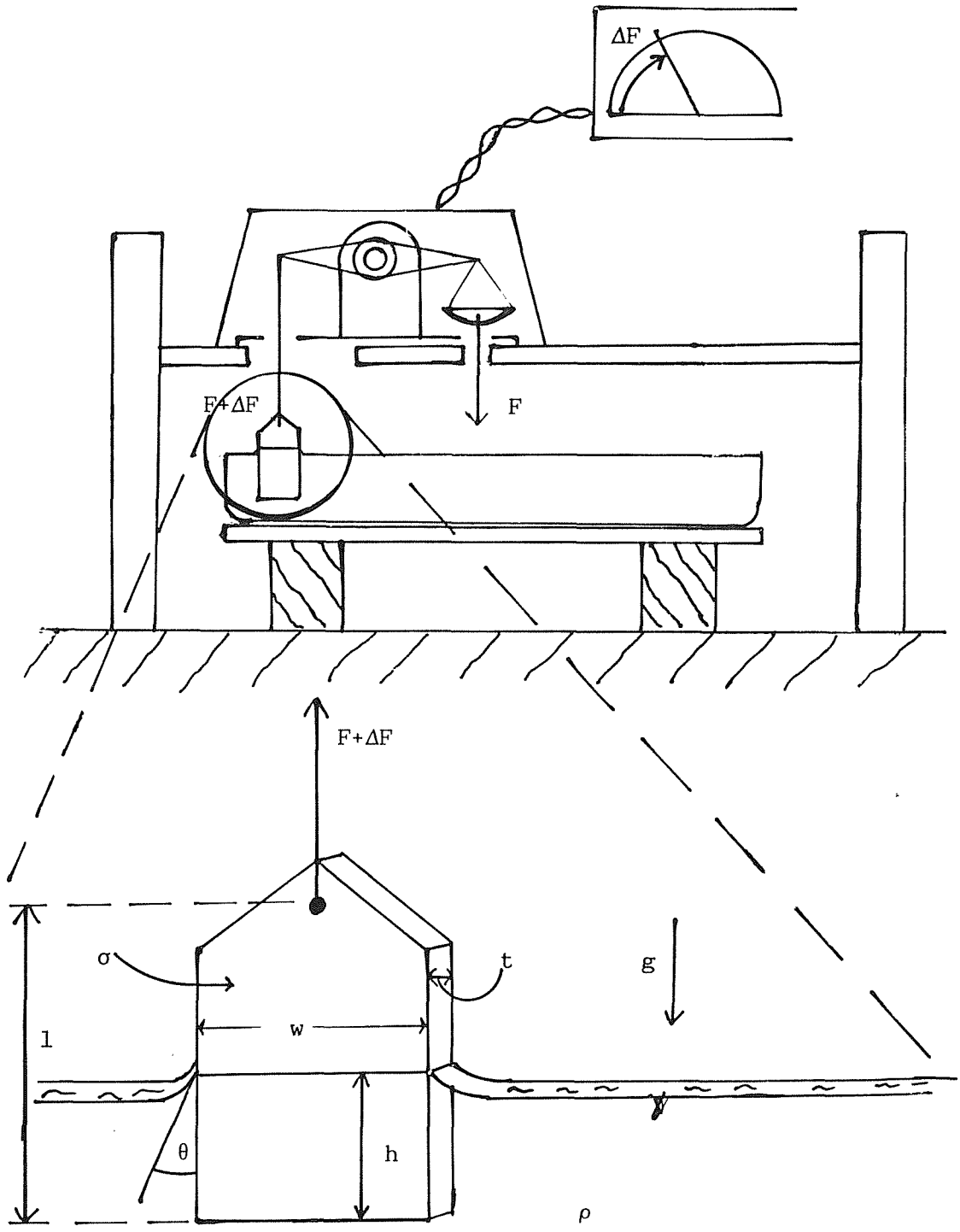

For Notation see text in sec 2.4.1

Fig 2.4 The Microbalance and Wilhelmy Plate

forces. The choice of filter paper for the Wilhelmy plate material was governed by consideration of the water/plate meniscus. Further consideration of this is given in section 2.4.2.

2.2.4 The Trough Water

A trough system requires a plentiful supply of pure water in order to clean the samples and trough as well as providing a suitable subphase. Pure water was obtained by passing doubly distilled tap water through a "Milli Q" system (Millipore (UK) Ltd) which contains one activated charcoal filter, two nuclear grade ion exchangers and one 0.22 μm membrane filter. This produces very pure water with a resistivity of 18 MΩcm in which all metal impurities occur at concentrations of less than 10^{-10} g/ml (based on a spectrographic analysis).

Temperature control was provided by a commercial chiller/heater unit (Grant Instruments Ltd) connected to a glass heat exchanger in the bottom of the trough. This gave enough control over the subphase temperature which could not change rapidly because of the substantial mass of water involved. (During the production of the final samples the heat exchanger had to be removed to provide a greater trough depth). The subphase temperature was measured with a mercury in glass thermometer, placed at the same end as a set of pH probes.

2.2.5 Anti-vibration

Surface waves on the trough, due to external vibrations can perturb the monolayer. Some experimentalists, e.g. Brown (1981), have had to work at night to overcome this problem. It was therefore necessary to "insulate" the trough from environmental vibration. The trough was clamped in an aluminium alloy frame which rested on three legs which could be removed to allow the trough to be lowered clear of the tape. The legs in turn were supported on a piece of kitchen worktop placed directly on a solid block of concrete. (The concrete was sealed in a polythene sheet to contain the cement dust). The concrete and trough formed a large mass all supported on a layer of foam in order to absorb high frequency vibrations which might have been transmitted through the bench from the floor. Other researchers have used heavy tables supported on rubber tubes filled with glycerine (Grunfeld 1983). More recently bubbled (large size) plastic packing sheet has been used successfully by Severn & Batchelder (1984).

2.3 SUBPHASE pH

2.3.1 pH Measurement

To measure the pH of the subphase a Philips PW9409 meter was used. Originally the pH was measured using combination probes, but they seemed to have a slow response when used in high purity water. Consequently we tried using separate reference and measuring probes. A "Quickfit" ground glass sleeve reference junction was used, as the manufacturers suggested "a more permeable" membrane was required. The reference probe was a Pye Unicam Ingold type 303W and a type 201E7 was used as the measuring probe. Some improvement was noted. (Similarly it is known that pH measurements in organic solutions need care, requiring a reference junction with a large surface area). All pH probes leak into the solution and the above one more than most. However we estimated that its contribution to subphase contamination was less than that due to the impurities associated with the $MnCl_2$ solution. The meter was also connected to a temperature probe which automatically corrected for variations in the subphase temperature while the pH probes were calibrated using buffer solutions of value pH 4 and pH 7.

2.3.2 Monolayer Doping

To produce magnetically doped monolayers we used a 10^{-3}M solution of $MnCl_2.4H_2O$ for the subphase as indicated by Pomerantz (1980). About 2 g of the salt was dissolved in about 100 ml of Millipore water (to enable easy addition along the whole trough length). A slightly weaker solution was used for cadmium ($5x10^{-4}$M $CdCl_2$). An alkaline subphase would cause ionisation of the stearic acid in the monolayer so then Mn^{2+} (or Cd^{2+}) ions from the subphase could bind to two hydrocarbon chains forming e.g. manganese stearate ($MnSt_2$). (However if the pH was much greater than seven then the hydroxyl ions would precipitate the manganese out of solution).

2.3.3 Subphase pH Control

The very pure Millipore water used for the subphase in our trough would quickly absorb carbon dioxide from the atmosphere to form carbonic acid, until it reached an equilibrium pH of 5.5. This effect has been noted by several authors (Grunfeld 1983, Walpitta 1977) and it was possible to observe the pH drop over some hours in the trough.

Pomerantz (1980) has investigated the pH required to obtain a $MnSt_2$ monolayer as against one of stearic acid (HSt). He found values between 6.5 and 7.0 were satisfactory so we chose to dip at pH 6.7±0.1. In order to obtain the required pH of 6.7, solutions of analytical grade NaOH or Aristar HCl (BDH Ltd) had to be added to the subphase. Since the natural pH of CO_2 saturated water is 5.5 it was usually alkali that had to be added. No buffer solution was used in order to avoid any possible contamination of the monolayer. The acid and alkali solutions used to control the pH had a concentration of 0.01M. It was much better to add "large" amounts of dilute alkali, rather than small quantities of a more concentrated solution. There are two reasons for this:

Firstly if a concentrated solution was dropped onto an area of the trough its pH would rise too much before mixing occurred. This could cause a precipitation of manganese hydroxide. To avoid this the initial adjustment of the pH could be done before the manganese chloride solution was added. However the addition of the $MnCl_2$ solution itself altered the pH, presumably by affecting the ionic balance. A similar change to an acidic solution has been reported by Grunfeld (1983). He suggested this was due to the metal ions "picking up" some hydroxyl anions. This means some pH adjustment has to take place with Mn^{2+} ions present.

Secondly mixing throughout the whole subphase was found to be a problem. If a large volume of dilute alkali was added it could be spread evenly over the whole length of the trough. Then local mixing was achieved by use of a pre-cleaned glass stirring rod kept for this purpose. The pH probe was located, necessarily, at one end of the trough so care was taken to add solutions uniformly along the trough to avoid local variations leading to errors in the pH measurement.

2.3.4 Subphase Mixing

Stirring could only take place before the monolayer was spread. Colbeck & Chase hung a rotating teflon plate in their trough to stir the subphase solution (private communication 1983). We had investigated the possibility of magnetic stirrers, but none was found suitable. This was probably due to:

i) the thick base of the trough frame

ii) the trough floor was a gentle arch across the width, i.e. it was

shallower along the centre than along the front and back sides. Hence a glass stirring rod was kept for this purpose, and used along the whole length of the trough whenever solutions were added.

2.3.5 pH Probe Cleaning

When the pH probes were transferred from one solution to another it was often necessary to vigorously wash off the old solution in order to reliably read the new one. This may be done by holding the probes under the "tap" of the Millipore unit to "wash" them, and then strongly stirring the new solution with the probes. We did not try wiping them with a "clean" cloth as suggested by some probe manufacturers as this might have caused unwanted contamination.

2.4 SURFACE PRESSURE

2.4.1 Measurement of Surface Pressure

Surface pressure is measured via a Wilhelmy plate, which is usually formed from a small strip of teflon, mica, glass or filter paper. Being half submerged as it hangs from a weighing balance it experiences a force which is the resultant of the surface tension, its weight, the bouyancy upthrust and the equilibrium force provided by the balance. The variations in the surface tension due to a monolayer are detected as apparent changes in weight. The change in surface tension, between pure water and film covered water is called the surface pressure, and is denoted by π being measured in units of mN/m. Consider a plate of thickness t, width w, length l, and density σ which is immersed by a length h in water of density ρ and surface tension γ; see fig 2.4.

Then the forces transmitted to the balance are:

the weight = $\sigma twlg$ where g = acceleration due

the Archimedean upthrust = $twh\rho g$ to gravity

the surface tension = $\gamma 2(t+w)\cos\theta$ and θ = angle of contact

Their resultant force F is

$$= \sigma twlg - \rho twhg + 2\gamma(t+w)\cos\theta$$

If the plate is completely wetted then $\cos\theta=1$, and if the depth of immersion is fixed, then the variations which the balance sees due to the monolayer are given by

$$\delta F = \delta\gamma 2(t+w)$$

and $$\pi = \delta\gamma$$

so $$\pi = \delta F/p \quad \text{where } p = 2(t+w), \text{ the plate perimeter.}$$

Since increasing the amount of monolayer material decreases the surface tension, the surface pressure, which is defined to increase with the compaction of the monolayer, is the negative of the change in surface tension. The Wilhelmy method is not the only method of measuring surface pressure; the Langmuir method has been described by Gaines (1966), and more recently a new method using strain gauges on a frame has been developed by Albrecht & Sackmann (1980). For example it can resolve 20 μN/m within a f.s.d. of 1 mN/m as well as measuring surface pressures normally used in troughs.

2.4.2 Errors In Surface Pressure Measurement

Although the compression of a monolayer took a relatively short time, dipping the monolayer could take hours. It was therefore important to know how much the surface pressure measurement system would drift during that time. The electronics drift was found to be about 1% of the dipping pressure of 25 mN/m.

The successful operation of a Wilhelmy plate according to the equation derived previously depended on the contact angle between the subphase and the plate being zero degrees. Many authors have noted that this can become a problem with time if the plate becomes coated in monolayer material hence changing the contact angle, e.g. Gaines (1977). In order to avoid the contact angle changing we used filter paper which remained soaked with water ensuring that the contact angle was zero but it did cause other problems e.g. soaked filter paper swelled so the perimeter length changed. We shortened the length to 15 mm which ensured total soaking, reduced possible evaporative effects (see below at 2.4.4) and the time to absorb water. A small hole allowed them to be fitted onto a "hook" hanging from the microforce balance. Experiments showed that a newly cut, dry, filter paper became fully soaked and gave a stable surface pressure after one hour. If immersed in water the time to stabilise was reduced. The filter paper was cut using a method devised by Colbeck & Chase

(private communication 1983), which consisted of placing three filter papers together. One acted as a cutting base which, together with the top paper, protected the central one from contamination. The plate cut out from the central paper was used while the outer two were discarded. It was possible to cut filter papers to within 5% of the required width. The expansion of filter paper on soaking with water was found to be about +2%. The filter paper thickness was 0.17 mm, which was also about 2% of the 10 mm width. For accurate work a suitable procedure would be to cut a filter paper, measure its width and add 4%.

2.4.3 Subphase Level Effects

A very important source of uncertainty was changes in the level of the Wilhelmy plate with respect to the subphase surface. Evaporation and surface cleaning changed the water level and hence the bouyancy effect and the amount of absorbed water above the subphase. The problem can be estimated by considering the bouyancy change due to the change in the amount of water displaced by the soaked filter paper. The filter paper and water entrapped in it, above and below the surface, are considered as one solid unit. A water level change of 1 mm would mean a displaced mass change of about 1.7 mg. Some crude experiments of observing the pressure deflection as the trough water was sucked out agreed with this figure within 20%. This indicated a systematic error of 1 mN/m for a 1 mm change in subphase level. This was 4% of the usual dipping pressure of 25 mN/m.

2.4.4 Evaporation

The previous analysis (see above at 2.4.2) assumed that the filter paper remained evenly soaked. Fortunately the evaporation of water from the exposed surface was not found to produce noticeable effects under normal conditions. (If the speed of the fan-filter unit was increased then about 1 mN/m change could be observed). To measure the effects of evaporation two different length filter papers were balanced against each other. When the trough fan was turned up it caused about a 4% change in the force measured. During normal dipping experiments the fan was switched off (to stop vibrations) and the trough fully enclosed (When the trough was left full of water for several weeks no lowering of the surface was noticed).

2.4.5 Errors In Π from Dirt and Solvent

Possible sources of "error" in the surface pressure were associated with unremoved "dirt" and the solvent used in the spreading solution. To assess these several tests were carried out:

i) The trough area was compressed after one suction cleaning. As the minimum area was reached the surface pressure rose to +3 mN/m and then quickly decayed to +1 mN/m. On further suction cleaning the pressure dropped to zero indicating the need for several cleaning cycles.

ii) A volume of solvent (chloroform) containing no stearic acid was spread on the trough (a "blank spreading"). The trough enclosure was shut and after ten minutes (to allow evaporation) the surface was compressed. The pressure peaked to +2 mN/m and then settled at +1 mN/m. Repeating the experiment but with the fan left on caused a +3 mN/m peak which then settled at +1 mN/m. The fan should be switched off before spreading.

iii) The above was repeated but with the trough enclosure left open. This caused a 6 mN/m peak and a +4 mN/m offset suggesting the trough should be fully enclosed after spreading.

At the areas used in dipping no pressure "error" was measured so we could ignore the peaking on full compression. (Following these experiments it was suggested that the solvent might dissolve off "dirt" from the barriers and that several blank spreadings, followed by suction cleaning, would remove this "dirt". This idea has not been investigated).

iv) Finally the trough was left enclosed but with the microbalance on for over four hours. Less than 1 mg change was noted. A large part of this could be accounted for by electronics drift (see above). Another contribution would probably come from unfiltered dust settling out on the trough. (If the surface was left for a several days and then fully compressed a π-A curve could be produced from the "dirt" which had settled on the trough's surface).

2.4.6 Summary of Errors

With a measured filter paper and a calibrated micro-balance we can estimate the uncertainty in π. Accounting for all the previous factors and the precautions taken, would suggest an overall random uncertainty

of ±2%. We also estimated ±1% constant error mainly due to filter paper cutting and the micro-balance calibration.

2.5 MONOLAYER CHARACTERISATION

2.5.1 Introduction

Several preliminary π-A curves were produced using stearic acid (HSt). The M_r(HSt) = 284.5 and its formula is $CH_3(CH_2)_{16}COOH$. It was obtained from Sigma Chemical Company. Then further investigations were made of the factors which affect monolayer behaviour and the functioning of the trough system e.g. the uncertainties involved with Wilhelmy plates made from filter paper as described in sec 2.4 above.

2.5.2 Monolayer Spreading

Stearic acid (Octadecanoic acid) was dissolved in Aristar chloroform (BDH Ltd) and made up to a concentration of 1 mg/ml or 5 mg/ml. This was stored in a refrigerator at approx 0^oC until required. The solution was deposited on the open surface of the trough with a Hamilton microsyringe. About 150 µl of a 1 mg/ml solution was required to cover the trough. (The whole trough was only needed when dipping large samples or building up a large number of layers). Drops were added to different parts of the surface to aid even spreading. (This also helped to avoid 3-D clusters). Walpitta (1977) has also reported spreading large volumes of "weak" solution on different parts of the subphase surface. Chloroform is denser than water, and will only stay at the surface because of surface tension. Hence it must be dropped from the micro-syringe in close proximity to the surface to avoid dropping through it and onto the bottom of the trough. After spreading the chloroform was allowed 5-10 minutes to evaporate leaving behind a dilute layer of stearic acid ready for compression.

2.5.3 Monolayer Compression

The speed with which the barriers could close was controllable between 0.5 cm^2/s and 10 cm^2/s. The compression effect, of the barriers on the monolayer, also depended on how much material there was in the monolayer. The compression rate was therefore normalised by the total number of monolayer molecules present. The shape of the π-A curve

depended on this compression rate as can be seen in fig 2.5, which shows the effect on $MnSt_2$ monolayers. It can be seen that for higher compression rates the surface pressure began to rise earlier in the compression. This could have been due to spaces between the molecules; at the higher compression the molecules did not have the time to re-arrange themselves into a more close packed configuration and so occupy a greater area. The change in the slope of the π-A curve produced from some monolayers indicated a transition stage in their arrangement.

2.5.4 LB Dipping

Langmuir Blodgett dipping usually requires the monolayer to be in the solid condensed phase. If the monolayer is too thinly spread holes will occur in the film transferred to the substrate. But if the monolayer pressure is too high then the chances of molecular overturning producing 3-D nucleation increase. The best pressure will depend on the ultimate use of the films.

The details of LB film preparation are given in chapter 3. However a basic outline is given here, so that the reader can understand the relevance of the following discussion of monolayer stability and our work on it. Once compressed the LB layers are built up by dipping a substrate up and down through the monolayer. This removes monolayer material from the surface, so it is necessary for the barriers to reduce the trough area correspondingly. This is done via a feedback system which aims to keep the surface pressure (as measured by the Wilhelmy plate) at a fixed value. If there is no decay of the monolayer then the change in trough area is a measure of the area of substrate that is being covered.

2.5.5 Monolayer Stability

After initial compression, if a monolayer is held at constant π then a decrease is observed in the Area. (Holding at constant π is the important method for LB purposes). There seem to be several conditions which affect this. These are:

i) the temperature

It is a rule of thumb that monolayers are more stable at lower temperatures. This is supported by the evidence of Heikkila et al (1970). Although we did not want to expose our monolayers to "extreme"

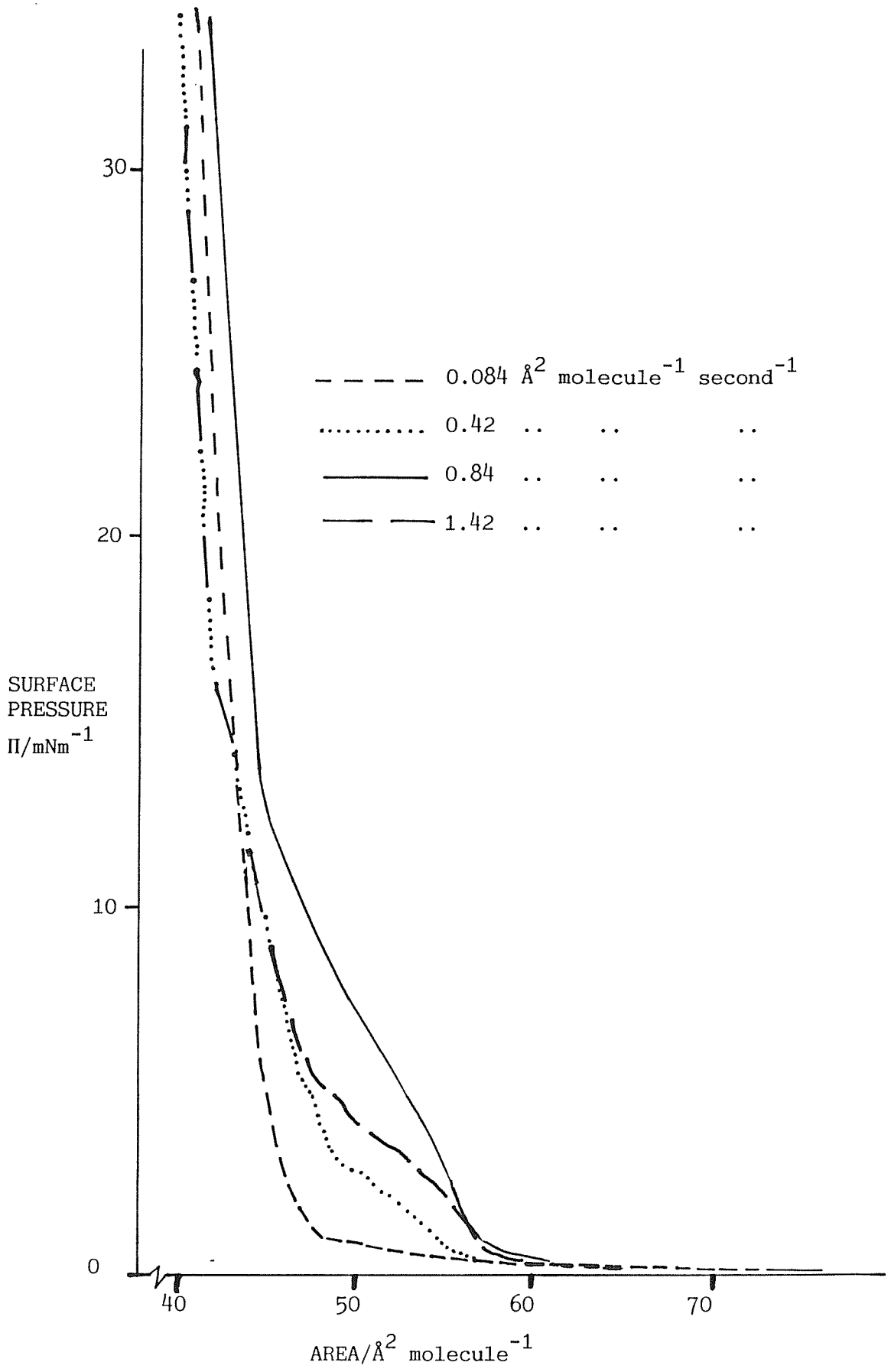

Fig 2.5 Compression Rate Effects on the $MnSt_2$

pressures, Grunfeld (1983) has noted that the pressure which a monolayer can withstand before collapse was much lower at higher temperatures. Surface pressure-Area curves of Rabinovitz et al (1960) appear to show a similar effect.

ii) the compression rate

There appears to be more monolayer decay if it was compressed quickly. This would be due to the monolayer having less time to respond. Smith and Berg (1980) have found that there is an initial fast decay proportional to the compression speed.

iii) cycling

Π-A curves show hysteresis. This occurs on expansion after monolayer compression. The expansion curves show lower pressures for the same area. This has been studied by Munden et al (1969) and Rabinovitz et al (1960). The larger the peak surface pressure on compression then the larger the hysteresis. (Which is really a form of surface pressure decay). Multiple cycling seemed to reduce the maximum surface pressure attainable on compression.

iv) the value of maintained surface pressure

This effect was shown by experiments in which the monolayer was compressed to a fixed surface pressure and held there. The consequential reduction in area required to maintain the surface pressure was then observed. The higher the maintained π then the greater the initial loss of area (Smith & Berg 1980). This was particularly relevant at the start of the LB dipping process.

v) subphase pH

When using fatty acid monolayers, a high pH was found to favour stability. At a fixed π there was a much greater area loss for monolayers spread on acidic subphases. This was explained by the degree of ionisation of the COOH headgroup (Xu et al 1982).

vi) chain length

It has also been noticed that molecules with an odd number of carbon atoms are more stable than an even numbered molecule with one more (or less) carbon atom. Otherwise increasing chain length usually imparted more stability (Sims & Zografi 1972).

vii) solution and evaporation

Most of the above references to decay indicate that monolayer solution or evaporation were not major factors.

2.5.6 The Origin of Monolayer Decay

Following Smith & Berg these effects can probably be explained by molecular rearrangement and expulsion from the monolayer. As the monolayer is compressed, little rafts of molecules are formed which collect together unevenly. Under a fast compression rate gaps are produced which are only filled after the required surface pressure is achieved. The surface pressure will begin rising at larger areas per molecule; see curves in fig 2.5. Then there is an initial fast area loss once the monolayer compression is completed.

However at higher pressures, the molecules may also be pushed out of the monolayer decreasing the area and producing 3-D rafts. This could be a smaller long term continuous process and would be dependent on chain length and the pH. The exact mechanism by which lower temperatures strengthen the monolayer is not known, but it is probably connected with lower thermal motion. Smith & Berg have produced further evidence to support this bulk nucleation hypothesis. Sprinkling of bulk monolayer material onto the monolayer accelerated the decay, but talc dust or lycopodium powder did not. (Solvents and "contaminated" water had little effect on monolayer decay). If the monolayer did form 3-D clumps on compression they would build up and cause further decay in future compressions. (There is some evidence that the rafts will partially disperse on expansion; see diagrams in Rabinovitz et al (1960) but Smith & Berg report that some 3-D rafts would remain).

2.5.7 Manganese Stearate Monolayer Decay

Since it was important for our work to avoid 3-D inclusions all work was done using fresh monolayers. These had not been cycled except when building the 101 layer sample. In this case the trough needed constant replenishing, and it would not have been feasible to clean off the remains of the previous monolayer. Sufficient time was allowed for the monolayer to rearrange itself (decay) before dipping began. This would help avoid holes in the film.

Similar to the reviewed work (above) on fatty acids we observed

monolayer decay in $MnSt_2$ films. Stearic acid was spread on a subphase of $MnCl_2$ solution (10^{-3}M) at pH 6.6-6.9. This was compressed to the set surface pressure, initially quickly but then reducing to a slower rate. An initial fast loss followed by slow decay was seen. Curves were obtained for π = 20, 25 and 30 mN/m at room temperature and 10°C. These values were possible conditions under which we would produce LB films. The area lost after thirty minutes is shown in table 2.1 and a diagram of the A-t curve for this phenomenon in fig 2.6.

π(mN/m)	pH	temp (°C)	ΔA (cm^2)
20	6.6	18.8	-11
20	6.8	17	-23
20	6.87	10	-32
25	?	?	-34
25	6.7	14.5	-14
25	6.85	10	-18
30	6.6	16	-18

Water + 10^{-3}M $MnCl_2$ + HSt spread.

Table 2.1 Area Loss after 30 mins by Monolayer Decay

Due to a miscalculation the total original area is not known, but can be estimated to be about 400-500 cm^2. No values of decay for $MnSt_2$ are known to have been given in the literature. However our few results are erratic and the trend of less decay at higher pressure and temperature is opposite to what we expected. We assumed this to be either due to large random variations or a misjudgement of the decay area as decay occurred very quickly at the start point. As we were mainly interested in these results because of their implications for our dipping we did not need to worry about this inaccuracy. As expected we had shown that manganese stearate monolayers would decay

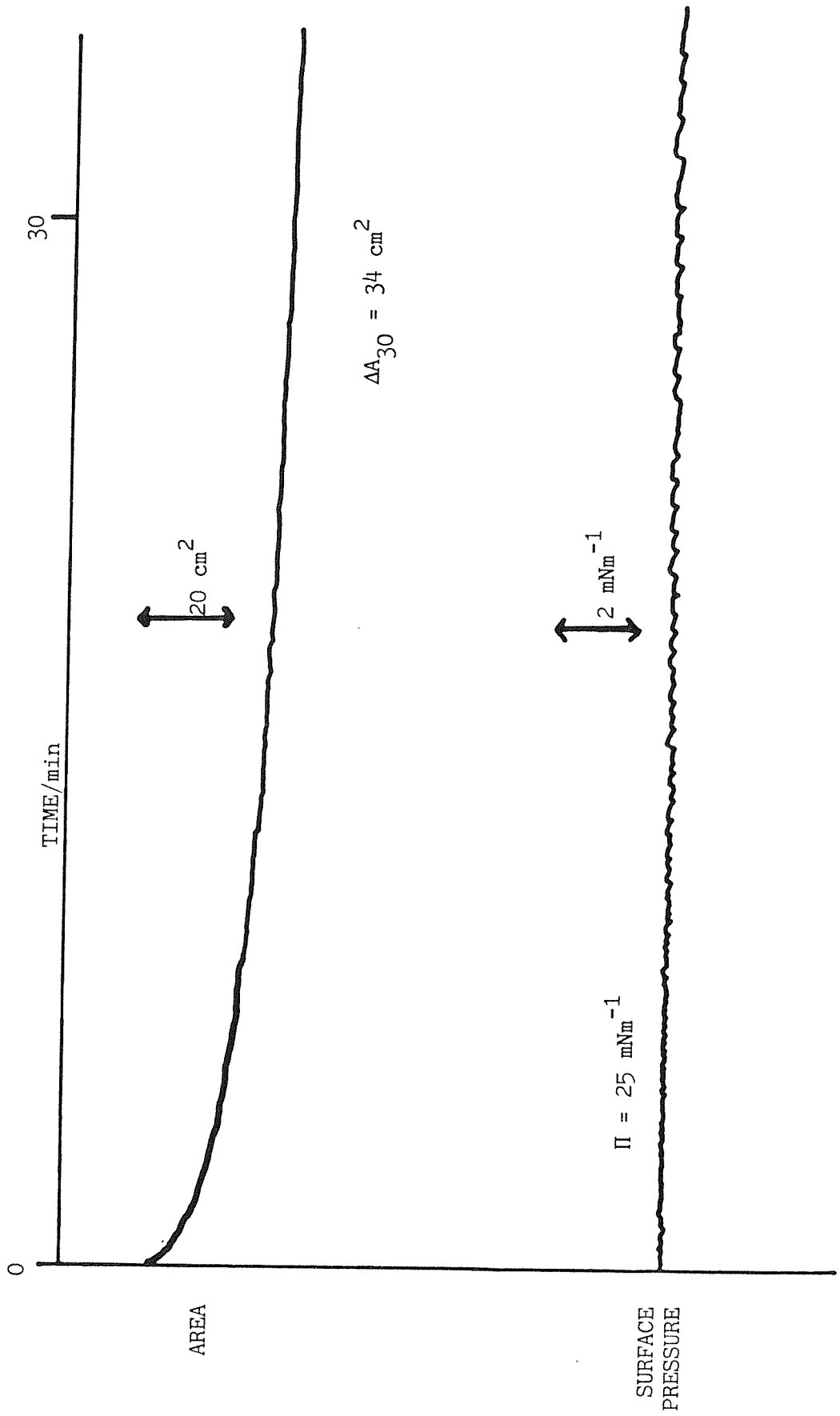

Fig 2.6 Monolayer Area Loss

and therefore we took the precautions previously indicated.

2.6 CLEANING

2.6.1 The Atmosphere

To keep the trough unit clean it was housed in a laminar flow cabinet (Fell Clean Ltd) which was maintained at a positive pressure with respect to the room. The cabinet was supplied with air through a fibre-glass pre-filter and a class 100 HEPA filter (i.e. High Efficiency Particulate Arrester). A class 100 HEPA filter can reduce the number of dust particles (with diameter ≥ 0.3 μm) to less than 100 particles per cubic foot of air. Large air flows did appear to increase the rate of "acidification" of the subphase due to CO_2 absorption (see above at 2.3.3). During compression of the monolayer and LB dipping the front of the laminar flow cabinet was closed with a perspex screen and the fan was turned down to avoid vibration.

2.6.2 The Clean Room

During the lifetime of this project it was also possible to set up a "clean room" where the trough and all the "cleaning" equipment could be housed. (The trough was still kept in the laminar flow cabinet). The clean room was pressurised by a fan similar to that used for the cabinet. The room also required a double door/lobby entrance system to maintain the positive pressure whenever someone entered/left the room. The room was regularly cleaned and several services were fed in, through the wall, from outside the room.

2.6.3 The Trough

As previously mentioned the trough needed to be kept very clean; however there is no agreed method in the literature for doing this (or for the cleaning of any sample substrates). The trough was quite large so it could not be readily washed out under a stream of pure water. So the "recipe" for cleaning it is given below in a chronological list.

1. The surface layer of water and impurities, from both sides of the barrier was sucked up using a peristaltic pump. (This stopped insoluble surface dirt from depositing on the trough walls when the

rest of the water was sucked out).

2. The majority of the subphase was then sucked out.

3. A clean wash bottle of Millipore water was used to apply a water stream to the trough sides (and the teflon tape if it had not been removed).

4. More Millipore water could be repeatedly poured over/into the trough and sucked out. (This constant dilution of any remaining solution and then sucking of it away was the closest we could get to holding the trough under the Millipore "tap").

5. If required the trough surface could be wiped down with Kimwipes (Kimberly Clark) which are reputed to be relatively fluff free tissues. If necessary the Kimwipes could be soaked in Analar grade propan-2-ol or trichloroethane as a degreasing agent. (Stage 4 would be repeated again after this).

For the majority of the time the trough was not dried out but left containing several litres of pure water. Then any contamination falling on the trough between uses would fall onto the water surface, from which it could be sucked away. This eliminated the possibility of any dirt drying onto the glass surface.

2.6.4 The Water Surface

It was not possible to produce an absolutely clean environment, so "dirt" of various forms would inevitably collect on the water surface of the trough. A large part of this would of course be the remanents of previous monolayers. This was removed by a remote suction pump. At its open end a disposable glass pipette provided a narrow orifice, to restrict suction to the surface region. Since the pipette was made of glass it could be rigorously cleaned before use - see method below at 2.6.9. To clean the surface the barriers were moved together, compressing the dirt into a smaller area, and then this smaller surface was sucked clean. The barrier compression and cleaning would be repeated several times until there was negligible change in π on compression.

2.6.5 The Filter Papers and Barrier Tape

These were difficult to clean because of their fragile nature. They could only be soaked in Millipore water and perhaps propan-2-ol so they were periodically replaced.

A Tygaflor (Fothergill Tygaflor Ltd) teflon barrier was used in this trough. (The closed tape is heat welded together at the joint). Teflon is inert, and soaking in organic solvent did not appear to affect the tapes, neither did boiling in Decon 90 solution, an alkaline decontaminant of pH 11 (Decon Labs Ltd). A concentrated H_2SO_4/HNO_3 pickling solution caused some discolouration of the tape after several hours. Like the trough there is no agreed method for cleaning the tape. It was first coiled loosely into a large, clean, beaker or bottle. It could then be soaked in a degreasing agent, such as trichloroethane, followed by propan-2-ol and Millipore water. (Otherwise it could be soaked or boiled in Decon 90 solution and then rinsed in Millipore water).

2.6.6 The Substrate & its Frame

During the project several substrates were considered. These included glass, quartz, silicon and finally aluminium foil. These substrates were clamped to the dipping frame by nylon screws and teflon blocks (see below at 3.1.4). Glass, quartz and teflon will withstand strong cleaning processes and were cleaned using the following procedure:

i) Ultrasonication (15 mins) twice in chloroform or trichloroethane to degrease the substrate.
ii) Pickling overnight in concentrated H_2SO_4/HNO_3 diluted by an equal amount of water.
iii) Ultrasonication (15 mins) twice in Millipore water.
iv) .. .. Analar propan-2-ol.

The alcohol is miscible with water which it could wash away, and would itself quickly evaporate to leave the material dry. (Other researchers have used different methods e.g. Walpitta (1977) used chromic acid and boiling Decon).

It was originally intended that the sample layers would be deposited on small glass or silicon slides and the method for handling these slides during cleaning has been described by Asaolu (1983). However, as is shown below in sec. 6.1, the SQUID magnetometer required a different form of sample using a large aluminium foil substrate. Since very large sheets (350x150 mm) were used, which would dissolve in any pickling acid, new cleaning and handling methods were developed. The aluminium foils were loosely rolled around thick teflon rods

(20 mm diameter) and placed in large measuring cylinders containing the solvents. The cylinders were then stood in an ultrasonicator. The foil was ultrasonicated twice in both chloroform and Millipore water, separated by alcohol, and finally alcohol again to aid in drying. It was soon apparent that, in alcohol and water, the foil could not withstand the forces imposed on it by "direct" ultrasonication for fifteen minutes; the foil became perforated. To overcome this problem ultrasonication was confined to much shorter periods of time, or the measuring cylinder was stood within a litre beaker filled with lubricating oil. The beaker and its contents were then placed in the ultrasonicator. (The use of the oil was unwanted but unavoidable).

There is no easy way to ascertain the effectiveness of this cleaning procedure. However, after cleaning, some foils were stored for several months and then inserted into the cryostat. The signals obtained implied that the foil was contaminated. We would expect to have a zero signal for a long clean foil on its own (see chapter 6). Fortunately when the foil was re-cleaned (using the above method) and re-measured it gave a zero signal implying that "de-contamination" had been achieved.

2.6.7 Pure Aluminium Rods and the Sample Holder

Some rods of high purity aluminium (Goodfellow Metals Ltd) were used as test and calibration samples for our magnetic flux detector and these needed cleaning. Also the foil sample holder was made from the same pure aluminium (99.999%) and they all had to be cut to the correct size using a lathe. Consequently, as well as removing any grease, we wanted to remove any inorganic surface impurities that might have been picked up from the lathe tool. It is not advisable to use Decon 90 with aluminium because of the way they react with each other. We therefore looked for some "etching" solutions. An acidic solution was chosen as this was slower than an alkaline one, giving us more control. This was made from a mixture of:

HCl acid	(relative density 1.18)	20%
HNO_3 acid	(" " 1.42)	10%
Millipore water		70%

The sample was etched for seven minutes, the material having previously been degreased. Then the sample was repeatedly washed in Millipore water and propan-2-ol.

The dural, used as part of the sample clamp, and the aluminium welding rod, used to roll the foils around, could not be cleaned in these "etching" solutions as black surface deposits would be formed. So we had to clean these in a proprietory neutral cleaning solution, Lipsol (Lip Ltd). This led to some "fizzing" and the surface layer of the material was visibly cleaned.

2.6.8 Our Gloves

It was occasionally necessary to handle either the inside of the trough e.g. the tape on its replacement after cleaning or the actual sample itself. The cleanliness required is greater than that in an operating theatre. Not only should the gloves be biologically sterile, but they need to be free from all organic and inorganic contaminants as well. We used Kimguard (Kimberly Clark) plastic gloves. These would be pulled from a box and after putting them on they would be "hand washed" in a stream of Millipore water. It was noted that the discarded water tended to be slightly "frothy", indicating that some impurity (assumed to be packing talc) was being removed. The gloves could then be dried by evaporation or by holding in the air stream of the air pressurising unit. We investigated the use of individually packed, sterilised, gloves but no advantage was achieved. They still had some powder coating to stop sticking. Unpowdered polythene gloves were of no use because of their lack of strength and elasticity. Also they were unsuitable since the rolling of samples (see section 5.5.3) required tightly fitting gloves.

2.6.9 The Glassware

To clean glassware two methods were tried.

i) A chromic acid solution was used, but it was suspected that this could "acidify" the glass surface (see below).

ii) Decon 90 was also used with the solution normally made up to 5% (approx.) and the articles were then left to soak overnight. For soiled articles it was found useful to scrub them with this solution, prior to soaking, for which several plastic toothbrushes were found to be useful. The manufacturers of Decon 90 (Decon Labs Ltd) claim that "three agitated rinses in demineralised water will ensure a film free finish"

(It was noticed that an irremovable deposit would be formed if a beaker was cleaned with Decon 90 after rinsing off a chromic acid

solution. Hence the suspicion that chromic acid solution can "acidify" glass)

2.7 SAMPLE STORAGE

i) Silicon and glass substrates - After cleaning or producing a sample, by LB dipping, the glass or silicon slides were placed in capped plastic containers and kept in a dessicated storage cupboard. They were handled by plastic tweezers which had been cleaned by ultrasonication in Analar propan-2-ol and Millipore water. (During the cleaning process plastic or stainless steel tweezers were used. The stainless steel does not degrade in the degreasing solvents but is of no use in the acid solution. Regretably the acid also partially attacked the plastic tweezers).

ii) Aluminium foils - Before and after sample deposition they were loosely rolled (on a cleaned surface) and placed in pre-cleaned test tubes and kept in a plastic dessicator. The solid pure aluminium rods used as calibration samples were stored similarly.

CHAPTER THREE - LANGMUIR-BLODGETT FILMS

3.1 THE LB PROCESS AND ITS USES

3.1.1 Introduction

The first detailed study of LB films was made by Blodgett in the 1930s e.g. one of her papers (1938) described an attempt to use LB films to produce optical interference so as to form an anti-reflection coating on glass.

Since then many more fundamental studies and applied projects have been carried out using LB films; e.g. Charles (1971) and Pomerantz & Segmüller (1980) used them to diffract X-rays. The latter were able to see single monolayers and investigate the structure within layers. Diffraction studies have also been made on fatty acids using neutrons e.g. Nicklow et al (1981), while Highfield et al (1983) saw neutron interference fringes. Much of the original work was carried out using fatty acids, but in the last decade there has been a great diversification into aromatic compounds as well.

3.1.2 Recent Interests

Examples of recent studies on LB films can be found in two volumes of Thin Solid Films; viz vols. 68 (1980) and 99 (1983). They contain articles on, for example:

i) The many factors affecting LB films which are still not understood, such as what causes the different types of LB dipping (see below at 3.2.1).

ii) Spectroscopy and other optical studies of LB films.

iii) Use of materials which will form polymerisable multilayers.

iv) Electrical studies of LB films and applications in electronics.

v) The addition of dye molecules within layers.

LB films for use in the electronics industry need to be stronger than fatty acid layers. To increase their strength layers of polymerisable material have been produced (Peterson et al 1983) and much new research has aimed at producing chemically active monolayers (Grunfeld 1983). There have also been attempts to produce multilayers of more complicated aromatic compounds. However these require aliphatic side

chains in order to form a monolayer; for example Vincett et al (1979) described how they succeeded in dipping an anthracene, which was only lightly substituted with aliphatic chains. Aromatic molecules have extended electron systems which might produce useful effects.

The most recent reviews of LB science and technology have been given by Tredgold (1987) and Roberts (1985). Roberts describes LB film applications, particularly within the electronics industry. However he draws attention to the relative "imbalance" of applied over pure research in LB films.

Langmuir-Blodgett films of manganese stearate ($MnSt_2$) was the system that was important to us. Several different studies of this material have been made, and reviewed by Pomerantz (1980). Much of his work has been referred to in the introduction, and except for a recent paper (Aviram and Pomerantz 1982) describing some modifications to his chemical procedure, his work is summarised in his review. These recent modifications have produced changes in results on bulk $MnSt_2$, but have not been applied to LB films of $MnSt_2$.

3.1.3 Outline of LB Dipping

Having obtained a compressed monolayer, it is necessary to maintain it at a fixed surface pressure using a feedback system. The Wilhelmy plate acts as the sensor and the barrier is the actuator. The up/down motion necessary to dip the substrates is provided by a large, vertically mounted, motorised micrometer (the "dipper"). This was attached to a rigid support which straddled the trough. The dipper had a variable speed (between 1 and 16 mm/min) which was adjusted via a calibrated potentiometer. It had adjustable end stops so that the dipping distance could be set as desired (up to 70 mm) and it was also possible to use these end stops to automatically reverse the dipper's direction. This could be done repeatedly, so that a pre-set number of layers could be built up. A diagram of the dipper is shown in fig 3.1.

The first pick up stroke would always be slow (e.g. 2 mm/min) - this is believed to help adhesion; see Roberts (1985) and Tredgold (1987). It was then possible to increase the speed. Often, as a precaution, with a large number of layers to be dipped this was increased in steps - i.e. dip two or more layers each at 2, 5, 7, or 10 mm/min. If the faster speed led to bad pick up we could then drop back to the previous speed. (This might be advisable if the control electronics

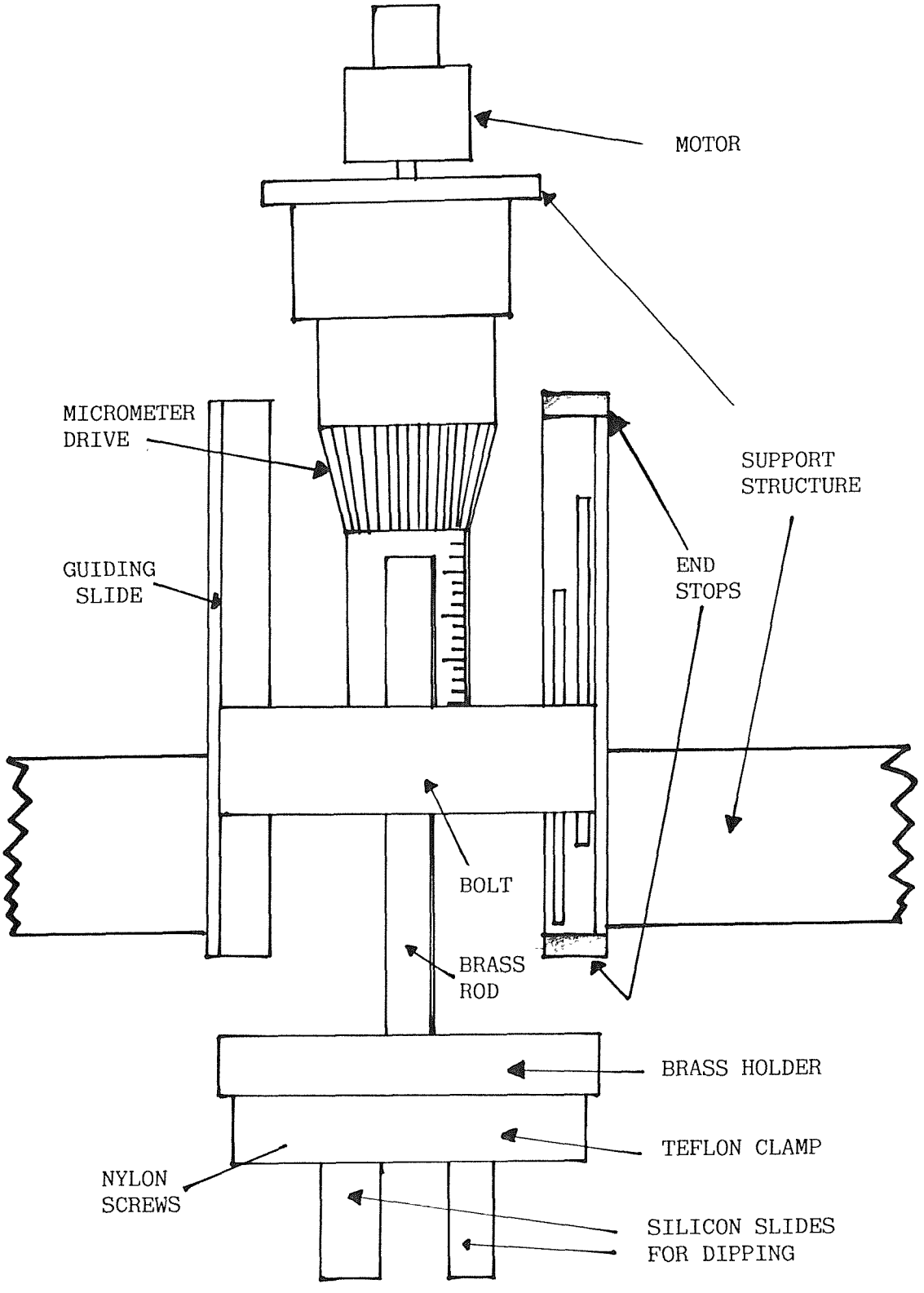

Fig 3.1 The Dipper

could not stop large excursions in surface pressure during dipping). The dipping process is followed over time by plotting the surface pressure (π) and the area, against time (particularly the A/t curve). An example is shown in fig 3.2. Then the amount of area picked up can be measured from the curve. Fig 3.3 (above the bar chart) shows the setting of the dipping speed controller as the multilayer is built up.

3.1.4 The Substrate Clamp

Two holders have been made for use with our trough. The first allowed one, or several, small slide(s) to be dipped. The substrates were clamped at their tops by nylon screws to a teflon holder. For the large and flimsy aluminium foils a second holder was made. This had two teflon legs suspended from a dural crosspiece to which the vertical brass rod was attached; see fig 3.4. The foil was folded in half, back to back, and its new edges fitted into two slots, one in each teflon leg which were clamped together by nylon screws. The part of the foil to be dipped could be positioned below the bottom of the teflon legs.

3.1.5 Substrates

Substrates can be sub-divided into two classes; either hydrophobic or hydrophilic. This determines how any monolayer transfer will start. Let us assume the substrate is just dipping into the water which is covered in a compressed monolayer. For a hydrophilic surface, e.g. aluminium, nothing happens as we push the slide down through the surface. Then if we reverse and slowly pull upwards, the meniscus will wet the aluminium with a small contact angle (concave up) and the monolayer will be transferred onto the aluminium. The headgroups bond to the metal surface with the hydrocarbon chains pointing away, perpendicular to the surface; see fig 3.5.

Before building further layers it is well known that we should now wait for some time, e.g. one hour. This allows any water to drain and the monolayer to dry. (If no drying period is given the monolayer will probably peel off on reinsertion through the surface). Then if we push the coated aluminium back through the surface the meniscus will be seen to turn over, and another layer will be added. This time the tails are pointing towards the aluminium, in contact with the tails of the previous layer; see fig 3.6.

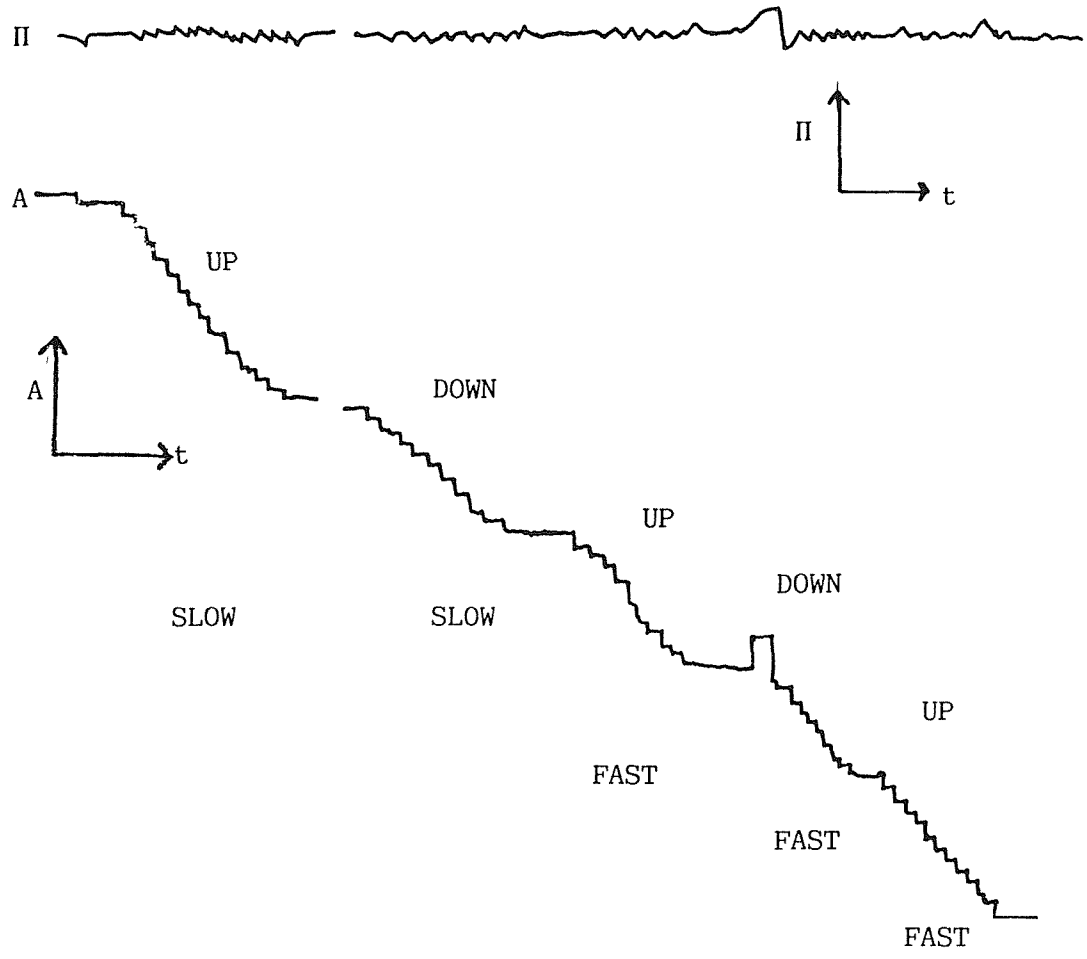

Fig 3.2 Π-t & A-t Dipping Curves

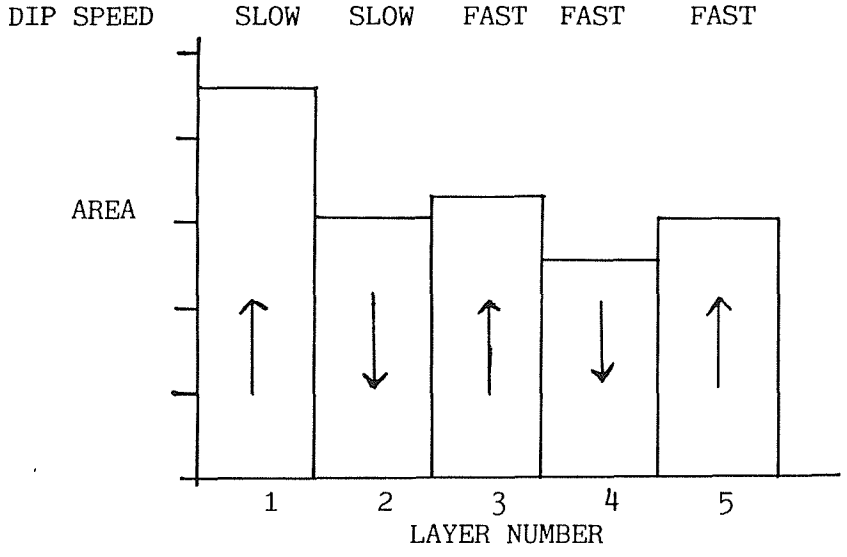

Fig 3.3 Area Dipped Histogram

Figs 3.2 & 3.3 Dipping Results

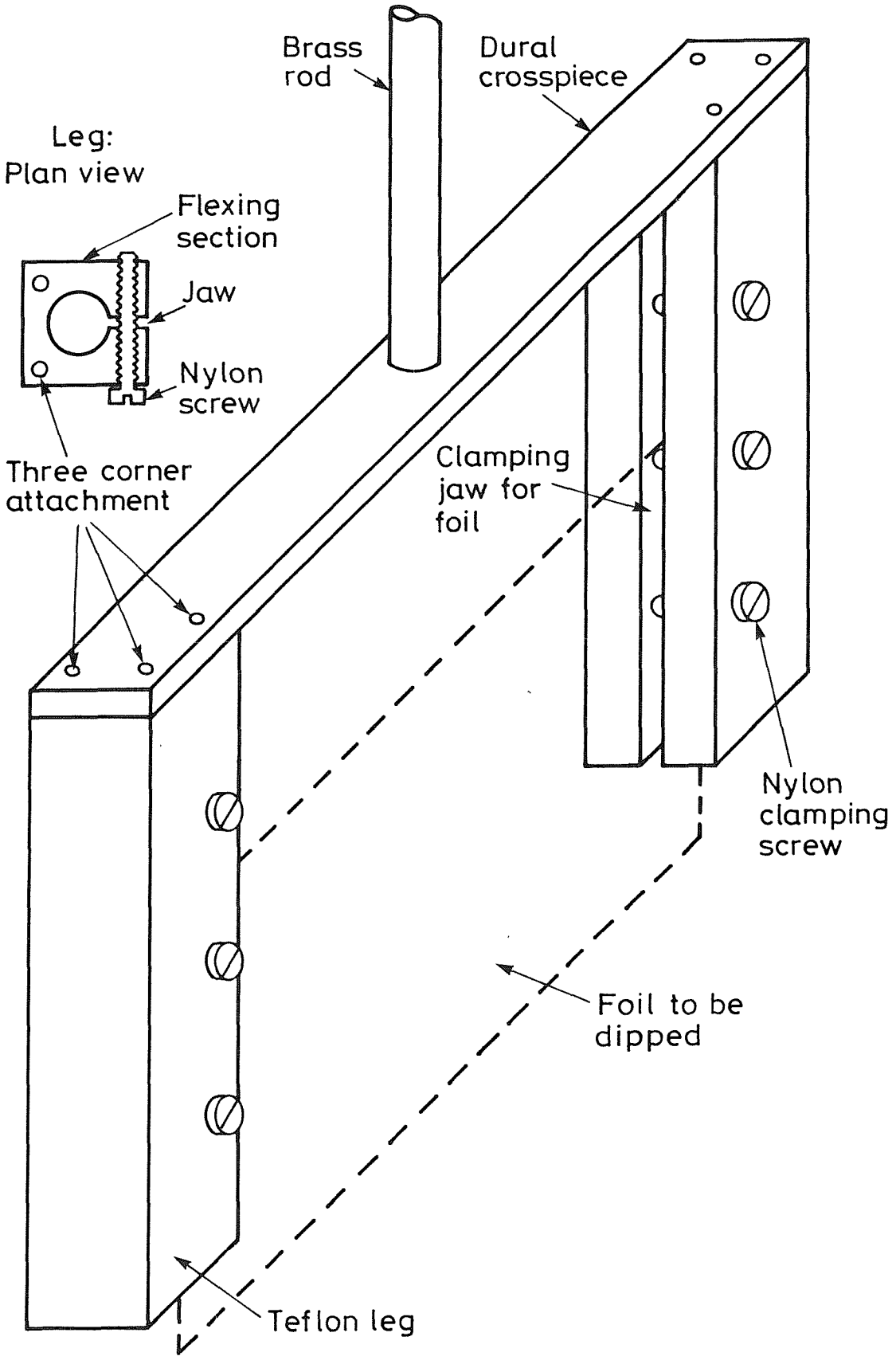

Fig 3.4 The Aluminium Foil Holder

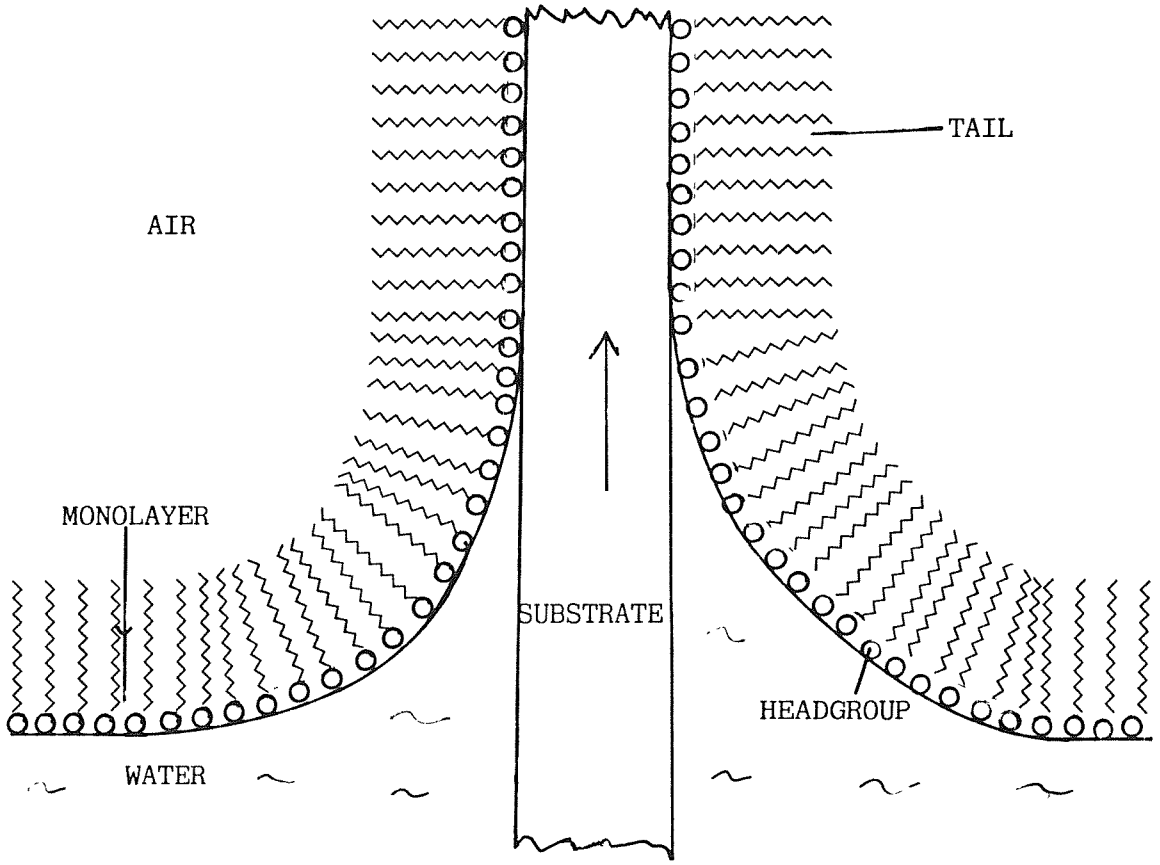

Fig 3.5 Substrate/Stearate Interface

Further up/down dipping produces more transfer, with the orientation of the headgroups alternating from layer to layer. If we had used a hydrophobic material, then, ideally, a monolayer would have been transferred on the first downstroke. The meniscus would be concave down and the monolayer has transferred with the tails in contact with the substrate. So now the headgroups project giving a hydrophilic surface which will pick up another monolayer head to head on the following upstroke.

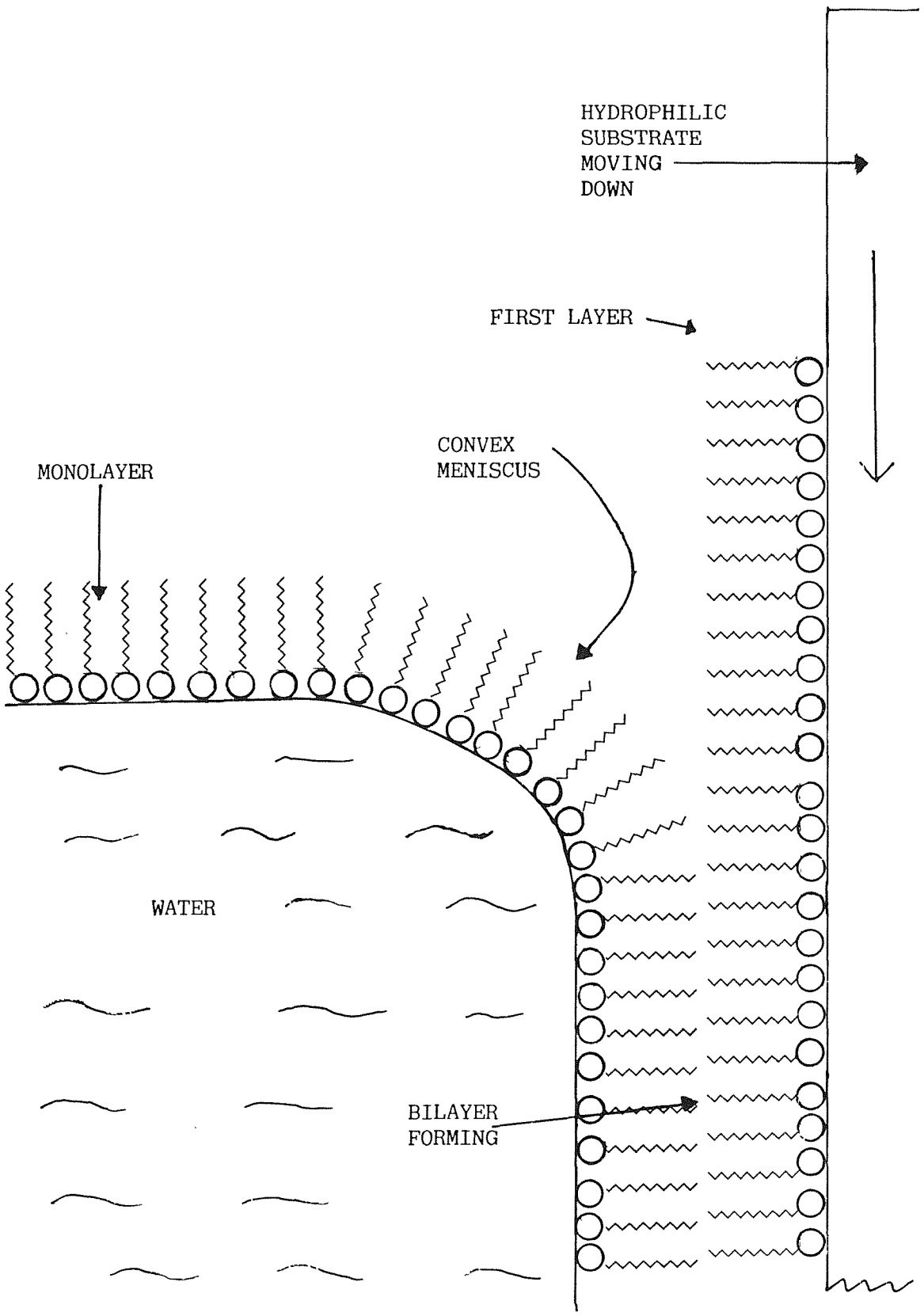

Fig 3.6 Bilayer Formation

3.2 NON-IDEALITY

3.2.1 The Transfer Ratio

The first non-ideality of the real world is that one does not get 100% transfer of the monolayer. In some cases transfer will only occur in one direction. A simple classification system has been formed to describe this. If the monolayer material is picked up on both up and down strokes it is called Y type deposition. If deposition only occurs on the upstroke then it is Z type, while deposition on the downstroke only is called X type. The type and amount of deposition can change during the process of building up multilayers. For example, the initial deposition might be Y type but in time the amount picked up on the upstroke falls until it becomes X type. It is possible to build hundreds of layers of some materials, though often the amount transferred will drop as the number of layers increase. A measure of the success of each transfer is given by the transfer ratio:

$$T = \frac{\text{decrease in monolayer area}^{1}}{\text{area of substrate dipped through the surface}^{2}}$$

(1 - allowing for monolayer decay)
(2 - allowing for meniscus effects)

so T=1 means full transfer and T=0 means no transfer.

This more precise definition follows Neumann and Swanson (1980).

3.2.2 Overturning

If one dips stearic acid at low pH Y type layers are obtained. But for salts at higher pH, there is a tendency for XY films to be produced (Hasmonay 1980). All X-ray tests have shown that for fatty acids the spacing of the layers in X type, Y type, and the more usual mixture of types give the same value for stearate layers (Stephens 1972). The layer arrangement is shown in fig 3.7.

The film surface is always hydrophobic, indicating that the last layer has tails outermost (Honig 1973). Thus if the sample builds with X, XY (or Z) deposition, there must be some form of overturning occurring.

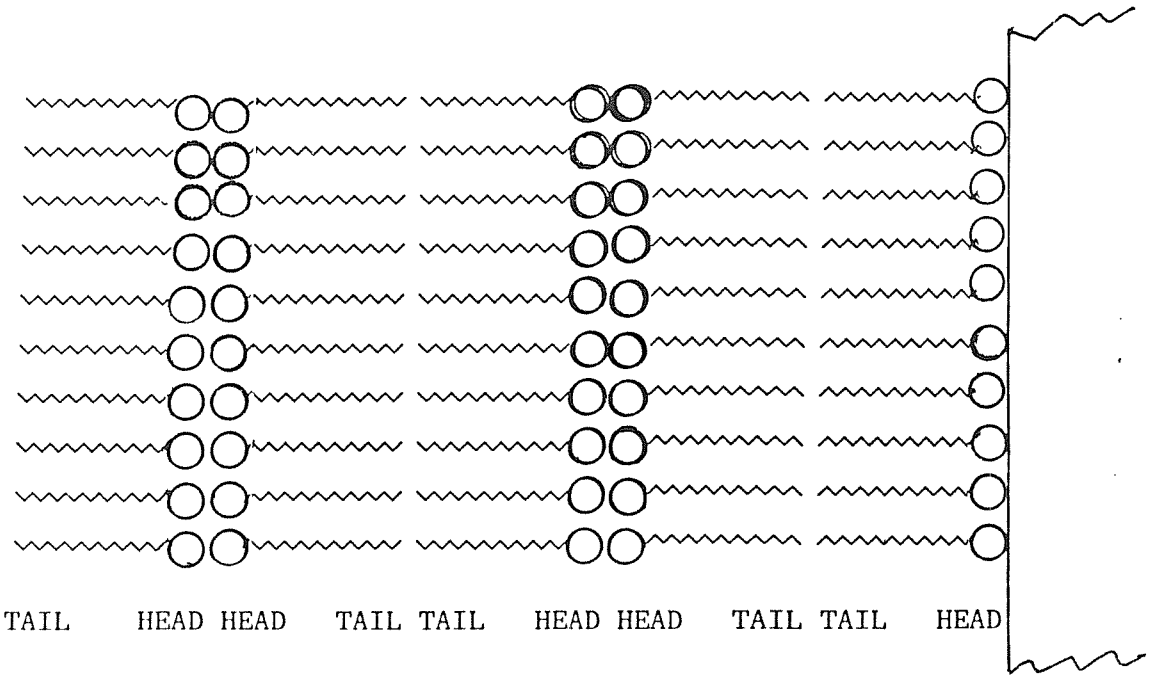

Fig 3.7 A LB Multilayer (on a hydrophilic substrate)

However no one has yet been able to show, convincingly, how or when this happens. More recently radioactive tracers have been introduced (Mizuno et al 1983). However we do not agree with the authors' interpretation of their results. We would like to suggest an alternative interpretation and so need to review some of the previous work.

Langmuir was the first to suggest the occurrence of overturning (1938) while Charles (1971) suggested that overturning occurred at the contact line as the dip occurred. Honig (1973) suggested that in X type deposition, after pick up on the downstroke, some of the chains detach themselves from the layer underwater, overturn and attach themselves to their neighbours. Hence instead of one extra monolayer half a discontinuous bilayer full of holes is formed. Then CH_3 groups are always outermost. If it was XY dipping then a smaller fraction overturn underwater. Later downstrokes could build a new layer and/or fill in some of the holes.

Neumann (1978) observed the contact angles during dipping using a cine-camera and reported that the contact angles support the idea of overturning to produce CH_3 groups, as the outermost layer. He also found that the results were independent of the time the sample was left underwater and thought that the overturning probably occurred quickly at the interface. This is contrary to the earlier report of Blodgett (1935) which indicated that X type films were more readily

formed if the substrate was kept underwater longer.

A further study was published later (Neumann & Swanson 1980) particularly concentrating on the upstroke, as this makes all the difference for X or Y deposition. They measured the contact angle, the transfer ratio and produced auto-radiographs of the films using Carbon 14. They noted that the contact angle was different on the substrate side closest to the barrier. They concluded that variations in dipping are heavily influenced by changes in the subphase monolayer and that during X type deposition interstices were formed during uplift which would be partially infilled on the downstroke; otherwise water would fill the gaps.

Hasmonay et al (1980) studied Y and XY films only, where XY means pick up in both directions but with a better transfer ratio on the downstroke. Hasmonay suggested that no overturning occurred; rather holes are formed which can be bridged by the downstroke. This meant that the final upstroke would leave some hydrophilic ends uncovered but no explanation was given for the fact that monolayer surfaces are consistently found to be hydrophobic. (Hasmonay did not observe X type multilayers so no explanation of them was given). It was also noted that the thickness of an XY multilayer varied at its two ends, one of which was where the meniscus overturning occurred. No dependence was found on the time the substrate spent underwater.

Pomerantz (1980) has shown that electron diffraction can be used to determine the number of layers. This might be used to determine which model is right. One would expect XY multilayers to have exactly the right number of layers according to Hasmonay. This might not be so for Honig as some of the material has to be used to fill in some of the holes.

Let us return to the more recent work of Mizuno et al (1983) who introduced a useful technique which nobody appears to have followed up yet. In their method a radioactive isotope of the usual cation was substituted in certain layers. (They experimented with Fe55 and stearic acid). Their dipping procedure was a form of "forced X type" using a modified trough and dipper which allowed the substrate to be withdrawn through pure water and not a monolayer. Their measurements indicate that cations can not occur at the outer surface in air. They suggest that the outer layer cations bond to the previous tails. We

believe most LB workers would reject this suggestion for stearate films as it contradicts X ray results. However it is possible that their results could be re-interpreted in terms of Honig's model. Because the forced X dipping was performed under conditions that normally produce Y type it indicates that overturning occurs quickly at the surface interface and not necessarily underwater.

Mizuno et al measured the distance from the radioactive cations to the surface by comparing the ratio of high energy to low energy electrons ejected by radioactive decay. In their fig 5 reproduced as fig 3.8, they show the various possibilities for the final layer. The ratio results indicate that the radioactive cations are one monolayer deep (their fig 5a) and two monolayers deep (their fig 5b) respectively. We suggest a different interpretation which is indicated in fig 3.9.

The first result gives one monolayer thickness between the surface and the radioactive cations. In the second suggestion parts of the two outermost layers are missing. Perhaps slow electrons ejected approximately perpendicular to the substrate could reach the detector through these holes giving a misleading ratio. The detector might then indicate a depth of two layers to the radioactive cations instead of the actual three. However as we do not know the form of their detector and its angular response, we were not able to make a quantitative assessment of our ideas.

3.2.3 Forced Z-Type Dipping

In order to avoid problems with partial pick up on the downstroke when good pick up is being maintained on the upstroke, it has been suggested that the deposition could be changed to a "forced Z type". This is done by having the monolayer decompressed during the down stroke. Then no pick up can occur. The monolayer is then re-compressed before the up stroke starts and good transfer can occur.

3.2.4 Transfer Ratio Correction

The important effect of meniscus changes on the apparent transfer ratio is best explained with an example. Consider an aluminium slide with one layer on it, about to descend into the water. The meniscus will be concave up, and let us say the contact line is 1 mm above the water surface (fig 3.10.1). (We will show only one side of the aluminium and the molecular orientation is also indicated - the

(a) & (b) suggest explanations for the actual results

● Fe 55 atoms

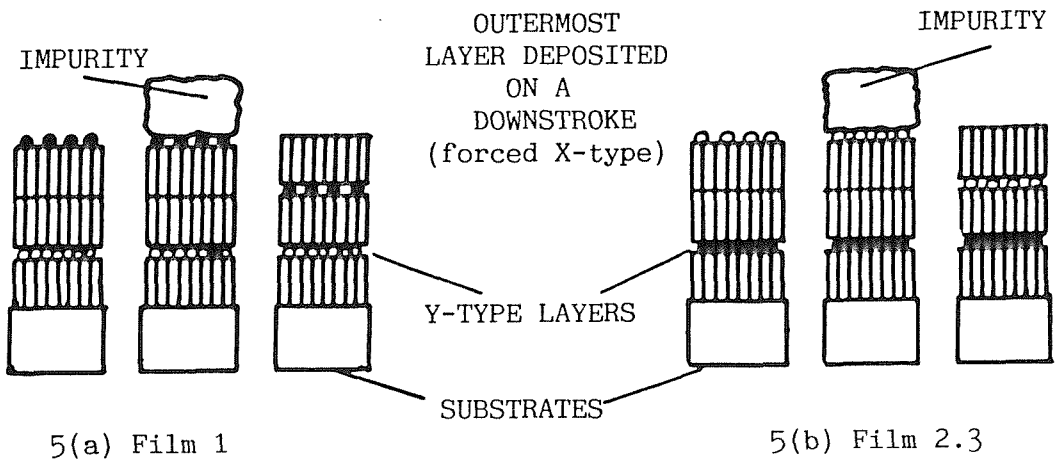

Fig 3.8 Possible Layer Arrangements (after fig 5 of Mizuno et al)

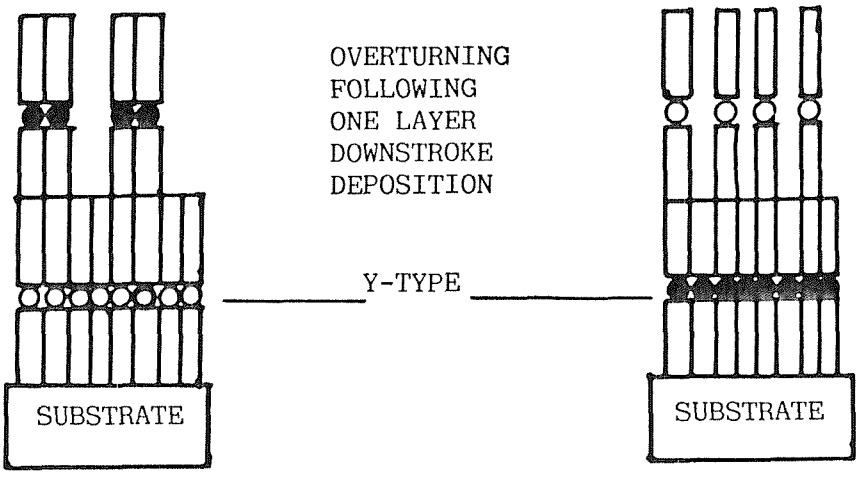

Fig 3.9 New Interpretation of Mizuno's Results

Figs 3.8 & 3.9 Radio-Tracers and Layer Overturning

circles represent the hydrophilic headgroups).

As the aluminium is pushed down, the meniscus turns over, but no transfer has occurred yet (fig 3.10.2). The letter M (meniscus) indicates the position of the meniscus contact line, on the substrate, and how the substrate has to travel 2 mm before pick up begins. (It is possible for the contact line position to move during the turn over. This would further complicate matters and would have to be allowed for in real life. For our example we assume an ideal situation). The substrate now travels another 8 mm to complete the 10 mm throw it was pre-set to (fig 3.10.3 S'→S). On the next upstroke a similar, but reversed sequence occurs. So we apparently would measure a transfer ratio of only 80%. It is better to define the transfer ratio allowing for these meniscus effects. This also means that if we wish to deposit layers of a specific length and between two specific points we must have some idea of what the meniscus will do and allow for it. This is important to us because we need to know the sample position within our magnetometer and its length. In our example above for a 20 mm long multilayer we would actually have to dip with a 22 mm traverse.

3.3 TEST SAMPLES

3.3.1 The Early Samples

The initial LB samples were prepared using coated glass and silicon substrates. Then some test LB films were produced on small pieces of aluminium foil. (Following this experience a set of large samples, which were actually measured in the cryostat, were produced). In fig 3.11 we show the Area/time (A/t) curve obtained from the first down and up strokes of a sample through a stearic acid monolayer.

The substrate was glass, aluminised on one side. The initial monolayer decay due to rearrangement was slowing down and as the sample was pushed down no pick up occurred (as expected). Then when the sample was pulled out good pick up occurred as the decrease in monolayer area was 93% of what we would expect for perfect coverage on both the glass and aluminised side.

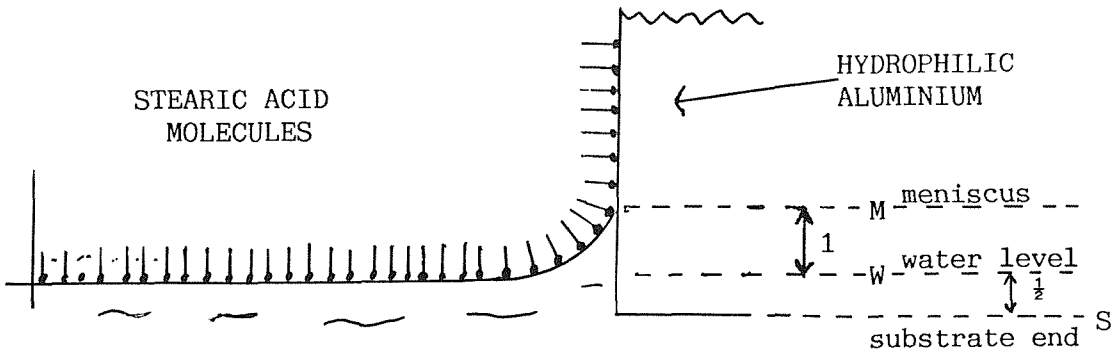

Fig 3.10.1 The Finish of the First Upstroke

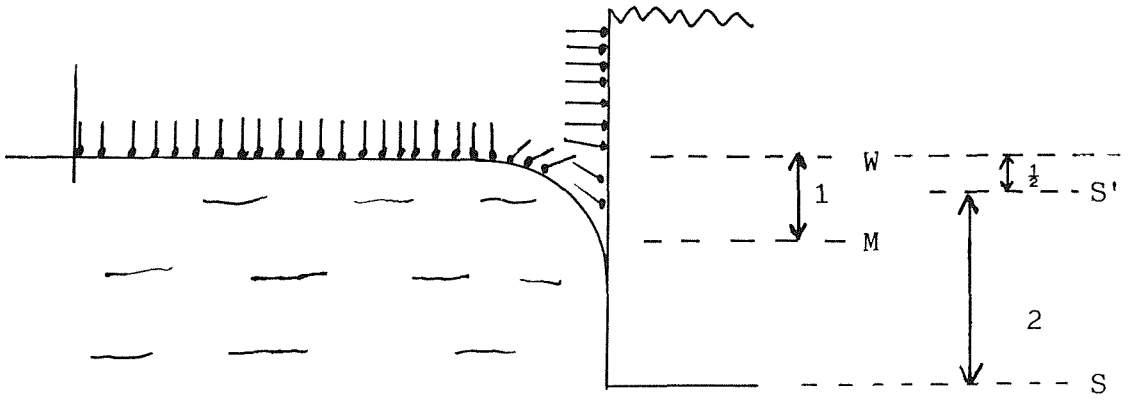

Fig 3.10.2 Meniscus Turnover at the Downstroke Start

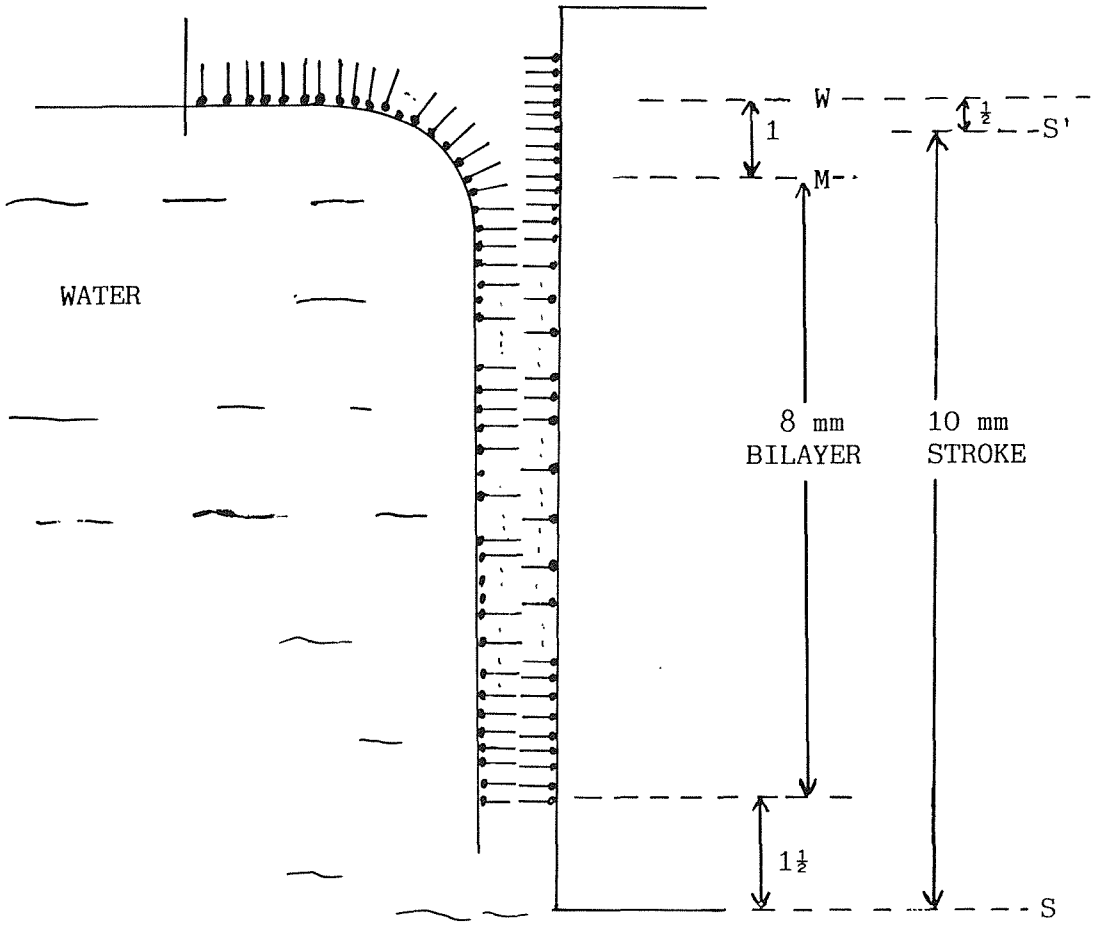

Fig 3.10.3 The End of the Downstroke

Fig 3.10 Meniscus Effects on the Dipped Area

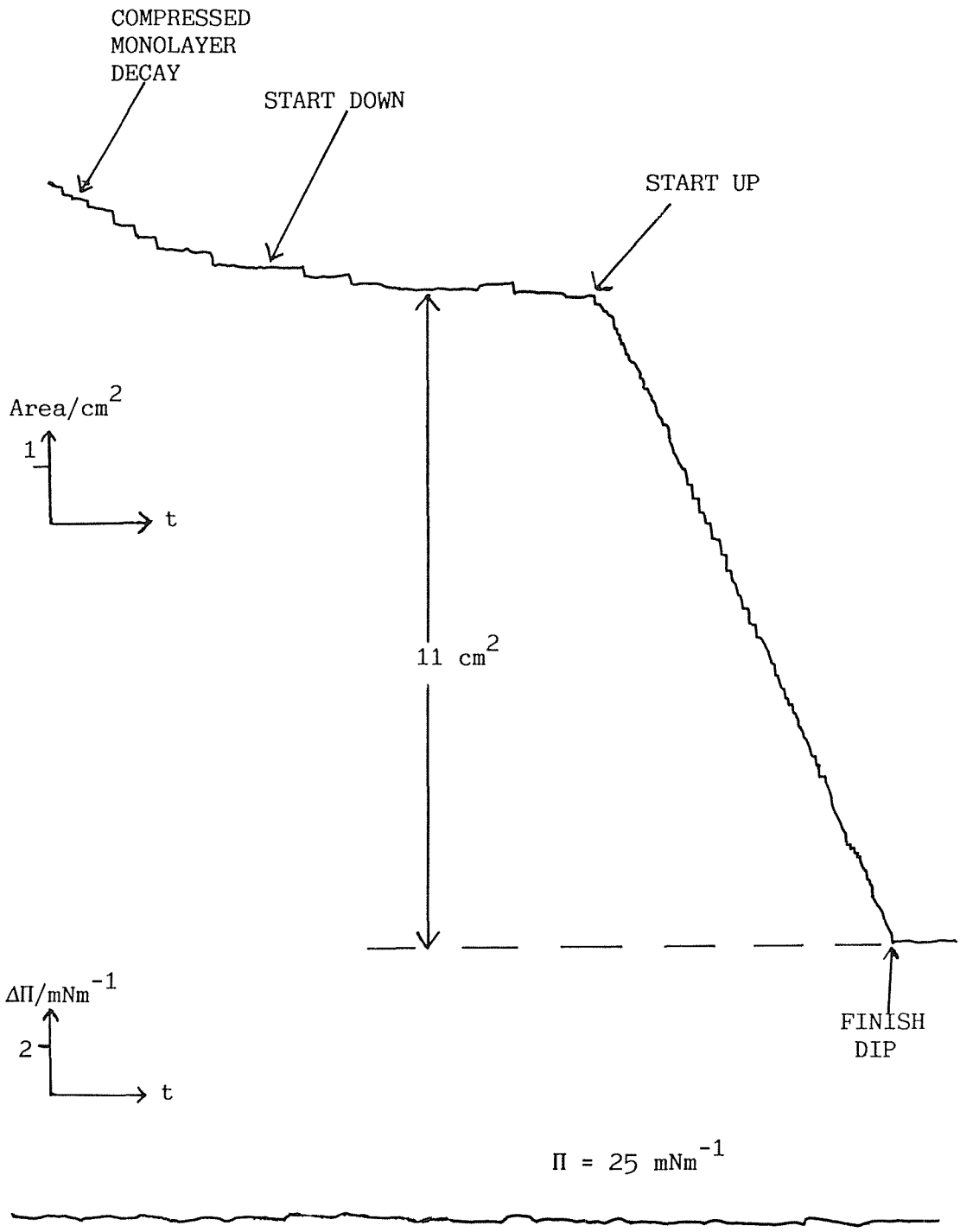

expected area for ideal pick-up = 12 cm^2

Substrate: aluminised glass

Fig 3.11 The First Dipping Strokes Through Stearic Acid

3.3.2 Dipping Meniscus Effects

The dipping of these initial multilayers allowed us to see some of the meniscus effects. As is commonly found, the first transfer had a larger transfer ratio than subsequent layers. This phenomena has been noted by others (Asaolu 1983 and Grunfeld 1983), and is usually attributed to monolayer decay or continued evaporation of solvent. However we suggest that this can only account, at most, for part of the effect. The beginning of the A/t trace shows how the monolayer decay is slowing, and an extrapolation of this will not account for the difference in area change between the first and subsequent dips. A possible explanation is as follows: During later downstrokes a hydrophobic surface (due to the hydrocarbon tails) will cause a greater depression of the meniscus than initially occurs with a hydrophilic aluminium surface. So it would be possible for a larger amount of monolayer to be picked up, because initially a larger length of slide passes the substrate/water contact line. Also the formation of a bigger meniscus as the upstroke began would lead to an apparent decrease in the monolayer area enclosed by the barriers. After the first upstroke each subsequent downstroke showed a meniscus effect at its start; see fig 3.12.

As the meniscus was pushed from concave up to down there was a sharp increase in trough area, followed by a sharp decrease. The exact shape of the A/t trace here was also a function of the feedback electronics which could not respond fast enough to keep the surface pressure constant. Sudden area changes did not occur on the transition from the down stroke to the upstroke and on this occasion the surface pressure did not deviate either. This may be because a hydrophobic meniscus tends to be smaller.

3.3.3 The Silicon Slides

In fig 3.13 we show an A/t trace for a silicon slide coated with a hydrophobic di-methyl di-chloro silane layer (silanised). Surprisingly it did not pick up any stearic acid on the initial, or later, downstrokes. Pick up occurred only on upstrokes i.e. Z type (our pH was 6.7). This was an unexpected result, though Daniel et al (1983) have also reported Z type deposition of amphiphilic material with cyano headgroups. Unlike the aluminium samples we did see a large meniscus effect at the beginning of the upstroke.

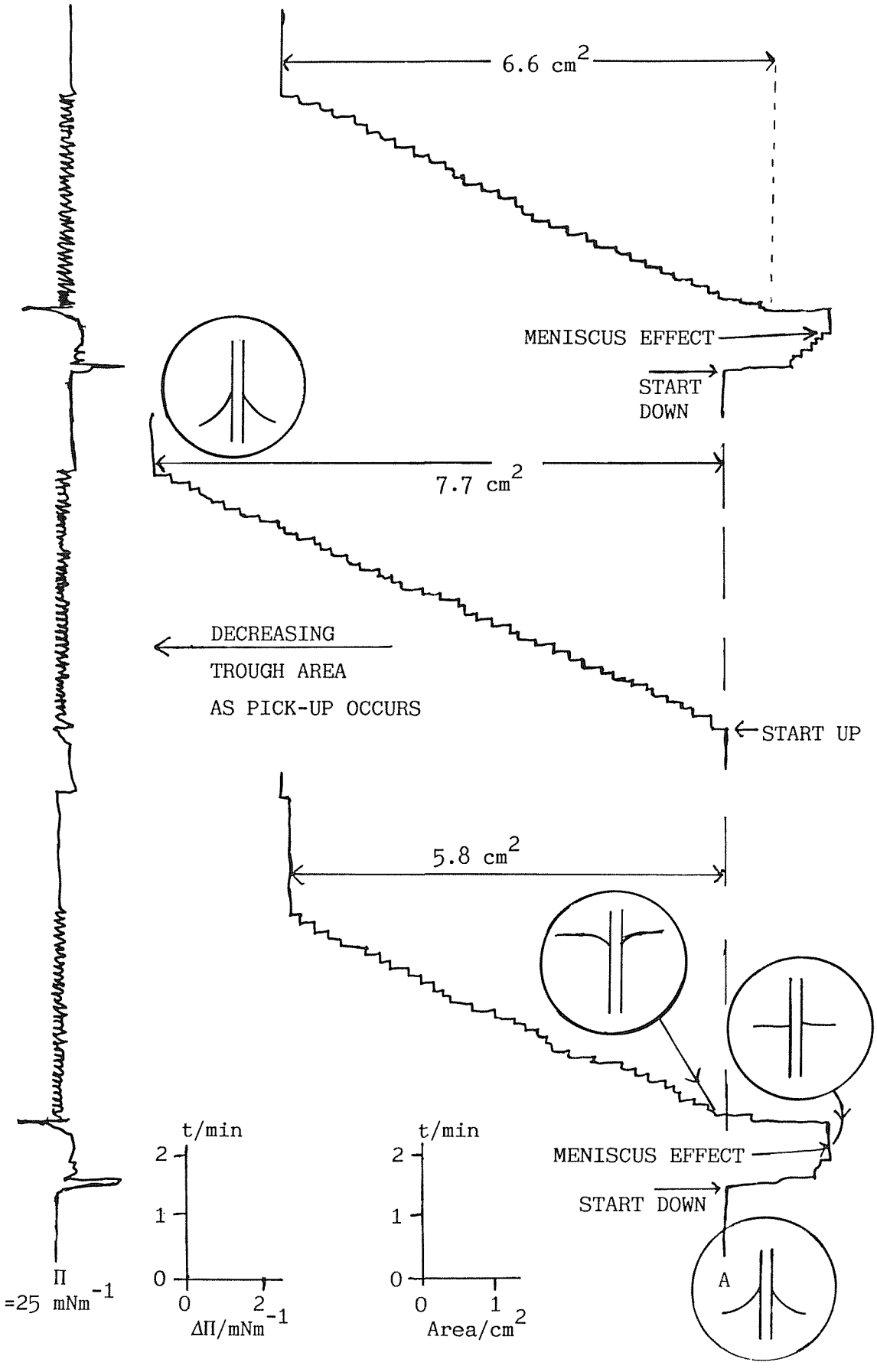

Fig 3.12 The Meniscus Effect

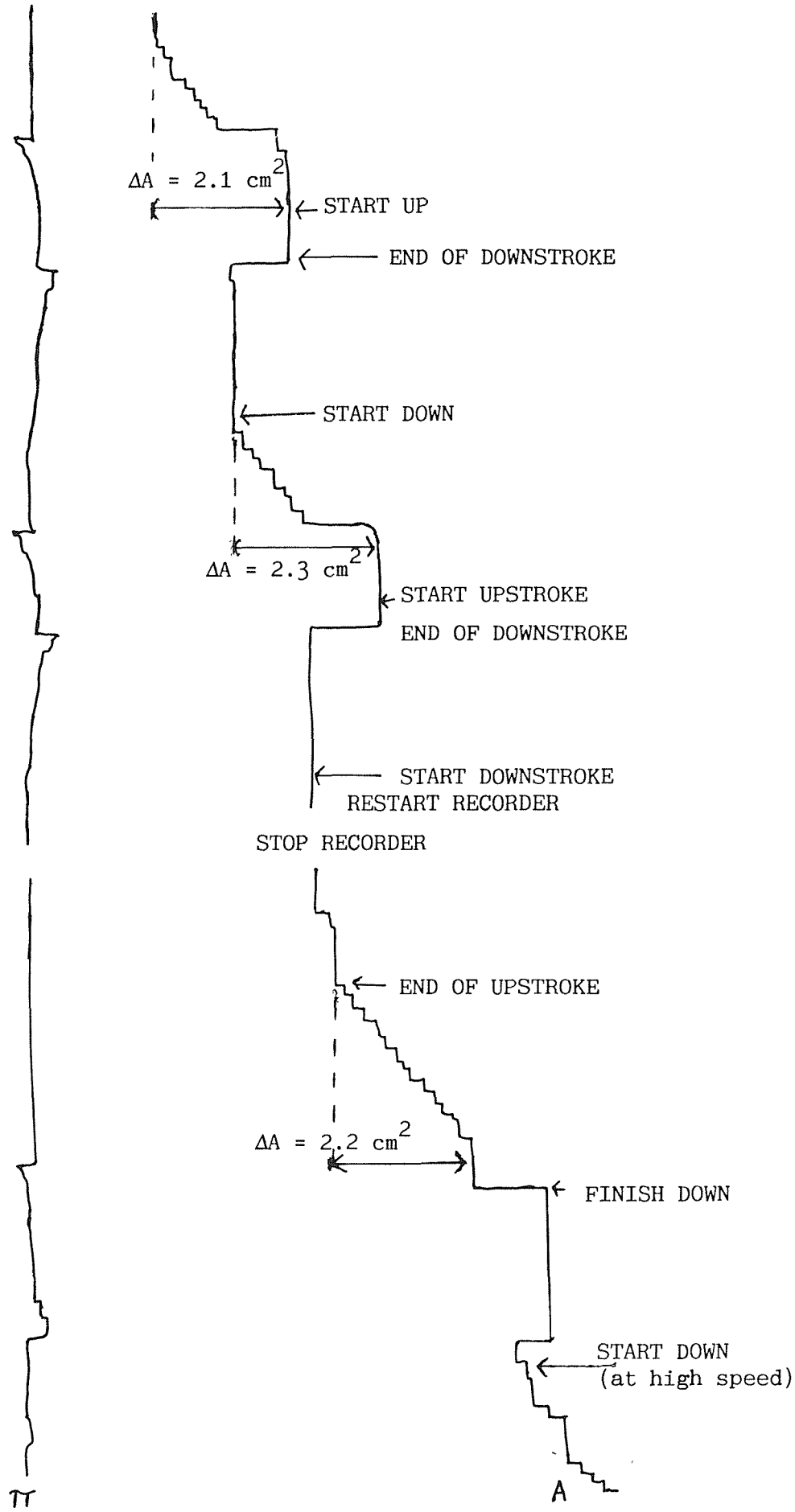

Fig 3.13 Z-Type Deposition - HSt on Silanised Silicon

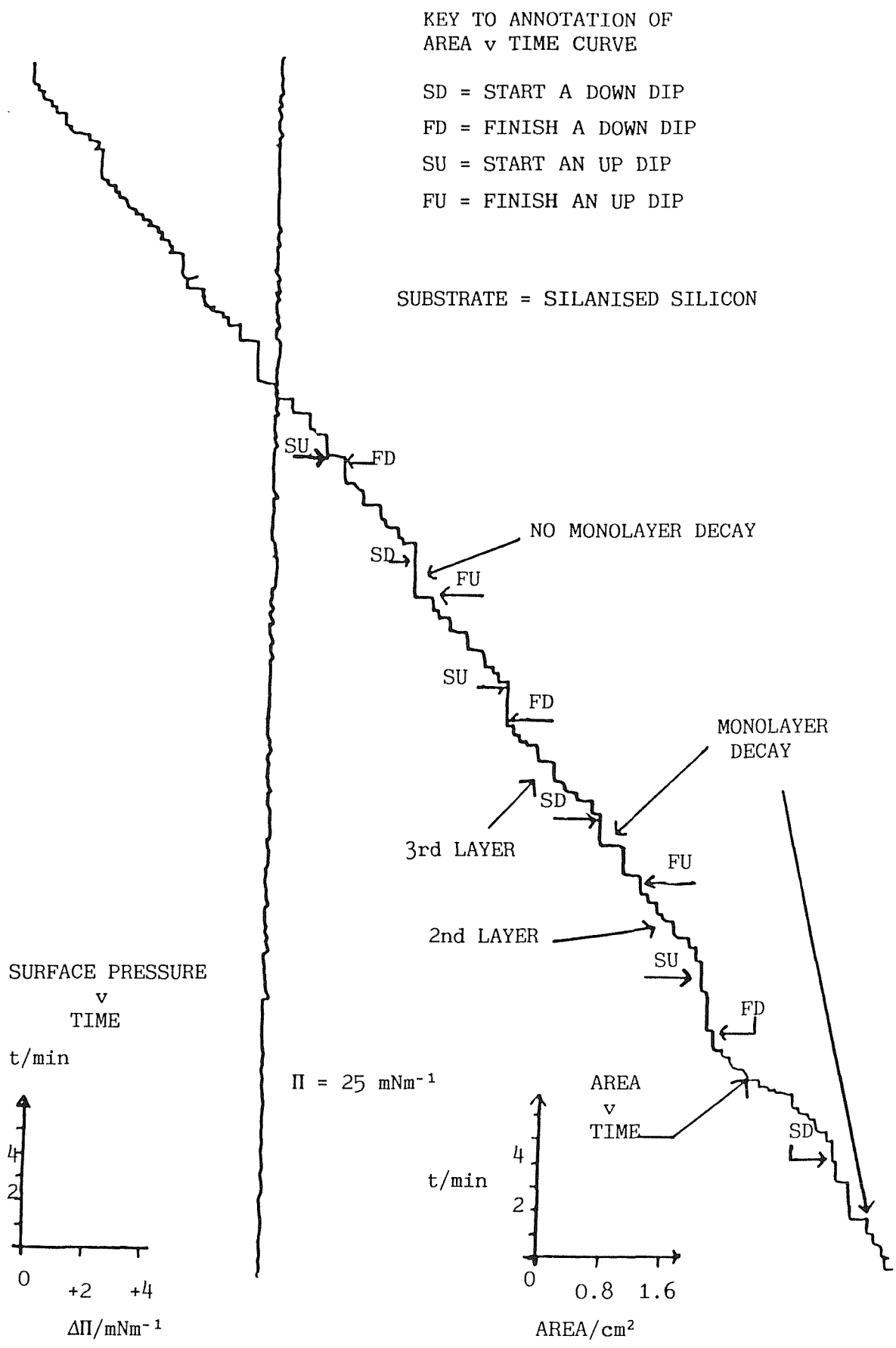

Fig 3.14 Dipping Record for a $MnSt_2$ Multilayer

Fig 3.14 shows the deposition of $MnSt_2$ on silanised silicon which is Y type (though deposition appears to be better on the upstroke). On this chart there is no noticeable effect from the meniscus. We have plotted a bar chart, fig 3.15, to show the dipped area per layer. This allows us to easily see any differences between upstroke and downstroke dipping, and any changes in the dipping type. It is also possible to use this data to plot a distribution of area transferred (strictly trough area changes); see fig 3.16.

3.4 THE MAGNETOMETER SAMPLES

3.4.1 The Trough and Substrate Clamp

The actual LB samples to be measured in the magnetometer were deposited on ordinary aluminium foil (Presto Supermarket). There was not enough time to make measurements using high purity foils. Some trial aluminium pieces were dipped but the meniscus effects associated with the teflon defeated any attempt at estimating the transfer onto the aluminium. So for the real samples the part of the foil to be dipped was arranged to hang below the bottom of the teflon legs. Because these foils had previously been cleaned and rolled, they did not present a flat surface as a glass or silicon slide might; rather they were "bumpy" and creased.

The magnetometer detector required the substrate to extend for some distance in both directions away from the sample position. (So as to provide a continuous background signal - see below in sec. 5.1). This meant a long sample so that there was no room in the trough for the heat exchanger even when brimful. The samples were dipped at the ambient temperature. Fortunately (!) this was $15\pm1^{o}C$, excepting for the 101 layer sample at $13.5^{o}C$, as the samples were formed between 31.12.85. and 8.1.86. when there was no heating in the building.

All the samples were dipped between pH 6.6 and 6.8 except the first $CdSt_2$ layer of sample 5 at pH 6.95. Pomerantz (1978) initially suggested that the pH should be maintained between 6.5 and 6.8 while later he gave a value of pH 7 (1984). This was to ensure conversion of stearic acid to manganese stearate.

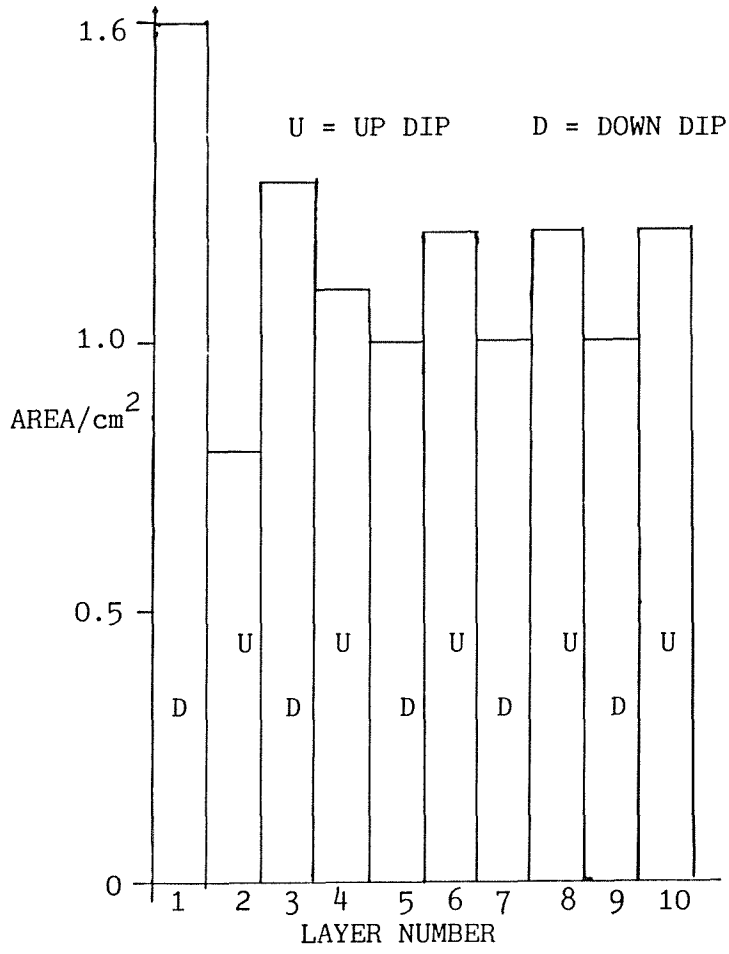

Fig 3.15 Area dipped against layer number

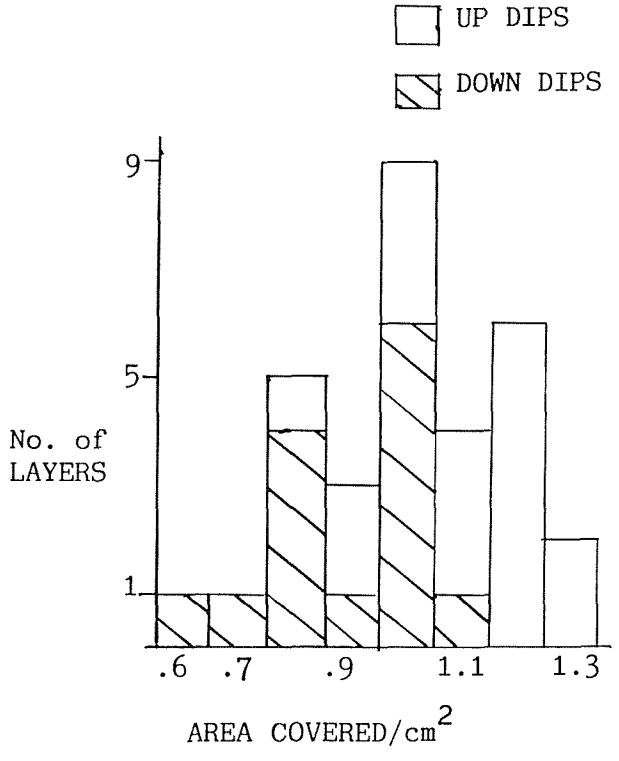

Fig 3.16 Distribution of Dipped Areas

Figs 3.15 & 3.16 Dipped Areas

3.4.2 Large Single Test Foil

This foil dip was started from the down position and as previously noted, for aluminised glass surfaces, there was a much larger reduction in trough area during the first upstroke. We only saw a meniscus effect at the beginning of the downstroke. At the start of the upstroke we noted that the meniscus actually did appear flat in the trough, and that it developed concave up after the upstroke began. So there was no need for a flipover. At the end of the first upstroke monolayer decay was seen to be small; for a time interval after the dip, equal to the time taken to dip the monolayer, the decay area was about 1% of the dipped area. So this will not explain the larger transfer ratio. Further evidence comes from sample two (see below at 3.4.5) which was produced by forced Z dipping. Then we obtained consistently large transfers, similar to the first layer, for all the layers.

3.4.3 Multilayer Appearance

With a multilayer LB film it was possible to see the deposited film. We could see that the top edge was smooth and straight - like the water surface, but the bottom, i.e. the part associated with meniscus flipover, was very ragged. It may be that after the first layer the bottom got damaged such that further layers had difficulty depositing there. Perhaps part of the meniscus effect at the beginning of the downstroke was loss of monolayer from the substrate back onto the subphase. The $MnSt_2$ multilayers had a pinkish tinge.

3.4.4 Meniscus Effect

It is difficult to work out where transfer starts so the total amount transferred for one down and up stroke (or one bilayer) can be much more accurately obtained from the dip curves. That is, we assume that the meniscus will be in the same position, at the same point, in the dipping cycle. (Our observations indicate that this was so for our foil samples. Observe the trace in fig 3.17).

If we take the apparent area change from both the downstroke and the upstroke separately and add them together they produce an area which is too big. Observing the curves individually there are several places where this overcounting can occur:

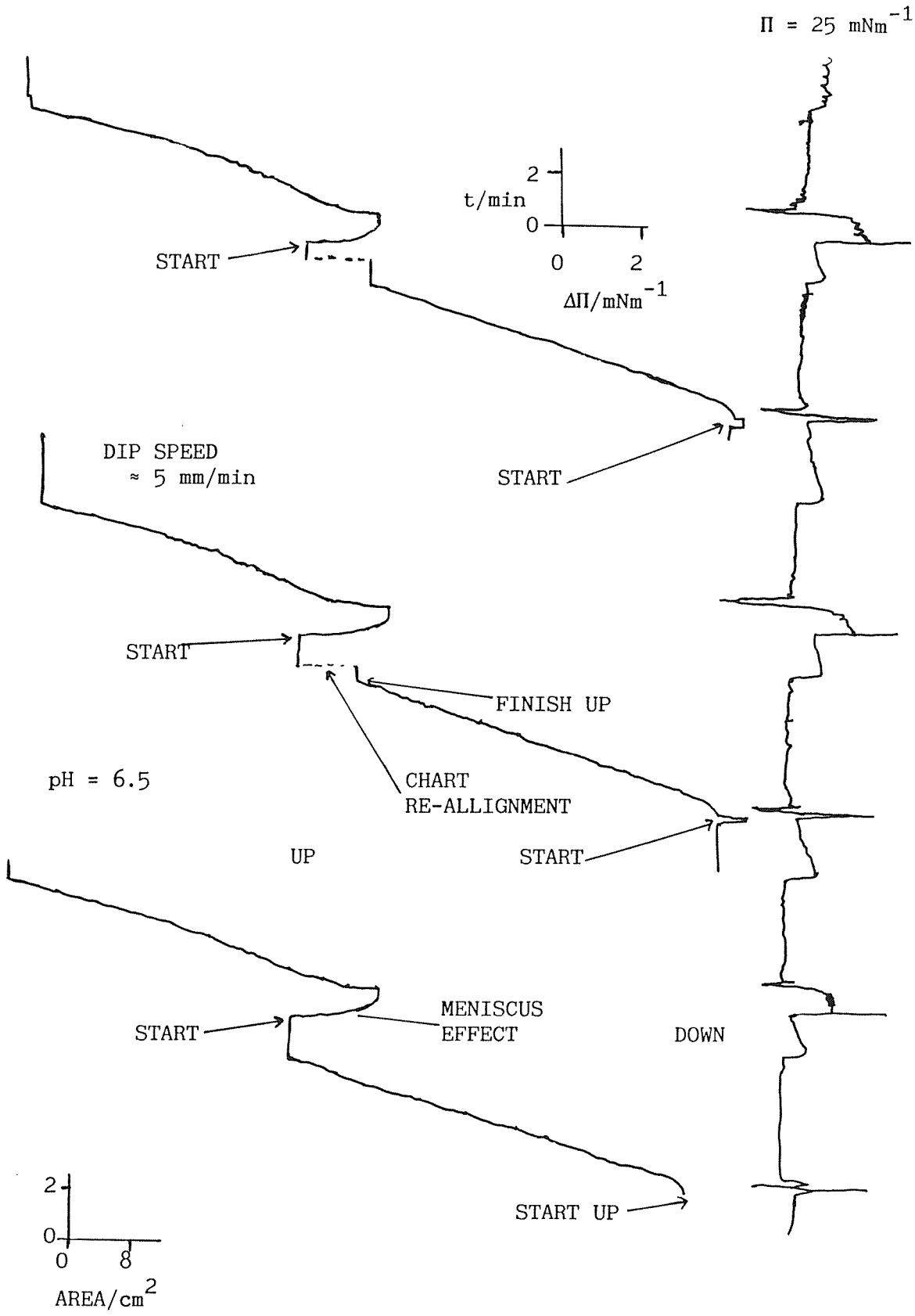

Fig 3.17 A/t & Π/t Traces Showing Stroke Similarity

i) At the beginning of the upstroke there is a meniscus effect as it lifts from horizontal to concave up.
ii) At the beginning of the downstroke it is possible that there could be some unpeeling of the monolayer, and again there is the meniscus effect.

Although the upstroke apparently produces a larger transfer it is possible that there is a large meniscus effect included in this - the magnitude of which is indicated by some of the initial area increase at the beginning of the foil downstroke. The transfer might start as soon as the meniscus is pushed flat. It might not become concave down. (This would also explain why the meniscus develops so "easily" at the start of the upstroke). However as we dont really know what is happening we can not produce accurate transfer ratio charts.

3.4.5 The Samples

Five LB samples were made and four used for measurement in the magnetometer. Sample 1 was built of 101 layers of $MnSt_2$ at pH 6.65 and a trough temperature of approximately $13.5^{o}C$. The solution of stearic acid in chloroform had a concentration of 5.2 mg/ml, and it was dipped at 25 mN/m. The dipping produced an Area/time trace similar to the previous aluminium test samples. The dipper's throw was set at 25 mm because of the large meniscus effects when using aluminium. The upstroke traces showed no meniscus overturning effects, and the first upstroke reduced the trough area by an amount greater than any following dip; see fig 3.18.

The trough had to be re-spread after the first three strokes. Then a further eight layers were added so that the sample finished in the up position. (Eight is the maximum number of layers which can be produced before the barriers will collide with the wide sample foil). The sample was then removed (for the night) and the trough surface cleaned. Interestingly no meniscus effect was noted for the first downstroke the following day! Also, the decrease in trough area appeared larger than for a usual downstroke. It was equal to the full initial amplitude including any meniscus effect; see fig 3.19.

After this initial difference all the following strokes occurred normally, except that by the time of the 75th layer, the excursions in surface pressure had become large. (These layers were being dipped fast). What looked like three dimensional inclusions were seen on the

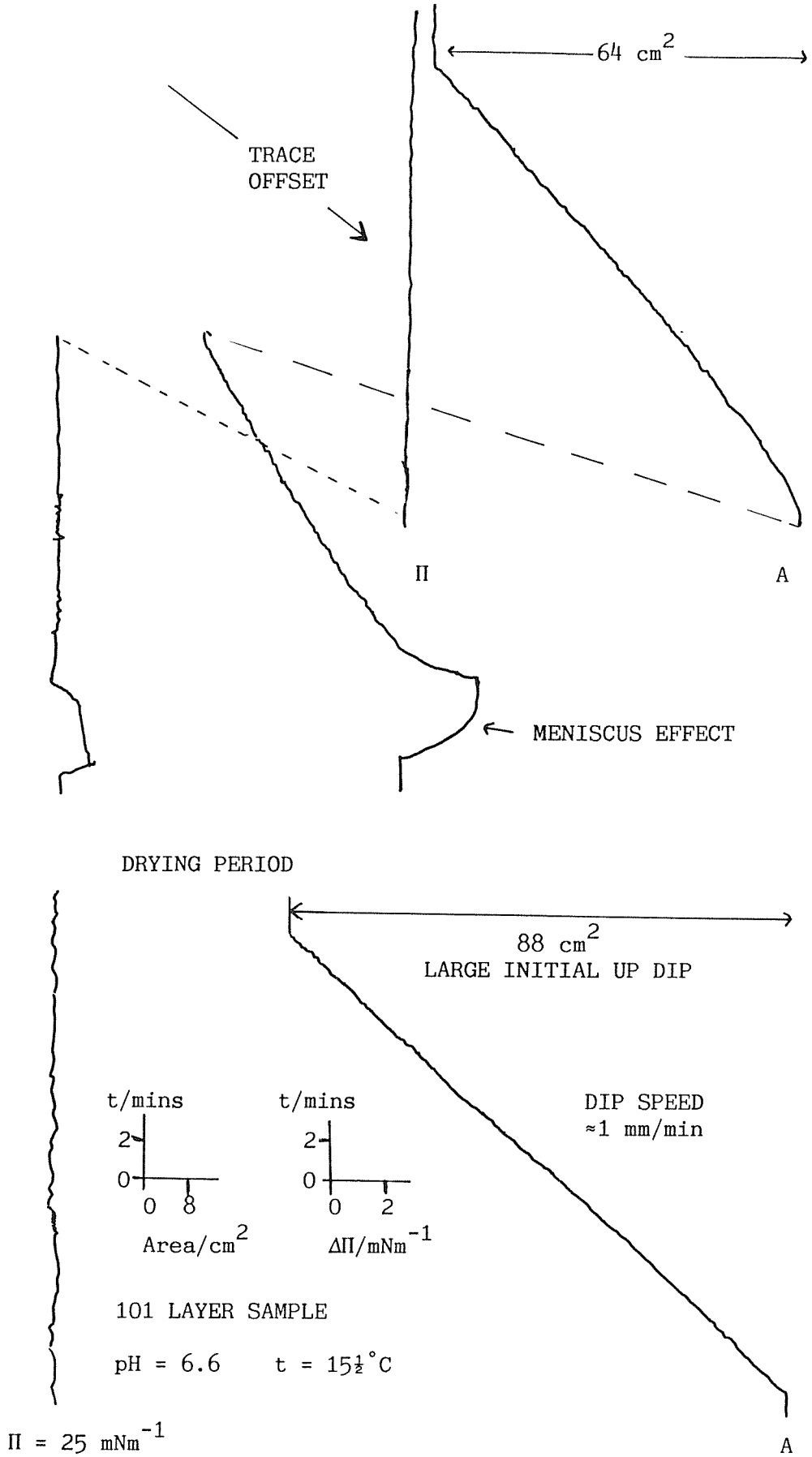

Fig 3.18 101 Layer Sample - Dip Start

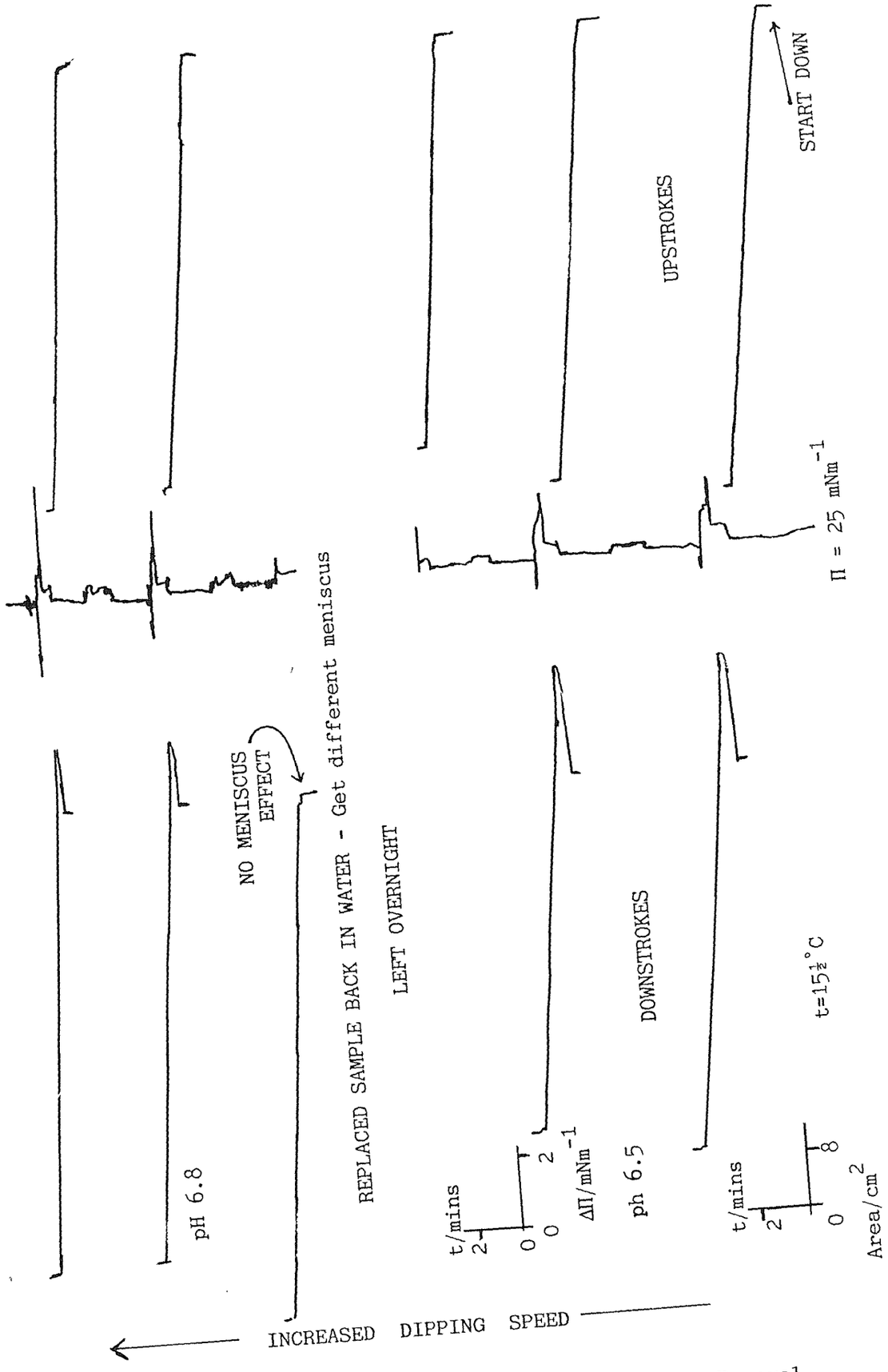

Fig 3.19 Loss of Meniscus Following Slide Removal

film. So the sample was removed, and the trough re-cleaned. The surface pressure during the monolayer transfer improved after this, and the "three dimensional inclusions" also "disappeared". We suspect that some of these problems occurred due to "overloading" the surface at each respreading, in order to get as many dips from each spreading as possible. On removal from the trough a 21 mm wide LB sample could be seen. There were also some "water marks" about 0.5 mm from each edge. (A similar "water mark" was seen 18 mm away, where the bottom of the lifted up foil had been left dangling in water overnight).

Our second sample was eleven layers thick and built by forced Z type deposition. The area changes were all similar to the first stroke, even though the last few were produced with a dipping speed ten times that used on the first layer, which was about 1 mm/min. Forced Z dipping avoided meniscus flip over and the associated large fluctuations in surface pressure (which the feedback system could not properly cope with); see fig 3.20.

Our third sample was a single $MnSt_2$ monolayer formed by one upstroke through the monolayer. This was a "Type 1" sample using Pomerantz (1980) notation.

Sample four was formed from one monolayer of non-magnetic $CdSt_2$ but was not measured as such. The $CdSt_2$ monolayer, on the trough, did not seem to be as stable as $MnSt_2$ monolayers.

Sample 5 was formed from one layer of $CdSt_2$ and a bilayer of $MnSt_2$ using forced Z dipping. This should form a "Type II" sample. The Area/time curves were as expected and the dip was adjusted to give a 22 mm high sample.

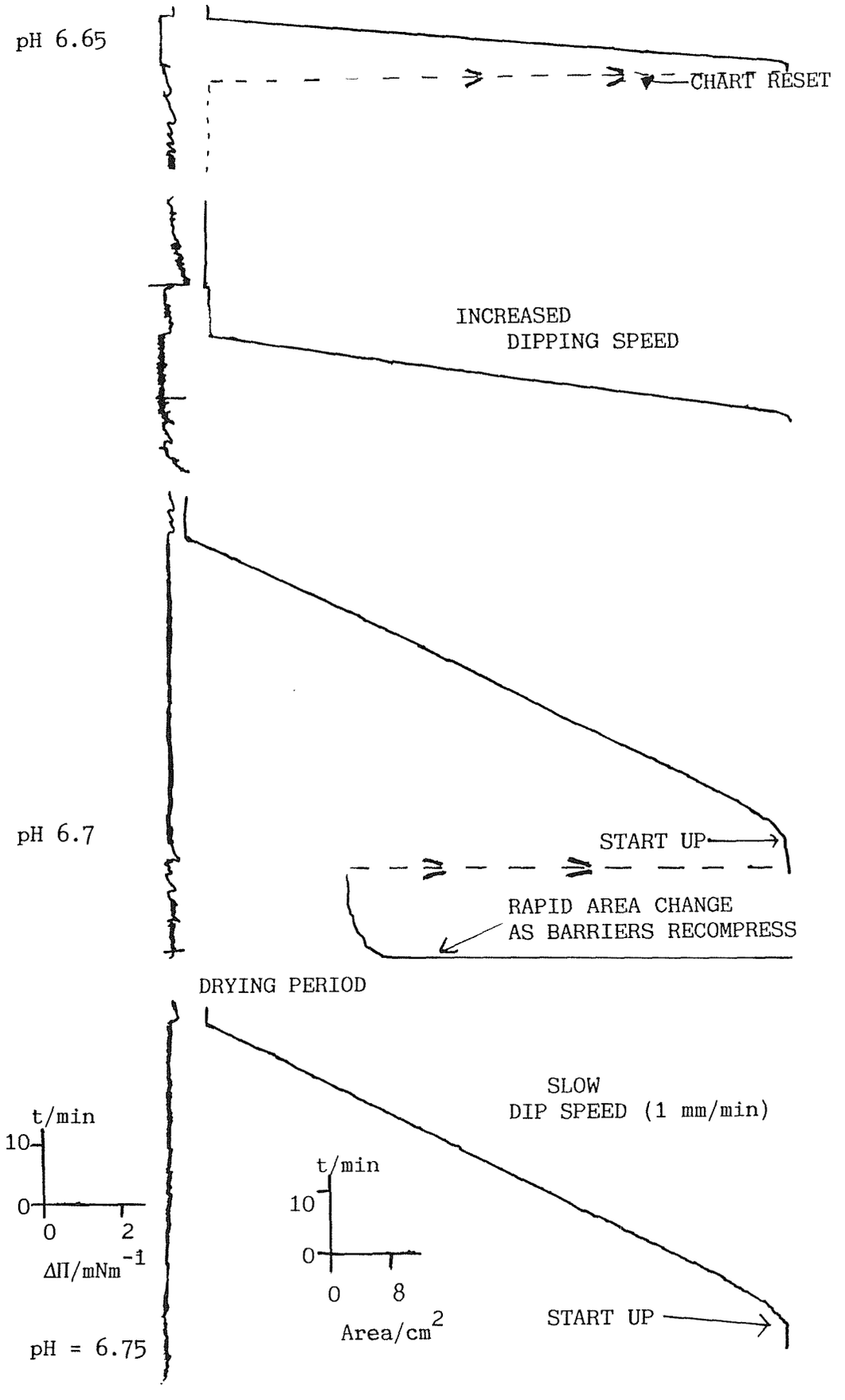

Fig 3.20 Forced Z-Dipping

CHAPTER FOUR - THE He3 CRYOSTAT

4.1 THE MAGNETOMETER

4.1.1 Introduction

Previous work (Pomerantz 1980) has indicated ordering temperatures below 4 K for LB samples of $MnSt_2$ and to obtain these temperatures a He4/He3 cryostat was required. It also provided the 4 K environment necessary to operate the SQUID detector, which was capable of sensing the very small signals produced by LB films. The mechanical details of the cryostat built by Oxford Instruments (O.I.) are given by Asaolu (1983) though since then several modifications have been made to it. After giving a brief outline of the cryogenics and some other SQUID magnetometers we will describe the cryostat system (see fig 4.1) and the modifications that were made to it. We will also mention several experiments which were carried out to characterise and calibrate various aspects of the cryostat's performance.

4.1.2 Cryogenics

Liquid helium provided a temperature of 4.2 K within the cryostat; the helium being shielded from room temperature by a vacuum jacket and liquid nitrogen radiation shields. The principles behind cryostat construction are given by, amongst others, White (1979). To obtain temperatures lower than 4.2 K the vapour above liquid He4 and liquid He3, contained in enclosed "pots", is pumped away, removing heat as the boiling point is lowered by the pressure reduction. Information on working at temperatures below 1 K may be found in the book by Lounasmaa (1974).

In order to detect the sample signal it was weakly magnetised by a superconducting magnet while being moved into a concentric pick up-coil which was connected to a SQUID (Superconducting QUantum Interference Device). Magnetometers based on this idea have become more common in recent years, making use of the superconducting properties that are available in several metals at liquid helium temperatures. As far as we know the Southampton SQUID magnetometer is the only one where the sample can be moved in and out of the detector while also being cooled below 1 K.

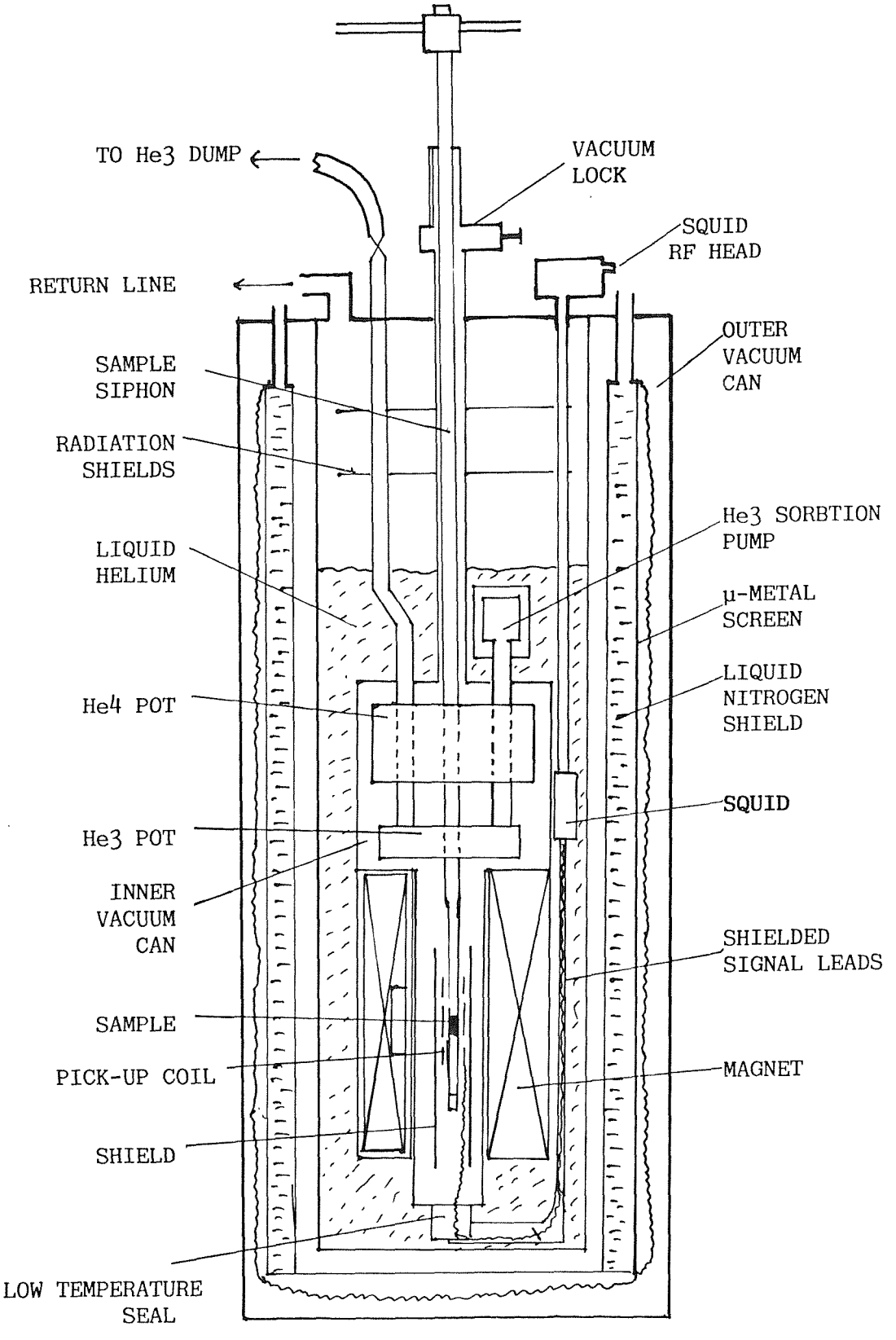

Fig 4.1 He3/SQUID CRYOSTAT

4.1.3 Magnetometers

During the 1970s magnetometers using SQUID detectors were increasingly reported in the literature. Cukauskas et al (1974) described an early superconducting magnetometer. It had all the main ingredients still used today: The sample was moved through a superconducting detection coil placed inside a superconducting screen which trapped and stabilised the field produced by a superconducting magnet. The sample could be measured over a temperature range of 1 K to 300 K. A review of this and earlier SQUID magnetometers has been given by Deaver et al (1978). Many subsequent SQUID magnetometers have been designed to operate over the same 1 K to 300 K temperature range. However Doran and Symko (1974) built a magnetometer operating between 2 K and 10 mK with the sample placed in the mixing chamber of a dilution fridge. This meant that the sample could not be moved, and the detection coils were also cooled down with the sample. Because of their sensitivity SQUID magnetometers have been used to measure the very weak signals from biological or chemical samples. These are often magnetically dilute and frequently only small quantities are available because they are expensive to produce or are inherently small such as the case of thin films; see Cerdonio et al (1976), Nave and Huray (1980) and Beauvillain et al (1985). Commercial magnetometers have also been produced, often designed as general purpose instruments - see Deaver (1978). All these magnetometers have had to overcome problems of:

i) Temperature dependent background signals e.g. Doran & Symko (1974) had problems with an epoxy resin.

ii) Mechanical vibration e.g. Hitzfeld et al (1984), Beauvillain et al (1985) or Pelizonne & Treyvaud (1981) where, at high magnetic fields, shouting at the cryostat was detectable.

iii) Eddy currents e.g. Philo and Fairbank (1977)

iv) External electromagnetic noise e.g. Gramm et al (1976) had three layers of mu-metal shielding in his cryostat, one of which was kept at 77 K.

Over the years sensitivity has been increased. The magnetometer described by Cukauskas et al (1974) had a magnetic moment sensitivity of 10^{-11} Am^2 while Gramm et al (1976) quoted $2x10^{-12}$ Am^2. These magnetometers usually work in a low applied field needed for the accurate detection of magnetic phase transitions e.g. 10 mT (Gramm et al 1976) or very low e.g. 0.01 mT (Ishizuka & Tohi 1980). On the other

hand Pelizonne & Treyvaud (1981) has built a system which will operate up to 8.5 T.

4.1.4 Description of Southampton Magnetometer

The cryostat had a main bath capacity of 20 litres of liquid helium. The inner vacuum can (IVC) with its sample tail was suspended within this bath while a high homogeneity (0 to 2 T) superconducting magnet surrounded the sample tail; see fig 4.1.

To provide cooling below 4.2 K there were He4 and He3 pots within the IVC. The He4 pot was filled via needle valves from the main bath and pumped by an external rotary pump. He3 gas was admitted from its room temperature dump through the He4 pot. The He3 could then condense in its pot to be pumped by an internal sorbtion cryopump situated just above the IVC. This would cool the He3 pot below 0.4 K. The He3 pot was attached to the movable 0.3 K platform, to which the sample was linked via several thick copper braids, which acted as heat links. Because of the sensitivity of SQUID systems to vibration, the cryostat was suspended from an anti-vibration platform. The cryostat was held at the top plate by a supporting framework which rested at its ends on two legs which were half sunk inside sand filled concrete tubes. Each leg was "de-coupled" from the framework by a thick layer of fan-folded computer paper. The paper and the sand isolated the system from both "horizontal" and "vertical" vibrations; see fig 4.2.

4.1.5 Vacuum

The cryostat contained several vacuum chambers. For high vacuum a 3" manifold connected four 1" lines from the cryostat system to the vacuum pumpset. The manifold could also be connected to a mass spectrometer, capable of detecting both He3 and He4, with an uncalibrated leak valve to check and tune it. The vacuum pumps consisted of an Edwards ES 200 1/min rotary pump for roughing and a large diffusion pump backed continuously by an Edwards 2S20B with a 2 litre backing space. The diffusion pump had a Peltier cooler suitable for long unattended pumping times. The cryostat was often pumped overnight, with liquid helium present so it was necessary to protect against power failures. One inch magnetic isolation/air admittance valves were fitted on the roughing and backing line to overcome this. On power failure they closed securing the vacuum.

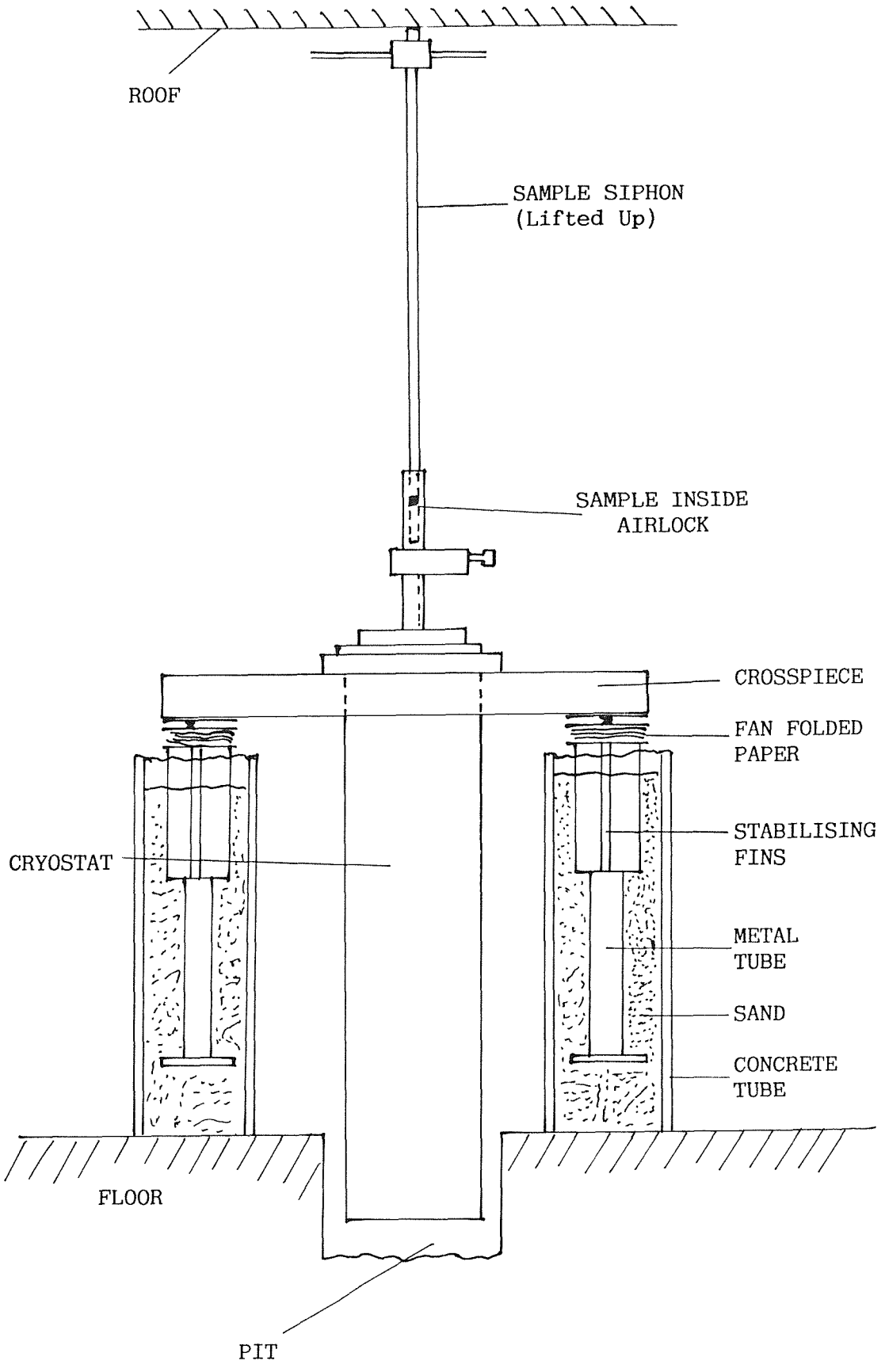

Fig 4.2 Cryostat Suspension System

The rotary pump used on the He^4 pot was an Edwards ISC 900 l/min pump. It pumped through a 1½" line and was connected to the pot via a NW40KF gate valve with a globe valve in parallel. The latter could be used at the beginning of the pump down when gas pressure was high, while the gate valve was opened later to give a greatly improved conductance at lower pressures. Diagrams of the vacuum pumpset and the pumped helium system are given in fig 4.3 and fig 4.4 respectively.

4.1.6 Sorbtion Pump

The He^3 was pumped by an internal charcoal sorbtion pump. This was situated above the IVC in the main bath space, but isolated from it by a vacuum space contained by the Sorb Vacuum Can (SVC). A vacuum tight copper container within the SVC was filled with the charcoal and thermometers and a heater were also attached to it. When heated to >40 K it did not act as a pump. However if a small amount of exchange gas was allowed into the SVC, it could be cooled down to the main bath temperature. The charcoal then adsorbed the He^3 vapour, so "pumping" the liquid in the pot. At the end of the experiments, when the cryostat was above 20 K, an external cryopump was used to suck all the He^3 out of the system. Then with the cryostat closed off, the gas was returned to the He^3 dump cylinder by warming the cryopump. The exact procedure was written into the O.I. manual. As the He^3 was removed from the cryostat when it was cold, any air impurities would be frozen out, and these could be pumped away using the high vacuum pumpset when the pot reached room temperature.

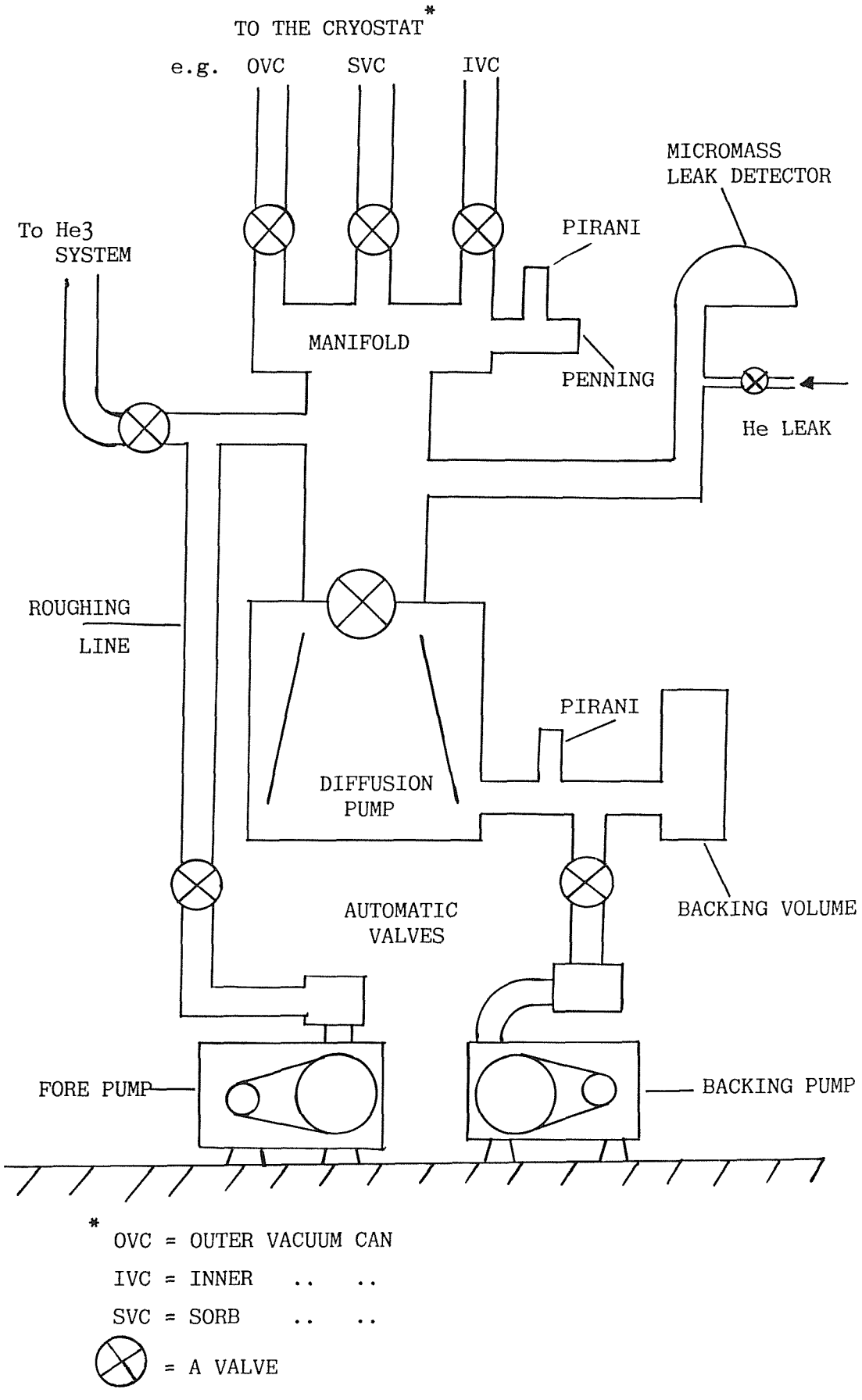

Fig 4.3 The Vacuum Pump System

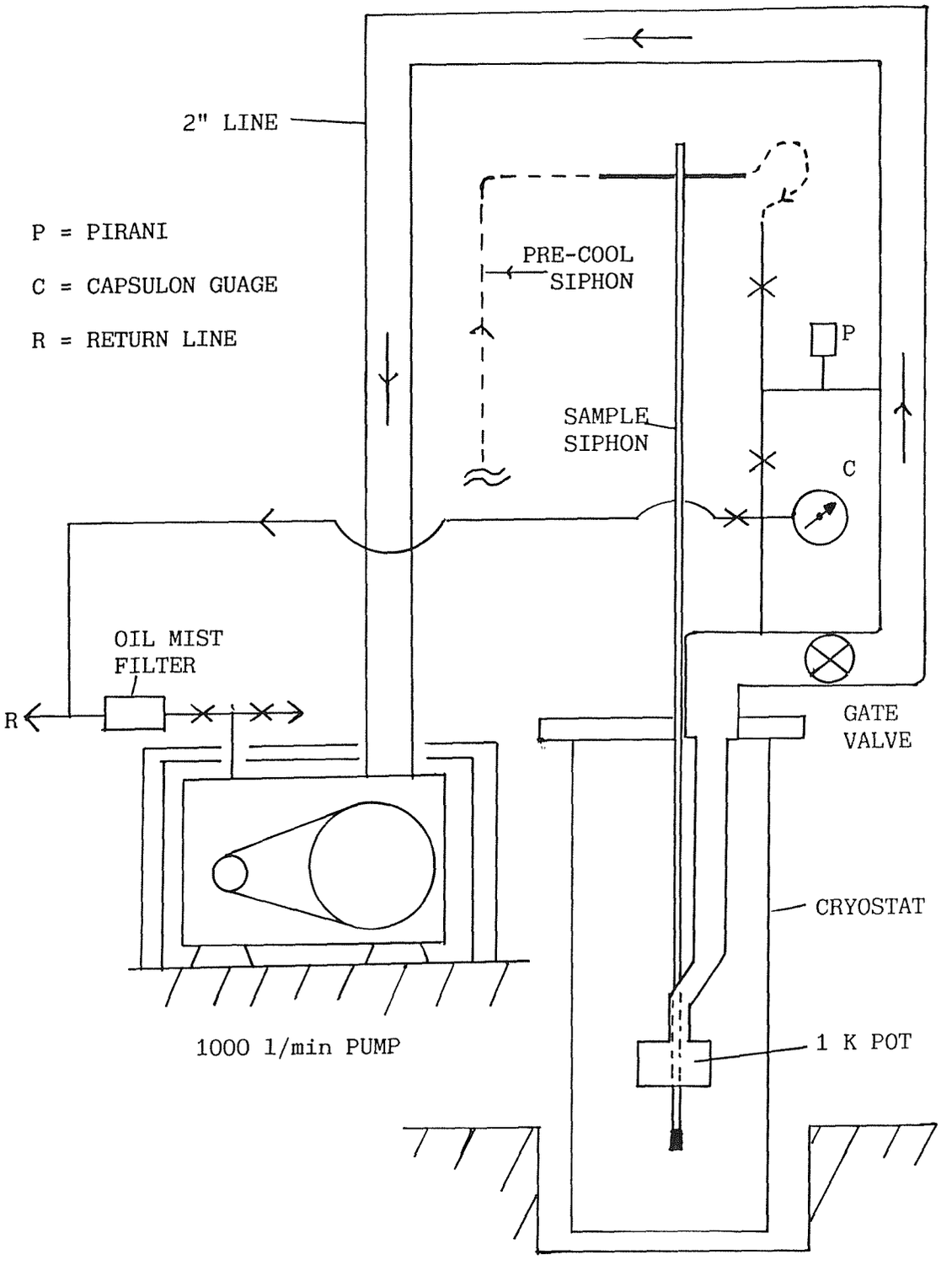

Fig 4.4 The Helium Gas Handling System

4.2 THE COOLDOWN

4.2.1 Nitrogen Cooldown

Prior to a cooldown all the vacuum spaces including the He3 pot would be pumped to remove any air that might have entered the system. The full details of a cooldown with leak testing is given in the O.I. manual. However in the latter half of this project, since the cryostat had been successfully cycled between helium and room temperature, the leak tests were omitted. Then we could use helium exchange gas in the IVC and SVC for pre-cooling from room temperature to 77 K. This decreased the time taken for the centre of the IVC to cool to 77 K compared with using nitrogen exchange gas. About 50 litres of liquid nitrogen were required to pre-cool the cryostat from 295 K to 77 K. If pumped in slowly then some of the cooling power of the gas was used and the first 25 litres would cool and cover part of the magnet. The cryostat must still be filled to the top to obtain proper pre-cooling. On occasions when it was not filled above the SVC, the following helium cooldown required more time and helium. Before the helium can be transferred the nitrogen liquid and gas must be removed. This can be done:

EITHER by blowing out with compressed nitrogen gas and then vacuum pumping immediately afterwards as described in the O.I. manual, usually with the nitrogen shields cold but empty of liquid;

OR the nitrogen can be blown out of the main bath in the evening, the nitrogen shields filled, and the main bath left empty overnight with a bunsen valve attached to the outlet port. Heat leaks mean any liquid left will evaporate overnight and the gas can be pumped out the next morning. After pumping, the main bath can be vented with helium gas.

4.2.2 Helium Cooldown

Helium is transferred via a "siphon" which should be pumped regularly to maintain a good vacuum. Cold helium gas from just above the liquid in the transport dewar was gently blown into the bottom of the cryostat so that the gas had enough time to absorb as much heat as possible. It is important to pass this cold gas from the bottom to the top of the cryostat as the largest mass requiring cooling is the magnet at the bottom of the cryostat. (Further operational details are found in the O.I. manual). A cooldown took four hours and used ten litres of liquid helium; liquid may then be transferred directly. The

"warm" cryostat took about an hour to fill. Once the cryostat was below 20 K any exchange gas in the IVC could be pumped out; a good vacuum was required before any cooling below 4.2 K could be attempted.

4.2.3 Boil Off

The cryostat capacity was about 20 litres and, once cooled, on average it boiled off 10 litres/day. The exact amount depended on the helium level, since the boil off rate decreased as the level dropped. As a rule of thumb the helium level halved every 24 hours. So if one filled on Friday night, the bottom of the cryostat would still be at 4 K on Monday morning. However as the 50% mark occurred at the top of the superconducting magnet, and this should be kept covered in helium when energised, the cryostat needed topping up each working day. When the sorb heater was used, the magnet energised, the 1 K pot pumped, or the sample siphon cooled by exchange gas then boil off would be increased. It was estimated that half of the static boil off was due to the heat leaks down the magnet leads.

4.2.4 Level Meter

The cryostat was fitted with a superconducting wire level meter. Using a dipstick with a vibrating rubber diaphragm it was cross checked and its level output related to the various features in the cryostat. A boil off against time plot was produced by Asaolu (1983) which is reproduced in fig 4.5. A comparison with a diagram of the cryostat, clearly indicates the effect of the flanges. As it was not possible to accurately convert level to volume, only approximate values of the latter are given.

4.2.5 Sample Siphon

The Southampton magnetometer is a top loading system. This means that the sample can be cooled down at the start of a "run" along with the rest of the cryostat and then removed, changed at room temperature, reloaded and re-cooled back to 4.2 K. To enable this the sample and its support are attached to the end of a special siphon - the "Sample Siphon". The sample siphon can leave or re-enter the cryostat using a sample "air-lock". To change a "cold" sample, it is slowly lifted up until clear of the IVC entrance tube. The gate valve is then shut so that the IVC is isolated. Once warm the air lock and sample can be removed. When a new sample is loaded the air lock can be re-attached

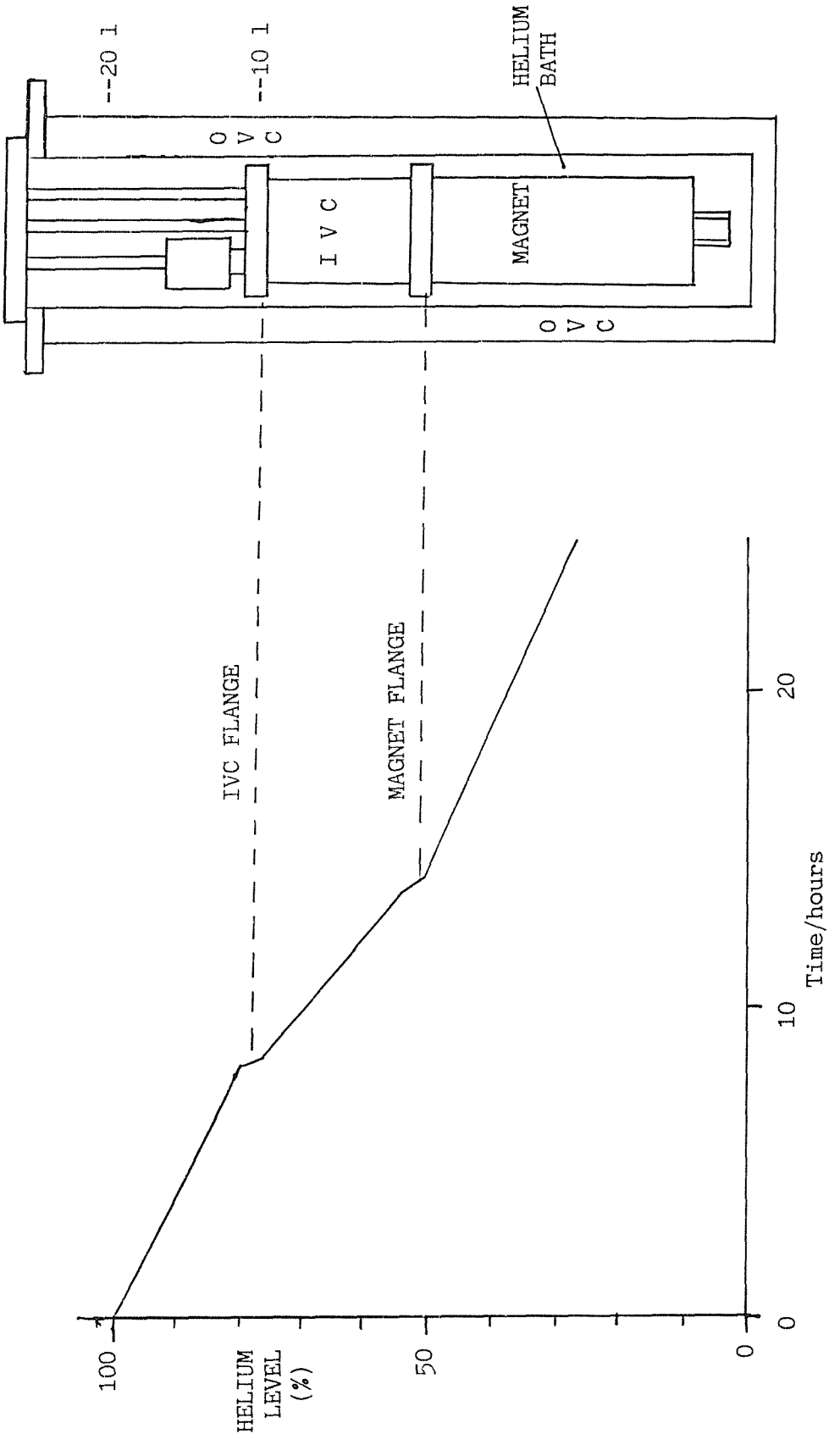

Fig 4.5 Cryostat Alongside the Boil Off Curve

to the cryostat and evacuated. Then the gate valve can be re-opened. The re-cooling can be done in two ways:
EITHER exchange gas can be added to the IVC and the sample on the end of its siphon very slowly lowered in. This means that it is cooled at the expense of the cryostat's helium and that long times are required to pump the exchange gas out of the IVC.
OR a "Pre-cool Siphon" can be attached to the sample siphon while it is half loaded into the IVC under vacuum. Then helium is transferred from a dewar via the "sample siphon pre-cool siphon" to the sample siphon. This is complicated to set up (requiring an external dewar) and has (in effect) two siphons to cool down.

The sample siphon is a long outer tube evacuated in the top half, through which two tubes run. One delivers helium to the copper nose of the sample siphon. The cold gas then fills the lower half, cooling it, before flowing out through the second tube; see fig 4.6. These inlet and outlet tubes form two arms at the top of the siphon to which the pre-cool siphon, and a small outlet siphon can be attached; see fig 4.7.

In order to cool the pre-cool siphon when connected to the sample siphon helium was sucked through it by a rotary pump. Two litres of helium was required and it took about half an hour to cool down. If the pre-cool was not finished then the Germanium thermometer on the He3 pot would show a large temperature rise when the sample siphon touched the "top hat". This effect could be used to check for the end of the pre-cool.

After successfully cooling, the pre-cool siphon was removed and a manifold attached to the sample siphon in order to pump out the remaining helium. (Otherwise this would produce a heat leak when cooling to 0.3 K). The nose of the sample siphon was threaded to engage the "top hat" of the 0.3 K platform. It was known as the upside down "top hat" because of its shape. The top hat was the lowest piece of the "sliding assembly" which was designed to keep the sample central and to thermally connect it to the He3 pot via a set of copper bundles.

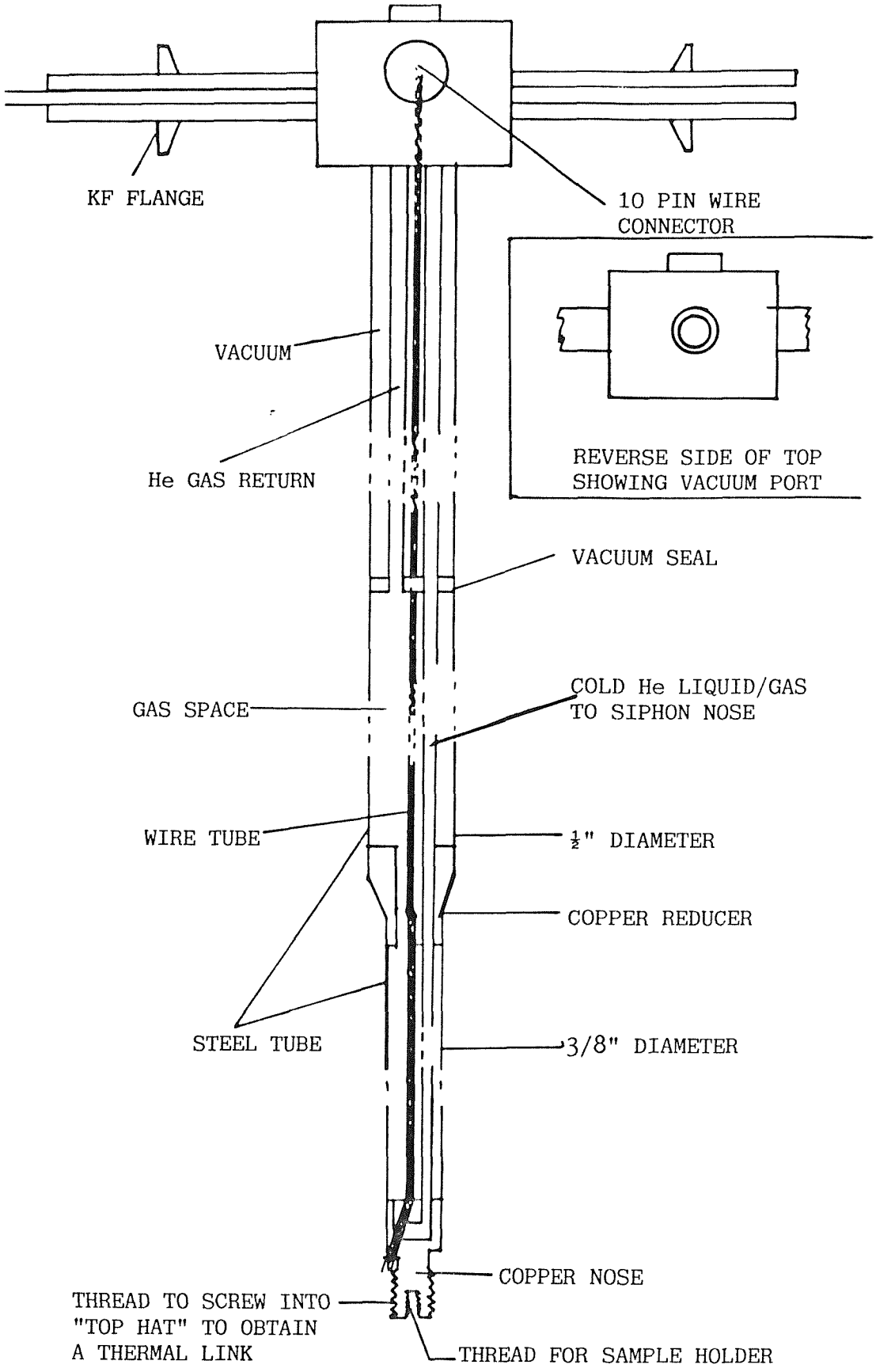

Fig 4.6. The Sample Siphon

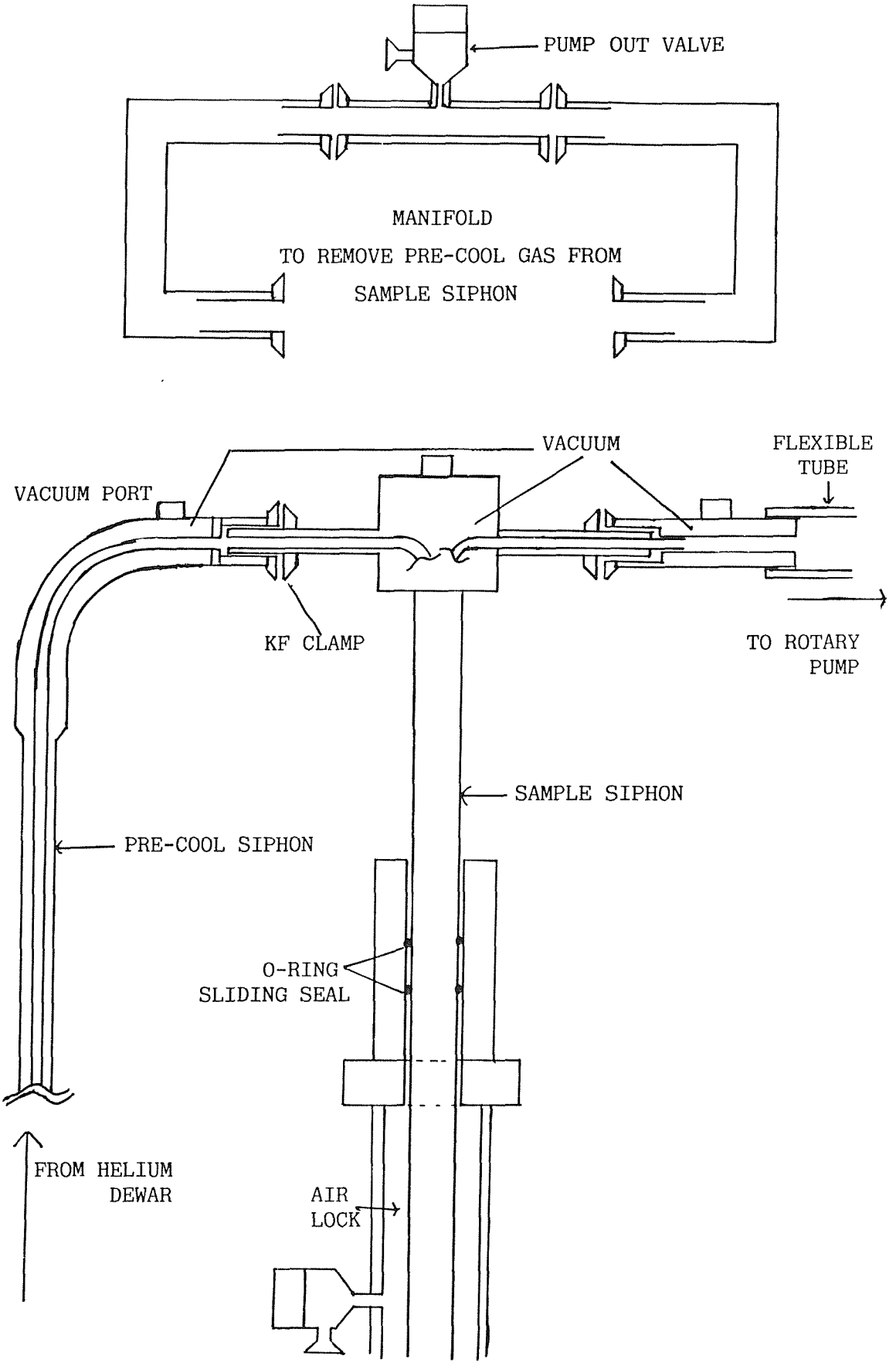

Fig 4.7 Attachment of Pre-cool Siphon & Manifold

4.2.6 Cooling To 0.3 K

In this cryostat only the pots, sample siphon and sample are cooled below 4.2 K. In particular the pick-up coil and its surrounds are maintained at 4.2 K. This keeps any temperature dependent background magnetic signals fixed, which can then be ignored (as long as they are small) because the detector will only respond to changes in signal. This is a special feature of the design of this cryostat. In systems where the surroundings change in temperature along with sample, there is the added complication of subtracting the background signal.

To start cooling the He4 pot is filled through the single shot needle valve. Then it is pumped to reduce the vapour pressure. After some time it will reach 1.2 K. Then He3 gas was slowly admitted from the room temperature dump (or the sorbtion pump). The first few mbar of He3 were let in gently, to act as exchange gas, to cool the He3 pot itself to the He4 pot temperature. The He4 pot condenses the He3 and the dump pressure falls to about 30-40 mbar. The sorbtion pump will reduce the temperature of the pot to 0.35 K. At the end of the experiment, if the cryostat is to remain "cold" the He3 can be left in the sorbtion pump until used again, otherwise it is cryopumped out as the cryostat warms (see above at 4.1.6).

4.3 THERMOMETRY

4.3.1 The Thermometers

The master thermometer in the cryostat was a Germanium resistance thermometer which was attached to the He3 pot. There were also several 220 Ω Speer and 270 Ω Allen Bradley (AB) carbon resistors. The Speer resistors were attached to:

i) the 4 K top plate of the IVC,
ii) the He4 pot,
iii) the He3 pot,
iv) the "top hat",
v) the copper guiding disc of the sliding assembly (later removed)
vi) the sample siphon (also later removed).

Calibrated Allen Bradley resistors were fitted to the He3 sorbtion pump (the "Sorb"). The Germanium and the Speer on the "top hat" were measured with four wires while all others were measured with two. During the cooldown, as well as monitoring the semiconductor thermometers, it was useful to measure the resistance of the magnet winding, as this is the lowest and biggest object in the cryostat. Its values were 2.34 Ω at 295 K, 2.02 Ω at 77 K and <0.1 Ω at 4.2 K. A thermometric resistor was also required on the niobium superconducting screen surrounding the pick up coils. This was to monitor the temperature of the screen when it was heated above its superconducting transition point to allow the magnetic field to penetrate.

4.3.2 Heaters

Heaters were fitted to the He3 pot, the "Sorb" and the outside of the niobium screen. Respectively, these consisted of a 500 Ω wire wound around the pot's circumference, a 33 Ω wire connected to a heat post and four carbon resistors in series. Resistance wire was not used on the niobium screen to avoid current induction problems.

4.3.3 Germanium Thermometer

Our Germanium thermometer was manufactured and calibrated by Lake Shore Cryotronics (see refs) for use between 0.3 K and 20 K. (Model no: GR-200A-100). The resistance of the Germanium was:

3.2	Ω	at 295 K
4.8	"	at 77 K
107	"	at 4.2 K
7200	"	at 0.3 K

Lakeshore supplied 52 calibration data points, with an uncertainty of ±5 mK below 10 K and ±15 mK at 20 K. An equation had been fitted and a set of interpolated resistances for specific temperatures were calculated. Since we read the resistance and wanted the temperature, this was inconvenient. So another fit to the original data using a seventh order Chebychev polynomial was performed by Dr C A Cornelius (then of Southampton University Physics Department - gratefully acknowledged). A tabulation of temperature from resistance was then produced. The seventh order polynomial provided a least squares fitting error of 5 mK and was found to be within 5 mK of the Lakeshore interpolation.

Resistance thermometers are known to shift their calibration when subjected to a magnetic field (Sample & Rubin 1977). Carbon resistors are less susceptible than germanium resistors, so our Germanium resistor was attached to the He3 pot, above the magnet, while a cross calibrated Speer resistor (R_6) was to be exposed directly to the magnetic field. A study of the magnet field data provided by the manufacturers (O.I.) suggested that the field experienced by the Germanium thermometer was 5% of the main field. Since our final experiments were carried out under a few mT, this meant that the Germanium then experienced a field equivalent to a few times the Earth's field.

4.3.4 Carbon Thermometer "Calibrations"

In order to control the temperature of the He3 pot between 0.3 K and 4.2 K there was a twin temperature controller which could drive the heaters on the Sorb and the He3 pot. The curve for the Sorb bridge thermometer is given in fig 4.8. Using the calibrated Germanium thermometer we could produce a plot of the He3 temperature against Sorb temperature; see fig 4.9 (no electrical heating applied to the pot). This information would be of use to coarsely set a temperature just below the desired value. A graph of R_5 the He3 pot Speer resistance (as measured by the bridge) against temperature is given in fig 4.10.

As R_6, normally on the "top hat", was closest to the sample (due to the removal of R_7 from the sample holder) it was also useful to have it cross calibrated to the Germanium; see fig 4.11. R_6 was calibrated by four wire measurements, with it temporarily attached to the He3 pot. During the actual foil sample measurements this thermometer became disconnected, and only the Germanium temperatures were available so the temperature at the "top hat" could not be monitored.

4.3.5 Aluminium Transition Temperatures

As we could not measure the temperature of the sample directly we tried using the superconducting transition temperature of aluminium, in a magnetic field, as a crude thermometer. This was not very successful. Changes in long foils will not be easily detected in a second order gradiometer. The SQUID detected flux changes which we assumed was the superconducting transition, but it was very broad and not very reproducible. (Using a "semi infinite" solid aluminium

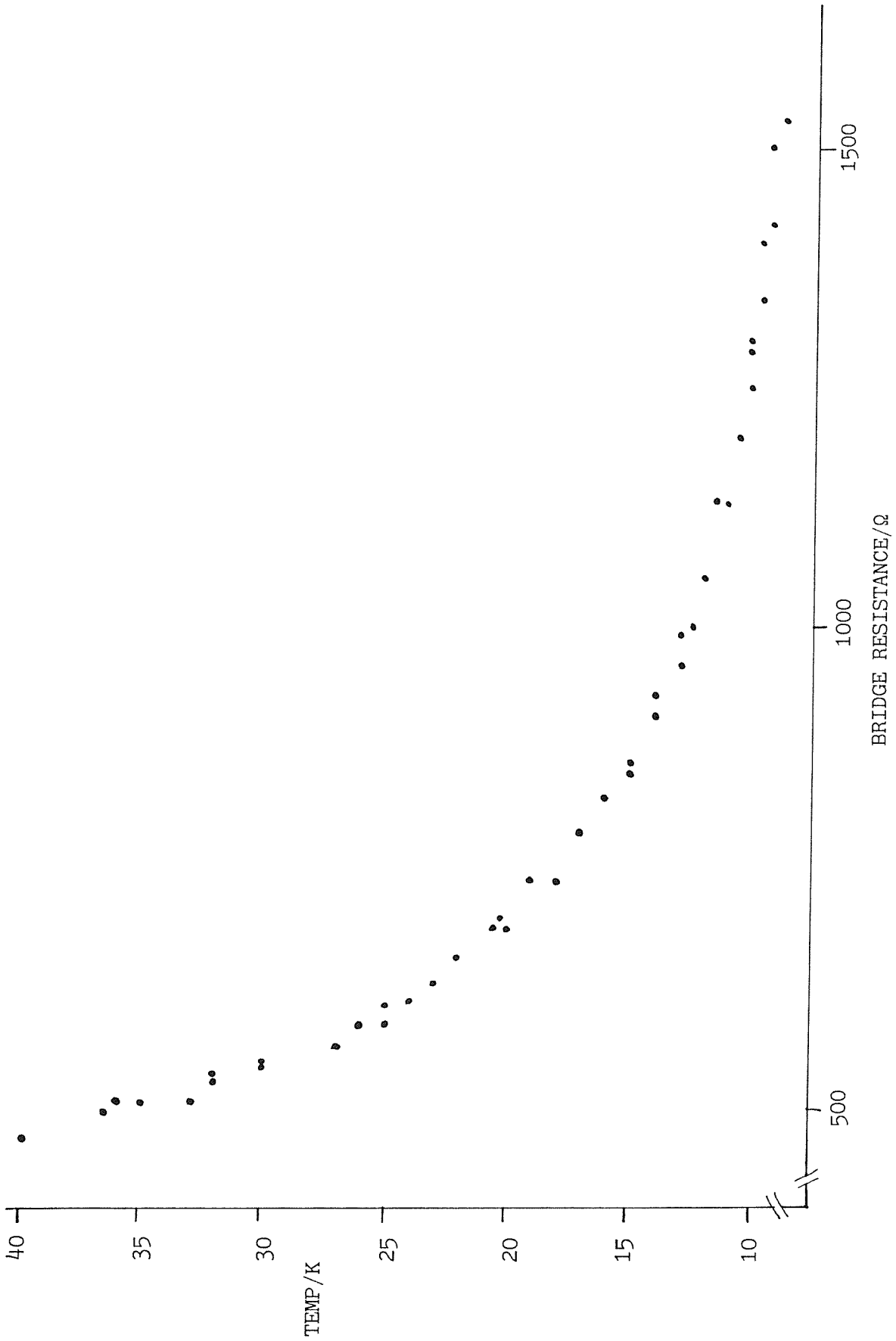

Fig 4.8 Sorb Temperature against Bridge Resistance

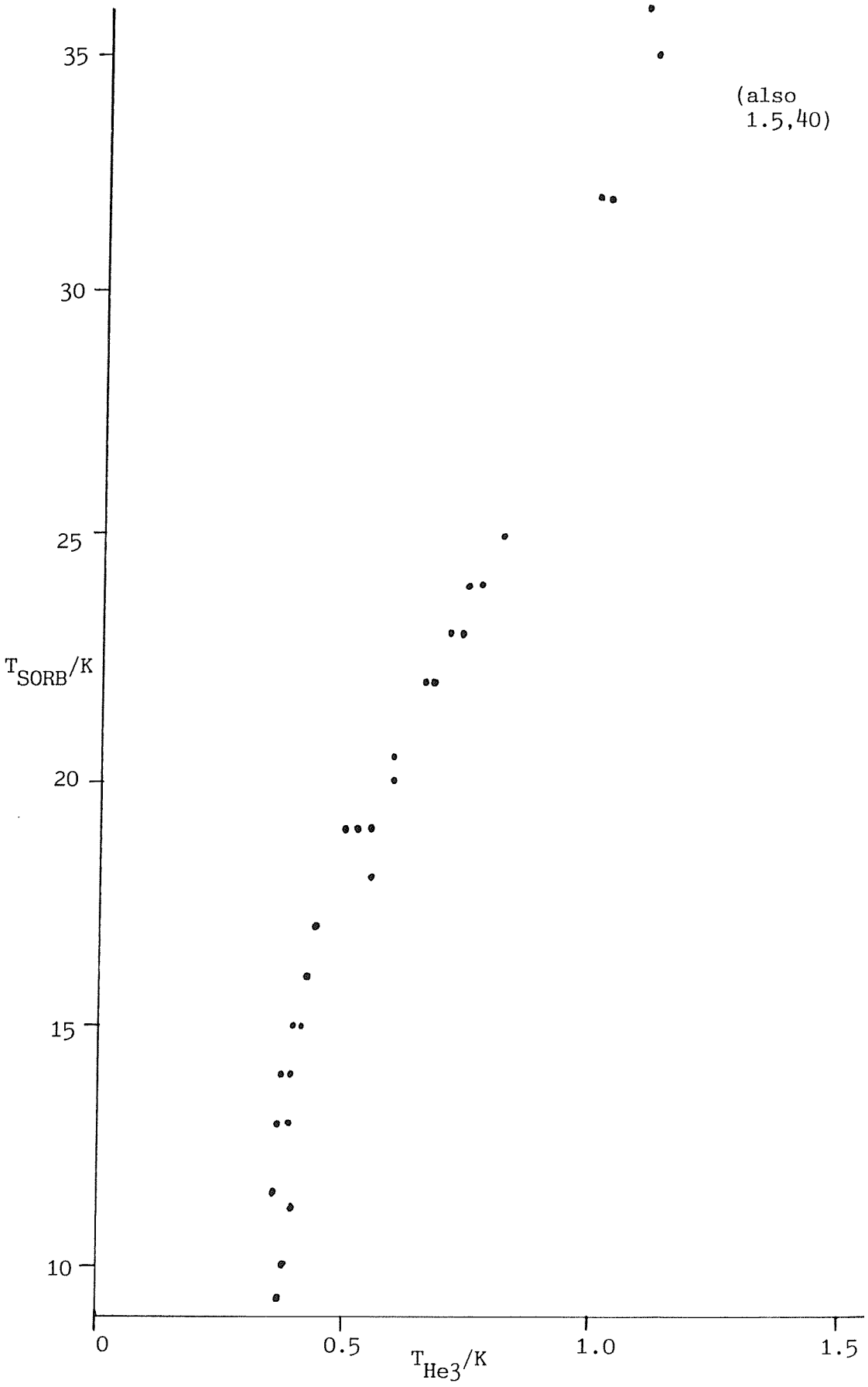

Fig 4.9 He3 Pot Temperature against Sorb Temperature

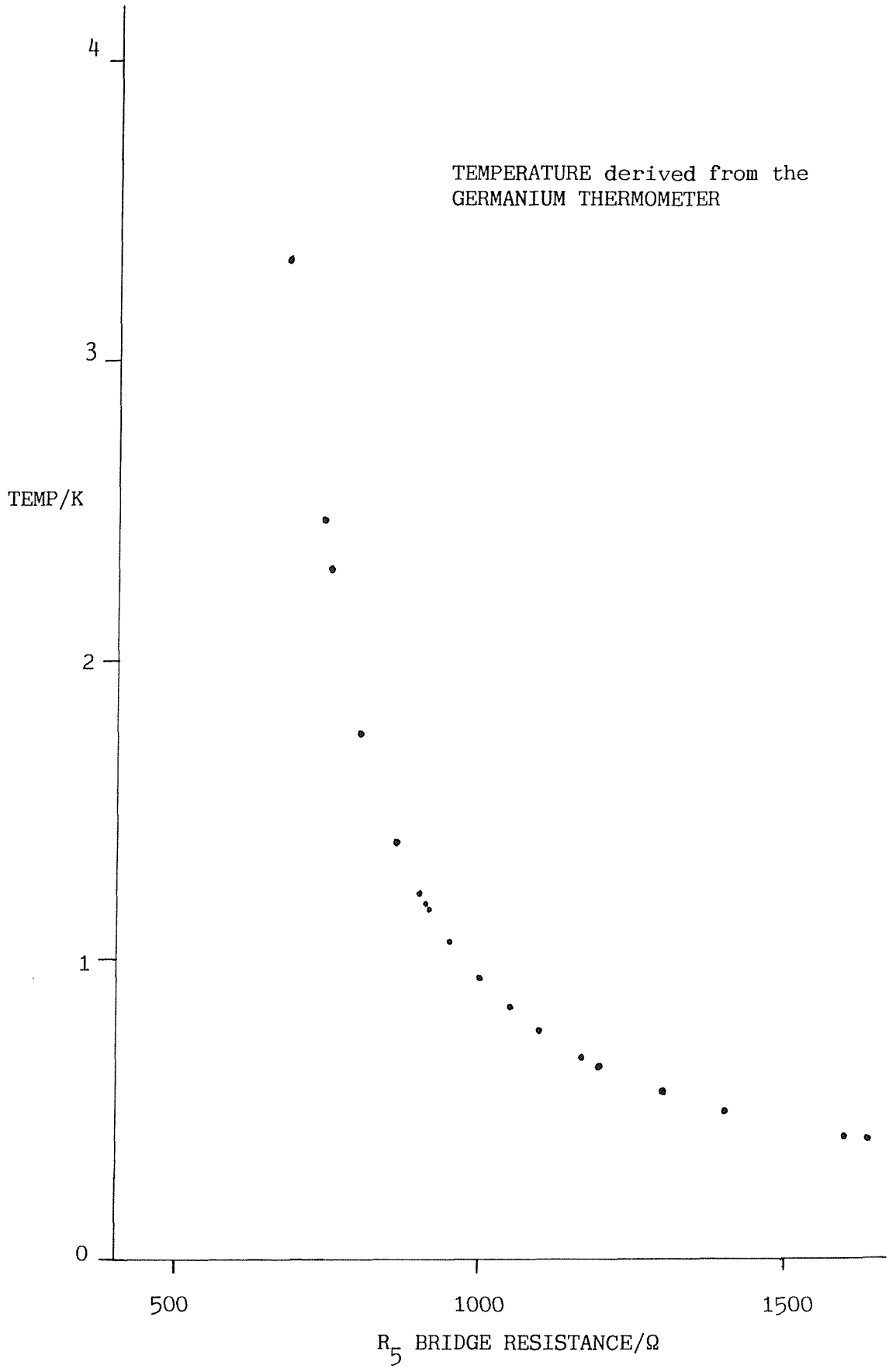

Fig 4.10 Plot of R_5 against Temperature

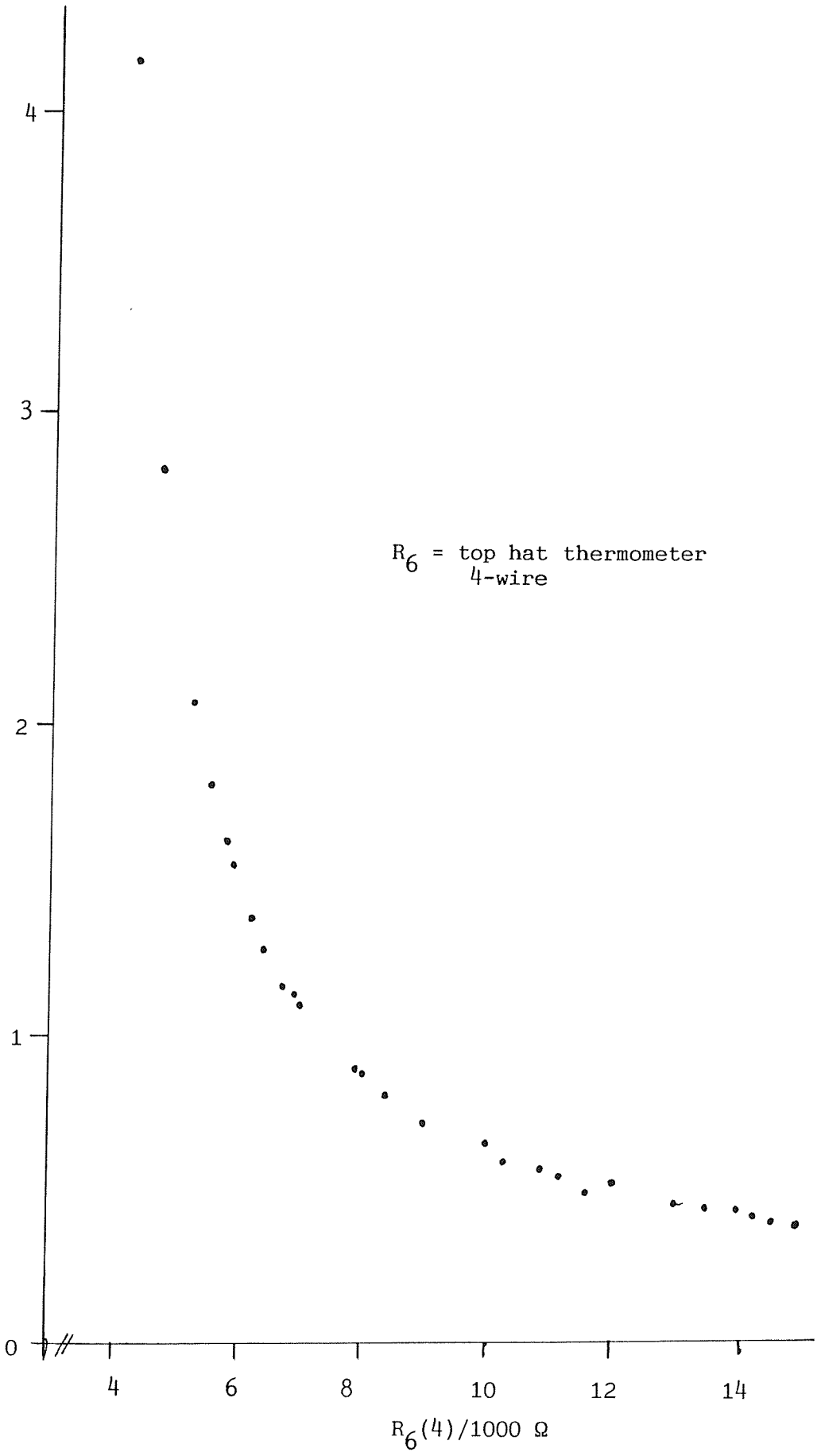

Fig 4.11 Plot of R_6 against Temperature

cylinder we were able to check that a real transition had occurred. At low temperatures the signal shape was inverted and much magnified (100s Φ_0), which agreed with a susceptibility change to -1 for superconducting diamagnetism). There was evidence for a transition, under a 2 mT field, when the Germanium thermometer was reading 0.5 - 0.7 K. One would expect the transition temperature of pure aluminium in a 2 mT field to be 1.1 K, according to the eqn:

$$T_c = T_0 \left[1-(B_c/B_0)^2\right]^{\frac{1}{2}}$$

where T_0 i.e. $T_c(B=0)$ = 1.20 K & B_0 i.e. $B_c(T=0)$ = 9.9 mT

This evidence might suggest that the sample was not at the same temperature as the He3 pot. But at worst the temperature was still well below 2 K, the magnetic "transition temperature" seen by Pomerantz. However our measured superconducting transition values were suspect because the foil samples were not pure aluminium and the possibility of remanent fields up to 1 mT (see 4.4.5 and sec. 6.4). We also saw a large SQUID signal for a sample, on warming, around 0.45 K when the applied field was 10 mT, at which superconductivity is not possible.

Later we found that the flux signal from a LB sample foil responded quickly to changes in the temperature of the He3 pot. After a temperature cycle the signal quickly returned back to the original value implying a good thermal link between the sample and the He3 pot. When the pot was left dry in vacuum, with a sample attached, it rose to 20 K overnight, due to the heat leak down the sample siphon. Further when the niobium shield was heated, while the He3 pot was being pumped, the Germanium registered a warming from 0.39 K to 0.42 K suggesting no thermal contact between the sample and the pick-up coil at 4 K. These latter pieces of information suggested that the sample would have been at the same temperature as the He3 pot. Also Oxford Instruments claimed to have checked that the sample holder cooled to the He3 pot temperature, using a calibrated carbon resistor.

4.3.6 The Cryostat's Temperature Profile

The change in temperature with height within the cryostat was measured using a silicon diode thermometer (Rao et al 1983). (The loan of which from the Institute of Cryogenics is gratefully acknowledged). The temperature profiles with the helium at 80% & 30% are indicated in fig 4.12. A very low temperature is seen over most of the cryostat

even at low helium level. This is partly due to copper braids hanging from the IVC flange, put there to deliberately maintain it at 4.2 K. However ice on the cryostat face indicated a heat leak probably due to the magnet leads. When they were re-arranged to keep a greater length in cooling gas ice no longer formed on the top face indicating a reduction in the heat leak. The copper vapour shields warmed to 77 K and 120 K when the helium level was low, otherwise the temperatures were 55 K and 90 K when the main bath was full.

4.3.7 The Sorbtion Pump Control

To coarsely control the temperature of the He3 pot the Sorb temperature was varied to change the adsorbtion, and hence pumping, rate. This was done by balancing the cooling power of the exchange gas in the SVC against the heater. More exchange gas was required if the SVC was surrounded by liquid helium, because some of the gas was then adsorbed onto the outer wall of the SVC. A twin three term temperature controller had been designed for use with the Sorb and He3 pot, such that it would feed heater power proportional to the temperature offset below the set point. The controller was tested and found capable of holding a temperature stable when the right bridge amplification and P.I.D. settings were made. However for the real sample measurements, the signals were only taken at natural points, given below:

20 K	the hottest one could easily get to
4.2 K	the main bath temperature
1.2 K	the He4 pot temperature
0.4 K	the coldest maintainable temperature.

There were some problems with this procedure at 0.4 K, due to friction heating as the sample moved. This was particularly noticeable in this cryostat because of problems with the sliding siphon. To obtain steady warming of the He3 pot from 0.4 K we found that it was more useful to apply electrical heat to the Sorb. Applying electric heat through the controller to the He3 pot caused a jerky rise in temperature.

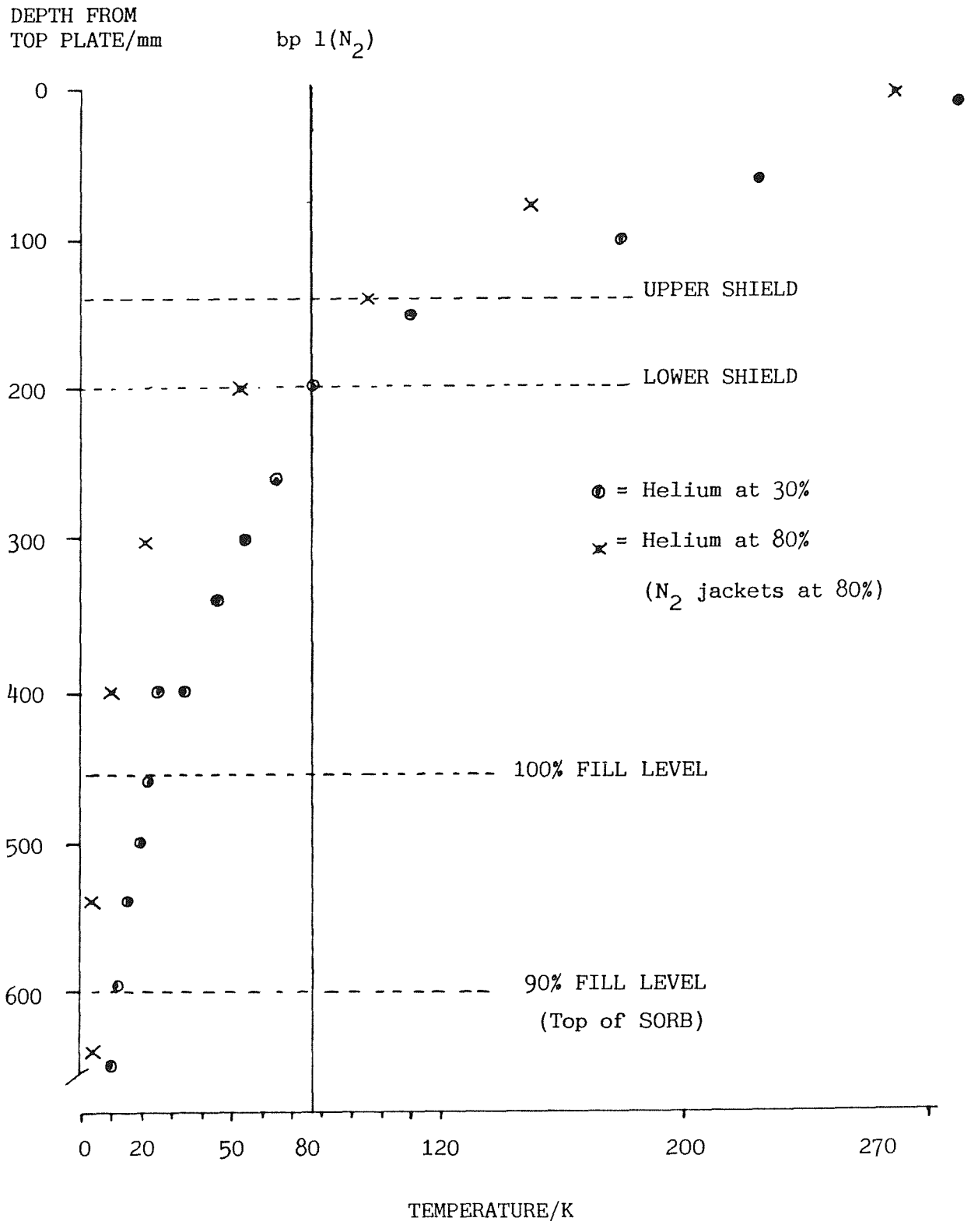

Fig 4.12 Cryostat Temperature Profile

4.4 THE MAGNET

4.4.1 The Magnet

The superconducting magnet had a main field which could be set between 0 and 2 T. Measuring the voltage across a standard 2 mΩ resistor allowed accurate control of the field setting. There were also eight shim magnets which were there to provide a field homogeneity of 1 in 10^5 over the central 50 mm x 10 mm (length x diameter) sample space. (It has been suggested that the main magnet itself would have a homogeneity of about 1 in 10^4). The shim values were only given for a 2 T field but because of vibration sensitivity we did not want to work above 10 mT so they were of no use. Different values are required for each field setting. All the shims had a mutual inductance with the main magnet, some quite strongly so that they could not be ignored. On energising the main magnet, currents would be induced in the shims. So these currents had to be "dumped" by opening the shim (heat) switches. This was done by cycling around the eight shims (about three times because of their own mutual linking). It was possible to see the effect of dumping all the shims with the SQUID, and the major shims (nos. 1,2,3 & 8) with a low temperature Hall probe. As the shims were superconductors, they will always retain some diamagnetic effect.

4.4.2 Magnet Energisation and the Niobium Screen

To remove power supply noise and provide temporal stability, the magnet was run in persistent mode, and a superconducting (niobium) tube placed, concentrically, within the bore. This will only remain useful up to a critical field of about 0.16 T. This tube with its natural strong diamagnetism (χ=-1) complicated the magnet energisation process. Once the magnet was energised the tube was warmed to destroy its superconductivity. This allowed the field in, which was then trapped on cooling. The heating had to be done before putting the magnet into persistent mode to avoid large induced changes in the magnet's supercurrent. (The niobium tube could support a field of over 0.1 T even if the main magnet was run down. However since it was then carrying all the current there could be problems of drift as occur in a persistent mode magnet. There would also be a loss of spatial homogeneity if the shield was short).

If there are any field drifts in the magnet the niobium tube will compensate for them (and since these would be minor the niobium will not be under the force strain which the magnet is; see Philo and Fairbank (1977)). If the IVC was fully evacuated it could take quite some time for the niobium to cool; so the magnet would be put into persistent mode before the niobium recooled. This mode of setting the field up, is different from some of the methods reported in the literature. Philo and Fairbank (1977) reported keeping the shield heated above the critical temperature all the time the magnet was charged. (They did not have to spend time dumping shims).

Unfortunately the normal/superconducting transition of the shield is known to cause an adjustment in the trapped field's magnitude. Steelhammer and Symko (1979) reported that it could cause an error in field value of up to 5%. Swithenby (private communication 1985) also reported a noticeable effect but that it was reproducible. We decided to study the effect for ourselves on our system.

4.4.3 Field Measurement

A low temperature Hall probe (Siemens RHY 18) was attached to the sample siphon and connected to a Hirst control box "Fluxmaster FM70". The probe required an increase in the bias resistor at the control box output to 470 Ω, which reduced the current, and the excessive self heating. There was also a heat leak down the probe's copper leads. It was found that exchange gas left in the sample siphon space provided cooling by supplying a heat path up the sample siphon to where it was in contact with the main bath. Other unwanted heating could be caused when the niobium screen was warmed up. Heating of the Hall probe changed its voltage output and hence its calibration which had been obtained using the magnet's current/field calibration provided by O.I., with the shield kept normal.

If an increasing field was applied from zero, with the shield cold, it was possible to see the shield forced normal, and the Hall field jump up. This usually happened at about 0.16 T, as measured by the Hall probe. However we also found that if we applied any field up to 0.45 T we could not be sure that it had penetrated unless the shield was also heated. This is a consequence of niobium being a type II with an B_{c2} of between 0.25 T and 0.9 T depending on the sample (Rosenbaum et al (1964)).

4.4.4 Field Trapping Experiments

We carried out a set of experiments where, with the magnet field fixed, the shield was thermally taken through the transition, in both directions. The Hall probe indicated the field change for seven different values of the applied field between 1 and 150 mT. Even though the probes self heating had been reduced it was still evident in the field/temperature plots of the field trapping. The output voltage of the Hall probe drops as it cools, indicating a decreasing field. Then at the trapping point it shows a sudden increase in field; see fig 4.13.

We found that for all, except the lowest field, the effect of trapping the field was an increase in field of 0.4 mT. It was a surprisingly small amount and it was not a constant fractional change as might be expected. From Steelhammer and Symko (1979) we had expected a bigger value. It has been suggested that the effect was small because we were cooling within a highly homogenous field. Another possibility is that the field is excluded from the inside wall of the tube first, and is then pushed radially out. We learnt later that the field, in thick niobium tubes, remains constant on trapping if the tube is cooled from the inside outwards. This is not so for the reverse. It is also advisable to cool the tube from one end only to get a uniform field (J Gallop - private communication 1987).

It was also possible to use the Hall probe, with its output connected to a digital voltmeter, to observe the field change over the 56 mm upwards from the magnet centre. The Hall probe was moved in as a sample might be. In "zero" applied field a 40 μT variation was found while there was a 2 in 10^4 variation over the distance when 1 T was applied.

4.4.5 Remanent Fields

It was found that after running the magnet down, dumping the shims and forcing the shield normal, that on its re-cooling there would still be a residual field. The Hall probe experiments showed that a field of several mT could get trapped on cooling. Some attempts were made to "demagnetise" by applying a smaller reverse field, and then de-energising. This was time consuming and not very successful. Two further problems with working at low fields came from the magnet power supply. It had a non-zero current output when its control helipot was

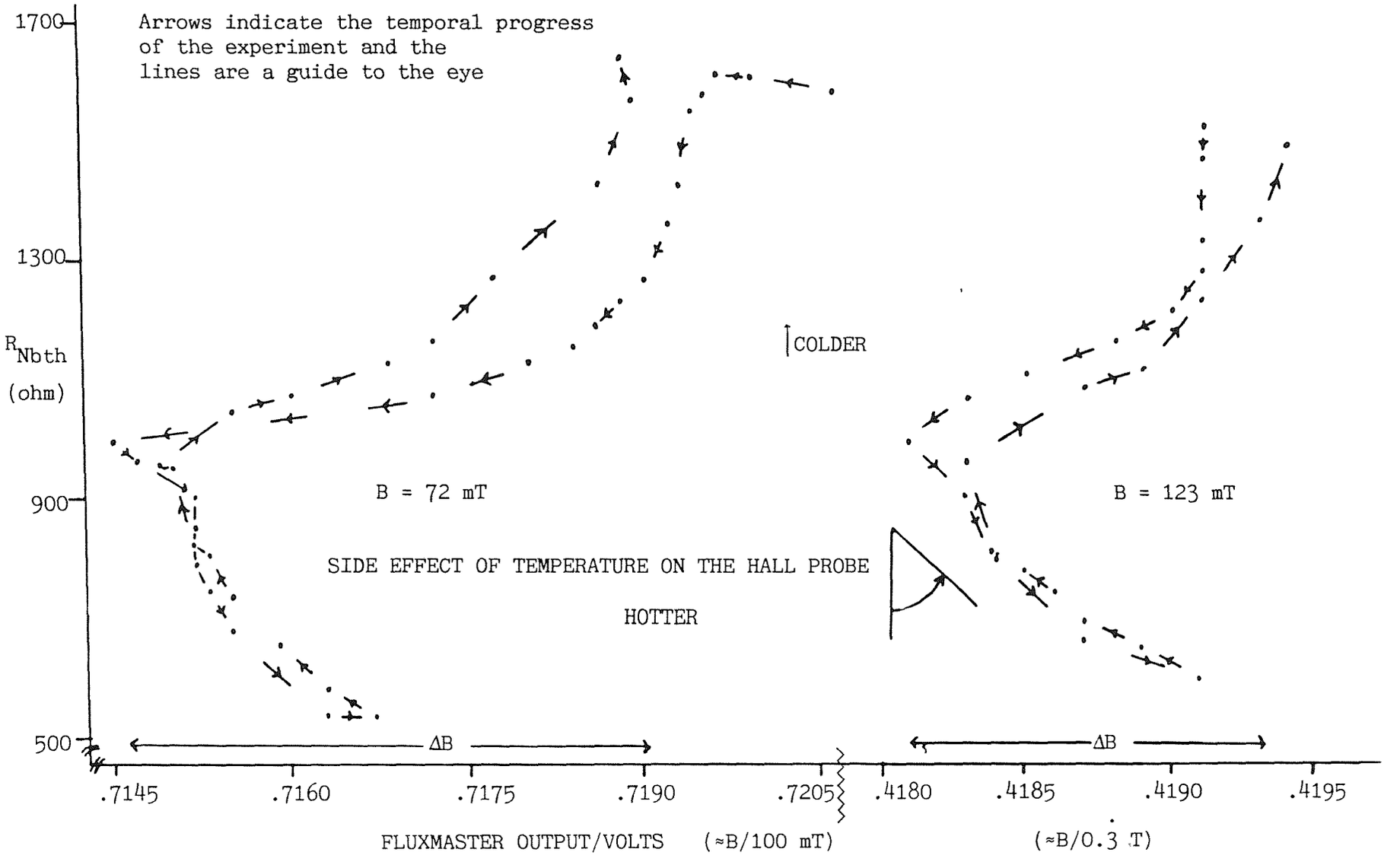

Fig 4.13 Flux Trapping in the Shield

turned to zero. This was partly reduced by adding a divide by ten resistor which could be switched in when desired. The other problem occurred when the magnet switch heater was turned off, to put the magnet into persistent mode, because the magnet supply would then jump up in current equivalent to a field of 0.2 mT. So for very small fields another smaller power supply was used to provide the current, through a resistor and ammeter to the magnet.

4.5 THE STAINLESS SAMPLE SIPHON

4.5.1 The Magnetic Stainless

When the original sample siphon was put to use in the presence of the magnet's field the SQUID detected some unusual signals. The siphon was externally inspected with a Fluxgate magnetometer which indicated something magnetic, though the field detected was only about 0.1 mT. The external tube was not obviously magnetic. The tube had been made of austenitic stainless steel AISI type 321, which should be non-magnetic.

We decided to have a new siphon made. Materials other than stainless steel were considered but were impractical e.g. CuNi was found incapable of taking the twisting forces involved in screwing the siphon into the He3 platform (or "Top Hat"). A literature search also showed that there had been problems with austenitic stainless steel transforming, under temperature cycling, to a martensitic phase which is ferromagnetic. This had caused problems for Larbalestier and King (1970) in a stainless steel former for a magnet. Their study of stainless steel transformation to a ferromagnetic phase (1973) indicated that it happened in many different types of stainless. It was also batch dependent because of slight variations in the alloying constituents and other impurities. So one should check a piece before using it. Steel AISI type 321 (as used for our siphon) had been found to transform on temperature cycling. They cycled between room temperature and either 77 K or 4.2 K and a magnetic field could be applied. The overall effect on AISI type 304 was much less than on type 321. Warnes and King (1976) studied transformation effects in specially produced samples and concluded that high carbon versions of low AISI grades (like 304) should be structurally stable and

anti-ferromagnetic rather than ferromagnetic. Weldable 321 was found more likely to transform. Collings and Hart (1979) also produced curves showing the susceptibility of 304N to be less than types 310, 316 or 330.

A set of experiments on various types of stainless tubes, some type 321 others type 304, was carried out. These tubes were inspected by a fluxgate probe before and after magnetisation in a one tesla electromagnet. No remanent magnetisation was detected though the tubes were pulled towards the poles of the magnet. Calculations showed that the deflection was greater than for a paramagnetic material, indicating a small ferromagnetic component. Short cylinders of 2 cm length were cut from these tubes, suspended in a VSM at room temperature and their B-H curves measured, with a maximum applied field of 890 kA/m (1.1 T). The VSM was calibrated with two nickel samples, one shaped as a thick disc, the other a short thin rod. (Demagnetising effects were allowed for throughout the experiments). The results for the different samples were similar in that small amounts of hysteresis were seen and the samples were almost saturated by an applied field of 1 tesla; see fig 4.14.

4.5.2 Temperature Cycling

We cycled the samples between room temperature and 77 K twenty four times and then measured their B-H curves. A similar procedure was applied to a piece of CuNi tube, but its magnetisation always remained too low to measure. After this we cycled strips of our tubes to 4 K with a magnetic field applied to them using SmCo magnets. Then using a continuous He flow insert, between an electromagnet's pole pieces, the samples were cycled in temperature and field. For the 321 there was an increase in the magnetisation by about 50% from beginning to end of this series of "mistreatments" - the biggest jump occurred after the first nitrogen cycling. However the 304 sample stayed about the same after similar treatment. Both magnetisation values started above the value given by Larbalestier and King (1973). However, although the magnetisation of our 321 sample increased, it was much less than Larbalestier and King's samples. Our 321 sample had a magnetisation of about 10 kA/m while the 304 was about 5 kA/m. Since 304 seemed less likely to transform, a tube of this type was used to build a new siphon. Prior to fabrication a piece was tested to make sure this particular tube was satisfactory.

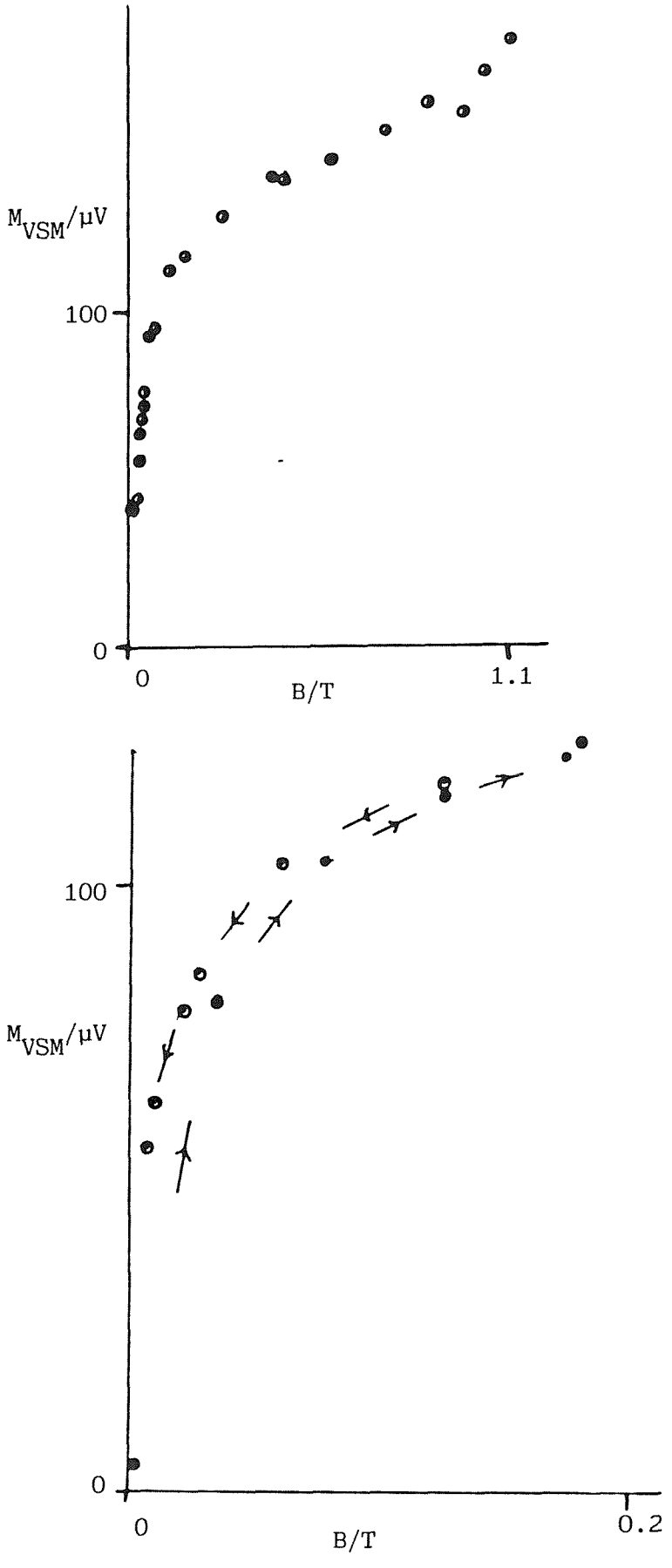

Fig 4.14 M v B Curves for Stainless Tubes

About this time it was discovered that the main source of the magnetic flux in the siphon was the helium carrying tubes within the siphon; see fig 4.6. They appeared to be ferromagnetic! Similar tubes were measured as having a magnetisation of 113 kA/m. (This may be compared with the saturation magnetisation for nickel of 480 kA/m). After the new siphon had been manufactured it was possible to cut pieces from the old siphon, and the old sliding assembly. These were measured in the VSM. The outer 321 tube was found to be no more magnetic than the 304 tube from which the new siphon was constructed. The ferromagnetic signal had been due to only the very small inner tubes, which were replaced by CuNi on the new siphon. (Unlike the outer tube they did not have to withstand any twisting force).

4.5.3 The New Siphon

Although the new siphon did not suffer from magnetic problems it was not straight and had a tendency to stick as the sample was moved in and out of the pick-up coil. It was also necessary to make sure that the siphon travelled along the axis so that the sample (at various temperatures) could not touch the insides of the pick-up coil former, which was fixed at 4.2 K. Another problem in the vicinity of the "top hat" concerned the copper braids connecting it to the He3 pot. These had been changed on the new sliding assembly, to a thicker braid. It was discovered that as the siphon was lifted they would bow out allowing them to touch the 4 K sides of the IVC tail. To overcome this they were spiralled around the sliding tube and laced together with copper wire to stop them deflecting outwards. Unfortunately the copper wires regularly needed replacing as they broke often. Possible problems with 4 K radiation onto the sample were discounted after it was calculated that this would be a negligible effect.

4.5.4 Sample Siphon Motor

The sample siphon was driven in and out of the detector coils by a linear drive which could be rigidly connected to the top of the siphon, after the sample had been loaded into the cryostat. The linear drive formed part of the position control system which could be set manually or by computer using a linear potentiometer as a position detector. Initially the sample was to be stepped in, with the flux detector being read when the sample was at rest. This allowed any transients to die down, but still relied on the SQUID being able to

follow them between measurements. However because of the sticking problem, the start/stop transients were too much for the SQUID to follow. So the position controller was modified, by our electronics workshop, and then used to drive the sample at an adjustable constant speed. This meant that the transients were less and the SQUID could usually follow them. However they then appeared on our chart recordings.

The motor itself was supported by three legs, which had been extended along with the siphon. The feet were firmly clamped to the top face of the cryostat.

CHAPTER FIVE - THE DETECTOR AND SAMPLE

5.1 THE SQUID SYSTEM

5.1.1 Introduction

In this chapter we will briefly outline how a SQUID works and how it is coupled to a sample through a flux transformer. We will also describe some of the electrical and mechanical noise which has to be overcome. More detail can be found in the many reviews such as Gallop and Petley (1976), Webb (1972), Swithenby (1980) or Giffard et al (1972). These reviews also discuss the many uses that SQUIDs have been put to, e.g. detecting the heartbeats of babies or maintaining voltage standards.

At the heart of a SQUID system is a Josephson Junction weak link. This consists of a ring of superconducting material with a restriction in the superconducting path around it, such that the path is almost broken.

But first, we need to remind ourselves of two results:

i) Consider a homogeneous ring of superconductor, with a magnetic field perpendicular to its plane. The superconductivity can be described by a single particle wave function. This is multiplied by a phase factor and leads to the phase being single valued around the ring. From this it can be deduced that the magnetic flux has to be quantised. (Gallop gives the derivation). A single flux quantum (denoted by Φ_0) is very small and has the value of 2.07×10^{-15} Tm^2. Any flux in the loop must be an integer number of these quanta of flux. A diagram of how the flux within an ideal ring would change is given in fig 5.1.1; a staircase pattern.

ii) Consider a ring of superconductor where, at one point, the amount of super current that it can carry is limited, i.e. a ring with a "weak link". In 1962 Josephson investigated the phase in a superconducting path that had to cross a potential barrier, formed by an insulating gap between two superconductors. (As long as the gap is small quantum mechanics predicts that some of the electron pairs will "tunnel" through the energy barrier). Josephson found that there was a

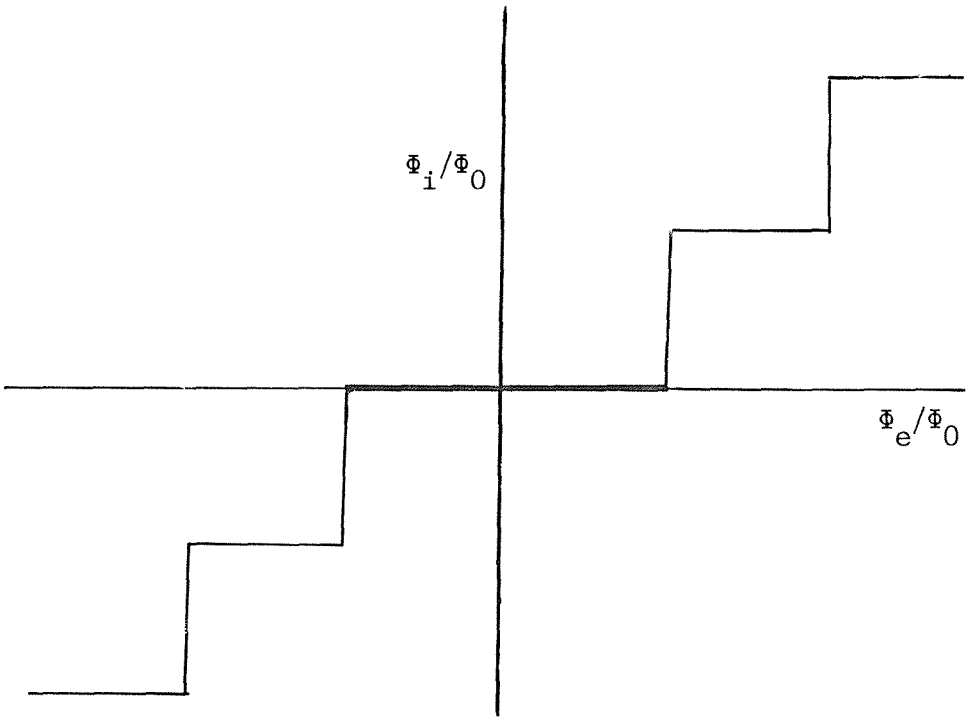

Fig 5.1.1 Internal Flux Response of a Superconducting Ring

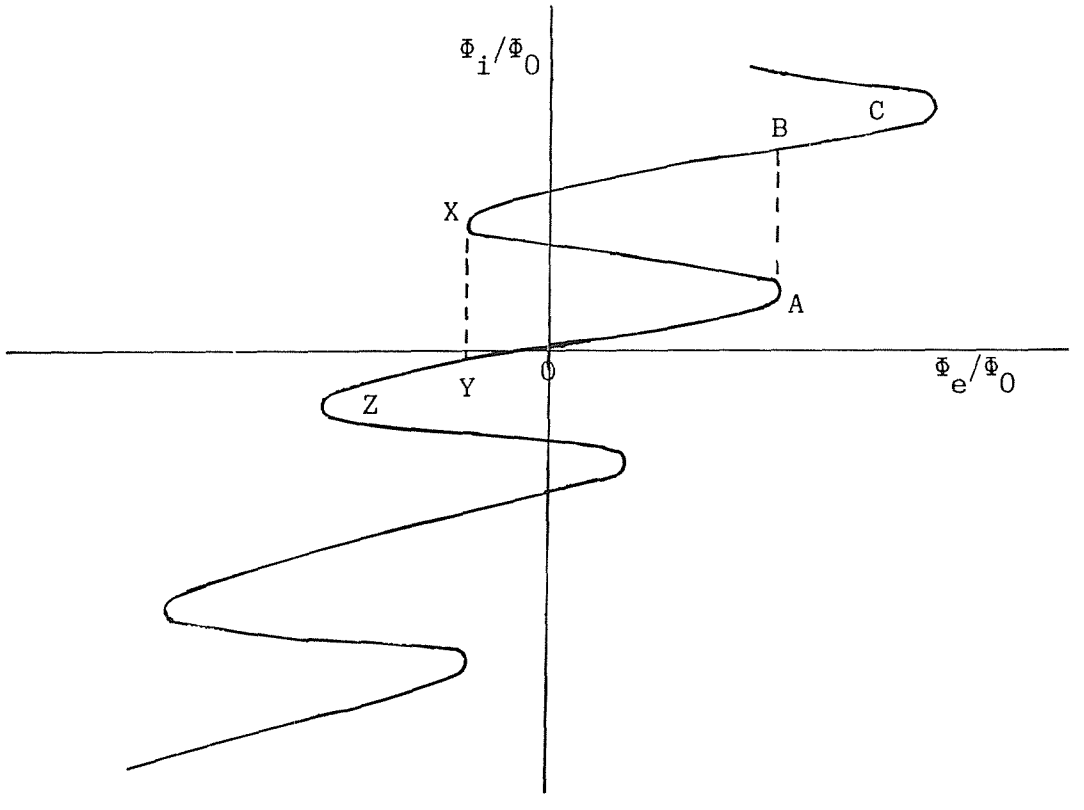

Fig 5.1.2 Response of a Ring with a Weak Link

Fig 5.1 Response to External Flux

phase difference (θ) across the barrier given by

$$\theta = \sin^{-1}(i/i_c) \qquad (5.1)$$

where i is the supercurrent flowing

and i_c is the "critical" or maximum supercurent that can flow without any voltage drop occurring.

It has also been discovered that this Josephson equation is applicable to other types of weak link. Some of these weak links are described and illustrated in the review by Gallop & Petley (1976).

5.1.2 SQUID Types

There are two types of "SQUID" depending on the way they are biased and the number of weak links that they contain. We used an RF SQUID which has only one weak link, as against a DC SQUID which has two weak links in parallel, and is biased by a constant current supply. Only RF SQUIDs are commercially available at the time of writing, so we will just describe this one type. However a lot more recent work has been done on DC SQUIDs, particularly in producing two good junctions simultaneously. One area of interest is their use to produce miniature gradiometers the size of electronic chips (Ketchen et al 1977). For the RF type, "SQUID" is really a misnomer as interference between two wavefunctions requires two "sources" such as provided by the two junctions in a DC SQUID.

5.1.3 The Effect of the Weak Link

The presence of a weak link alters the equations which lead to flux quantisation in a homogeneous superconducting ring. Suppose that we now apply a flux to our weak link ring (this is usually done indirectly via a flux transformer; see below at 5.1.6). Supercurrents will flow to try to oppose this, but the net flux is no longer quantised, so the net flux that threads the ring changes with the external flux as shown by OABC in fig 5.1.2. Once an increasing external flux passes point A the ring current can not be supported and the amount of net flux must jump to B and continue increasing to C. If we were now to reduce the external flux the net flux would decrease in a different manner via CBXYZ. So hysteresis occurs and energy is dissipated. Suppose that this external flux was only "slowly" changing - "quasi DC". In order to measure how much external flux there is, at some point in time, we couple some extra sinusoidal flux into the

ring. We can then see what amplitude of extra flux is required to obtain this energy dissipation.

This modulation is at radio frequencies using an L-C tuned circuit, operating near its resonant point. The execution of a hysteretic path takes energy from the tuned circuit and the RF tuned voltage falls, making the transition detectable. Thus the peak RF voltage gives us a measure of the flux already in the ring from the external source. If a slowly increasing external flux was applied then the peak RF voltage would periodically vary up and down in value, producing a triangle wave pattern. Because of non-linearities, instead of counting triangles to measure the amount of flux, it is usual to apply more reverse quasi DC flux to the ring as negative feedback to cancel the external signal. Then the signal is held at one of the triangle peaks and now the feedback flux becomes the measure of the flux coming from the experiment. To help in detection an audio frequency signal is also superimposed and used for phase sensitive detection. The SQUID is now in a "flux locked loop". To get an output signal the voltage across a resistor in the feedback circuit is monitored. This gives a measure of the current, and hence, the flux required to balance out the external signal. The SQUID junction is then used as the null detector; see circuit in fig 5.2.

5.1.4 The SHE SQUID

The SQUID used in this project was a commercial System 330 produced by S.H.E. (now B.T.I. - see refs). Its weak link was formed by a niobium thin film tunnel junction within a bulk niobium toroidal body. The latter provided shielding from external noise. The unit had a 2 μH input coil to which an external superconducting coil could be attached, in order to form the flux transformer. Separated from this input coil was the RF "interrogation" coil which also carried the audio and quasi DC signals.

The electronic control system allowed the SQUID to be operated in three modes, determined by their cut-off frequencies; FAST, MEDIUM and SLOW. It also enabled a test signal to be introduced into the ring while the feedback was switched off to produce the "triangle output" previously described. This could be used to check on the performance of the SQUID and on any deleterious side effects of the flux transformer.

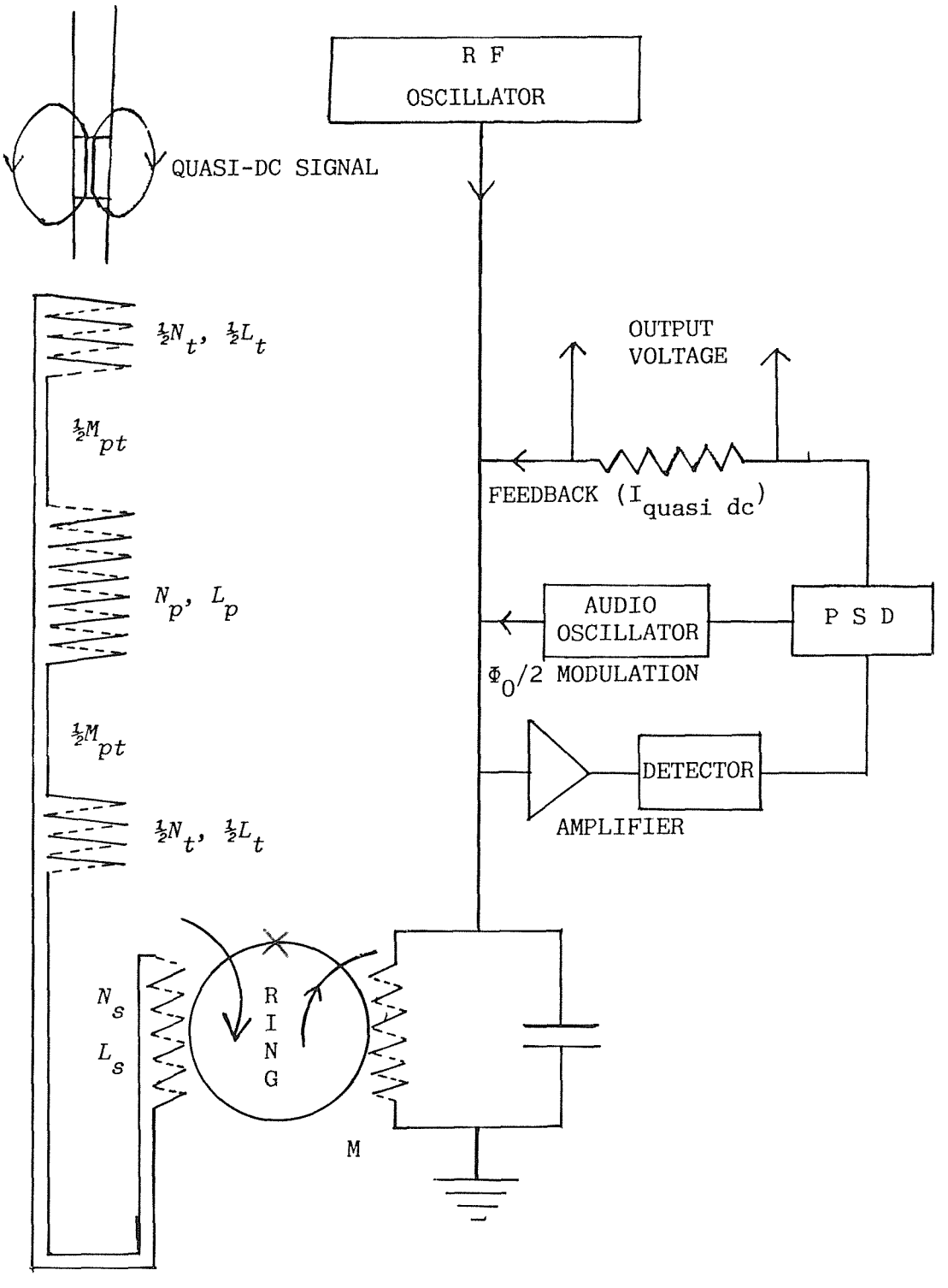

M = SQUID Mutual Inductance

Note the reverse winding of the terminal sub-coils
Coil notation - see text 5.1.7

Fig 5.2 RF SQUID Electronics and Coil Notation

In the highest amplification range (x100) the electronics produced 2.15 V/Φ_0. This value could also be seen in "flux jumps" superimposed on a steady trace. ("Flux jumping" occurs when noise, usually RF, makes it impossible for the feedback electronics to hold the flux in the SQUID ring fixed. It breaks "lock", and then tries to reset itself, often offset by an integer number of flux quanta).

5.1.5 SQUID Protection

Because of the great sensitivity of a SQUID it needs to be electrically screened and free from vibration. In order to make sure that the SQUID could not move in a field we clamped it to the IVC via the support for the signal leads; see fig 5.3. The tail of the IVC containing the pick-up coil hung down the magnet bore so a ring of duralumin was fixed between the tail and bore. (Duralumin was chosen as this was the magnet former material and would clamp onto the copper tail by thermal contraction during cooldown).

5.1.6 The Flux Transformer

The pick-up coil was a second order gradiometer making it insensitive to signals from afar off and consequently less sensitive to external noise. If properly balanced it also has a low response to variations in the magnitude of the high homogeneity field.

The coil was wound from 0.37 mm NbTi wire onto a tufnol former of O.D. = 10 mm. The coil centre was arranged to coincide with the magnet's centre point. Being second order the coil was in three parts. The two outer sub-coils (of 16 turns each) were half the size of the central one (32 turns) and wound in opposition to it. The dimensions of the coil are given later in fig 5.4. The bottom of the tufnol former was supported by a soft solder coated copper bar which was part of the 57 mm basal flange of the IVC tail. The coil former also had three aluminium rings around it, spaced along its length. The niobium screen fitted over these and covered the pick-up coil leads to the top of the copper bar. An adjustable ring (shown later in fig 5.5) was fitted over and around the top of the niobium tube. Its eccentric bolts could then be turned to expand this copper ring, so clamping it rigidly to the walls of the IVC tail.

The wires from the coil travel down through the former support to a low temperature epoxy seal and into the main bath. A diagram of the

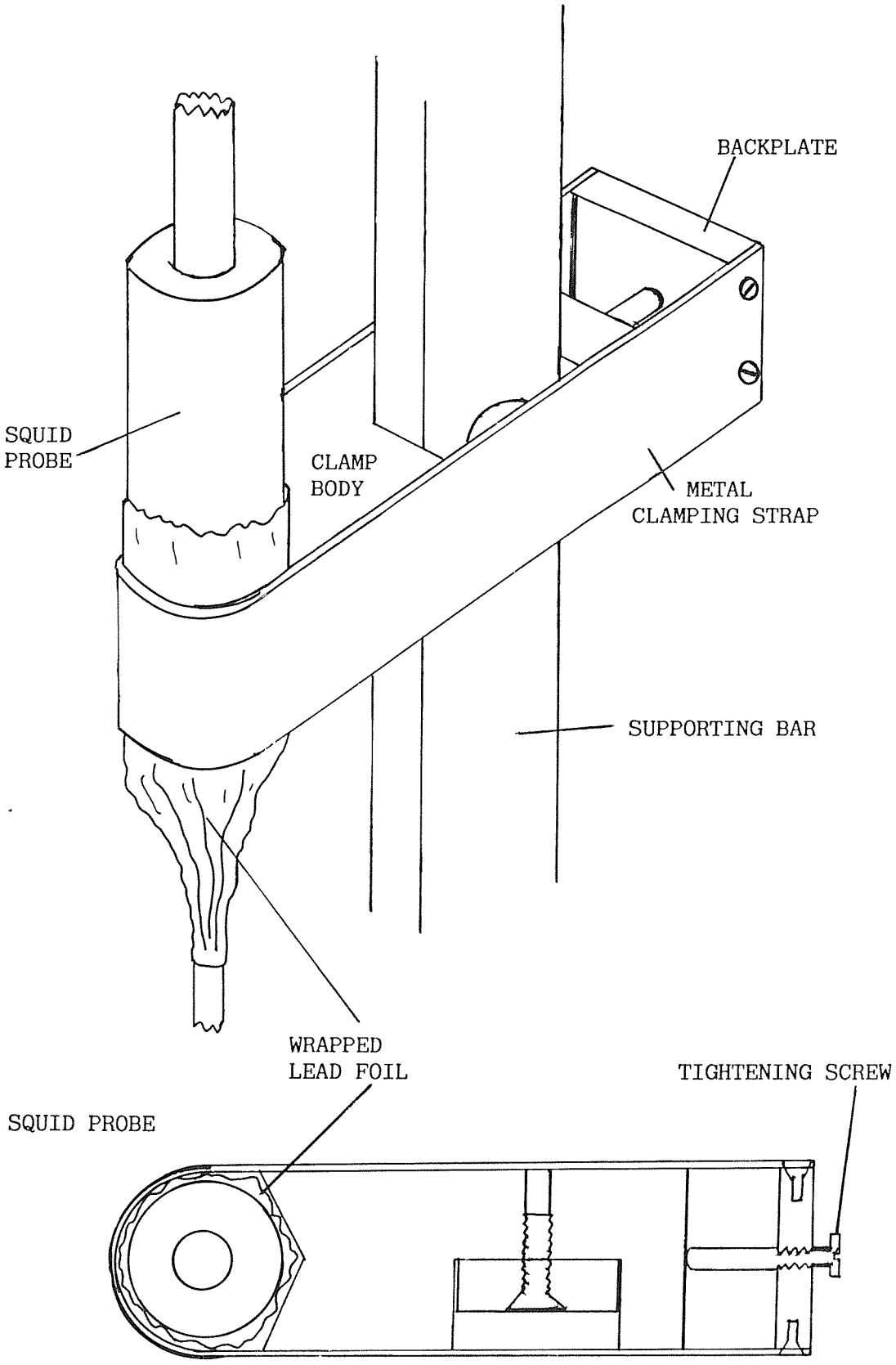

Fig 5.3 The SQUID Clamp

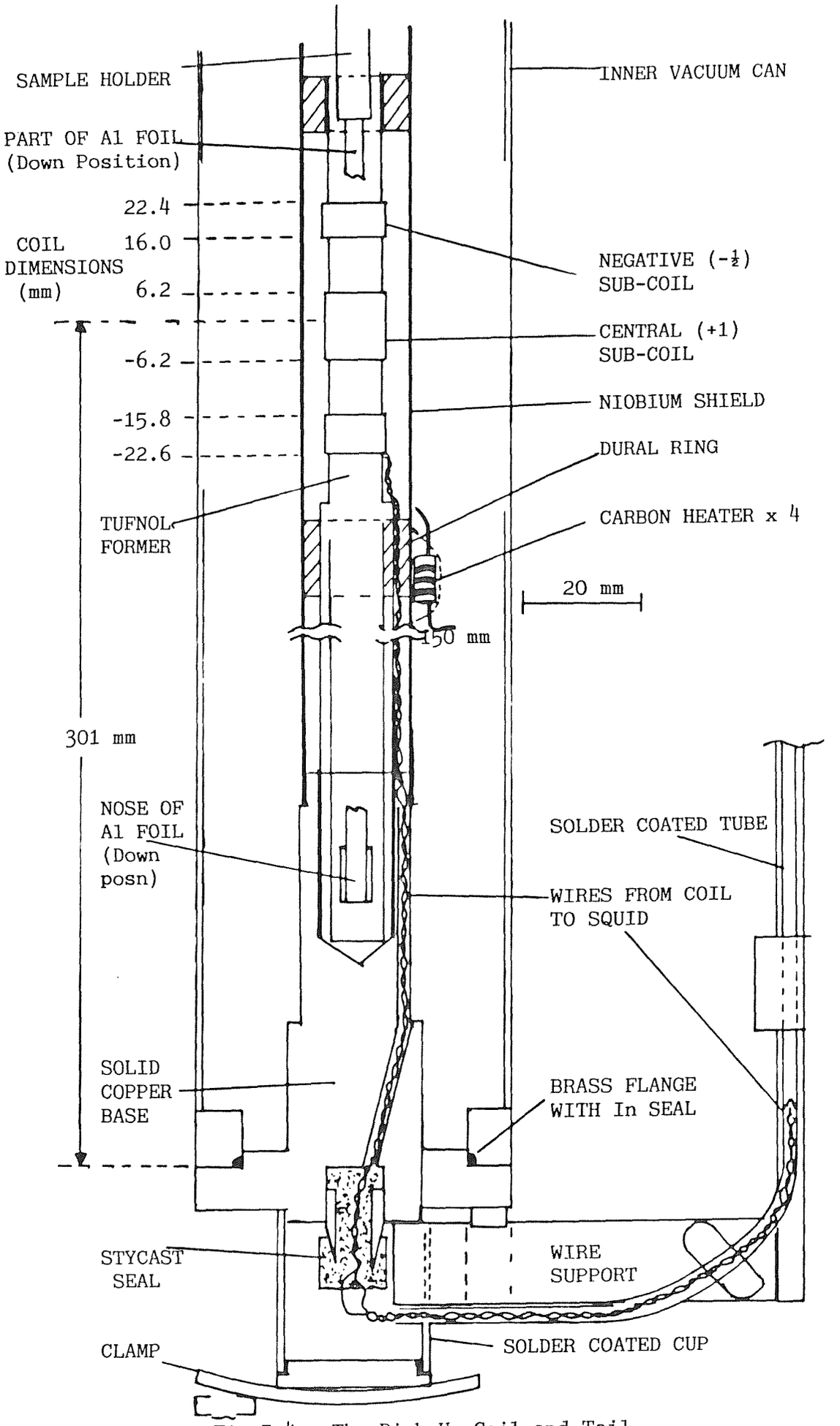

Fig 5.4 The Pick-Up Coil and Tail

coil set and supports is given in fig 5.4.

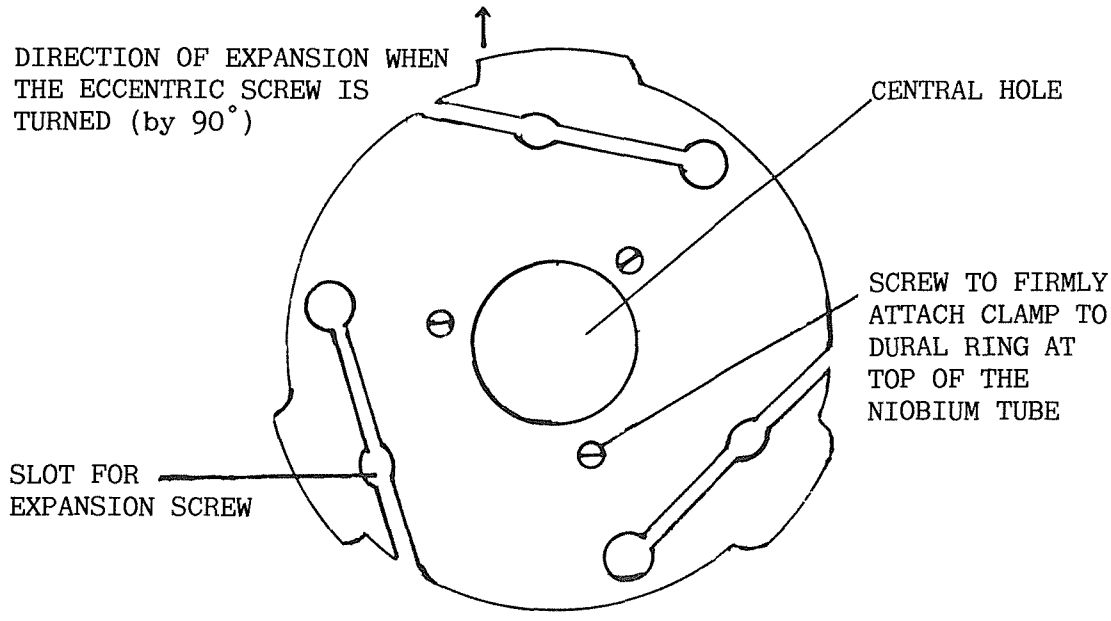

Fig 5.5 Niobium Screen Clamping Ring

The wires travelled up the outside of the magnet in a solder coated copper tube to connect with the SQUID probe. (Solder coated tubes were used by Giffard et al (1972)). The copper tube was mechanically attached to the SQUID probe by a teflon adaptor. The wires were tightly wound together to minimise pick up and further mechanically protected by a teflon sleeve within the tube. (The sleeve was used because some problems had previously occurred with insulation breaking and shorting to the copper tube). Vacuum grease was injected into the tube to provide mechanical packing. Extra electrical shielding was provided at either end; a solder coated copper cup covered the lower end while lead (Pb) foil was wrapped around the connection of the tube to the SQUID probe.

5.1.7 Coupling Factor

Although a flux transformer allows one to couple a signal from a sample in a "high" magnetic field, it can not couple all of the flux to the SQUID. We needed an estimate of the coupling factor for this coil. For a basic flux transformer the equation for the coupling factor had been derived by Claasen (1975) using the fact that the total flux-turns in such a superconducting circuit must remain constant. This equation also assumed that the flux coupled to each loop in the pick-up coil was the same.

Asaolu (1983) extended these ideas to a second order gradiometer. He assumed that the terminal coils coupled a fraction, K'_{pt}, of the flux coupled to the central coil (Asaolu 1983 p127). He also assumed that the sample was at the centre of the coil set and that there was an equal flux coupled to all the loops within each of the sub-coils. (The actual coupling for each loop would be slightly different, but an average value can be taken). Similar to Claasen, Asaolu derived an equation for the coupling factor (his eqn 4.65b) given below in its non-reduced form.

$$\text{coupling factor} = \frac{M N_p (1-K'_{pt})}{L_s + L_p + L_t - 2M_{pt}} \qquad (5.2)$$

where N_p = No. of turns on the central coil
L_s = SQUID input coil inductance
L_p = central sub-coil inductance
L_t = total inductance of terminal sub-coils
and M_{pt} = mutual inductance between the central and terminal sub-coils.

The notation is as Asaolu. The value of all the numbers are positive and any sign changes due to winding orientation have been written down explicitly in the equation. Asaolu derived this equation in passing but made no attempt to evaluate it. This would require knowledge of the various inductances and the terminal/central coupling fraction. We therefore took relevant values from the literature or calculated them in order to obtain a value for the coupling factor.

We obtained a value for the coupling fraction (K'_{pt}) by assuming a small sample in the centre of the coil set and summing the calculated

flux through each loop in the central and terminal coils. This was a one dimensional calculation using a program Flux Couple, based on the program Flux Calc (YO),1; see Asaolu (1983 p164). The total flux for both the terminal and central coils was found and hence their ratio, K'_{pt}. For a small sample $K'_{pt} = 0.029$. However this ratio is dependent on sample size. The above figure is useful for samples up to 2 mm long. In table 5.1 we show the values for different length samples. Of particular interest is the figure for a centrally situated 20 mm sample, where $K'_{pt} = 0.074$, because many of our final LB samples were of this size.

Sample Position/mm	Sample Length/mm	K'_{pt}
±15	30	-0.22
±10	20	-0.074
±5	10	-0.036
±1	2	-0.0293
±0.01	0.02	-0.0291

Table 5.1 Coupling Fraction K'_{pt} as a Function of Sample Length

To calculate the self inductances we need the equation:

$$L = 2\times10^{-7}\ \pi^2\ a\ (1/\beta)\ N_p^{\ 2}\ K(\beta) \qquad (5.3)$$

(i.e. eqn 4.56 of Asaolu)

where a = coil radius

β = reduced length = 1/2a

and where we used the tables of $K(\beta)$ produced by Grover (1946).

(This equation is an extension of the more familiar

$$L = \mu_0\ n^2\ l\ A$$

which may be found in undergraduate texts e.g. Halliday & Resnick (1978), and gives the inductance for a section of an infinite solenoid).

For our central coil

$N_p = 32$, $l = 12.0$ mm, $a = 5.19$ mm and $K(\beta) = 0.7195$

which gives $L_p = 6.53$ μH;

while for one of our terminal coils

$N_t/2 = 16$, $l = 6.0$ mm, $a = 5.19$ mm and $K(\beta) = 0.5611$

which gives $L_t/2 = 2.55$ μH.

This means that the total inductance of the pick up coil is 11.6 μH. (Later we measured this inductance using a four terminal bridge, at room temperature. It gave a reading of 12±2 μH).

The mutual inductance can be calculated from the formula:

$$M = \frac{\mu_0 \pi a^2 a^2 N_p N_t}{2z^3} \qquad (5.4)$$

(Bleaney & Bleaney 1976)

where z = the distance between the coil centres (19 mm) and z>>a (which is satisfied in our coil set). This gives an answer:

$$M_{pt} = 0.107 \text{ μH}$$

(The mutual inductance between the two parts of the terminal "coil" was assumed negligible).

The SHE manual tells us that the mutual inductance (M) between the input coil and the SQUID is 20 μH, while the SQUID's self inductance (L) is 0.5 nH.

We can now substitute these values into equation 5.2, giving us a coupling factor of 4.6%. This can be compared with other quoted values given below, which are all for first order gradiometers:

0.6% - Pelizonne & Treyvaud (1981); but this had been deliberately lowered to get a better S/N ratio.

4.2% - Gramm et al (1976)

1.5% - Cerdonio & Messana (1975)

We assume these coupling factors were experimentally determined and not calculated. We have also used some of our experimental results to obtain a value for the coupling factor. The answer for it was much lower; viz 0.17% (see sec. 6.4). We do not know the reason for this difference.

5.2 NOISE

5.2.1 RF Noise

When the SQUID was originally operated in the cryostat it was found to be very susceptible to RF interference. For example switching on the computer caused excessive "flux jumping". This occurred even though the SQUID was in an all metal cryostat which should screen it. The triangle waveform had a low amplitude confirming that RF interference was occurring even when the SQUID input was supershorted. The SQUID was tested in a shielded external dewar, again with a supershort across its input terminals, and produced the expected 80 mV peak to peak (p.t.p.) triangle pattern from the test signal. The cryostat screen seemed satisfactory until we discovered that the anodised screw cap which compressed the O-ring seal between the SQUID and cryostat top plate was non-conducting. A brass copy was substituted and amazingly the supershorted SQUID gave the full 80 mV triangle pattern. Obviously, either RF had been getting in at the top through this "gap" in the screen or the continuity of the earth had been broken. However when the pick-up coil was attached the triangle wave amplitude fell to 40 mV p.t.p. So a small resistive shunt, of about 2 Ω, was added across the input terminals of the SQUID forming a low pass filter with the SQUID's superconducting input coil. The RF noise reaching the SQUID was reduced and the triangle wave amplitude increased to 60 mV p.t.p.

As the amplitude was not back to the full 80 mV, noise was still entering the cryostat, probably because of the many wires going to the magnet (about 40) and all the thermometers. Because of the number of wires, many of which went down the pumping tubes, no RF filters had been fitted. If a portable RF noise generator (a hot air blower!) was taken near to the point where leads connected to the cryostat then RF noise could be seen on the triangles; particularly when brought close to the SQUID head.

5.2.2 SQUID Response To Magnet & Helium Level

As expected, the SQUID could "see" the energisation of the magnet, and the magnet heater signal as well as the superconducting transition of the shield. At several times during the project we energised the magnet and then left the SQUID observing it in persistent mode. When the magnet was run down we could also watch the field trapped by the

niobium screen alone. Some of the things seen were:

i) For high fields (1 T) if the magnet was not carefully energised, and in particular all the shims fully dumped, then the SQUID signal would not settle down even after several hours. It would drift continually, usually in the same direction. Later when we carefully dumped all the shims we obtained a 1 T field where the SQUID signal drifted by only 2 Φ_0 in eight hours.

ii) Moderate fields, less than the critical field of niobium, could be trapped and supported by the screen alone when the magnet was run down. In one experiment, with the Hall probe in place, 90 mT was trapped by the shield alone and the drift was only a few Φ_0. The major part of the drift occurred when the helium level fell low. We also observed the drift in a trapped 5 mT field when a "semi infinite" piece of aluminium was in place as a sample. Initially for a few hours flux jumping was noted, then it went quiet and there was less than 1 Φ_0 drift in ten hours.

iii) Once the helium level dropped below 60%, the SQUID signal started drifting in one direction. For small fields this would only be noticeable over some hours and the drift would be negligible in the time taken to obtain a flux signal from a sample.

iv) There was some evidence that the SQUID was more prone to RF noise, and therefore more flux jumping, when the helium level was high. It has been suggested that our SQUID might operate better slightly above 4.2 K. We also noticed that it was much easier to get a noise free signal from a sample when the helium level was low. Ishizuka and Tohi (1980) deliberately regulated the main bath pressure because variations in it were affecting the SQUID. Taber and Cabrera (1985) reported substantial reductions in noise from a SHE SQUID when the helium fell below the SQUID probe. Whether the phenomena they describe is the same as ours we do not know. The levels of noise they measured were very small and it did seem dependent on the actual SQUID and cryostat. They attributed the noise to convection cells in boiling helium. This caused thermoelectric currents which were "picked-up" when they were near the input coil, the SQUID or its casing. They greatly reduced the noise by filling the space around the input terminals with quartz microspheres, so inhibiting convection.

v) We also noticed that the triangle waves would sometimes increase in amplitude when the helium level was low. This effect was seen just

after helium began to collect during a cooldown. Triangles of 80 mV amplitude would initially be seen, but after filling they were only 60 mV.

5.2.3 Vibration Noise

The detector's sensitivity to noise was surprising because of the care taken over field homogeneity and the use of a second order coil as well as the large anti-vibration structure that the cryostat was hung from. We investigated the noise by whistling near the cryostat which lead us to believe that the vibration was air-borne as against ground-borne and that the detector was very sensitive at specific frequencies. We set up a loudspeaker within one metre of the cryostat and resonances were seen at over fifteen frequencies under different magnetic fields and helium levels. Resonances increased (non-linearly) in bigger fields with one of the largest resonances around 1150 Hz. This produced a noise signal of $\pm 10\ \Phi_0$, when the field was at 1 T and the "noise level" from the speaker was uncomfortable to stand by. We also noted that bursts of 1100 Hz resonance occurred when the cryostat was tapped. Moving the sample siphon caused all the resonances to occur and the SQUID was unable to track the noise. This vibration noise had, apparently, not occurred in the time of Asaolu. We adjusted several things e.g. extra clamps on the tinned copper tube taking the leads to the SQUID, or we took out the "jamming" ring between the magnet and IVC but the resonances continued. We checked the SQUID itself with a superconducting short, but it gave no noise signal. When we super-shorted the pick-up coil at the point where the leads left the IVC NO vibration noise was detected in a 0.1 T field. This indicated that the noise was generated by or near the gradiometer; probably the gradiometer is vibrating in the magnetic field even with the niobium shield still superconducting. This suggests that the pick-up coils could vibrate with respect to the niobium screen as well as the magnet. The IVC tail resonance occurred at the wrong frequency (100 Hz) to produce the noise.

5.2.4 Room Temperature Noise Detection

Calculations suggested that it might be possible using a nanovolt amplifier, with "lock in" detection to see the noise source at room temperature. The coils were re-connected to the amplifier and a large resistive coil was hung in place of the superconducting magnet. The

magnet was run at 10 mT and to produce vibration a mechanical oscillator was touched against the cryostat. We were only able detect a vibration induced magnetic signal at around 985 Hz and 1050 Hz. This was found by watching the output as the frequencies were slowly stepped through. Holding at this frequency, the magnetic field was varied and the signal was found to respond proportionally, giving evidence that it was magnetic pick-up. (Initially there were problems of electrical noise pick-up). We tried clamping parts of the niobium shield, but did not get any useful changes.

Overall we had detected some vibration noise at room temperature but apart from identifying the bottom loop as a possible source, we had not solved the problem. We decided to change the bottom of the coil former and remake the superconducting wire joint and the low temperature seal. The original leads had the disadvantage of forming a loop which might be vibrating in the magnetic field, which was inhomogenous at the bottom of the IVC.

At this time we made up a small test coil, on a support rod, and drove it through the pick-up coil. An a.c. signal was applied to the test coil, which was detected by our pick-up coil and lock in amplified. This produced a room temperature approximation to the pick-up coil "instrument function"; see fig 5.6.

5.2.5 New Coil Base

The original support to the tufnol former was made from a brass tube which connected the former to the brass flange at the bottom. As we had doubts about movement of the gradiometer leads this tube was replaced with a solid copper bar which had a recess at the top into which the tufnol was glued. A narrow hole was drilled obliquely half way up the copper tube from the bottom end. The leads from the pick-up coil went through this hole to the seal. The design of the new base was shown in fig 5.4. Some other changes were incorporated in the new design. A lip was formed around the top of the copper bar, over which the niobium tube could be pushed/forced, giving a tight fit. This had the added advantage that the niobium tube could cool much faster in a vacuum, because of the direct connection to the main bath. A new clamp which gripped on both the inside and outside of the top of the niobium tube was introduced. This was bolted to the adjustable copper expansion clamp which opened up within the IVC to jam against the

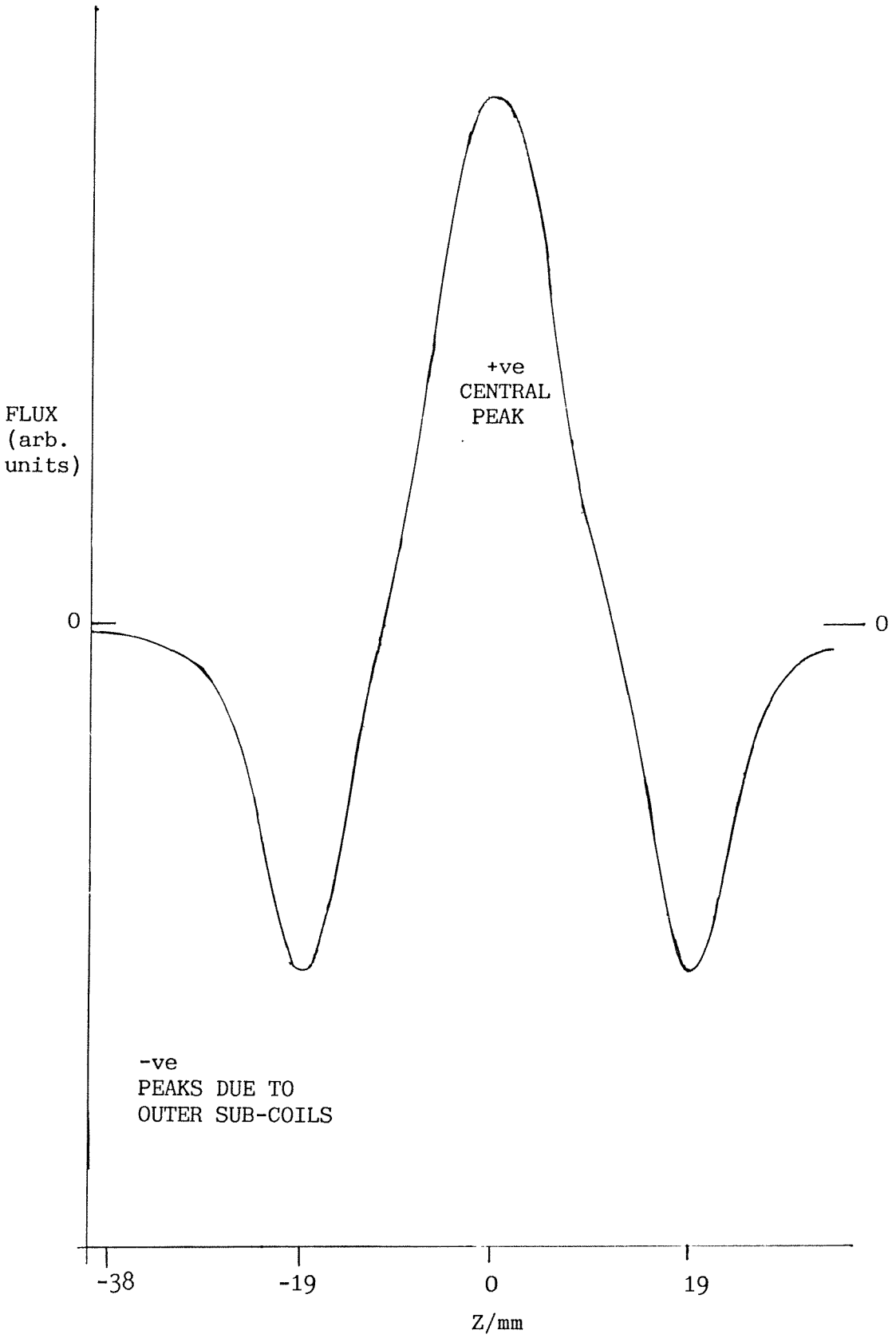

Fig 5.6 Room Temperature Instrument Function (Small Coil Response)

wall; see figs 5.7 & 5.5. At the same time the actual pick-up coils were re-varnished and the aluminium spacers re-glued. This was all aimed at reducing the possibility of relative movement. (We also re-measured the coil dimensions and their position with respect to the base flange. The corrected values are given in fig 5.4).

We used Stycast 2850 GT for the seal which filled the recess at the base of the former. Below the seal a new clamp was added to hold the copper cup which shielded the seal. A new bar was made to support the tube carrying the wires to the SQUID and was clamped more firmly to the IVC.

5.2.6 Results on Re-assembly

After the modifications to the coil support it was re-assembled to the cryostat. However the first cooldown showed that we had a resistive flux transformer and only a.c. signals were detectable. One of the spot welds at the IVC seal had to be re-made to produce a superconducting circuit. It was also found that our Stycast seal was leaking at 4 K so it was re-made around a knife edge. The knife edge was formed at the end of a small copper tube which had been soldered into the recess at the base of the copper bar. This seal held. (Recently a new type of low temperature wire seal, using indium and varnish, has been described by Kessel and Sapp (1986)). The sliding assembly was also altered to reduce friction. This meant that it would be pulled up slightly higher; so the throw of the sample was re-measured as just over 57.1 mm using our cathetometer. (The unhindered contraction of copper between 295 K and 4 K might reduce this by 0.15 mm).

The cryostat was now re-cooled but unfortunately tests for the noise showed that it was present, though the amplitudes seemed less. Probably we had failed to lock the flux transformer to the magnetic field trapped by the niobium screen. The aluminium rings may contract sufficiently to allow the tufnol and the coil to vibrate within the shield.

Using our sample drive motor we could set a steady speed, at which the sample was driven in or out. Then the SQUID output was fed directly to a chart recorder. When a small copper rod was introduced into the pick-up coil the SQUID detected a greater amplitude of vibration noise. Since the sample is hanging in the coils some vibration of it

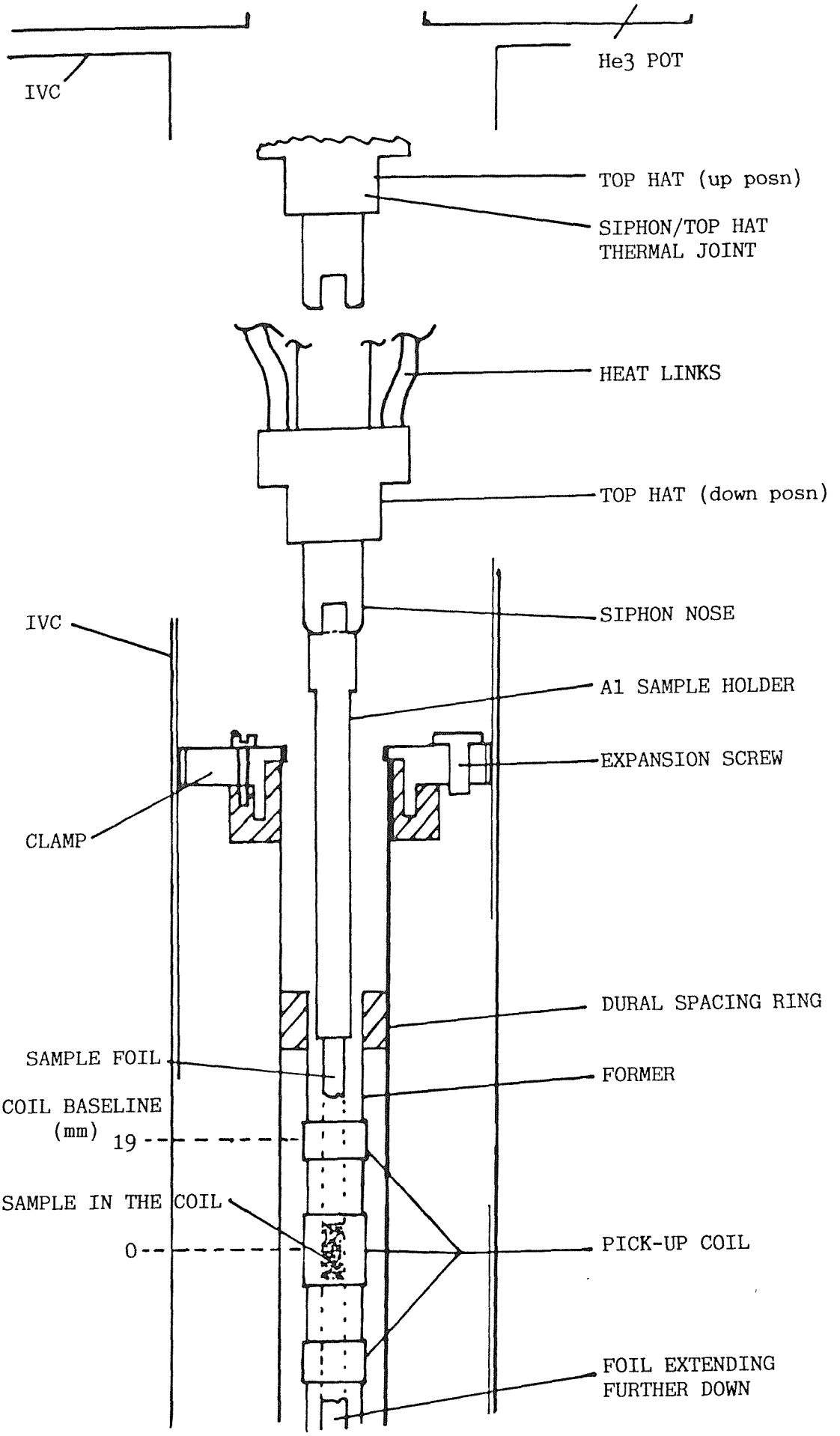

Fig 5.7 The Sample in the Down Position

must be inevitable. It was decided that the maximum usable field would be 10 mT. Moving the copper sample in and out appeared to produce a repeatable signal though often with vibration noise superimposed so we had to repeat the measurement in order to get one "good" result.

5.2.7 Flux Pumping

After some experience running the cryostat, we discovered that we had to be careful whether we set the SQUID in FAST, MEDIUM or SLOW mode. The FAST mode could pick up RF noise leading to repeated flux jumping, while the real signal remained steady. But if there was other noise, then in SLOW mode, and sometimes MEDIUM, the SQUID could not track it and the signal produced was meaningless. Sarwinski (1977) explains that for a detector to be able to track a specific signal, the SQUID must be able to track all the signals present at the input, including the noise.

It was the realisation that SLOW mode could not always follow the signal, that explained an apparent phenomena of "flux pumping" which was observed in some of the results of Asaolu (1983). In these the signal continued increasing in the same direction on both withdrawl and insertion of the sample. One would have expected the signal to be re-traced on reversing the direction of the sample movement. We obtained a similar effect when large amounts of vibration noise occurred and the SQUID was in SLOW mode and the field was 0.1 T. It could not follow this but if any filter was in, or the signal was being monitored by just the computer, one might not notice this. The SQUID signal goes off in one direction only - an artifact of the electronics and nothing to do with the signal. The magnitude of the sample signal also depended on the speed the sample was moved; faster speeds meant a smaller magnitude.

Flux pumping might also explain why Asaolu did not notice the vibration noise. Perhaps it was there but masked. Now it has been made worse by the "stickiness" of the new sample siphon. It is a great pity that the first siphon had been ruined by the use of incorrect materials during manufacture.

5.3 THE SAMPLES AND HOLDER

5.3.1 Substrate Choice

Two dimensional molecular films are incapable of supporting themselves, so a substrate must be provided and ideally the substrate should be magnetically "invisible". Although we can never obtain total invisibility, we used three methods to approach it:

i) We required a substrate of as low a bulk as possible, so reducing the amount of magnetic material there.

ii) We required a substrate that was as close as possible to being "non-magnetic".

iii) We used the second order gradiometer characteristic to cancel out the background substrate, by making it long and uniform.

In practice we had to modify these approaches, as they conflicted with practicalities e.g. a substrate needs to be suitable for the formation of Langmuir Blodgett (LB) films and a reasonable heat conductor at low temperatures. Furthermore, the substrate must be physically strong and large enough to provide a detectable signal from the LB film.

The initial samples of Asaolu did not fulfil these requirements. So he introduced the concept of a "Minimum Support System". This consisted of a long thin piece of glass, which was evenly aluminised, with the LB film deposited only on a central section over a 10 mm length. (See fig 6.13 of Asaolu 1983). However the composition of glass can not be easily controlled increasing the possibility of impurities. Glass also has a much higher susceptibility than the elements silicon, copper or aluminium (Asaolu 1983) which are other possible substrates. Furthermore the glass and aluminium film would not provide a good heat conduction path to the sample and it would be difficult to get reproducible and even aluminisation over that length. Finally we would only get 4 cm^2 of LB sample, making detection difficult when the number of layers is small. So we set out to improve the implementation of the "Minimum Support System".

We considered a variety of other substrates and their associated sample holders including a pure aluminium plate or tube. Since aluminium was needed to get a good film why not dispense with the glass? In addition the aluminium would be a good heat conductor, except when it went totally superconducting. A tube is naturally

stronger than a plate but, though there is an increase in surface area by a factor of π, only the outside can be used, while on plate two sides are available for deposition. The real advantage of a tube comes from its strength/thickness ratio and a possible reduction in the size of the substrate signal. It is also a better symmetry match to the pick-up coil, which has a response slightly dependent on the radial position of the sample as well as its z position.

To reduce the background signal we wanted as thin a substrate as possible, which led us to consider a tube of very pure aluminium foil. If we rolled a sheet of this up, to form a light but sturdy tube we would increase the magnitude of the overall signal because a much larger area could be coated.

5.3.2 Susceptibility

When considering the material from which the sample substrate and sample holder were to be made we needed some idea of their susceptibility at 4 K. For example mylar is very thin and strong and was used by Asaolu (1983) as an outer shield to the sample. However it has the disadvantage of a high susceptibility. Asaolu had found some susceptibility values for other materials so we extended the literature search enabling us to produce a new table of susceptibilities. We have summarised these values in table 5.2.

Both copper and silicon have the lowest susceptibilities and are diamagnetic which can be an advantage when looking for the weak paramagnetic signal expected from a LB film of $MnSt_2$. However supposedly "pure" copper can contain a significant amount of iron impurities, as seen in a force balance used by some of our colleagues. The compound quartz is generally considered to have a low magnetic susceptibility (see Pomerantz 1980 and Swithenby 1980). Meanwhile aluminium has a reasonable value for susceptibility and from Steelhammer and Symko (1979) we found that any magnetic impurities present do not "clump" together to form a net magnetisation, due to the trivalent nature of aluminium. Swithenby (1980) also remarks on the surprising suitability of aluminium as a possible construction material within SQUID magnetometers.

The magnetometer works on a cold finger basis so only the signal from the sample, its holder and the siphon will change as the sample is moved, or its temperature altered. The siphon is made from

	TEMP/K	$\chi/10^{-6}$SI	REFERENCE
Al	4.2	24.1	HEDGCOCK & LI (1970)
	296	28.2	HEDGCOCK & LI (1970)
	room	20.1	LAKNER (1977)
Cu	1.45	-7.54	BOWERS (1956)
	4.2	-8.64	BOWERS (1956)
	300	-9.30	BOWERS (1956)
	298	-9.62	GRUBE & WACHTEL (1976)
Si	"low"	-6.6	HUDGENS, KASTNER, FRITSCHE (1974)
	room	-4.1	"Rubber Handbook" 55th Ed.
quartz	6.4	-13.7	HURD (1965)
	4	72	SALINGER & WHEATLEY (1961)
Ag	room	-23.9	"Rubber Handbook" 55th Ed.
Au	4	-33.9	Physica 61,389
	room	-34.9	"Rubber Handbook" 55th Ed
GE varnish	4	21	SALINGER & WHEATLEY (1961) & ρ(GE Varnish mix)=0.85g/cc
mylar	4	886±150	SALINGER & WHEATLEY (1961) & ρ=1.40g/cc

Table 5.2 Susceptibility of possible Substrate Materials

"non-magnetic" austenitic steel, and the detector can only "see" over a short range, so the siphon should not contribute to the signal. For the holder and the substrate we have to be more careful in our design and choice of materials.

5.3.3 Aluminium Foil

The first test of the feasibility of aluminium was made using household foil obtained from a supermarket. We were led to believe that this foil would be 14 µm thick (±<1%), 98.5% Al, 1% Fe (!) with some Si and Mn. We also discovered that the foil was extruded in doubled over sheets. The shiny side was outermost and in contact with the steel rollers, while the dull side faced the other half of the sheet. There was also a possibility of organic residue on the foil from the processing.

The methods for cleaning the foil and depositing LB films on it have already been described in chs 2 & 3. We had chosen foil sheets of size 350 x 150 mm and to get a tight tube "gloved finger contact" was needed to roll the foil around a former. An aluminium welding rod, of diameter 3.1±0.1 mm was used for this. The foil with its LB sample on its top surface was laid upon a larger cleaned sheet of aluminium placed on a work-top. The foil was then rolled up in about thirty revolutions by hand, but wearing cleaned gloves. Inevitably there was a small air/crinkle gap between the layers. Attempts to do the rolling indirectly, e.g. by holding at the ends of the rod failed. Once rolled up the rod was slid out. (This usually required one reverse turn on the rod to loosen it from the innermost roll of the foil). After making several foils we found the outer diameter came to 4.1±0.1 mm.

5.3.4 The Clip and Holder

Using very pure aluminium rod (99.999% from Goodfellow Metals) we bored out a short thin tube (o.d. = 5 mm) and very slightly cut a thread (M4.5) on its inside. This tube could then be slid/screwed over the bottom end (or nose) of the foil to strengthen it and hold it together. This tubular clip gave us something reversible so that we could roll an uncoated foil, measure it in the magnetometer and then unroll it to deposit a film before re-rolling it to measure the actual film. However this nose piece was a break in the uniformity of the foil, and in many of the final sample foils it was left off after it had been found unnecessary. Instead the end was gently crimped to make a firm, tapered, nose. In the actual experiments before we used foils with LB samples deposited on them we measured some uncoated foils. We found that the signal from a properly cleaned foil was negligible, so they could be "irreversibly" rolled (i.e. crimped) after the sample had been deposited.

To connect the foil to the sample siphon another piece of pure aluminium rod was used. A large diameter head (8 mm) increased the thermal contact with the copper siphon nose, but below this the rod was thinned down (o.d. = 6 mm) and drilled out (i.d. = 4 mm) to reduce its signal. The inside of this holder was lightly threaded (M4.5) at the bottom allowing the foil to be "screwed" into the holder - a case of "inverted self tapping". This joint was strong enough for our purposes and had the advantage of being magnetically clean. The sizes of the substrate foil, the holder and clip are given in fig 5.8.

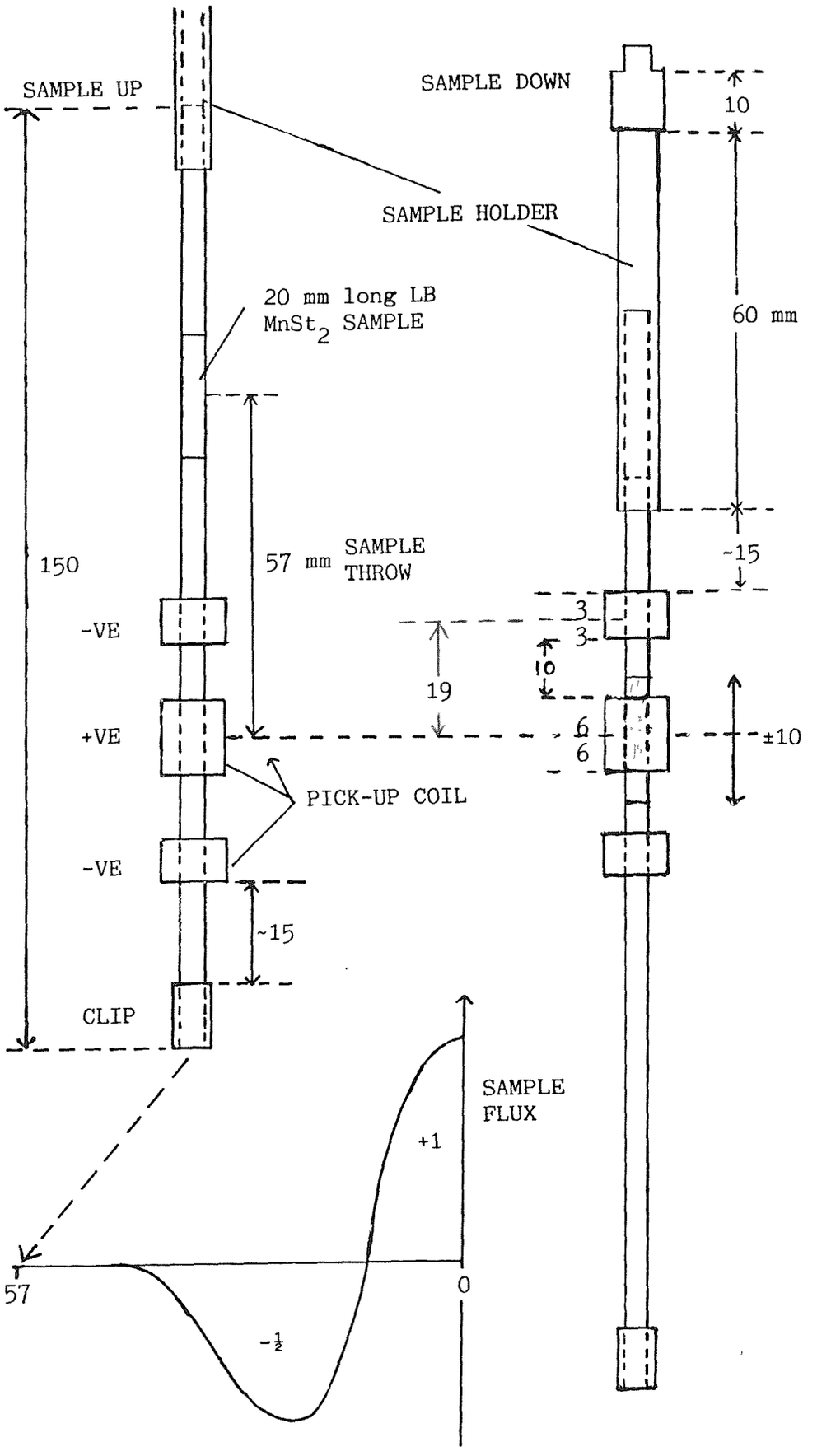

DIMENSIONS: mm (approx scale 1:1)

Fig 5.8 The Aluminium Foil Sample

We tested the loading of these foil tube samples at room temperature and discovered that some of them would catch on loading, consequently crumpling and jamming up. If this were to happen at 4 K it would imply a warm up to clear the blockage. In fact, all our LB samples survived, but when a foil carrying a layer of bulk $MnSt_2$ was loaded it caught and jammed. (This might have been due to some squashing of the tube, done to this sample only, to help contain the powdered $MnSt_2$ which could have caused a loss of strength). The jammed sample meant the termination of our experiments.

5.3.5 Optimum Sample Length

To decide on the sample length we developed two sample simulation computer programs; see secs. 6.2 & 6.3. These programs were run to calculate how the central peak signal varied with sample length. For the dimensions of our gradiometer they produced an optimum value for a 22 mm long sample (i.e. ±11 mm about the coil centre). We decided to dip samples to the slightly shorter (and therefore easier) 20 mm length.

To decide on the length of the foil substrate we had to take into account both the cryostat's dimensions and the trough's, as well as the length of the actual LB sample. To fulfil the constraints of both of these the 20 mm sample was deposited 40 mm from one end of the foil. So when the LB sample is fully inserted into the centre of the coil there is about 15 mm between the top of the pick-up coil and the pure aluminium sample holder. (See fig 5.7 of the sample in the down position). This is just enough not to be "seen" by the pick-up coil. It also suggests that we should start the foil (from the up position) with an equivalent 15 mm projection of unadulterated foil below the bottom of the pick-up coil. The limited depth of the trough means that the sample holder has to be 70 mm long overall. If the trough was deeper, the holder could be made shorter and then the foil could be made longer in both directions, so reducing background end effects.

5.3.6 Calibration Samples

In order to turn the SQUID's signal into sample magnetisations we needed a calibration sample. This was because:

i) We could only estimate the coupling factor between the pick-up coil and the SQUID

ii) There could be deviations from the idealised winding of the

pick-up coil.

We reviewed how others had calibrated their magnetometers. Some workers used spheres of niobium or lead to produce a signal with $\chi = -1$ e.g. Nave & Huray (1980); but then the signal can be too large, and there may be problems of trapped flux in the superconductor. Alternatively Cukauskas et al (1974) used a known signal coil, similar in shape to their sample. Steelhammer & Symko (1979), working at lower temperatures than us, used the nuclear paramagnetism of aluminium to obtain their calibration. Other suggestions have been semi-infinite wires of niobium. (In this a long piece of wire is partially introduced into the pick-up coil and the peak value used). The shape of a calibration sample was important because any demagnetisation factor is shape dependent as well as the coil response being slightly shape dependent. Ideally any calibration sample should have the same shape as the sample under study.

With the change to the foil system, and the availability of pure aluminium rod, we decided to use a "semi-infinite" bar of aluminium to provide a calibration sample. ("Semi-infinite means a sample that starts in the centre of the pick-up coil and continues outside the coil end for a long distance, beyond detection range). A more ideal 20 mm strip of pure aluminium foil rolled up inside a foil tube was not available to us. However as a variant of this, an aluminium foil containing an extra 20 mm wide strip of the ordinary foil, in place of the LB sample, was measured. We could then compare its signal shape and amplitude with that from a LB sample and from computer simulations; see 6.4.5 & 6.5.1. With long samples the demagnetising factor becomes very small along their lengths. (The only problem with very pure aluminium is its softness. A rod of it can be easily bent between one's fingers). The semi-infinite rod had a 7.5 mm diameter and was 106.1 mm long.

The preparation of the LB 101 layer, 11 layer, bilayer and monolayer samples has already been described in chapter 3. We also produced a semi-infinite aluminium foil. The experimental results from these samples are described in sec. 6.4.

CHAPTER SIX - SIMULATION & RESULTS

6.1 ESTIMATION OF SIGNAL SIZE

6.1.1 The Paramagnetic Moment of Free Ions

To estimate the magnitude of the expected signal we firstly worked out the magnetic moment: For a paramagnetic collection of free ions we estimate a theoretical magnetic moment by calculating the normalised sum of the ions states multiplied by their probability of occupation, the sum being over the magnetic quantum number. This leads to the Brillouin function, the derivation of which is given by Bleaney & Bleaney (1976). For B/T <<1 this can be simplified giving a result for the magnetic moment (μ) of:

$$\mu = \frac{Ng^2J(J+1)\mu_B^2B}{3kT} \qquad (6.1)$$

where μ = total magnetic moment
N = total number of ions
J = total angular momentum
μ_B = Bohr magneton
B = applied field
k = Boltzmann's constant
T = temperature
g = Landé g factor

(The magnetic fields used in our experiments satisfied the low B/T requirement).

In three dimensions (3-D), $M = \mu/V$ and $\chi = M/H$ where M is the magnetisation, V is the volume, χ is the susceptibility and H is the field (in A/m). These concepts can also be used with LB films, though with some modification. The difficulties in accommodating the third dimension used in the normal definition of M and χ can be overcome by careful formulation.

6.1.2 Volume and Bilayer Susceptibilities

Consider the whole $MnSt_2$ multilayer (or single bilayer) as a three dimensional (3-D) object, then;

$$M = \mu/V \quad \text{implying} \quad M = \mu/Atb$$

where A = bilayer area
b = no. of bilayers
t = bilayer thickness, 5 nm for a stearate bilayer

In this equation we are effectively smearing out the total magnetic moment (mainly due to the Mn^{2+} ions) over the whole of the layers.

Since $\chi = M/H$ we have $\chi = \mu/HAtb$ (6.2)

We now introduce

$$n_b = N'/A$$

as the bilayer ion density (or planar density), where N' is the total number of ions in a bilayer and A is its area. If we substitute into eqn 6.1 and 6.2 and use $B = \mu_0 H$ we obtain the "volume susceptibility" (χ_V):

$$\chi_V = \frac{n_b g^2 J(J+1)\mu_B^2 \mu_0}{t \quad 3kT} \tag{6.3}$$

For LB samples the number of bilayers is a more useful concept than the actual thickness. So, alternatively, we can write an equation for the bilayer magnetisation M_b:

$$M_b = \mu/bA$$

then substitute for μ and N using $N = n_b Ab$
where N is the total number of Mn^{2+} ions in a multilayer.
Dividing by the applied field we get the "bilayer susceptibility" (χ_b):

$$\chi_b = \frac{n_b g^2 J(J+1)\mu_B^2 \mu_0}{3kT} \tag{6.4}$$

(If we wanted to include a single monolayer we can consider this as 1/2 a bilayer).

6.1.3 Magnetic Moment of Manganese Stearate

Using LB layers of $MnSt_2$ Pomerantz (1980) measured the spin parameters and lattice dimensions. The latter leads to a planar density of 5.33×10^{18} Mn ions/m^2 (Asaolu 1983). So we have:

$n = 5.33 \times 10^{18}$ ions/m^2

$g = 2$

$J = S = 5/2$

$\mu_B = 9.27 \times 10^{-24}$ J/T

$\mu_0 = 4\pi \times 10^{-7}$ H/m

$k = 1.38 \times 10^{-23}$ J/K

and $T = 4$ K say.

substituting into eqn 6.3 gives the volume susceptibility χ_V:

$$\chi_V = \frac{5.33 \times 10^{18} \times 4 \times (35/4) \times (9.28 \times 10^{-24})^2 \times 4\pi \times 10^{-7}}{5 \times 10^{-9} \times 3 \times 1.38 \times 10^{-23} \times 4}$$

$$= 2.4 \times 10^{-2}$$

or the bilayer susceptibility $\chi_b = \chi_V t$

$$= 1.2 \times 10^{-10}.$$

So we can now estimate the bilayer signal in a 1 mT field at 4 K.

Normally $\mu = \chi HV$

for our LB sample $\mu = \chi_b HbA$ and using $H = B/\mu_0$

for 1 cm^2 of bilayer $\mu = \dfrac{1.2 \times 10^{-10} \times 10^{-3} \times 10^{-4}}{4\pi \times 10^{-7}}$

$$= 9.5 \times 10^{-12} \text{ Am}^2$$

If the same size sample went ferromagnetic, a simple calculation of the signal would produce

$$\mu = nJg\mu_B bA = 2.4 \times 10^{-8} \text{ Am}^2$$

which is a bigger signal by a factor of 10^{-3}.

Both of these can be compared with the signal from a similar area of substrate. Consider 1 cm^2 of pure aluminium foil, of thickness 14 μm and susceptibility χ of 2.4×10^{-5} at 4 K under a field of 1 mT then:

$$\mu = \frac{\chi AtB}{\mu_0} = 2.7 \times 10^{-11} \text{ Am}^2$$

This indicates that the LB films should be detectable against the aluminium background (assuming the theoretical calculation for the susceptibility of the manganese stearate is applicable).

6.2 COMPUTER SIMULATION

6.2.1 One Dimension

The first sample simulation program used in this project has been described by Asaolu (1983). This was a one dimensional (1-D) calculation, with the sample assumed to be concentrated on the z axis. The program ignored the responsivity of the pick-up coil as a function of radial position, and no allowance was made for the superconducting shield effect. It also assumed that the sample diameter was fixed at 8 mm. The initial program was upgraded and transferred to a BBC computer. This 1-D program was used to estimate the signals from various samples such as a semi-infinite piece of aluminium, or a 10 mm length of niobium rod and as well as calculating the best sample length to maximise the signal. These early 1-D calculations and the later 3-D calculations all made use of the principle of reciprocity (Mallinson 1966 and Asaolu 1983). This relates the signal detected by a pick-up loop, from a magnetised sample, to the magnetic field the sample would experience if instead, a unit current was passed through the pick-up loop.

The next step was to introduce a three dimensional sample simulation program. By assuming an axially symmetric sample we could transform the problem into one of calculating the mutual inductances between several coils.

6.2.2 Garrett's Equations

The equations for calculating the mutual inductance between co-axial coils have been derived by Garrett (1963), following the work of Snow (1939) and Jones (1898). Of relevance here are Garrett's eqns (8) and (9), viz:

$$M(S,S) = zM(S,L)+(2/3)\mu_0 arr_1[K-(2/k^2-1)(K-E)]$$

and (6.5)

$$M(S,L) = \mu_0 z[r_1(K-E)-(a-r)^2(Q-K)/r_1]/2$$

where:

a = 1st coil radius and $r_1 = (a+r)^2+z^2$

r = 2nd coil radius while z = distance between "coil ends"

$\mu_0 = 4\pi x10^{-7}$

K = the complete elliptic integral of the 1st kind

E = ... 2nd ..

Q = ... 3rd ..

It is important to realise that Garrett's equations are given for unit current and unit turns per metre. To obtain the mutual inductance between two solenoids one must combine the four values of the M(S,S) function, obtained by substituting for z the four different coil end separation lengths; see fig 6.1.1. For further details and diagrams see Montgomery (1969).

Using the associated eqn (12) from Garrett we also calculated the axial field within a solenoid to check the program's accuracy, by comparing its results at special points which could be calculated from simple formulae. We were also able to re-derive the equation for the radial field:

$$B_r(S) = \{-i_L/(2\pi rL)\}M(L,L)$$

It is used in 6.3.2.

All these equations make use of elliptic integrals of the 1st, 2nd and 3rd kind, which were calculated in our programs using Hasting's approximation (Abramovitz & Stegun 1964). The computer code for these was produced by G. J. Daniell (Physics Dept., Southampton University) and the results of this code were checked against the tables of Abramovitz and Stegun (1964).

Further checks were made by calculating the mutual inductance using our implementation of Garrett's formulation and the simple equations from Bleaney and Bleaney (1976) as well as the more accurate tables of Grover (1946). Three examples using our implementation agreed within 3% with results obtained using Grover's method.

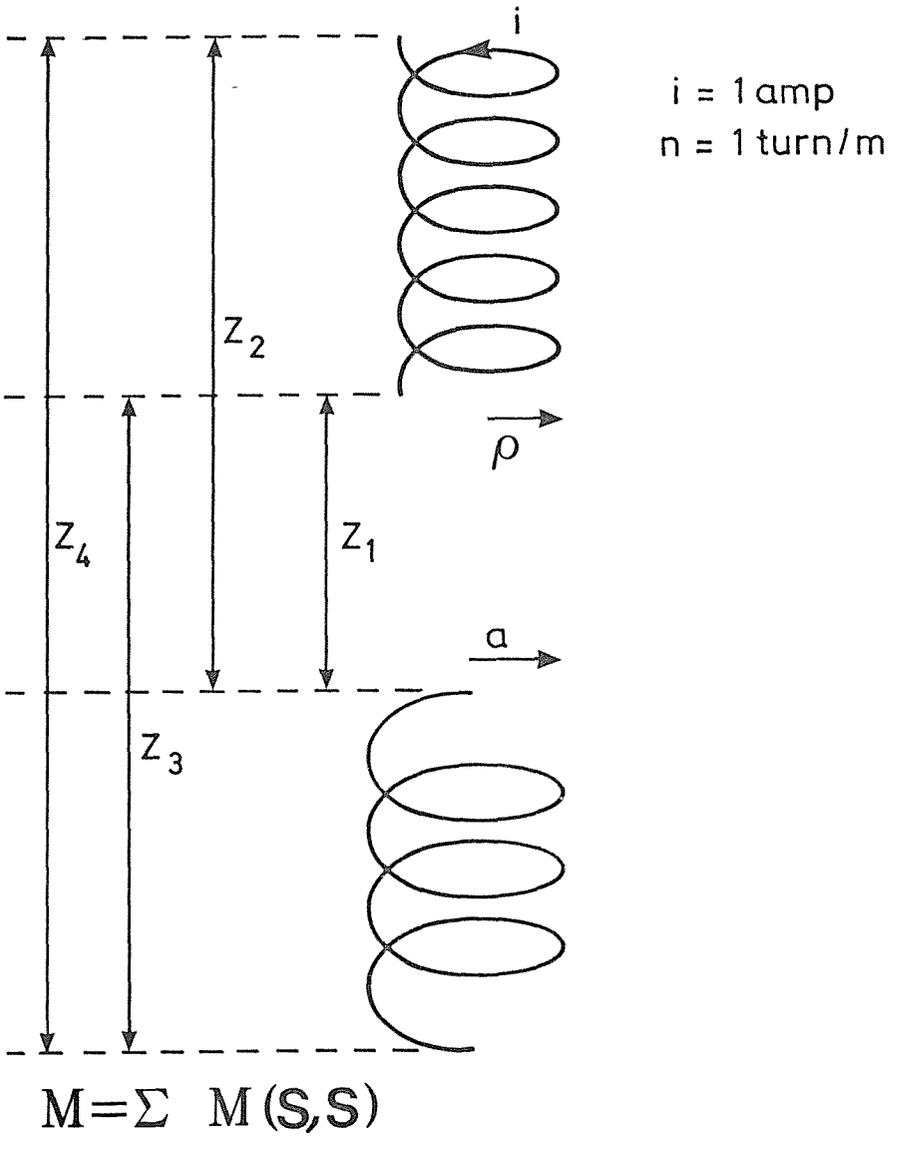

Fig. 6.1.1 Calculating the Mutual Inductance for Two solenoids

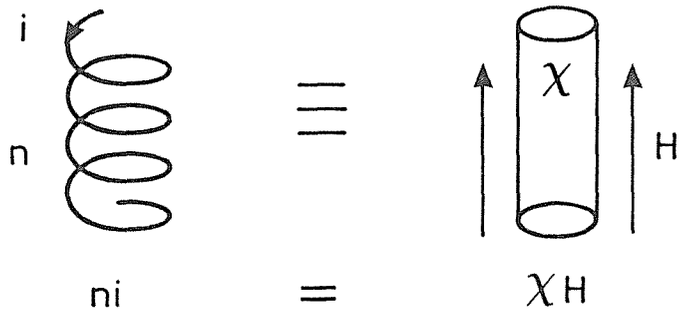

Fig. 6.1.2 Solenoid-Sample Equivalence

Fig 6.1 Solenoid and Sample Calculations

6.2.3 Transformation from Sample to "Coil"

To use Garrett's equations we assumed that our solid samples could be represented as solenoids. This transformation is based on the equivalence of the magnetic moment that is produced by a current carrying solenoid and a uniformly magnetised cylindrical sample; see fig 6.1.2. The magnetic moment (μ) for a solid and a solenoid are given, respectively, by:

$$\mu = MV = (\chi)HV \qquad \text{and} \qquad \mu = Anil$$

where

M = sample magnetisation	A = solenoid area
V = .. volume	n = no. of turns/m
χ = .. susceptibility	i = solenoid current
H = applied magnetic field	l = .. length

n.b. lA = V and nl = N; where N is the total number of turns in the coil. Combining these two formulae:

$$\chi H = ni$$

Thus we can replace ni in the solenoid formulae by χH when we are representing a solid sample.

6.2.4 The Three Dimensional Programs

We tested our BBC BASIC version of "FLUX 3D" by comparing calculations of samples split into two or three parts, each being separately calculated, with the results for the parts considered as a whole. We also compared it with our 1-D program which gave similar results (within 10%) but, as expected, not the same. Further checks suggested that rounding errors on the BBC computer were significant and that there was a maximum limit for the furthest part of the sample from the pick-up coil of 250 mm (sample diameter 8 mm). It was decided to set the upper limit at 106 mm because this was the distance to the bottom of the sample siphon.

The rounding error problem was overcome, and the run time improved, by translating the BBC BASIC program into FORTRAN and running it on an ICL 2970 computer. This program was found to be reliable and could be used accurately for any single layer coil, not encompassed by a superconducting screen. It also showed that for samples of radius 1 mm

or more the BBC version was accurate to three significant figures or more. (The BBC program had the advantage that the results could be easily displayed graphically on both screen and printer). The BASIC version of FLUX3D is printed out in Listing 1. For a simple 4 mm radius sample there was a 6% difference between the results from the one and three dimensional programs run on the 2970.

6.2.5 Development

The next development in sample simulation was to alter the program to allow different parts of the sample to have different radii. Following this we calculated the three dimensional signal that would come from tubular samples e.g. aluminium foil. These foil tubes had an inner and outer radii and the result was calculated using superposition; two values for solid samples of radii equal to the inner and outer radii were calculated. Then the value for the thinner sample was subtracted from the other. (The programs produced for the BBC and the 2970 to do this were entitled FLU).

Using one of the FLU programs we estimated the error due to "mis-rolling" of an aluminium foil. If it was rolled to a diameter 0.1 mm greater or lesser than normal the magnitude of the flux signal would vary by less than 0.5%, which is quite acceptable.

6.2.6 Room Temperature Coil Test

Our unscreened program was appropriate for the one occasion when a superconducting screen was not present. This occurred when the pick-up coil was used at room temperature to detect an a.c. signal coil (see sec. 5.2.4). When the calculated and measured results were compared a small difference (a few per cent) in the ratio of the inner and outer peak heights were found. This is probably because of inexact winding. Otherwise the good agreement in the shape gave us confidence in our programs. No other simulations using the above programs will be reported as they were superseded by a new three dimensional method which allowed for the superconducting screen.

6.3 SHIELD EFFECT CALCULATIONS

6.3.1 The History

For the last decade physicists have wanted to calculate the effect on a sample signal of a superconducting shield, which is usually in the form of a tube. Below its critical field a superconducting material will not allow field lines to pass through it. Instead it sets up opposing supercurrents, on its surface, to exactly cancel any such field lines.

These shields have been used for three main purposes:
i) To confine and enclose the field from a solenoid.
ii) To shield a pick-up coil from any outside field source.
iii) To trap and hold a steady field, previously applied by an external solenoid which may or may not be continuously applied.

The references to many of the early papers relevant to this subject have been given by ter Brake et al (1985), particularly in case (i). For example Smith (1973) calculated the effect of having the shield outside the field producing solenoid. His shield was designed to improve the homogeneity and to confine the field.

Muething et al (1982) improved upon this type of calculation by using the equations of Garrett (1963). However they did make one algebraic slip in the derivation of their eqn (6). Repeating the derivation from Garrett's equations will give an extra π in the denominator. Unfortunately Israelsson and Gould (1984) seem not to have noticed this mistake in their paper.

When a solenoid is energised within a superconducting shield, then supercurrents flow on the shield to produce an opposing radial field. This exactly cancels the radial field from the solenoid, at the shield's surface. These supercurrents flow around the tube's circumference, and their magnitudes will vary along the length of the tube. By splitting the tube into many sub-sections, and assuming the current was homogeneous within an individual sub-section, Muething et al (1982) were able to calculate the current distribution along the tube.

Zieba and Foner (1983) also discovered the problem of superconducting currents when using a V.S.M. (at low temperatures). They observed

distortions of the sample flux in the presence of superconducting magnets and cylinders. They likened the problem to the "image effect" in electrostatics. However they stated that the method of images is not strictly applicable to circular cylinders. So they approximated the circular cylinder to one with a hexagonal cross-section.

About the time of Zieba and Foner's paper, Asaolu (1983) had tried introducing two "image current rings" and he used matching of longitudinal fields by an iterative process in order to calculate the "image currents" within these rings. Two image rings were used because of the two "opposite" sides of a cylinder. This had limited success.

The idea of an image ring was also used by Guy & Park (1984) as one of two methods for calculating screening currents. (They wanted to calculate the effect of the screen on their magnetic monopole detector). Firstly they managed to accurately calculate the super-current distribution caused by a current carrying circular coil placed inside a long co-axial superconducting cylinder. Using a fast Fourier transform method, and working with the magnetic vector potential **A**, they developed a method which was analogous to Muething's but more accurate, effectively with a much finer sub-division of the cylinder. The second method considered an image ring outside the cylinder in which a fictitious current would flow. By varying this current they could approximate the "shielding effect".

6.3.2 Recent Work

Some more recent work on shielding effects has been carried out by Feng (1985) and ter Brake et al (1985). Feng was interested in using superconducting tubes to shield apparatus from large fields in high energy physics experiments. He was able to calculate the current distribution for this mode, and suggested the use of a variable diameter tube to increase the ability of a shield to "withstand" a high field.

Working on a rock magnetometer ter Brake et al had a problem closer to ours. They wanted to correct for the effect of the shield on the signal detected by their pick-up coils. However their pick-up coils were different from ours, being saddle coils. So to calculate the shield effect they developed a different mathematical method from that described below in 6.3.4.

Meanwhile we had followed the idea of Muething et al and produced a program, using matrix inversion, which split the tube into many small cylinders. Using the equation for the radial field from a solenoid that we had derived from Garrett (see 6.2.2) and our knowledge that the net radial field must go to zero at the superconducting surface we calculated the average supercurrent that the cylinders carried. We obtained the same shape as the accurate distribution of Guy and Park, but with a different multiplier. The difference was not resolved as this method was discontinued in favour of the more direct treatment discussed in the next section.

6.3.3 The Osterman Approach

A new calculational method was produced by Osterman & Williamson (1983) which made a significant advance. All the attempts until then had aimed at calculating the current distribution on the niobium screen. It would then have been necessary to calculate the effect of these currents on the detector. However Osterman and Williamson derived a direct solution to the problem. They were the first to find a way of calculating the signal from a sample moving into a pick-up loop, both of them being concentrically inside a superconducting cylinder. They used a Green function to describe the magnetic potential, and hence the field within the tube, with the boundary condition that the radial component must vanish at the shield surface. This formulation led to the linked sample flux being given in terms of a sum over a series of Bessel functions and associated exponential terms.

The zero's of dJ_0/dx are also needed and are listed in the tables of Abramovitz and Stegun (1964), which also provide useful functional relations for these zero's. The Bessel functions themselves were numerically calculated within the program using a code written by G. J. Daniell, and based on the equations in Abramovitz and Stegun.

Osterman's eqn (5) in his units, but using our notation, was:

$$\varphi = Mra \sum_{n=2}^{\infty} F_n \exp\{-x_n|z|/s\}\sinh\{x_n l/2s\} \qquad |z| \geq l/2$$

or (6.6)

$$\varphi = -Mra \sum_{n=2}^{\infty} F_n \exp\{-x_n l/2s\}\cosh\{x_n z/s\} + 4\pi^2 Mr^2(1-a^2/s^2) \qquad |z| \leq l/2$$

where

$$F_n = \frac{16\pi^2 J_1(x_n a/s) J_1(x_n r/s)}{x_n^2 J_0^2(x_n)}$$

and φ = the flux detected by the pick-up loop

M = sample magnetisation

r = sample radius

a = pick-up coil radius

s = shield radius

l = the sample length

z = the distance from the loop to the sample centre
(see fig 6.2.1)

x_n = the nth zero of the function dJ_0/dx
i.e. $dJ_0(x_n)/dx = 0$.

J_m = the mth order Bessel function

We also communicated with David Osterman, who kindly sent us copies of his (Fortran) program and some notes. We tried applying the equation on our microcomputer but we ran into several problems. Firstly we found it necessary to expand his equation out to avoid multiplying very large numbers by very small numbers. We also found that when z=l/2 his equation did not converge at all well; (z=l/2 implies the end of the sample was in the same plane as a pick-up loop). He appears to have overcome this with "brute force" computing. However we could not do this, so we needed an alternative approach.

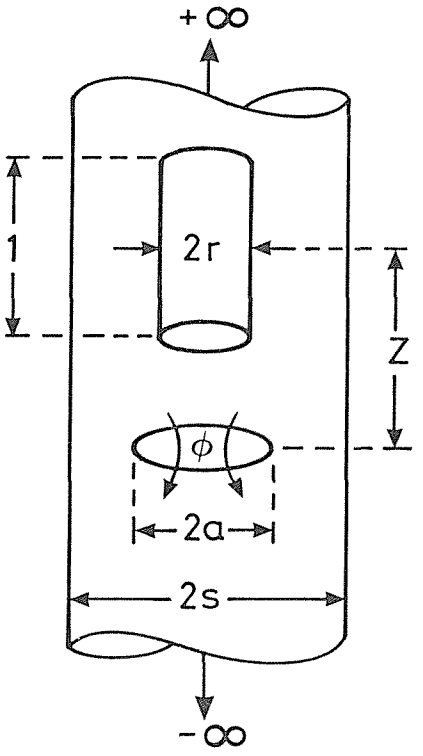

Fig. 6.2.1 Ostermans Sample-Loop.

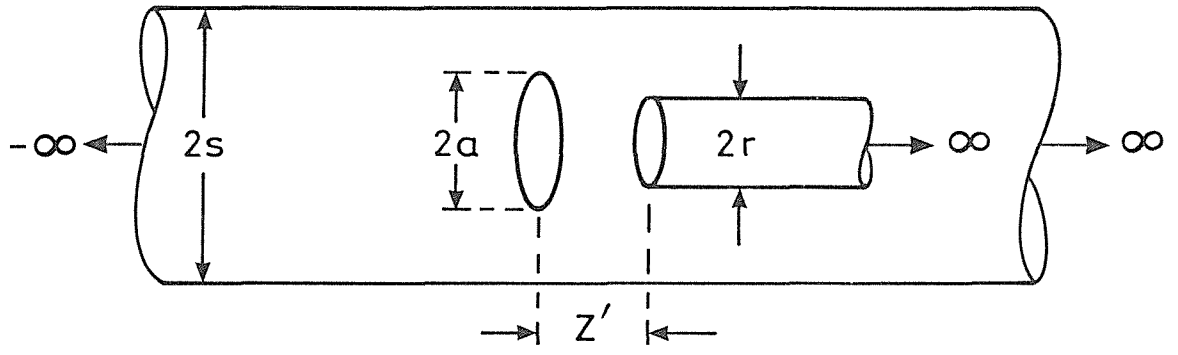

Fig. 6.2.2 Loop Solenoid.

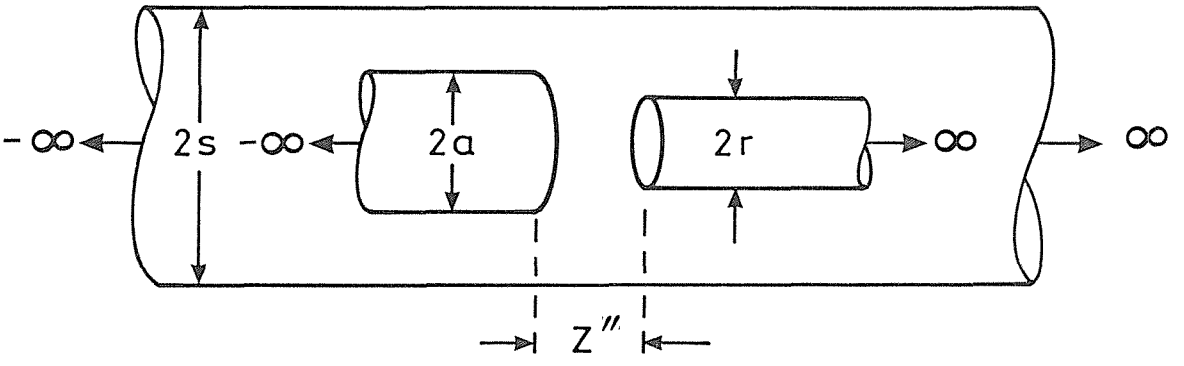

Fig. 6.2.3 Solenoid / Solenoid

Fig 6.2 Notation for the Shielded Coil Equations

6.3.4 The Daniell Method

The mathematics of this problem required the help of G. J. Daniell (University of Southampton). He overcame the problems of Osterman's equations by using an alternative form of the Green function expressed in terms of modified Bessel functions. In this formulation the "discontinuity occurs in r not z". Using generalised cylindrical coordinates (r,φ,z):

$$G(\underline{r},\underline{r}') = \frac{2q}{\pi}\sum_{m=-\infty}^{m=\infty}\int_0^\infty \{I_m(\lambda r')/I_m'(\lambda s)\}\{[K_m'(\lambda s)I_m(\lambda r) - I_m'(\lambda s)K_m(\lambda r)]\ x\ [\cos\lambda(z-z')\exp(im(\varphi-\varphi'))]\}d\lambda \qquad (6.7)$$

for r>r' (interchange symbols for opposite case)

where q = magnetic "charge"

s = shield radius

λ = variable of integration

and r & r', φ & φ' and z & z' are generalised cylindrical, azimuthal and axial distances respectively.

From this equation the flux (Φ) linking a loop with a solenoid can be derived, where the loop lies co-axially with, but separated by z' from, one end plane of a semi-infinite solenoid.

$$\Phi(r,z')=2\mu_0 nira\int_0^\infty \frac{\sin(\lambda z'/s)I_1(\lambda r/s)}{\lambda\ I_1(\lambda)}[I_1(\lambda)K_1(\lambda a/s)-K_1(\lambda)I_1(\lambda a/s)]d\lambda \qquad (6.8)$$

where r = radius of source solenoid (or sample)

a = radius of loop (a pick-up loop)

z'= length to the end of the source solenoid

s = radius of shield

λ = another variable of integration

and ni is the current-turns per unit length. (ni = 1 in Garrett's convention).

This can be evaluated by Cauchy's theorem and then the contribution from the poles, corresponding to the zero's of $I_1(\lambda)$, give the "reduced" form of Osterman's series:

$$F(z') = 2\mu_o niar\{\pi\Sigma_n \frac{e^{-x_n z'/s}J_1(x_n a/s)J_1(x_n r/s)}{x_n^2 J_0^2(x_n)} + \frac{\pi r}{4s}[\frac{a}{s}-\frac{s}{a}]\} \quad \frac{z'}{s}\geq 1$$

$$F(z') = -F(-z') \quad \frac{z'}{s}>1 \qquad (6.9)$$

where the notation is as previous.

If this equation is only used where appropriate (i.e. $|z'/s| > 1$), the sum can be truncated after 15 terms with sufficient accuracy. However these equations led to poor convergence when $z \to 0$, so as an alternative to cover the range $0<|z'/s|<1$ the integral in eqn 6.7 can be split into two parts. The first part viz:

$$F1 = \int_0^\infty \frac{\sin(\lambda z'/s)}{\lambda} I_1(\lambda r/s) K_1(\lambda a/s) d\lambda \qquad (6.10.1)$$

will give the value of flux in the absence of a shield, while the second part gives the shield "correction" viz:

$$F2 = -\int_0^\infty \frac{\sin(\lambda z'/s)}{\lambda} \frac{I_1(\lambda r/s) K_1(\lambda) I_1(\lambda a/s)}{I_1(\lambda)} d\lambda \qquad (6.10.2)$$

The first part of the equation can be reduced to a linear combination of elliptic integrals:

$$F1(r,z') = \mu_0 niz' r_1 [(E-K)+(\Pi-K)(a-r)^2/r_1^2]/2 \qquad (6.10.3)$$

where $K = K(k)$ the complete elliptic integral of the 1st kind
$E = E(k)$ .. .. 2nd ..
$\Pi = \Pi(N,k)$ .. .. 3rd ..
and $k^2 = 4ar/\{(a+r)^2+z^2\}$
$N = 4ar/(a+r)^2$ (or c^2 in the notation of Garrett)
$r_1 = (a+r)^2 + z'^2$

while a,r and z' are as before,
and μ_0 = permeability of free space
n = number of turns per metre
i = solenoid current.

The above equation is the same as the M(S,L) equation of Garrett (1963).

For the second part of the equation giving the shield "correction", it was not possible to provide an analytic solution. But if z' is not too large, (we require $z' \leq 2s-r-a$, which is equivalent to $z'/s < 1$ for our values of s and r), then it could be calculated by using the Gauss-Laguerre (G-L) method. This turns the integral into a form of weighted sum. The integrand goes as $\exp\{-(2-r/s-a/s)\lambda\}$ for large λ, where λ is again the variable of integration, and a ten point G-L

formula gave sufficient accuracy. The equation becomes:

$$F2 = 2ar\mu_0 ni \sum_{i=1}^{10} w_i \sin\left(\frac{x_i z'}{\sigma s}\right) \frac{I_1(x_i r/\sigma s) K_1(x_i/\sigma) I_1(x_i a/\sigma s) \exp(x_i)}{x_i I_1(x_i/\sigma)} \qquad (6.10.4)$$

where I_1 = a modified 1st order Bessel function

K_1 = ...

$\sigma = 2 - a/s - r/s$

and w_i & x_i are the Gauss-Laguerre constants

while all other symbols are as before.

For large z' the shield "correction" is of similar magnitude, but of opposite sign, to the unshielded value. This leads to rounding errors. However at large z' the Osterman equation converges quickly so it can be used instead.

So far we have only considered a semi-infinite solenoid the end of which is a length z' from a co-axial pick-up loop that is positioned at the "origin". Using the superposition method of Montgomery (1969) enabled us to derive the flux linked to the pick up loop from a solenoid of length l with centre at a distance z from the pick-up loop:

$$\Phi(r,z) = F(z+l/2) - F(z-l/2) \qquad (6.11)$$

This equation will produce the expanded out version of eqn (6.6) above as given by Osterman and Williamson (1983). The notation for the new method is shown in fig 6.2.2. In the calculation of Φ we can combine the F functions which have been calculated by different methods as long as we remember the constant given in eqn. 6.9. So we can always choose the most appropriate method of obtaining F depending on the value of z'.

6.3.5 Extension from Loops to Solenoids

So far we have written our equations in terms of loops and solenoids, but a solenoid is equivalent to a sample where ni = χH. So to go from describing a solenoid to a sample we merely alter "$\mu_0$ni" to "χB"; where χ & B are the susceptibility and magnetic field, which were the two quantities normally used in our experiments.

These equations could be calculated via a BBC Microcomputer: though the programs became quite long, and took some time to run they worked well. To obtain the signal from our pick-up coil simply meant

appropriately adding up the contributions from the 64 turns in the coil. In the earlier FLUX3D program (see 6.2.4) we had been able to calculate directly in terms of just three sub-coils (or little solenoids) using the M(S,S) equation of Garrett (1963). So this idea was extended to the shielded case. We again needed to have alternative methods to carry out the calculation, depending on the sample distance from the coils. The new equations are obviously more complicated. We now have four distances involved, i.e. the distances of the two ends of the sample from the two ends of the solenoid that made up a pick-up sub-coil. They were obtained by the integration of:

$$\int_{Z-L/2}^{Z+L/2} F\left(\frac{z+l/2}{s}\right) - F\left(\frac{z-l/2}{s}\right)\, dz$$

where z = distance from a loop within one solenoid (the pick-up coil) to the centre of the second solenoid (the sample)
l = length of the second solenoid (the sample)
Z = centre position of the first solenoid (the pick-up coil)
L = length of the first solenoid (the pick-up coil)
s = shield radius

i.e. we are adding up the signals from all the infinitesimal loops that go to make up a uniform solenoid. This leads to four terms which can be produced by substituting the four coil end - coil end lengths in the functions given below. (This is similar to the arrangement for the unshielded equations shown in fig 6.1.1 and previously referred to in 6.2.2) except that a shield is also now present. The flux is then given, in appropriate S.I. units, by:

$$n_1\mu_0 n_2 i 2ras\left[+f\left(\frac{Z+L/2+l/2}{s}\right)-f\left(\frac{Z+L/2-l/2}{s}\right)-f\left(\frac{Z-L/2+l/2}{s}\right)+f\left(\frac{Z-L/2-l/2}{s}\right)\right] \quad (6.12)$$

and $\mu_0 n_2 i$ can be replaced by χB if the second "solenoid" is actually a sample (with r,a & n as before).

The function f is defined by:

$$f(z''/s) = \int_{z''/s}^{\infty} F(z)dz$$

which can be calculated by different equations in different regions of z" space.

$$f(z'') = \pi\Sigma_n \frac{\exp(-x_n z''/s)J_1(x_n r/s)J_1(x_n a/s)}{[x_n^3 J_0^2(x_n)]} \qquad z''/s>1 \qquad (6.13.1)$$

i.e. for large separation c.f. Osterman's equation for a loop.

$$f(z''/s) = f(-z''/s) - \frac{\pi r z''}{2ss}\{\frac{a}{s}-\frac{s}{a}\}\{\frac{-z''}{s}\} \qquad z''/s<-1$$

$$f(z'') = f1+f2 \qquad 0<|z''/s|<1$$

where:

$$f1 = [\frac{a+r}{sk\sqrt{N}}][(\frac{N}{3k^2}-\frac{N}{3}-\frac{k^2}{N}+k^2)K + (1-\frac{N}{3}-\frac{N}{3k^2})E - (1-N)(1-\frac{k^2}{N})\Pi] - \frac{\pi r z''}{4as} \qquad (6.13.2)$$

$$f2 = \int_0^\infty (\frac{\cos(\lambda z''/s)-1}{\lambda^2})\frac{I_1(\lambda r/s)K_1(\lambda)I_1(\lambda a/s)}{I_1(\lambda)}d\lambda + \frac{\pi r a z''}{4s^3} \qquad (6.13.3)$$

Again this requires the use of the Gauss Laguerre method;

and $N = 4ar/(a+r)^2$ while $k^2 = N/[1 + (z/s)^2/(a/s + r/s)^2]$

z'' = separation of sample/solenoid ends.

As with the solenoid loop equations there is a constant of integration which is not easily derived analytically. However in our calculations it was necessary to have a value for it when combining the f functions calculated by the different methods (because of the value of z"). To obtain it we compared the values for the f function calculated by the two different methods when z"/s = 1. The difference gave us this constant. Then the f functions can be safely combined as superpositions to calculate the flux between one solenoid and another (or a sample). The resultant notation for shielded coils is shown in fig 6.2.3.

6.3.6 Program Validation

We checked our new programs by comparing the results of the Osterman and Daniell equations where they overlapped. We considered the results for single loops and a sample before introducing the whole coil set. As before we also sub-divided a constant sample, and checked that we obtained the same answer for it in parts as compared with it as a whole. By allowing the shield to grow large (say x100) we could make a direct comparison of the curve shapes with that from the FLUX3D program. This allowed us to confirm that the function was of the right form. However since Osterman and Daniell used "quasi-c.g.s" units to

convert to S.I. we used a comparison between FLUX3D and our programs to confirm that the required constant multiplier before the function was $2\pi\chi$Bar (S.I.) instead of "Mra" (Osterman "c.g.s."). Later we made some comparisons between the calculated results and some experimental results provided from a coil at 4 K, with both a.c. and d.c. excitation.

6.3.7 Additions to the Programs

A plotting routine was added to enable output of the results in a graphical form. Furthermore versions were adapted to calculate the results for tubular samples, and to display the differences in signal with and without the shield.

Further improvements were made to speed up the calculation time. This was done by producing a "one off" calculation of the "instrument function" for the pick-up coil (for a specified sample radius) and storing it on a disk. This took several hours, but thereafter it could be quickly retrieved, reducing the calculational time for a sample signal to a few minutes. The only small loss was that the instrument function was only calculated for every 0.1 mm, so all sample distances had to be given to the nearest 0.1 mm (or linear interpolation can be satisfactorily used). Again we adapted the programs to calculate the signal from a sample with changes in radius and for "tubular" samples such as our Langmuir Blodgett films. We then required a two-dimensional array to contain the instrument functions for different radii.

The relevant parts of these programs are printed out in Listing 2 (SAMPAC) and Listing 3 (TUBERS). The BASIC code for the calculation of the actual function is shown in Listing 4 (GJDOst2) while the code for the production of the instrument function is given in Listing 5 (SQDGRDS).

6.4 3-D EXPERIMENTAL RESULTS

Once the magnetometer was repaired we worked towards measuring the LB foils. After measuring a few large "easy" samples to test the system we tried measuring foil substrates followed by an "imitation" sample,

which we expected to be similar in magnitude to our LB films.

6.4.1 Resistive A.C. Signals

In a previous section (6.2.3) we have seen that a coil is exactly analogous to a solid sample of the same dimensions. However until we repaired the resistive section of our "superconducting" flux transformer the SQUID was only able to respond to a.c. signals. So we compared the experimental results from a coil with calculated results from our 1-D and 3-D programs (unshielded and shielded). The results were scaled to the central peak height. A very good fit was obtained from the shielded 3-D calculation, noticeably better than the unshielded 3-D or the 1-D calculation; see fig 6.3. (The unshielded calculation gave a peak height 17% greater in magnitude than the shielded calculation).

6.4.2 Superconducting A.C. and D.C. Signals

After re-connecting the super-break in the flux transformer we could pick up d.c. signals, either from steady currents in the sample coil or from solid samples. We could now detect the sample coil former so when we applied various direct currents to the sample coil the results obtained were the superposition of the copper rod former and the sample coil signal. After digitisation the former signal was subtracted off.

The net signal was of the expected shape with sign corresponding to a "paramagnetic" sample. The current in the sample coil was varied giving different magnitudes to the peaks; see fig 6.4. Knowing the current in the coil and by comparing the digitised experimental result with the calculated theoretical result we estimated the coupling factor to be 0.16% if we compared the +ve peaks, but 0.17% if we matched the -ve peaks. This difference may indicate some imbalance in the pick-up coil. The linearity of the system could also be checked by plotting the peak height against the current. The linearity was confirmed to be within the experimental/digitisation uncertainty of a few per cent; see fig 6.5.

6.4.3 Aluminium Semi-Infinite Rod and Foil Holder

The first "real" sample that we tried to measure was a solid "semi-infinite" rod of alumimium of radius 3.75 mm. (Semi-infinite

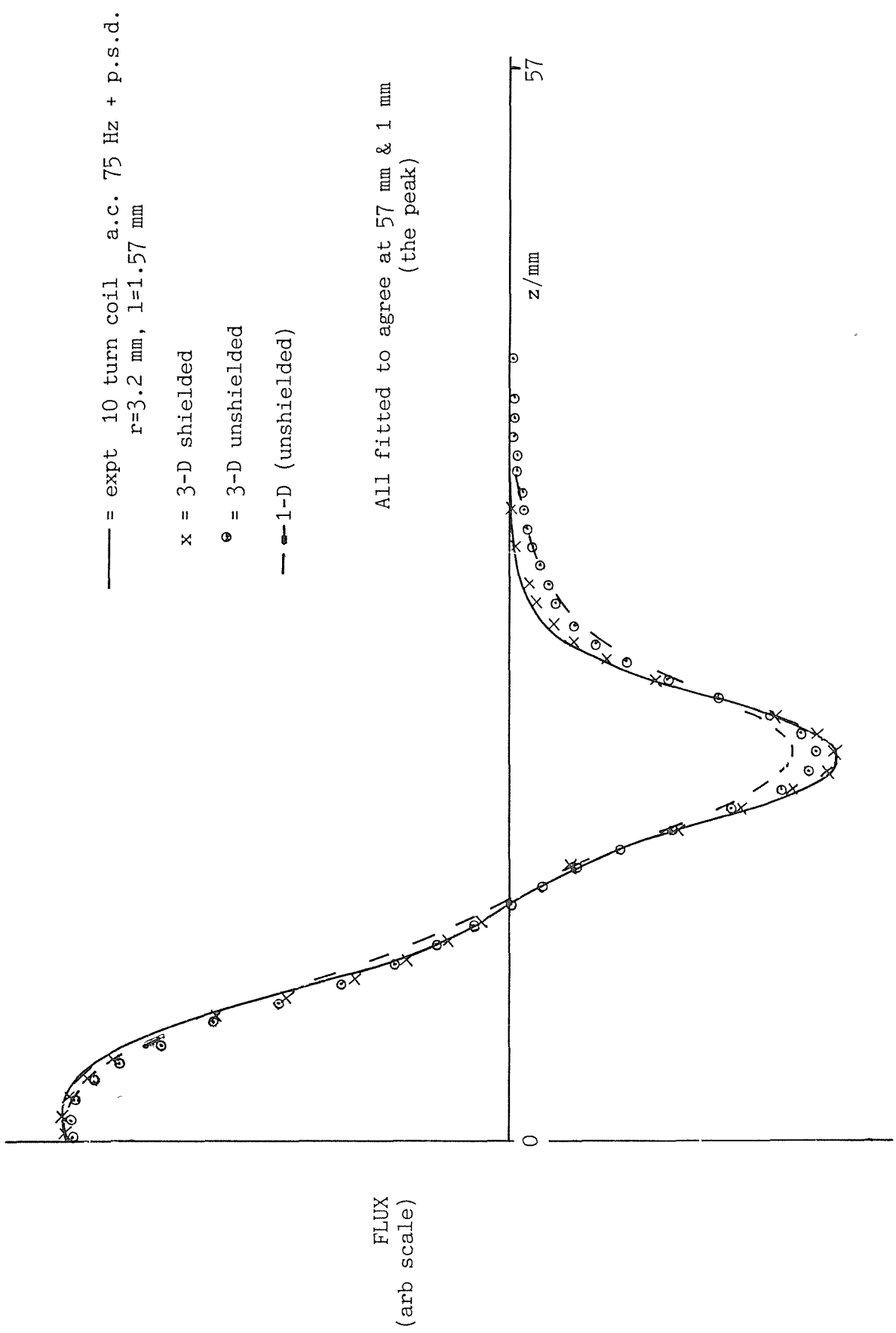

Fig 6.3 Comparison of Expt, 1-D, 3-D and Shielded 3-D Calculations

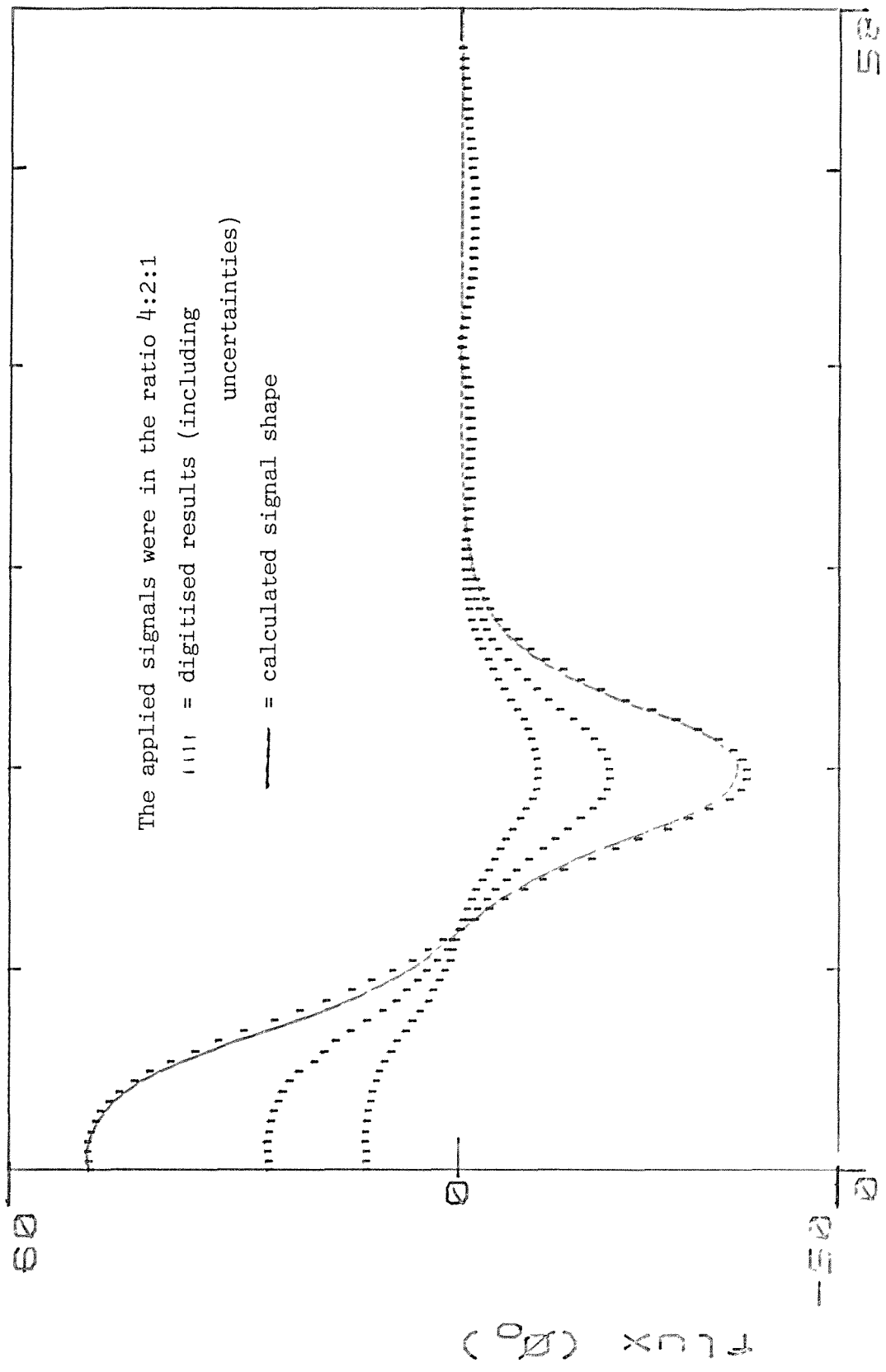

Fig 6.4 Several Coil Signals (D.C.)

Plot of Flux Signal (p.t.p.) against Applied Signal

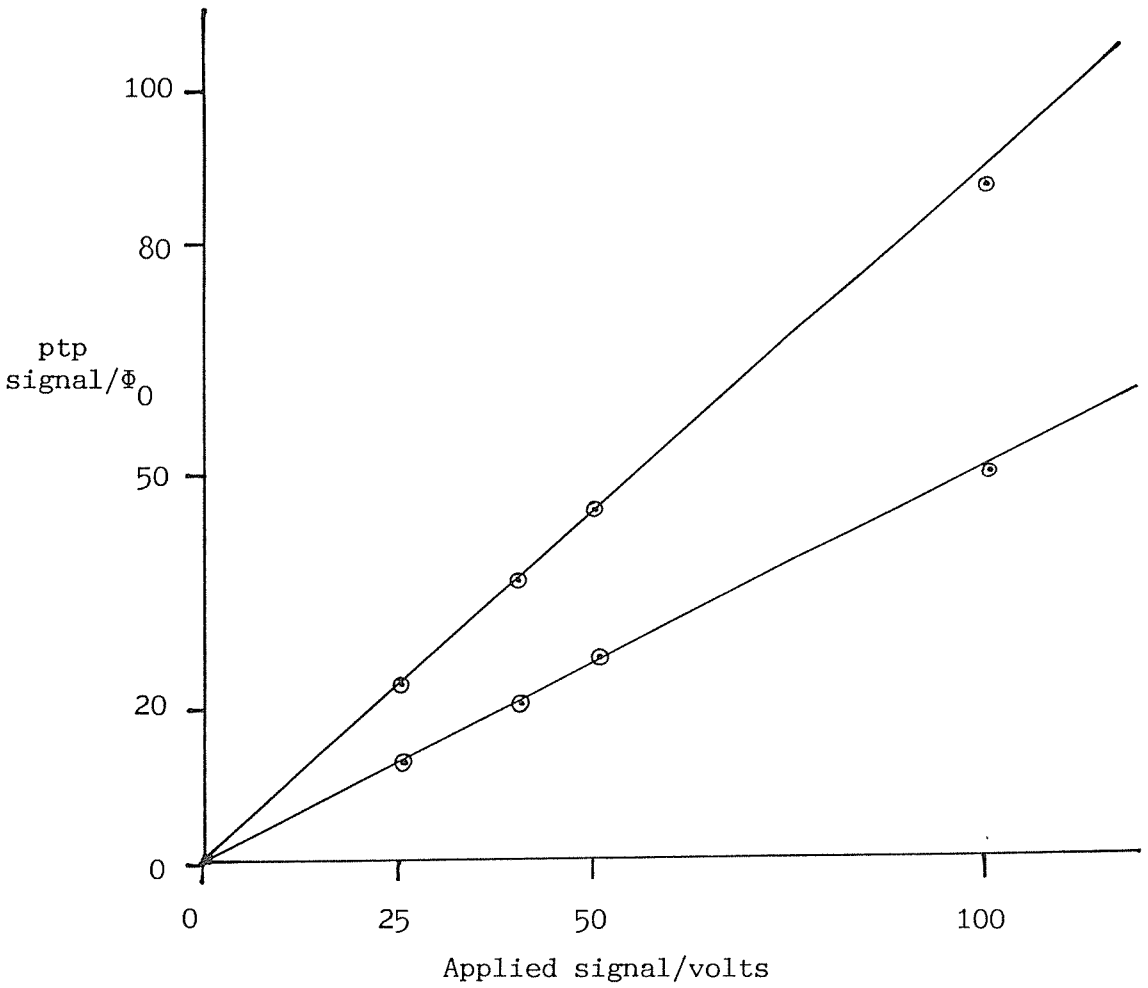

Fig 6.5 Signal Amplitude from D.C. Coil

means only one end of the sample passed through the gradiometer, the other being well outside the region of significant sensitivity). The semi-infinite rod was initially measured at 4 K and only later did we lower the temperature. The first measurement suggested that we were suffering from remanent fields of around 1 mT and contamination of the rod. So the sample was re-cleaned by ultrasonication in various solvents. (It had been stored for a long time in its container between the time it was previously cleaned and the time that it was measured). During the re-cleaning we checked that the sample siphon on its own produced zero signal, when driven towards the pick-up coil. When we re-measured the semi-infinite aluminium rod sample in "zero" field we observed no signal suggesting that the remanent field and any contamination had been properly removed. On application of ±4 mT we obtained more reasonable signals with peak amplitudes similar to each other, but in reverse directions. Comparison with the computer simulation gave a value of 0.17% for the coupling factor.

Later we re-measured the semi-infinite pure aluminium rod in 0 mT and 2 mT and obtained a signal shape closer to that expected; see fig 6.6. Comparisons with the computer simulation in 2 mT gave an unusually high coupling factor of 0.22%. The 2 mT signal showed an assymmetry, which was much more pronounced in the nominally zero field signal. It is noticeable that the B=0 mT bump coincides with the skewed peak of the B=2 mT signal. The computer simulation did not fit the shape of the experimental curve as well as some later samples. If we were to subtract the 0 mT signal from the 2 mT signal we would get a lower coupling factor - approx. 0.18%.

We also made a Φ v z traverse after we had cooled the aluminium rod down below its superconducting transition temperature (1.2 K). Its signal deflected in the opposite direction to that at 4 K, confirming a change from paramagnetism to diamagnetism. Because the signal was so large the SQUID repeatedly reset every 500 Φ_0. However the reset rate and direction did change at the right point i.e. at the peak position expected. An approximate count of the number of deflection lines gave an estimate of the peak signal size. Comparing this with the 4 K paramagnetic signal ($\chi = 2.41 \times 10^{-5}$) gave a low temperature susceptibility close to -1 as expected. The actual foil holder was also machined from pure aluminium. Although it never entered the pick-up coil we still checked that there would be no background signal from it.

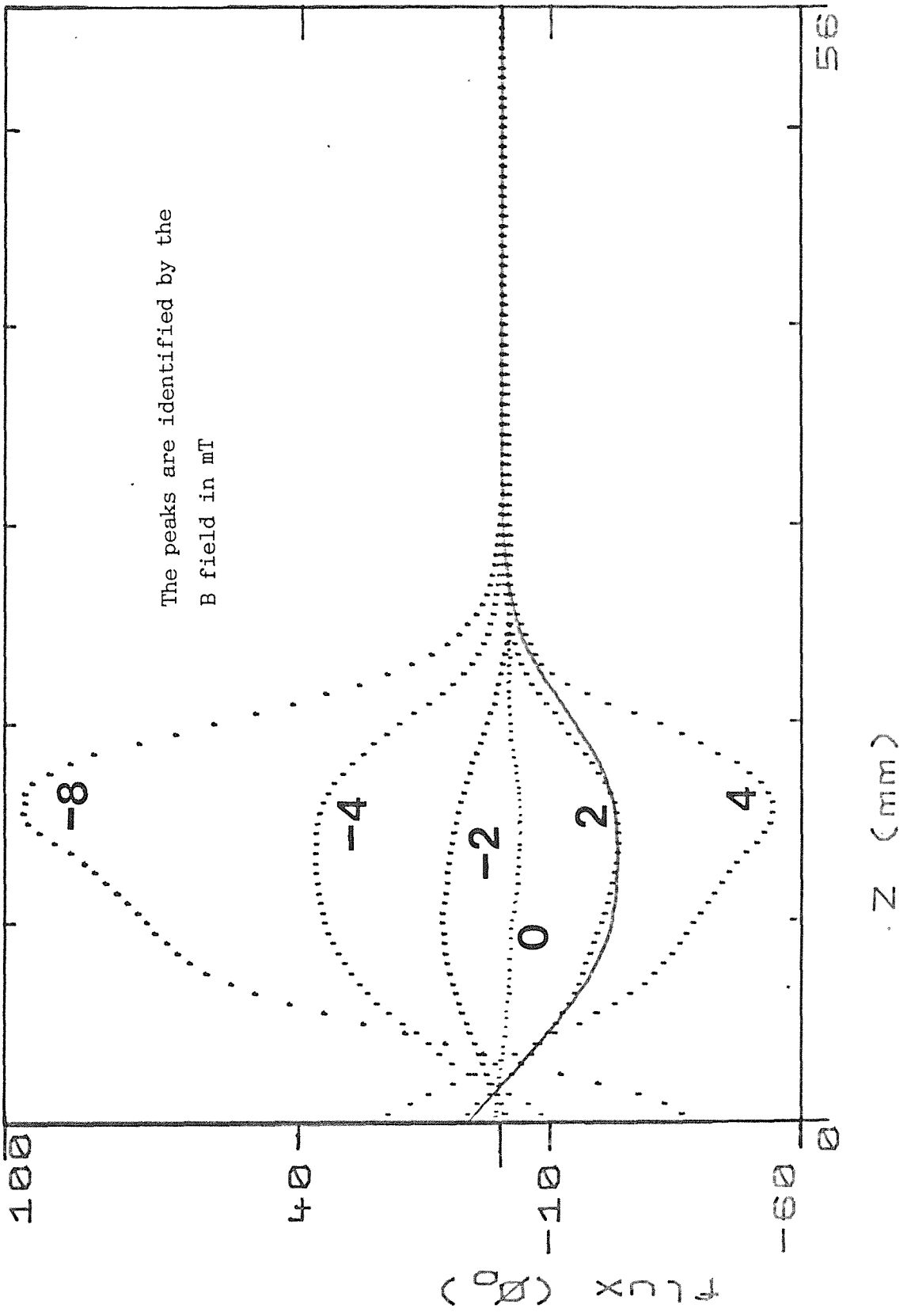

Fig 6.6 The Semi-infinite Aluminium Rod in Various Fields

6.4.4 Infinite Aluminium Foil (Alone)

Before measuring an actual LB sample, we measured two foil substrates to check for any background signal. The foils were not pure aluminium so they might have impurity effects. We measured the first foil in several increasing fields and there did appear to be a small signal, unusual in that it seemed to get bigger with time increasing to 2 Φ_0 p.t.p. Based on our experience with the solid aluminium we thought this might be due to "dirt", so the second foil was re-cleaned. When we measured this foil there were some signs of a signal at 4 mT, but it remained small at about 0.2 Φ_0.

We also examined the foils for remanent effects following the application of ±1 T. There was a remanent signal with p.t.p. value of ≈7 Φ_0 which gave an approximately reversed signal on reversal of the field. So we adopted the precautions of recleaning the foils and avoiding their exposure to high fields. Later we measured an old foil in 2 mT between 20 K and 0.4 K. At 4 K we picked up a contamination peak of about 2 Φ_0 increasing to 4 Φ_0 on further cooling. Our substrates needed to be very clean if we were to detect monolayers!

As well as recording the SQUID signal as the sample moved through the pick-up coil at fixed temperatures, we also measured the signal as the temperature of the sample was varied, while maintaining its z position fixed usually in the centre of the pick-up coil. In zero field the foil signal changed by <0.1 Φ_0 between 20 K and 0.65 K (as measured by the Germanium thermometer). But below 0.65 K the signal suddenly deflected by 9-15 Φ_0. Cycling in temperature from 0.4 - 0.65 - 0.4 K produced different deflections. We assumed that this was due to the foil tube becoming superconducting but with the output signal being reduced as the gradiometer was designed not to detect the substrate signal.

In a field of 2 mT we charted the cooldown to 1.3 K and observed a deflection of ≈1 Φ_0. The signals from the LB samples were expected to be much bigger than this. We did not cool further than this as we would only see the superconducting transition.

6.4.5 Aluminium Strip in Foil Tube

Before loading a LB film we took a strip of aluminium foil 20 mm wide (like a LB film) and rolled it up in a foil tube, in the position a film would occupy. There was no signal in zero field, except when the sample was a long way out at the beginning of the throw - suggesting that it was due to the substrate foil. When the field was applied the signal shape was similar to what we expected; see fig 6.7.

As usual we made several runs to make up a clean traverse of the 57 mm sample throw. We also found that driving the sample in faster to reduce the "sticking" reduced the amount of flux jumping. The signal in -2 mT was the reverse of +2 mT, except for the "bump" at the top of the throw (assumed to be due to the foil). Using our simulation program "TUBERS" we could calculate the theoretical signal from a foil tube. (TUBERS = TUBE with variable Radii, in a superconducting Shield). Hence we could derive a calibration factor, assuming the susceptibility value of pure aluminium for the foil. This again came to a value of 0.17%. As the foil was rolled into a tube we used its inner and outer rolled radii, but because the foil did not completely fill the volume between these two radii, we multiplied the susceptibility of aluminium by a filling factor:

$$\text{filling factor} = \frac{\text{Area of foil (as viewed from end of the tube)}}{\text{Area of a solid tube with equivalent radii}}$$

$$= 0.87 \text{ (based on the sizes given in sec. 5.3)}$$

The results of this experiment showed that the cryostat was usable even with the difficulties of vibration noise, and strengthened confidence in our ability to measure a LB multilayer of $MnSt_2$.

We also measured the signal from the strip sample as the temperature was varied. In zero field we only measured between 1.2 and 0.4 K and observed a change $\approx 1\ \Phi_0$. In 2 mT the result was ambiguous, any change down to 1 K was $<1\ \Phi_0$. Below this temperature we saw, on two occasions, either no change or almost $10\ \Phi_0$ change. In higher fields the change seen on cooling was also about $1\ \Phi_0$. These results were disappointing since we had expected a simple paramagnetic increase as the temperature decreased.

After a further semi-infinite Al rod measurement (mentioned earlier) the foil strip was remeasured but with the foil tube connected "upside

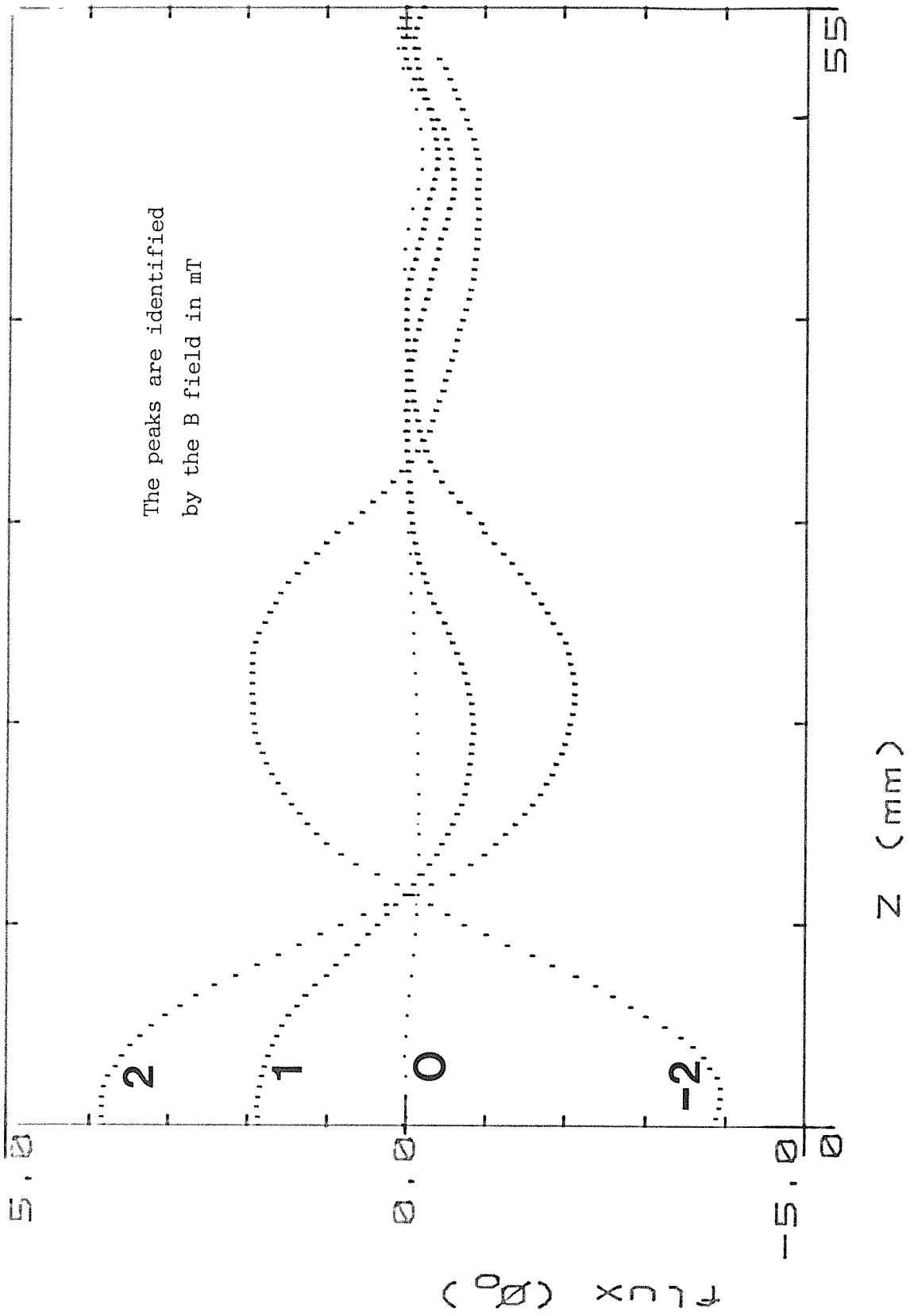

Fig 6.7 2 cm Aluminium Foil Strip in Various Fields

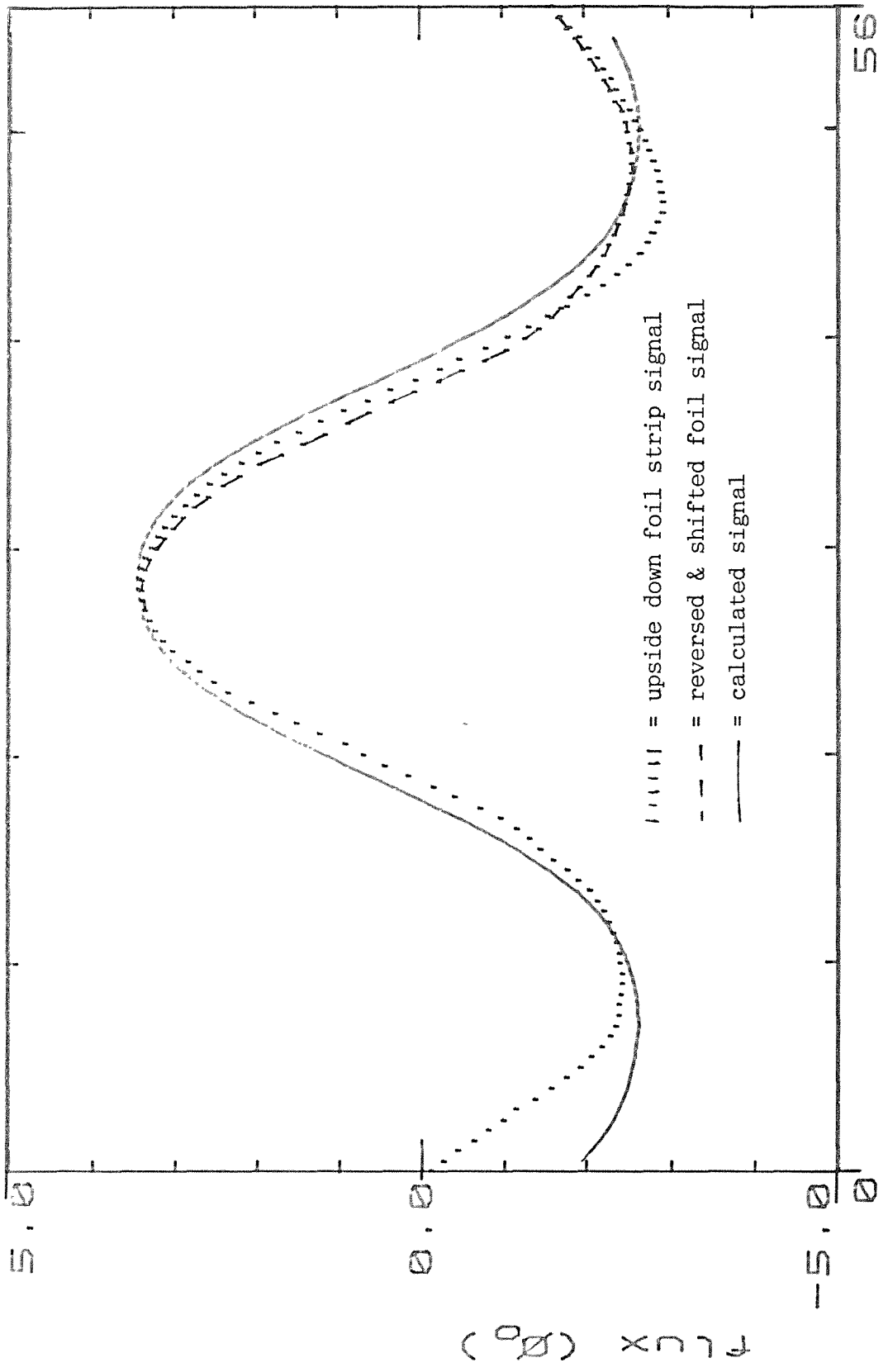

Fig 6.8 Upside-down 2 cm Al Strip with a Simulation

down"; see fig 6.8. (Because the end of the foil was damaged, this meant that we had a slightly shortened "infinite" foil). Now the sample strip started from a much lower position giving rise to two negative peaks from the two outer sub-coils. Comparing the two negative peaks showed differences in magnitude and shape. This could indicate some imbalance in the pick-up coil, though it might have been due to a small contaminant effect. Fig 6.8 also shows a comparison with the original 2 mT foil strip signal, taken before the application of +1 T (but reversed and with an origin shift to match the peak). The amplitudes are very similar. A comparison with a computer simulation (also plotted) indicates that the foil strip was at -28±10 mm below the pick-up coil centre (at the end of insertion).

6.4.6 Semi-infinite Aluminium Foil

We also measured a semi-infinite foil sample of length 119 mm. This allowed us to go beyond the semi-infinite null point and to see all the peak as the centre coil was filled. The sample was measured in 4 mT and the signal was as expected except that the peaks were "narrower" than calculated; see fig 6.9. Comparison with the computer simulation gave a coupling factor of 0.24%.

When the temperature was varied from 25 K to 0.4 K in fields of ≤4 mT the signals were within 1 Φ_0. We observed no large excursions due to superconductivity. We expected that both the semi-infinite aluminium foil and the 2 cm strip would give much bigger signals than this, especially when we consider the changes between their Φ v z curves at different temperatures.

6.5 QUASI 2-D RESULTS

6.5.1 101 Layer LB Sample

Having established the satisfactory operation of the system we measured a LB sample with 101 layers of $MnSt_2$ (see 3.4.5). The signals under equivalent conditions to the foil strip previously measured were considerably bigger from the LB sample but they were of the same sign indicating a paramagnetic susceptibility.

The initial measurement in "zero" field at 4 K showed a very small

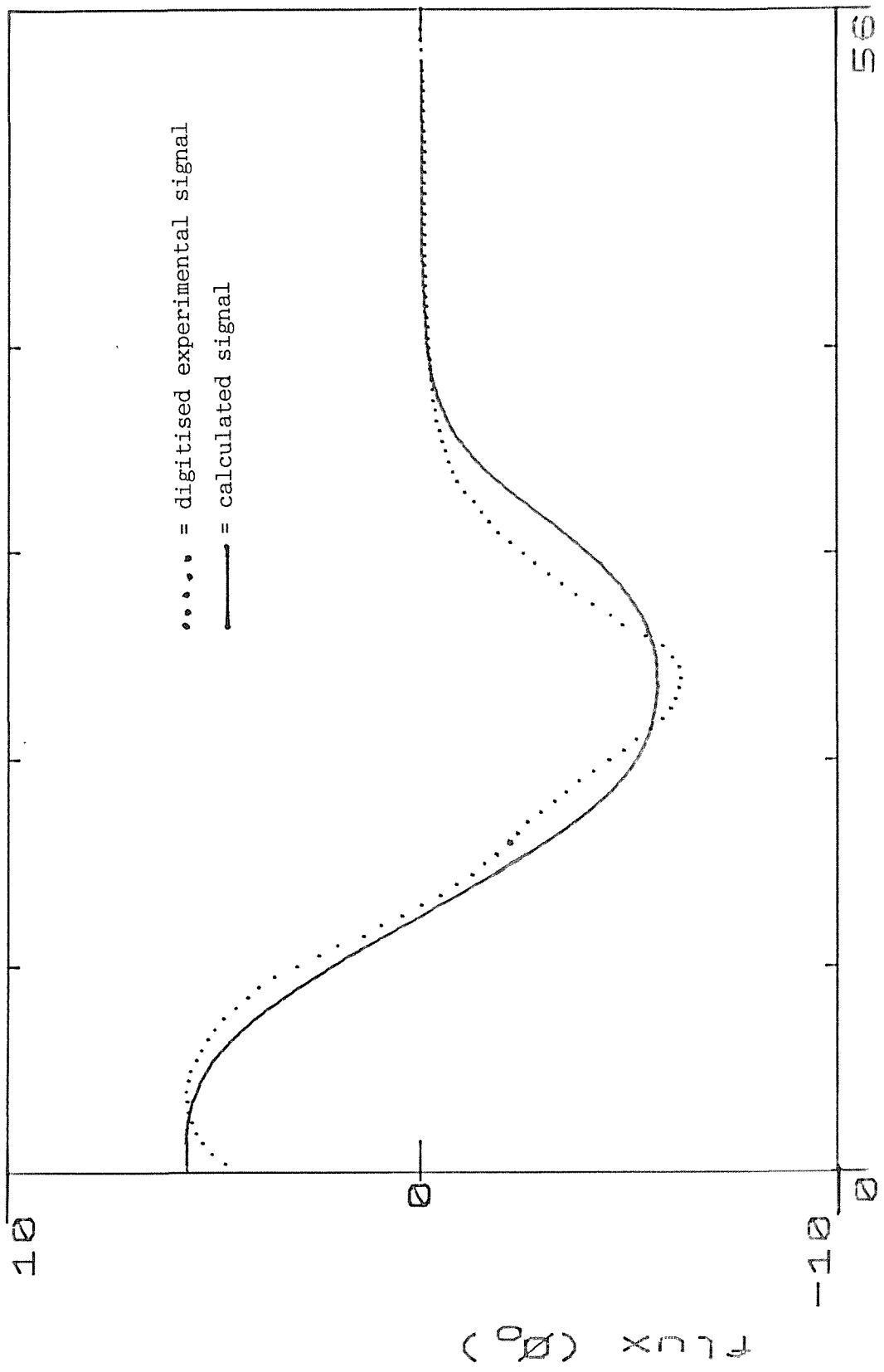

Fig 6.9 Semi-infinite Aluminium Foil

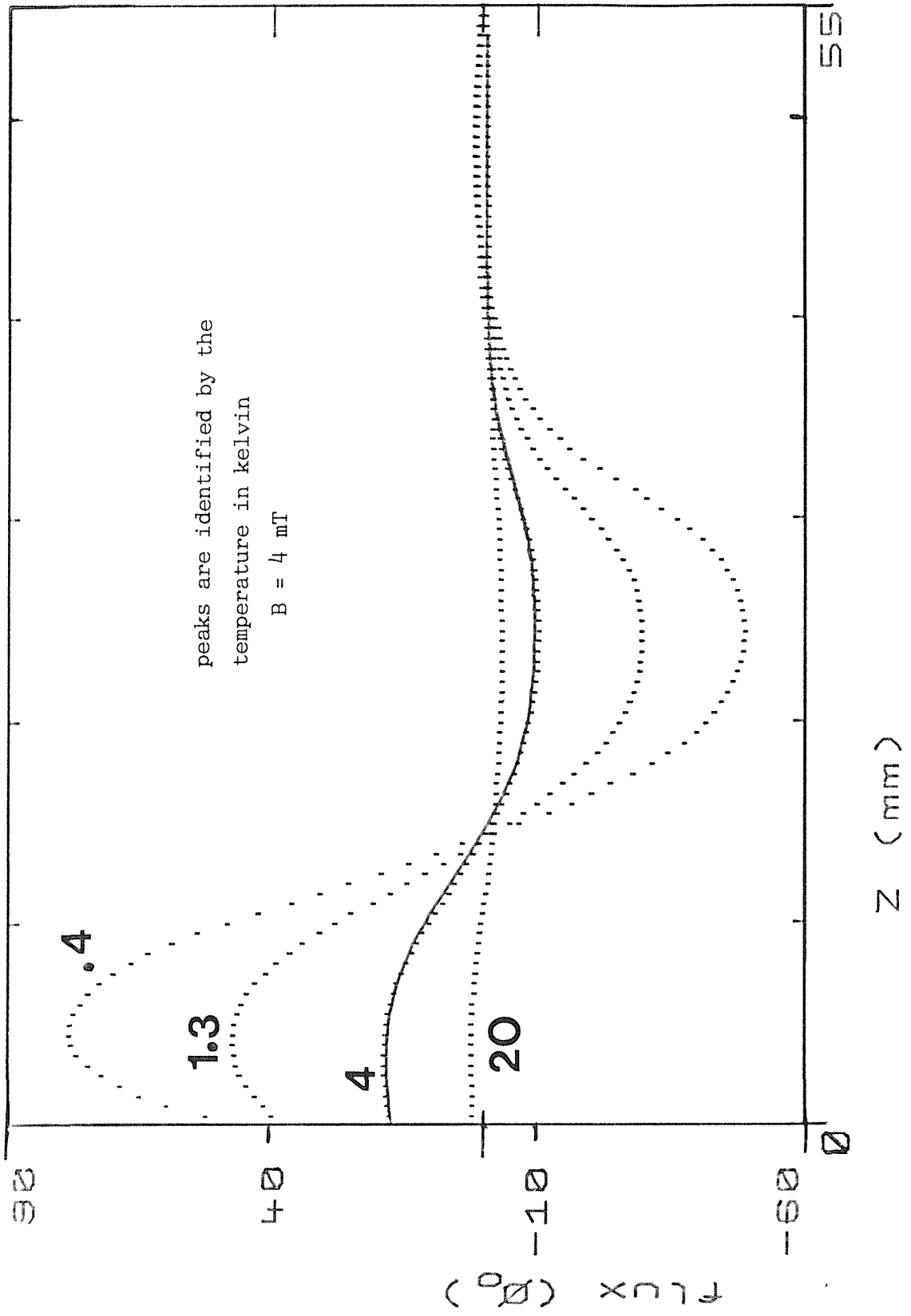

Fig 6.10 101 layers, 2 mT, various T

signal. After this we applied 2 mT and made measurements at 20 K, 4 K, 1.3 K and 0.4 K (as given by the Germanium thermometer on the He3 pot) to seek evidence for any magnetic transitions. The signal amplitude increased with decreasing temperature as shown in fig 6.10. Using the computer simulation and the derived coupling factor we calculated a value for the LB volume susceptibility of 6.4×10^{-3} at 4.2 K. Raising the field increased the signal magnitude but fields higher than 6 mT produced far too much noise, and were unlikely to give any useful information.

The majority of traces showed an unexpected bump at the start of the trace before the LB sample entered the upper sub-coil. We used the computer simulation to check whether this could be some "nose effect" from the foil but no adequate fit to the evidence was found. The computer simulation indicated that the ratio of the +ve/-ve peaks should be two, suggesting that the real zero of the signal had been offset by the "bump".

We also produced Φ v T curves, with the LB sample in the centre of the pick-up coil (the "down position" i.e. when Z = 0). In zero field little signal change occurred, as the temperature was lowered until some way below 0.6 K, when the signal deflected by ~15 Φ_0 down to 0.4 K. (Similar to the Infinite aluminium foil signal; where the majority of the superconducting transition would be "invisible" to a second order gradiometer). In a field of 2 mT the curve showed a steady deflection as the temperature dropped and the overall change from 23 K to 0.4 K was ~100 Φ_0; much bigger than that for the foil alone; see fig 6.11.

We were able to cross compare the down position (~"peak") signal from the Φ v z results, taken at set temperatures, with the equivalent points on the Φ v T results in which the sample was held at the bottom of its throw while the temperature was varied. However the agreements were limited; comparing the B=2 mT Φ v T deflection (fig 6.11) with the change in Φ v z peak signal we find that in going from 20 K to 0.4 K the peak signal has increased by 83.7 Φ_0 which is less than the the Φ v T change of ≈95 Φ_0. It is likely that the change in peak values from the Φ v z curves are more accurate because it is easier to repeat them in order to identify and remove errors from them; see Philo & Fairbank (1977) and compare with the results of 6.4.6.

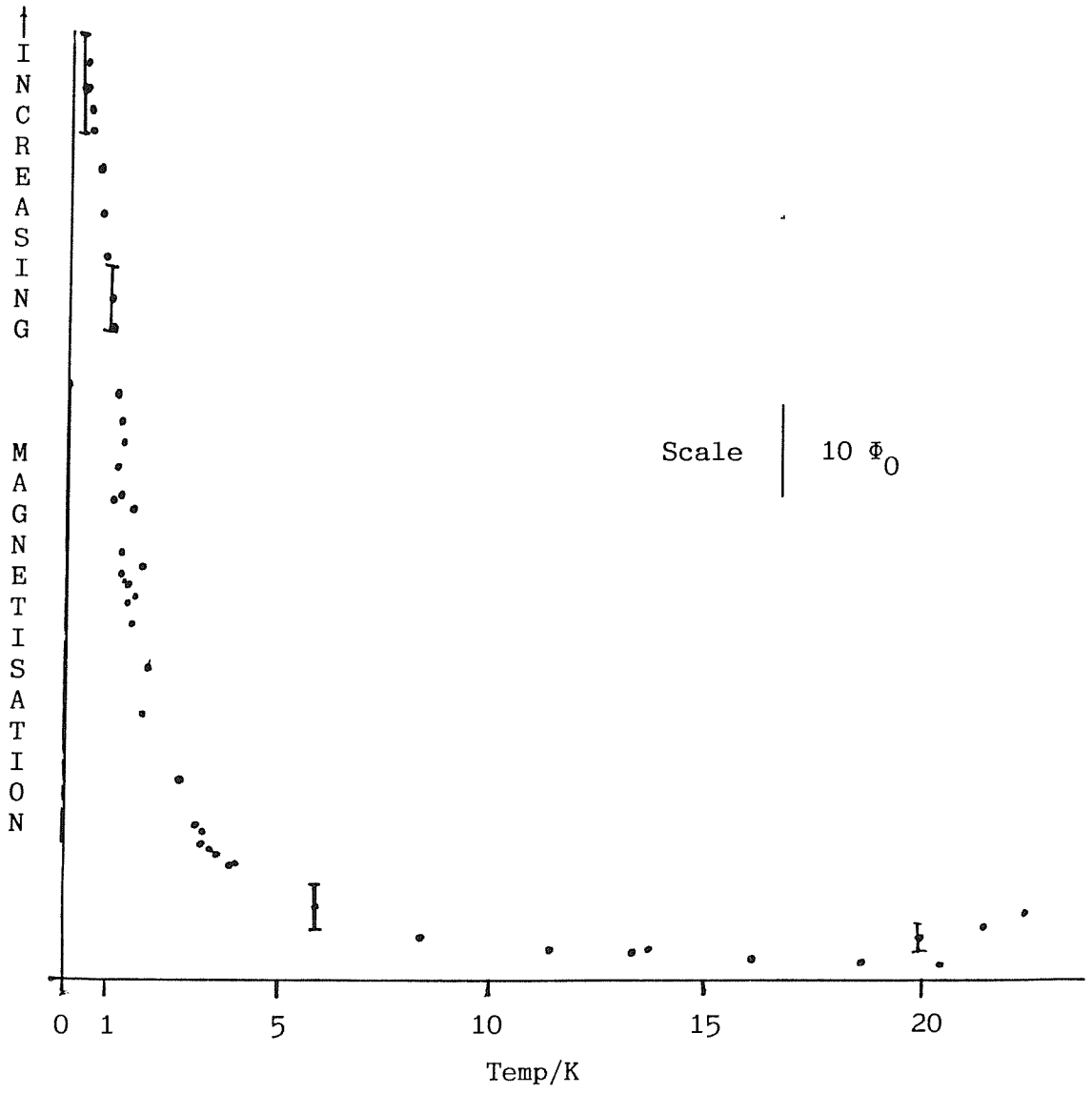

Fig 6.11 Magnetic Signal against Temperature (101 layers, 2 mT)

The Φ v T curve showed that the temperature dependence was "smooth". However, as we were not sure about the quantitative value of the Φ v T curves and because the Φ v Z curves had a similar shape we used the p.t.p. values from the Φ v z curves for comparison purposes. (Measuring p.t.p. values avoided the problems due to the uncertainty of the zero level position which occurred on some curves). The signal increases with decreasing temperature and higher fields. To assess whether the data followed the Curie-Weiss law:

$$1/\chi \propto T-T_c \qquad (6.14)$$

we plotted the inverse of the p.t.p. signal from the various Φ v z traces against temperature; see fig 6.12. (We could not plot the inverse of the flux signal from the Φ v T deflections because the zero was offset. This offset should be equivalent to the positive peak signal from the sample at 20 K, the highest temperature we went to. However the uncertainty in estimating it was too great). Although we had fewer points the p.t.p. signals gave "absolute signals" and not just offset changes. We also made some Φ v T measurements in ± 4 mT and 6 mT; see fig 6.13. In 4 mT between 6 K and 0.4 K, there was a 185 Φ_0 change which compared with the 2 mT signal where there had been about 90 Φ_0 change between 6 K and 0.4 K. The signals again increased monotonically as the temperature decreased and the large increase in signal may indicate that a transition is being approached. However no cusp or saturation of the signal was actually reached.

6.5.2 Eleven Layer LB Sample

Measurements were made on the eleven layer LB sample, in fields of 0, 2 & ± 4 mT, at up to four different temperatures each. Some of the +4 mT results are shown in fig 6.14 and 2 mT in fig 6.15. The latter also has a 4 mT curve (at 4 K) for comparison. The two curves taken below 4 K (2 mT) do not scale with the rest, however the shapes of the curves were similar to those expected, giving us confidence that our system was capable of measuring an 11 layer sample.

There were some extra feature(s) observed as the sample entered the upper sub-coil. As with the 101 layer sample there was a positive deflection ("bump") on some of the curves at the start of the run, followed by a dip. These deviations were not noticeable on the low amplitude signals, indicating that their magnitudes were also dependent on field and temperature. Unlike the 101 layer signal we

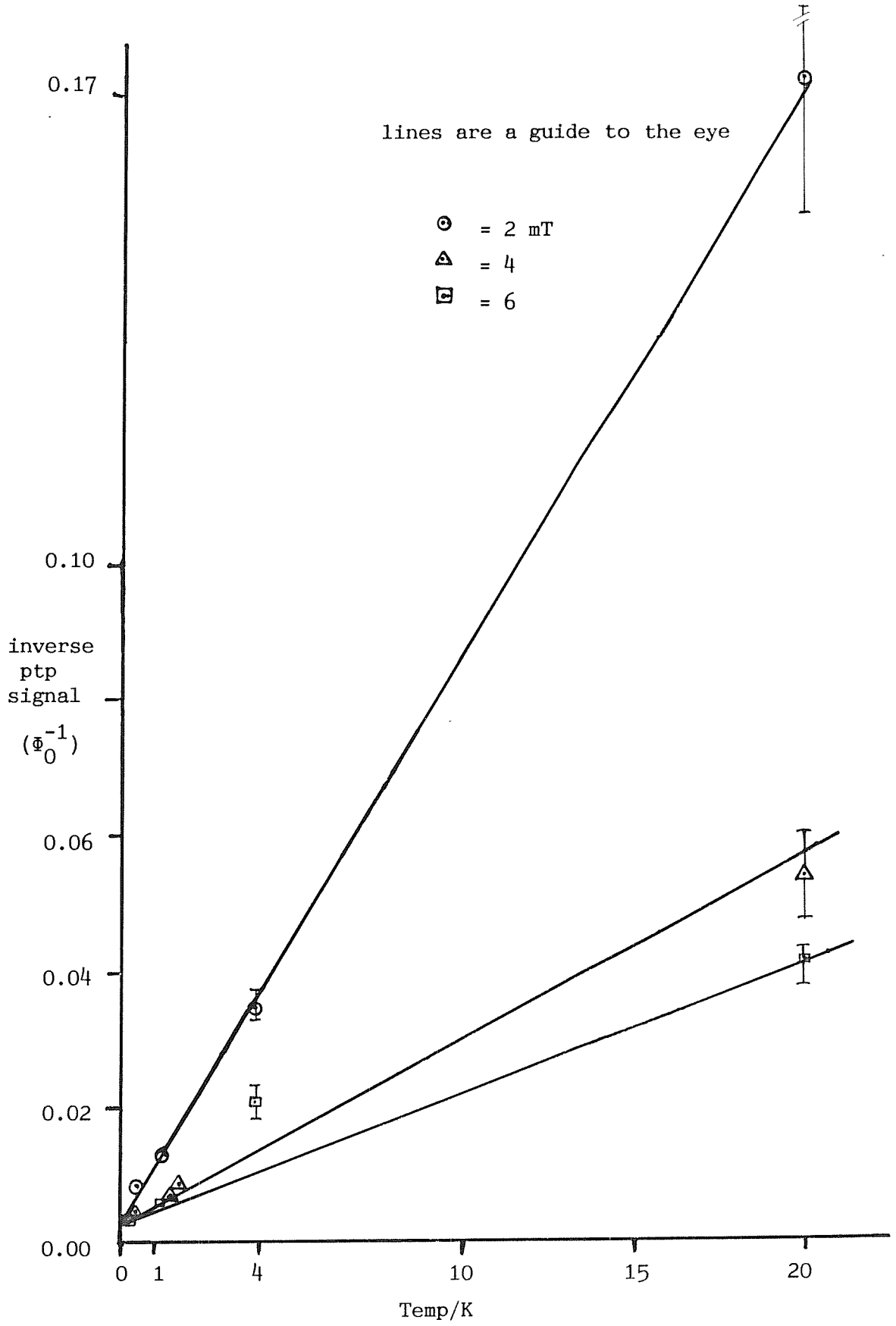

Fig 6.12 Inverse 101 Layer p.t.p Signal against Temperature

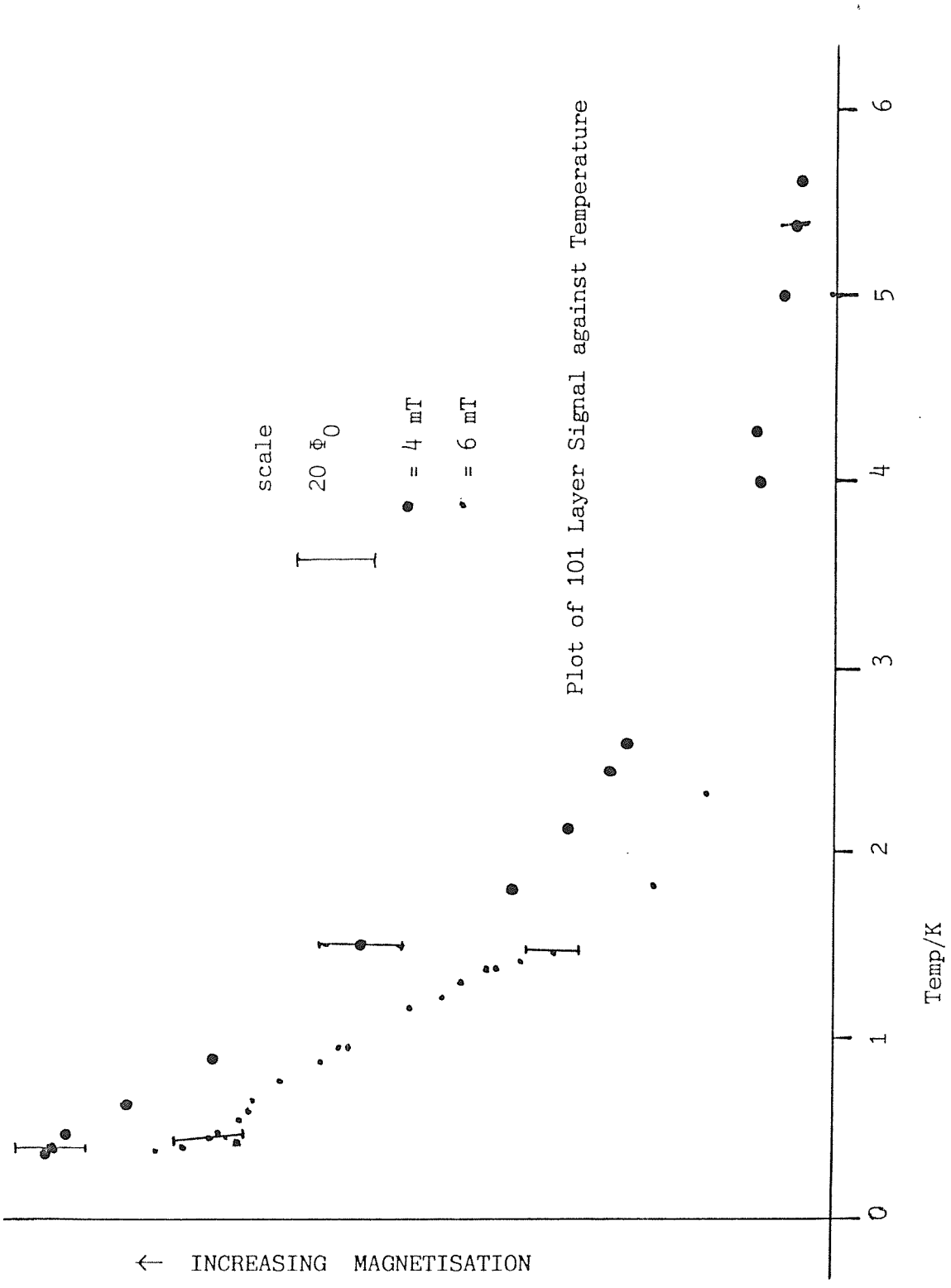

Fig 6.13 101 Layer LB Sample against Temperature (4 & 6 mT)

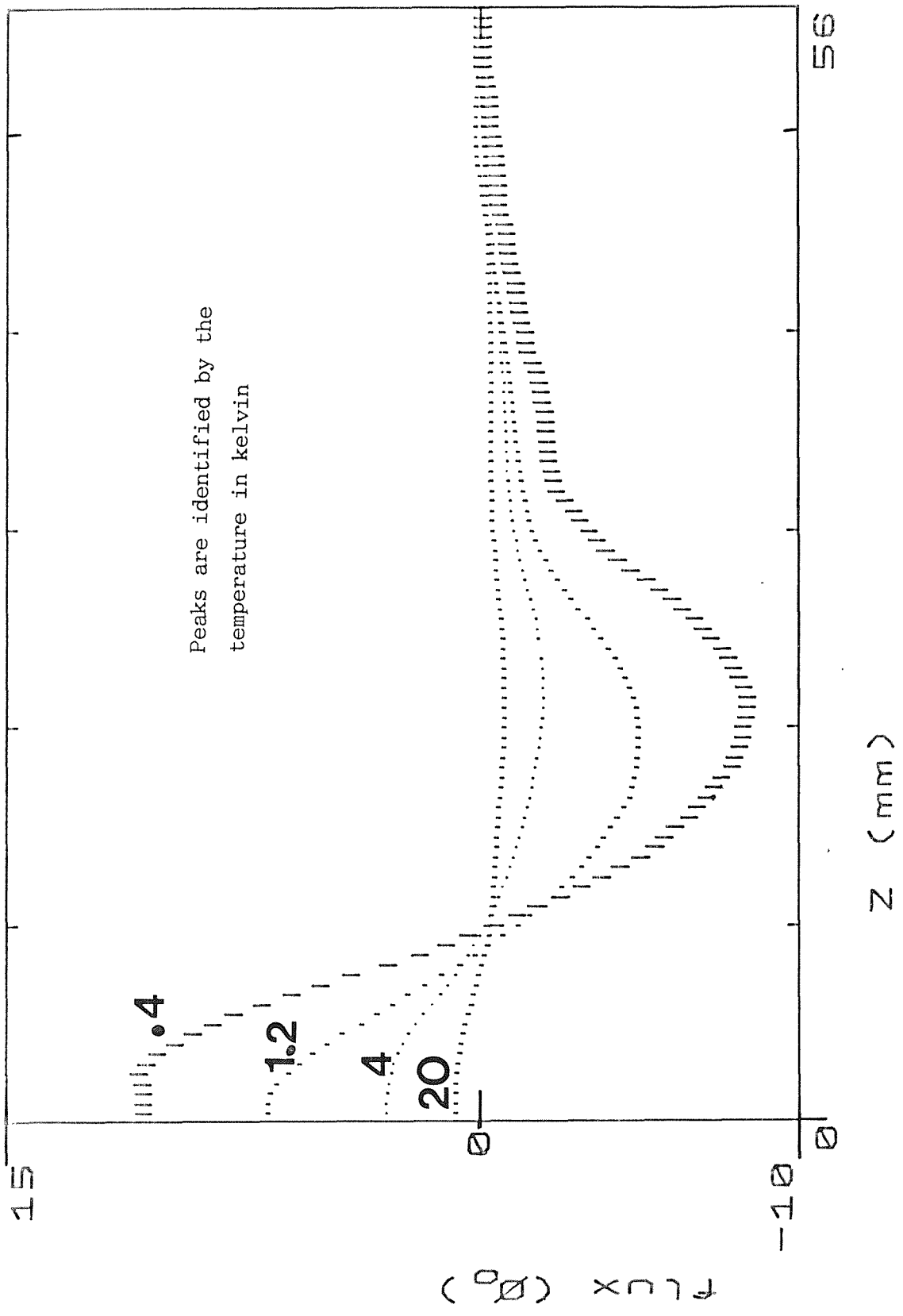

Fig 6.14 11 Layer Φ v Z (B=4 mT)

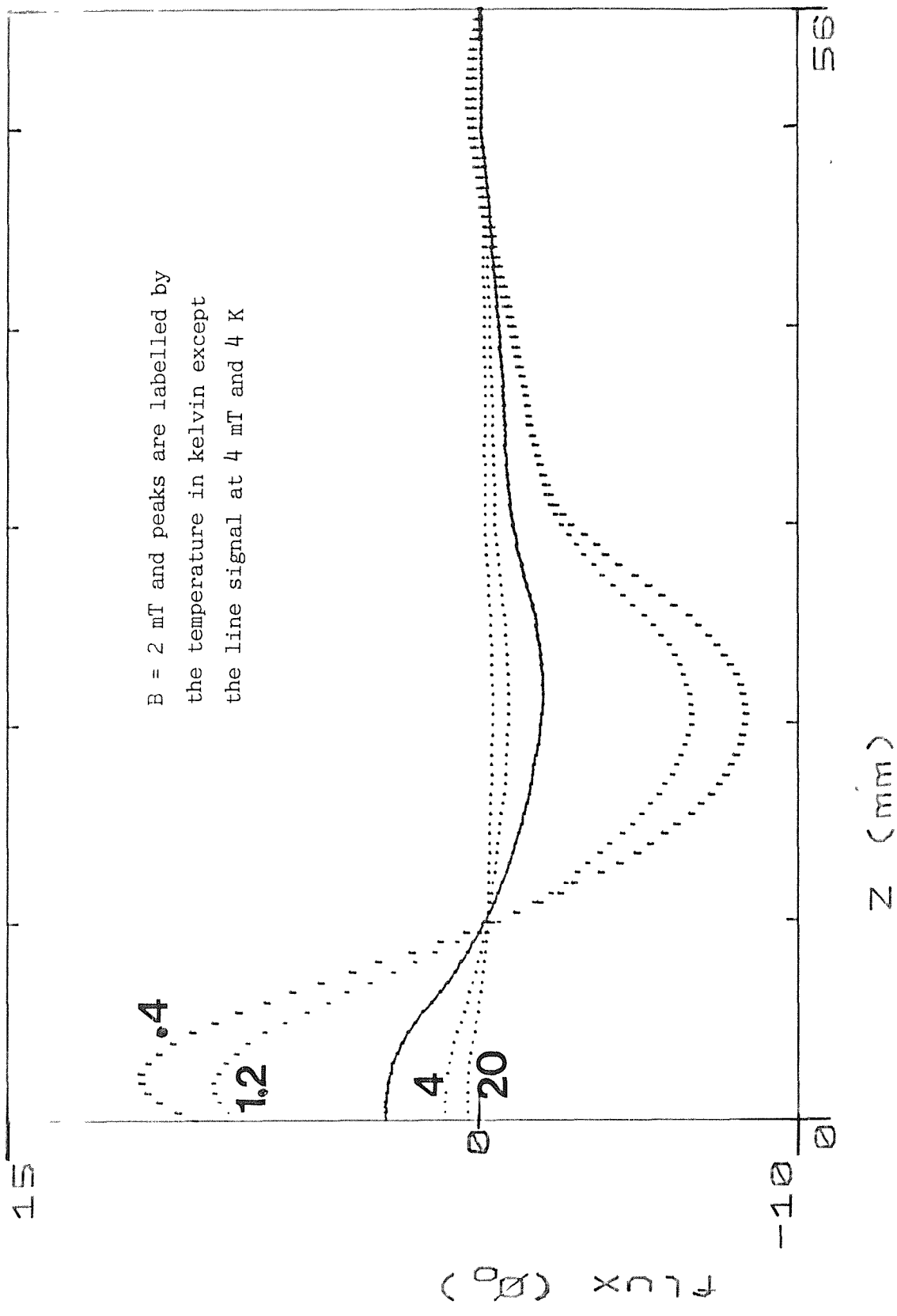

Fig 6.15 11 Layer Φ v Z (B=2 mT)

were able to approximately fit a possible impurity signal to it. If we assume that the "bump" was due to a small piece of material (≈1 mm) about 55 mm ahead of the centre of the LB sample we get an approximate fit using a susceptibility of 1.7×10^{-4} with a filling factor of 0.015; see fig 6.16. However this model does not account for the odd shape to the side of the positive peak.

For ease of comparison and the problem of deciding on the zero level on the Φ v z curves (masked by the "bump") we have again used p.t.p. amplitudes. The reciprocal of the p.t.p. signal from the 11 layer sample was plotted against temperature as shown in fig 6.17. The results only are presented there; fitting is discussed in chapter seven along with the results from the previous sample. Comparison of the 101 layer and the 11 layer data showed that, on average, there was a factor of twelve difference in magnitude; we might have expected a factor of 9-10.

We also measured this sample as the temperature was changed in various fields. In B=0 mT the main deflection occurred at 0.65 K by about 10 Φ_0 (similar to the previous sample). However on two different traverses, they deflected in different directions. We attribute this phenomenon to a superconducting transition in the aluminium foil. On changing the field to 2 mT we saw a steady increase in signal which was repeatable from 5 K down to 0.6 K giving a total deflection of about 6 Φ_0; see fig 6.18. Going below this on one trace caused a very large change (about 200 Φ_0) which we again attribute to the superconducting transition of the aluminium foil. This compares with an approximate 5 Φ_0 change in the peak signals from the Φ v z curves. Doubling the field to 4 mT produced a steady signal rise of about 12.5 Φ_0 as the temperature dropped from 6.5 K to 0.4 K which is in accord with the 2 mT Φ v T signal above. The Φ v z curves suggest a smaller change of about 10 Φ_0

As with the 101 layer sample the signal from the 11 layer sample increased monotonically with decreasing temperature, at an increasing rate, but did not appear to reach the transition point. Perhaps a break in the rise of the signal might have been seen if the temperature could have been taken a bit lower. The intercept of any extrapolation of the results shown in fig 6.17 would be suggestive of Curie-Weiss behaviour, so we would then have to look for a cusp in the magnetisation signal.

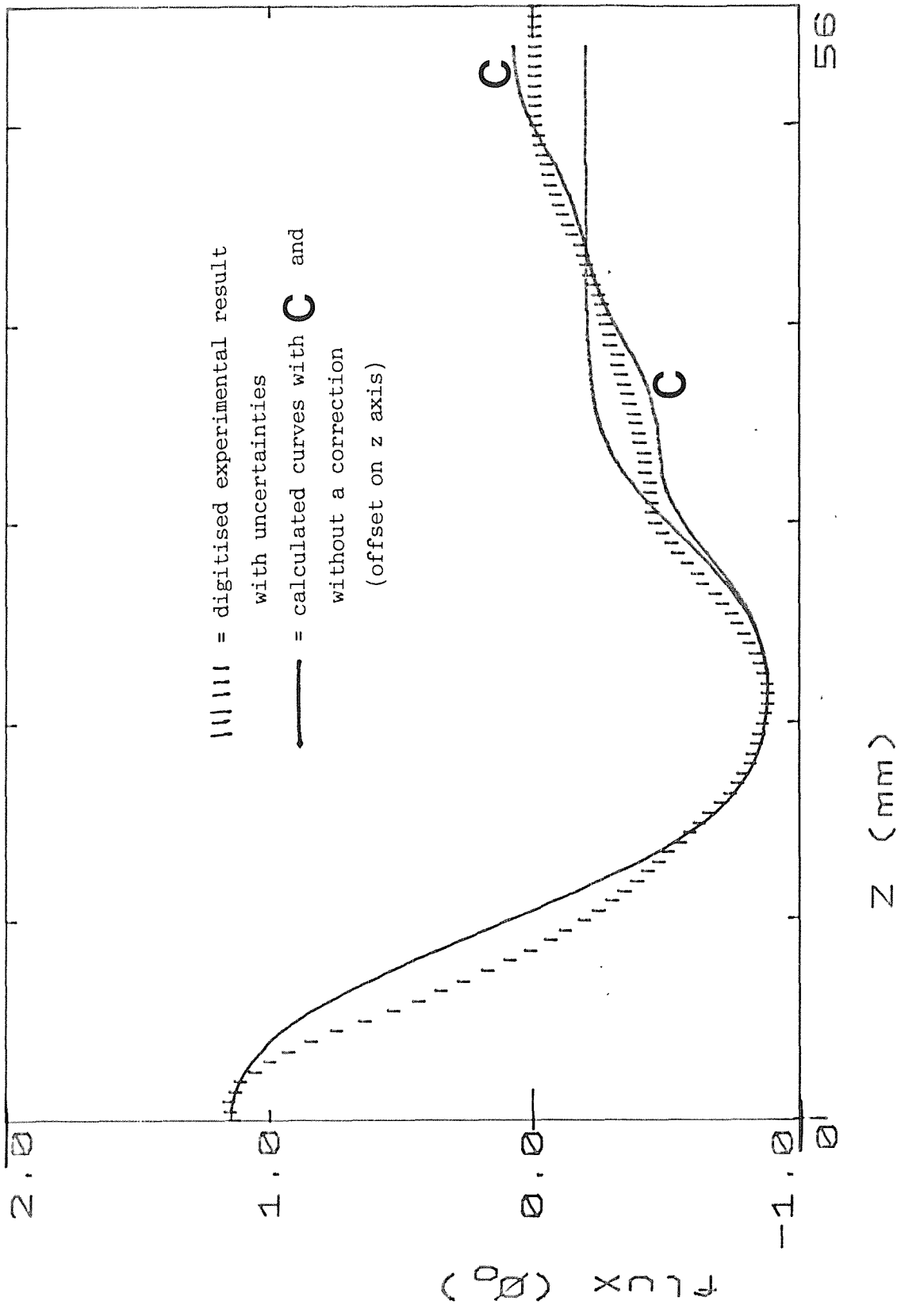

Fig 6.16 Comparison of Simulation and Experiment

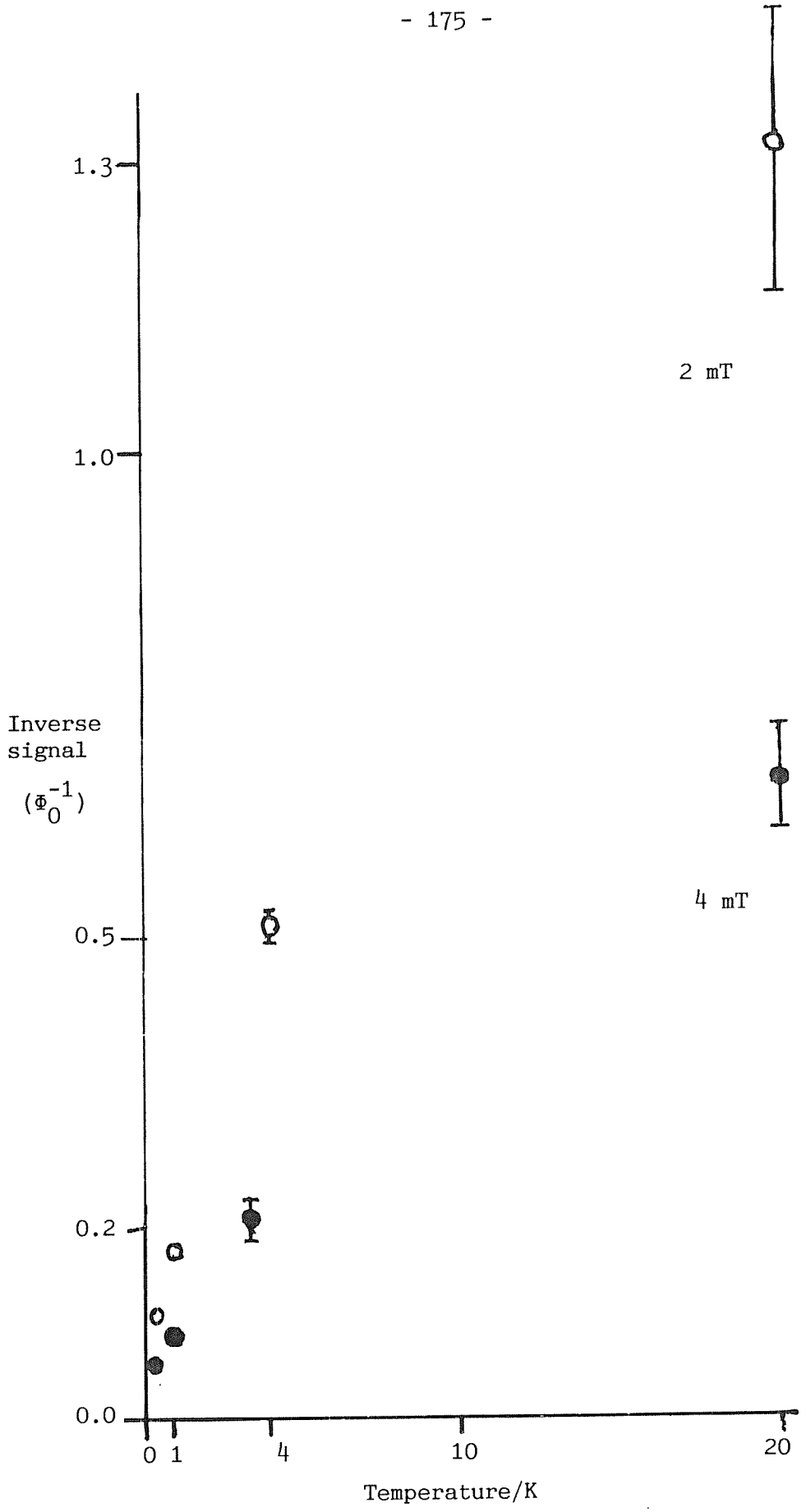

Fig 6.17 11 Layer Inverse Signal against Temperature

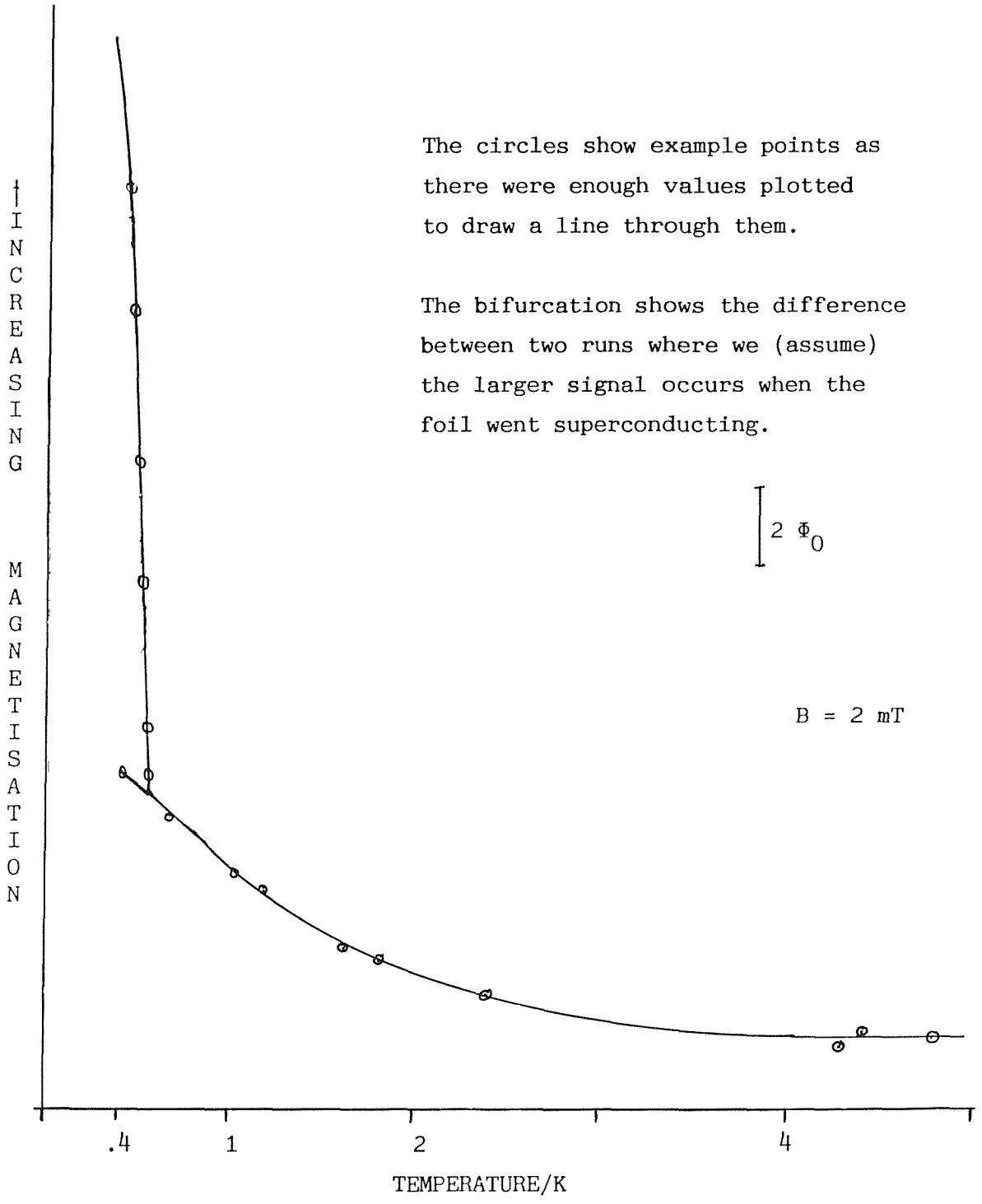

Fig 6.18 11 Layer Signal against Temperature

6.5.3 Type II LB Bilayer

This sample should have produced a very good approximation to a truly two dimensional sample. When measured at 4 and 1.3 K this sample, not surprisingly, provided very little signal in zero field. In a field of ±2 mT and a temperature of 20 K and with the small signal amplified on the chart recorder it was seen to have an unusual shape, but nevertheless consistent with signals obtained later at lower temperatures. Reversal of the 2 mT field at 20 K produced approximately mirror image signals. Most of the other 2 mT signals at lower temperatures had similar amplitudes to each other. When the field was increased to 4 mT and the sample measured at 1.3 K and ~0.4 K, only slightly larger signals were obtained, not double those at the 2 mT field. An example of one of these curves (1.3 K & 0.4 K, 4 mT) is shown in fig 6.19.

For the Φ v T measurements in zero field no signal change was detectable on cooling, starting at 1.2 K, until 0.8 K when there was a sharp deflection of ~6 Φ_0. This was again attributed to superconductivity. In 2 mT no useful signal could be obtained, the signal drift being <1 Φ_0, until the superconducting transition was seen around 0.4 K.

The general curve shape, produced by all the Φ v z measurements was unusual in that it never reached the positive peak; see fig 6.19. If the signal was from the LB film, then the indication from the negative peak position is that the sample was displaced upwards along the z-axis from its intended position.

The magnitude of the negative peak can be compared with that of the 101 and 11 layer samples (i.e. 50 and 5 bilayer samples). The amplitude of the "bilayer" sample was half that of the 11 layers, much bigger than expected. This anomalously large signal which did not change with temperature, and the strange shape, suggested that the source of the signal was some contaminant and not the bilayer. Because of the nature of the results we could not plot p.t.p. variations against field and temperature.

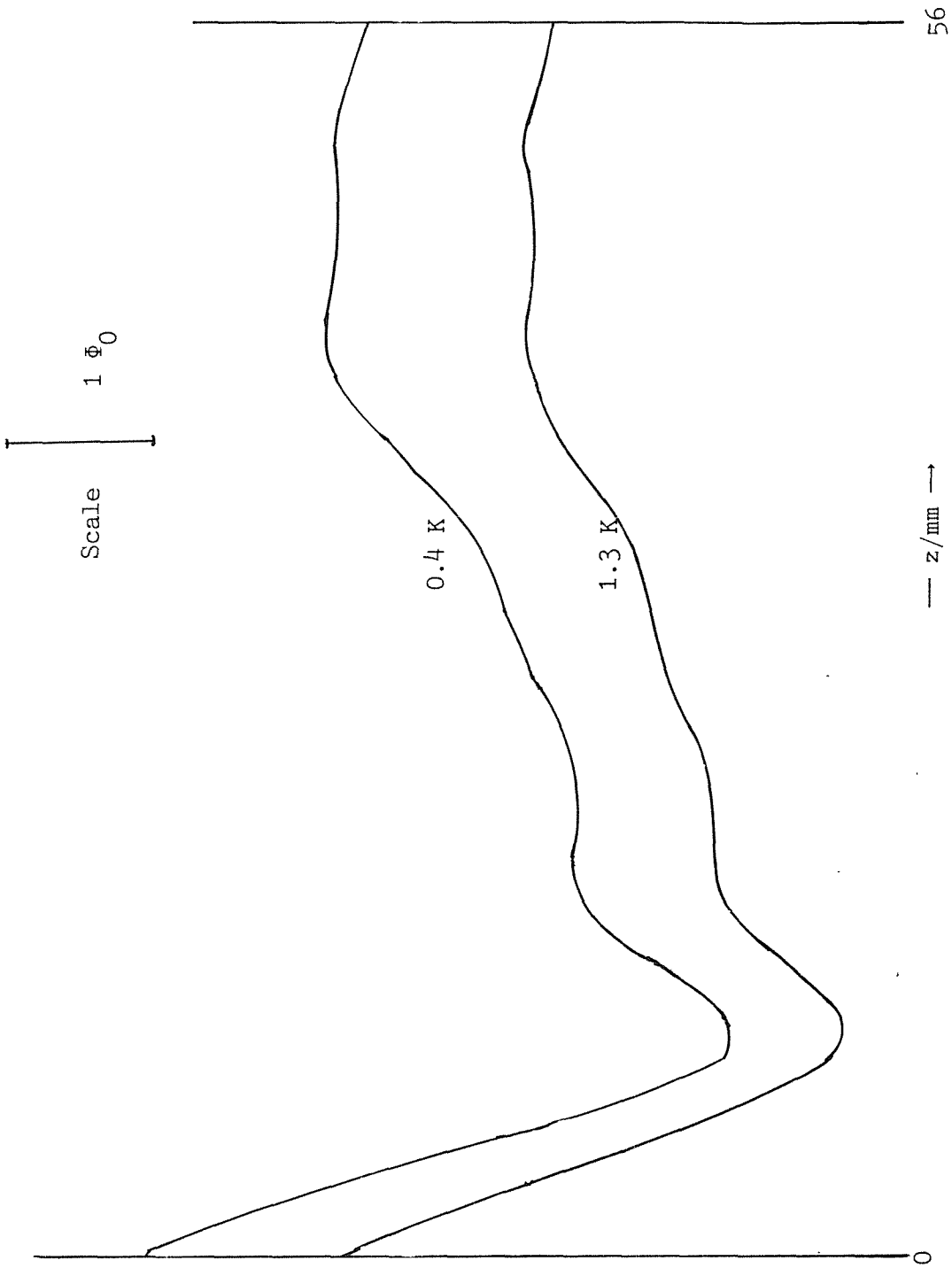

Fig 6.19 Bilayer Sample in 4 mT at 1.3 K

6.5.4 The Manganese Stearate Monolayer

As with the bilayer, virtually no signal was observed in zero field at 4 K or 1.3 K. At 0.4 K the signal from the superconducting foil was dominant. When fields of 1, 2, 2.5, 3 and 4 mT were applied and the temperature lowered a shallow negative peak was observed which increased with the field, and with lower temperatures. The monolayer signal was better behaved than that from the bilayer.

The monolayer curve started to rise towards a positive peak but the sample reached the end stop before reaching the appropriate position in real z-space. If this was the signal from a monolayer then it would mean that a misallignment of at least 5 mm along the z-axis had occurred. However the signal was again larger than expected (based on the 11 & 101 layer results) and the shape was unusually broad. So we concluded that the sample had also been spoiled by contamination. Yet again this observation impresses the great need for a clean environment and very pure materials for measurements on such a small amount of material.

Finally we planned to measure a "3-D" powder sample of $MnSt_2$ (kindly provided by Dr M. Pomerantz) but the cryostat sample tube became jammed during loading. The powder was dissolved in Aristar chloroform and dripped onto the foil and allowed to dry out. To stop the powder falling down the foil tube it was slightly pinched, and this may have contributed to the jamming. Retracting the sample siphon left the foil behind. Unfortunately the jamming of the cryostat sample tube prevented a repetition of these experiments in the time available.

6.5.5 Summary

After using some known samples to calibrate the magnetometer we have been able to measure two quasi two dimensional samples of 101 and 11 layers. Both of their signals increased monotonically with decreasing temperature and no inflections were seen indicating that any transition temperature had not been reached. However the plots of the inverse signal were suggestive of a Curie-Weiss behaviour - intercept offset from the origin - which is discussed further in chapter seven.

CHAPTER SEVEN - IN CONCLUSION

7.1 SUMMARY AND DISCUSSION

1. We have successfully produced magnetically doped Langmuir Blodgett (LB) films of between 1 and 101 layers. These have been deposited onto large sheets of aluminium foil. To the best of our knowledge aluminium foil has not previously been reported as having been used as a substrate.

2. We have operated a SQUID magnetometer below 1 K with a sample that can be moved in and out of the detector. However vibration still remains a problem which means that the magnetometer is limited to fields below 10 mT.

3. We have used the magnetometer to detect our LB films, having successfully removed the substrate signal by the use of a gradiometer and a very long substrate. We measured the 101 layer and 11 layer samples deposited on aluminium foil rolled into a tube, and have shown that the magnetic signal from only one layer is just detectable. However the unusual signal profile for our bilayer and monolayer samples indicated the presence of external contamination. At this level, cleanliness of the samples is very important.

4. We have also improved upon the mathematical/numerical formulae available to model the effect of a superconducting shield. The computer simulations have been validated and have been useful in understanding the experimental signals.

5. The magnetic signal from our LB samples increased on cooling, in keeping with paramagnetic behaviour, but no phase transition occurred, at least down to 0.4 K. This differs from the work of Pomerantz (1980) who reported a transition around 2 K. We took our inverse magnetisation results (of figs 6.12 & 6.17) and multiplied them by the magnetic field and calculated the results per monolayer. (If we were to divide the signal by the number of bilayers this would bring some of the susceptibility results of the two samples closer together. Pomerantz reported that the single monolayer nearest the aluminium does not show a transition, so it might have been better to work in

bilayers).

All these inverse susceptibility results have been plotted for our full temperature range in fig 7.1.1. There is no evidence of any discontinuity or inflexion in the signal around 2 K. Fig 7.1.2 shows an expanded portion of these results below 5 K. The line is a best fit (uncertainty weighted) to all the points (including 20 K). However there may be some systematic errors within each of our field settings, arising from the possibility of remanent fields. We have no accurate estimate of these so they are not included but it is conceivable that even after our precautions they might have been as large as 0.5 mT and therefore responsible for some of the spread in our data.

Another comparison of our inverse susceptibility results is with fig 16 of Pomerantz (1980); reproduced as fig 7.2. E.S.R. intensity is proportional to the susceptibility, so he plotted the inverse intensity against temperature for a "thick" multilayer and this has an inflexion occurring around 10 K. Pomerantz does not comment on this difference from his E.S.R. field shift data which shows 2 K as the ordering temperature, other than to say that there are signs of anti-ferromagnetism below 10 K. We observe no such inflexion in our inverse susceptibility results.

Although we did not have any p.t.p. values around 10 K the Φ v T curves show no indication of any inflexion such as Pomerantz suggested in fig 7.2. Compared with Pomerantz's results our curve indicates a much smaller negative intercept of -0.6±0.4 K on the temperature axis. So our data shows no transition within its range. This difference in the results could be attributed to the preparation route of the different material. Aviram & Pomerantz (1982) have reported a change in the transition in their powder samples of $MnSt_2$ when they were prepared by a revised method. They obtained anti-ferromagnetism with a T_N=10 K instead of weak-ferromagnetism below 5 K. Furthermore a closer study of the data produced by Pomerantz shows that his transition was most visible when the field was perpendicular to the film. Our field was parallel (and it would mean a total sample redesign to alter this). Also Pomerantz's field was around 100 times larger than ours. It is possible that there is a transition just below the lowest temperature that was obtainable in our cryostat. Figs 6.11 and 6.13 show the signal rising rapidly and the temperature intercept of the inverse susceptibility curve suggests the possibility of

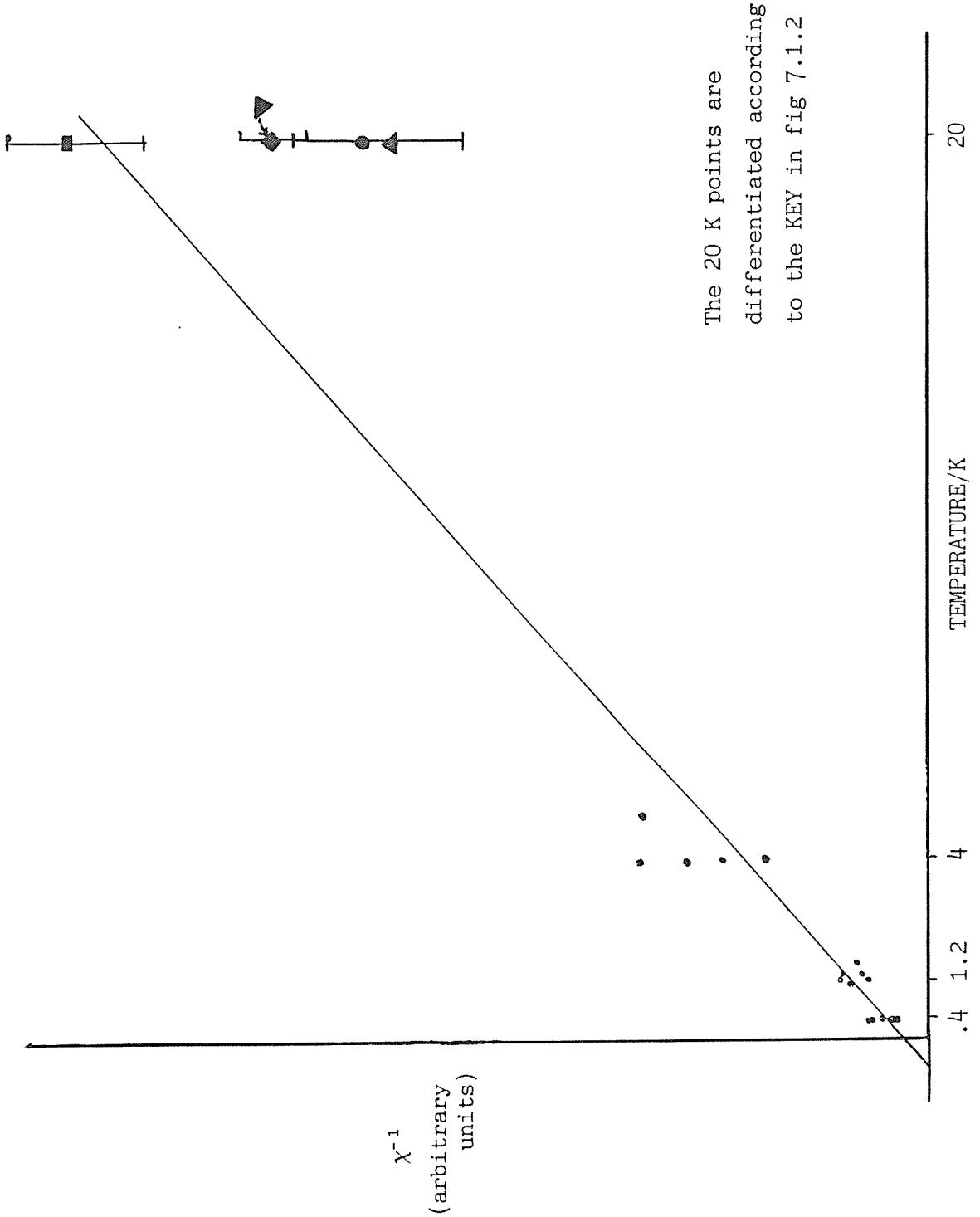

Fig 7.1.1 Inverse Susceptibility against Temperature (T<20 K)

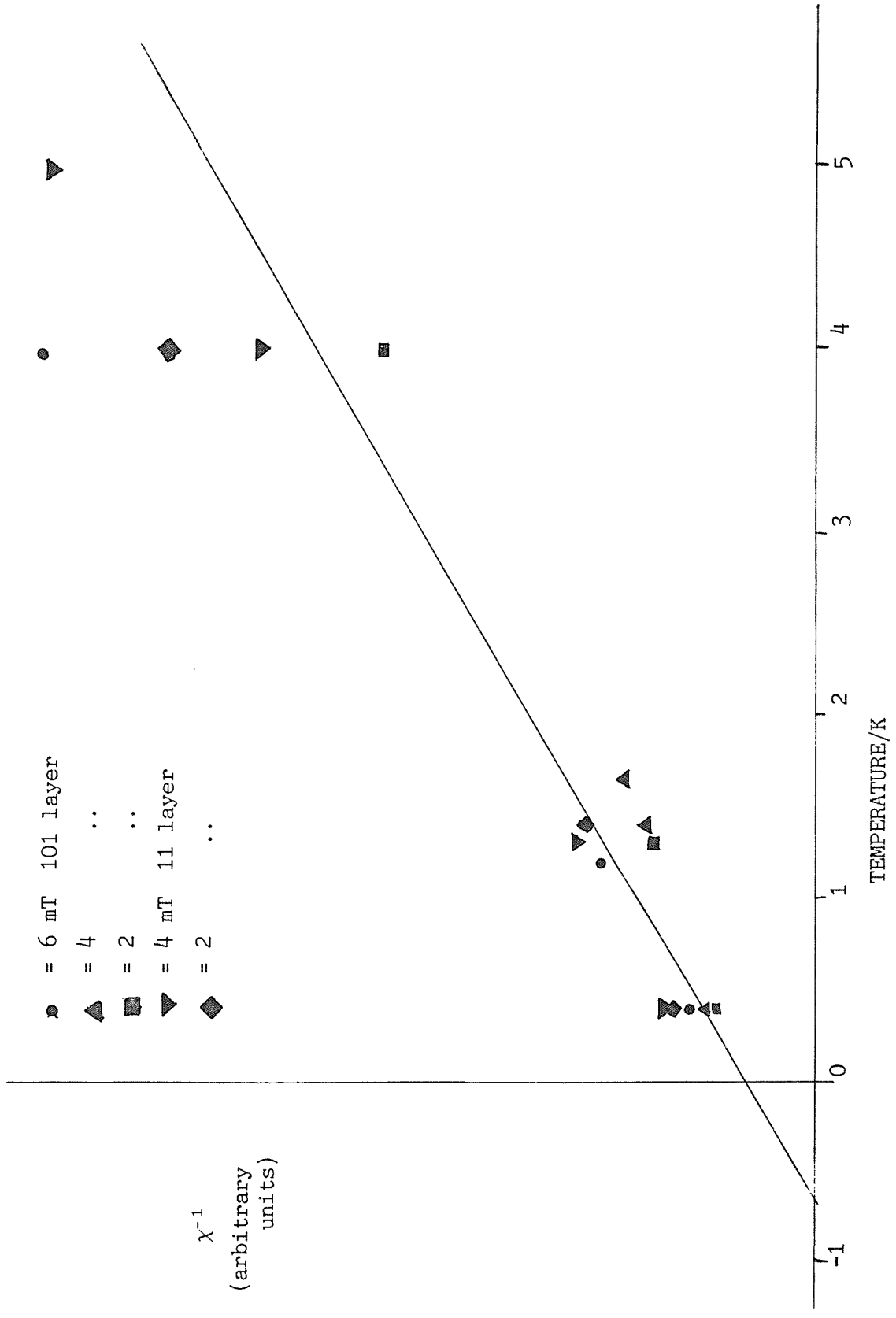

Fig 7.1.2 Inverse Susceptibility against Temperature (T<5 K)

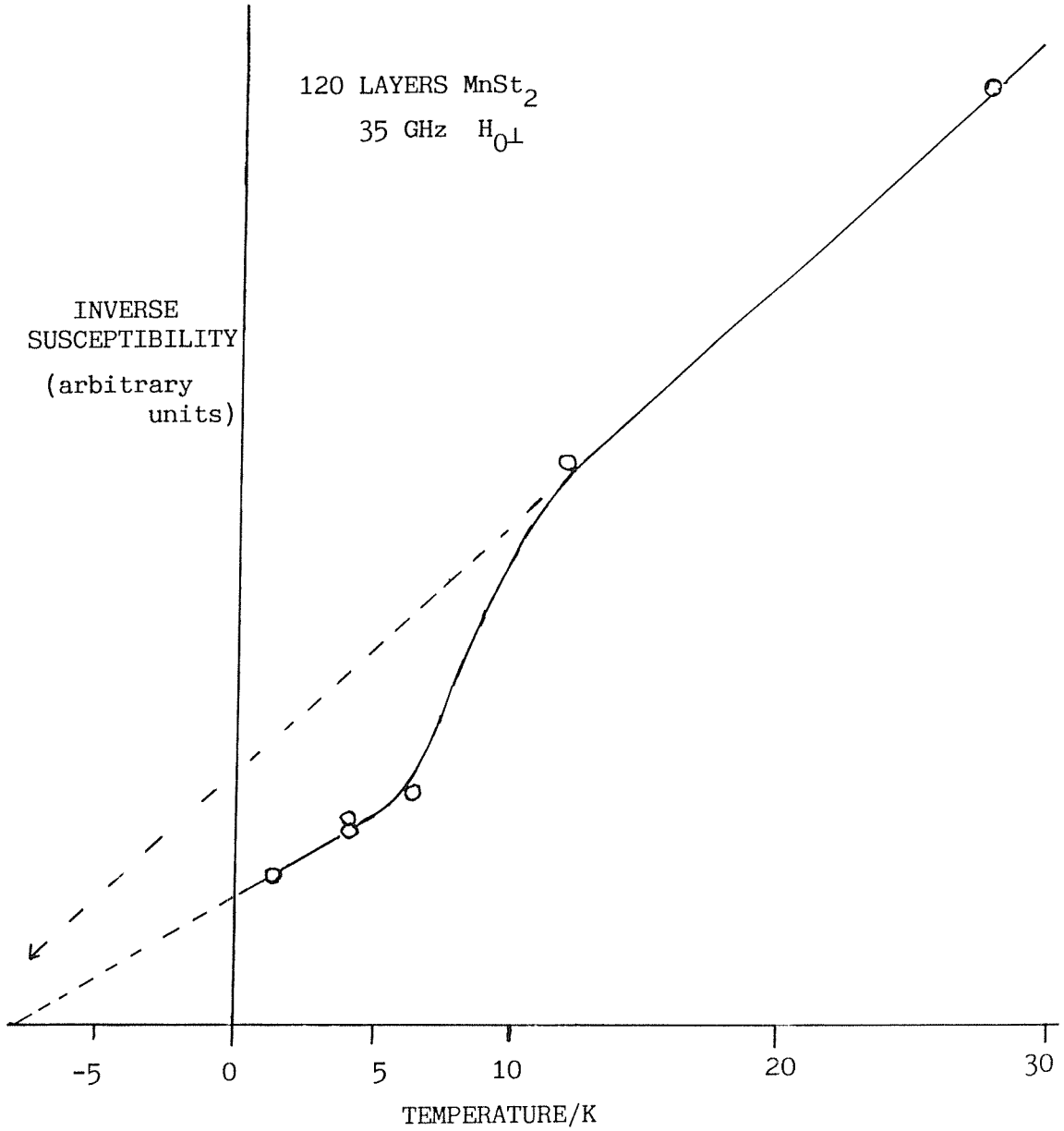

Plot of the inverse susceptibility against temperature for a 120 layer $MnSt_2$ sample (After Pomerantz 1980)

Fig 7.2 The Results of Pomerantz

anti-ferromagnetism within this temperature range.

Finally the measured 4 K value for the 101 layer susceptibility is 6.4×10^{-3} which is close to, but smaller than, the calculated paramagnetic susceptibility of 2.4×10^{-2}.

More detailed and accurate work needs to be done to confirm our experimental results, though first it would probably be useful to make some modifications to the experimental systems as described below. (However a different system might be required if the temperature was to be pushed low enough to detect any transition properly).

7.2 FUTURE APPARATUS IMPROVEMENTS

During this series of experiments we have realised some of the deficiencies of our apparatus. We will summarise these and discuss possible solutions for some of them.

7.2.1 Trough

Since such large samples are needed, it would be much easier if there was a deeper trough or one which contained a deep rectangular pool at its centre. With the larger volume of water allowance should be made in its construction for the use of magnetic stirrers. Also the heat exchanger would have to be constructed with a central gap down it, to allow for long samples.

For cleaning purposes it would be useful if the minimum area on compression was reduced. This could be done if:
i) the dipper and surface pressure system could be easily lifted up,
ii) the barriers were constructed with the tape holders projecting forward of them and
iii) the dead channels were made thinner by use of smaller diameter tape holders.

Better automatic control over the surface pressure is needed. (Large excursions in π occurred during the dipping of our foil multilayers). This might be obtained by replacing the present proportional system with P.I.D. control.

At the air/water interface there is still a need for a better understanding of the meniscus changes during dipping. It might also be possible to use radioactive tracers in the further study of X, Y & Z dipping and the overturning phenomena found in stearate LB films. Furthermore the orientation of "forced Z" samples should be checked.

7.2.2 Cleaning

There is a constant need to improve the level of cleanliness in the sample preparation. A source of truly clean gloves is still lacking. Also the last cleaning material to touch the substrates before use is Analar propan-2-ol, so it would be logical to improve its purity to the same standard as the Millipore water, by some similar filtration system.

If further results are obtained, then a check on the effects of material purity (viz stearic acid and $MnCl_2$) could be made. The different synthesis methods of Aviram & Pomerantz (1982) could also be tried. Finally the cleanliness of the foils still remains a problem particularly as they necessarily have a large surface area. It would be advantageous to be able to check how clean they are, and if they become contaminated with time - perhaps by repeated measurements in the cryostat? Also the "hands on" method of rolling the foils up should be improved upon.

7.2.3 Substrates and Samples

All the samples that we have measured have been deposited on aluminium foil substrates and it will probably be necessary to continue using foils of some type to achieve a discernable signal from a few multilayers or less. Foils made from pure aluminium could be tried, but there remains the problem of its superconductivity in low fields. It might be possible to use gold foil, but it would dip differently (see Peterson et al 1986) and would be expensive.

It would also seem a good idea to continue the use of "infinite" foils, as this reduces the need for background subtraction. In fact a slightly longer foil and a shorter sample holder would further reduce the end effects of the present "not quite infinite" foils. (But this would also require a deeper trough - unless the foil could be folded over at the end which is to be submerged, and then unfolded after the dipping is complete).

For monolayers and bilayers it was difficult to tell exactly where deposition had occurred (as there was no obvious colour tinge). This problem could be magnified by large meniscus effects or some effect from forced Z dipping. So it would be useful if some optical (polarisation?) technique could be used to establish the exact position where deposition had occurred on the substrate.

As well as altering the substrates, different sample material could be used, possibly cadmium or ferric stearate. Since Prakash et al (1987) have now been able to make LB films of ferric stearate, perhaps revised techniques could also be used to produce cobalt and nickel stearate films. These materials are expected to have much higher signals than $MnSt_2$.

It would be an advantage to produce and measure several similar samples to check for consistency of results. So far we have only made one sample of each size. When loading the samples they had to be transferred some distance to the cryostat. Perhaps a carrying box could be made for them and a new type of side opening put into the present air lock chamber. Then a sample might be changed without totally removing the sample siphon. Otherwise and perhaps more usefully as the present siphon is heavy and was constructed with a kink in it, it could be replaced by two simple sample tubes; they would have no pre-cool facilities but would be cooled by exchange gas. If a sample was changed at the end of the day the gas could be pumped out overnight. (To achieve the lowest temperature the O.I. manual suggests using exchange gas even with the present sample siphon). If there were two sample "siphons" and two identical sample holders, then the sample change could be speeded up as the new sample could be loaded while the old one was still warming up to room temperature.

7.2.4 The Cryostat

1. Cryogenics

Instead of blowing gas across during a cooldown it is easier to suck it across from a freely vented dewar, with the siphon dipping into the liquid. This method is used at NPL using a rotary pump and control valve. This method should be tried in the He3/SQUID cryostat.

It would be useful to cross calibrate the temperatures at the base of the sample foil and the copper top hat with the Germanium thermometer

on the He3 pot. This would give us a better indication of how the foil was cooling. At the same time a better method is needed to ensure that the copper braids leading from the He3 pot to the top hat do not touch the side walls of the IVC at 4 K. It might be necessary to hang a short, but wide, guide tube from the He3 pot to stop any possibility of the braids splaying out. The copper wires used at present break too easily. Otherwise the lower half of the braids might be replaced by solid copper rods and the flexible braiding kept above the He3 pot.

2.The Magnet

Because of the requirement for small fields (a few mT) it would be useful to have a small stabilised magnet power supply. There is also a need to check the value and profile of these small fields within the present large magnet and shield system as well as a further need to check on the size of any remanent fields. This might be best done by making a low temperature n.m.r. probe using p.t.f.e. as the detector material (S. Swithenby private communication 1985). The Hall probe lacked sensitivity and its bias current caused self heating.

Of course if one is going to continuously work at low fields, it might be worth while replacing the present magnet with a a small one made by winding it directly onto the I.V.C. tail. The field would then have to be maintained by the superconducting shield, unless a heat switch was added to allow persistent operation. With the small fields there should be less magnetic strain on the cylinder. (Otherwise perhaps two concentric cylinders could be used, the outer one to maintain the field, while the inner one compensated for any drift in the outer shield). The removal of the present magnet would solve the problem of the redundant shims and perhaps reduce the remanent fields. There would be less wires meaning less heat leak, and a bigger volume for the helium liquid at the bottom of the cryostat.

3.Shield

To obtain good field trapping the top clamp of the shield, to the I.V.C., might have to be changed to a slightly less (thermally) conducting material. This would ensure cooling from the bottom up to obtain a more uniform trapped field (J. Gallop - private communication 1987). There is also a need to change/replace the present pick-up coil to stop any possibility of it vibrating with respect to the shield. (Maybe this could be done by packing the interspace with a lot of vacuum grease, or potting them?). It would also be a big advantage

when making cryostat alterations if the connections of the superconducting leads at the very bottom of the I.V.C. were made of some form of shielded screw joint, instead of the present spot welding. These welds have caused continuity problems as well as being prone to breakage.

Because the SQUID is so sensitive, particularly to R.F. noise, then the leads to the thermometers and the magnet should be screened; particularly at their connection points at the top of the cryostat top face. This would require a different type of connector to the one already provided by Oxford Instruments. At the same time the screening of the pick-up coil leads going from the base of the niobium shield to the connection point should be improved; perhaps by encasing in a thin grease packed niobium tube. A similar niobium tube could replace the present solder tinned copper tube that goes from the I.V.C. base up to the SQUID.

4.SQUID

To actually improve the SQUID's noise performance there are several things that could by tried. We have already mentioned the effect of a lower helium level. If there was a bigger volume for liquid at the bottom of the cryostat it would not need to be filled so high. However to ensure the SQUID's temperature was kept fixed thermal links to the liquid would be required. Based on our previous observations there might be long term drift problems, though this should be acceptable if there was a reduction in short term noise.

Otherwise the cryostat might be run at a higher pressure, to raise the temperature, to see if the SQUID responded better. (There might be safety problems and heavier stoppers could be required on the fill and dip ports). On a smaller scale several authors have reported controlling the gas pressure above the helium, to remove temperature fluctuations, to increase SQUID stability. In a similar vein to stop convection cells in the boiling helium from affecting the SQUID, quartz microspheres could be packed around its superconducting terminals as described by Taber & Cabrera (1985).

7.2.5 Sample Measurement

In processing the data, for detailed comparisons, we have had to digitise our chart recordings. We have also noted the problem that these readings were taken on the move, and subject to eddy current

effects and any vibrations that were present. Perhaps with new smoother sample "siphons" it would be possible to use computer control for sample insertion. As long as there is no excessive vibration noise the sample could be stopped at several points and the D.C. signal measured, as was originally intended. (Excessive vibration noise means noise that causes the SQUID to break lock). Another possibility, if the computer was fast enough, would be to read the output directly onto the computer during a smooth insertion (similar to Beauvillain et al (1985)). The run would then have to be repeated several times to produce an average. However there would still be a requirement for the software to remove the occasional flux jump.

With a better measuring system a more accurate value for the pick-up coil coupling factor could be obtained. A measured sample coil, carrying a known stable direct current, wound on a cleaned "infinite" substrate might be helpful in obtaining this as well as further confirming the system's linear response to signals.

7.3 CONCLUSION

Experimental

There is no evidence for a magnetic transition temperature in LB films of manganese stearate above 0.4 K. However the increasing signal and the plots of inverse susceptibility suggest that a transition to anti-ferromagnetism may occur just below the lowest temperature that we were able to obtain.

Theory

As we do not seem to have reached a transition we have not been able to see if any comparison with theory could be made. Hence with regard to the effect of dimensionality on any LB transition, the question that Pomerantz (1980) originally posed still remains, "2-D or not 2-D? That is the question."

Applications

As for the practical use of LB films as magnetic memories in superconducting computers: This may now be irrelevant with the discovery of high T_c superconductors, unless such things as iron based LB compounds have a higher ordering temperature somewhere above 77 K.

APPENDIX

Listing 1 FLUX3D

```
100 REM 3D FLUX USING GARRETT
110 REM D I HEAD
120 REM Date 10.10.84 & MAR & APR 85
150 DIM Y(5),X(5),Z(4),W(4)
165 REM---------INITIALISATION---------
170 A=.005185: R=.001: REM Coil radius, sample radius (m)
172 PRINT:PRINT"SAMPLE RADIUS= ";R;" METRES":PRINT
175 R=R/A :REM REDUCED R
180 B0=.001:REM Field in tesla
182 PHI0=.207E-14 :REM Flux quantum in Wb (Tm^2)
185 S=0 :T=0
190 NC=2667:REM pick-up coil turns/m
195 REM -------SAMPLE DIMENSIONS------
196 REM -------& SUSCEPTIBILITY-------
197 REM S.I.UNITS
200 Y(1)=-.1   :Y(2)=-.010 :Y(3)=.010
201 Y(4)=.05   :Y(5)=.1    :REM Y(5)=YMAX
210 X(1)=1E-5 :X(2)=5E-5  :X(3)=1E-5
211 X(4)=-3E-5:X(5)=0     :REM X(5)==0
255 PRINT"SUSCEPTIBILITY","POSITION"
260 FOR I=1 TO 5
265 PRINT"X(";I;")= ";X(I);TAB(20);"Y(";I;")= ";Y(I)
270 NEXT I
280 PRINT
290 PRINT"Z","FLUX IN PHI0"  :REM Table Headings
295 REM-----MOVING SAMPLE IN-----------
300 Z0=.056 :REM THROW OF SAMPLE (m)
305 FOR ZK=0 TO 56 STEP4
310 ZE=Z0-ZK/1000
320 FOR J=1 TO 4 :REM 4 SECTIONS OF SAMPLE
325 IF X(J)=0 THEN 480
330 FOR C=-1 TO 1 STEP1 :REM COUNT THRU COILS BOT MID TOP
340 Z(1)=ZE+Y(J+1)+1E-3*(+6-3*C*C-19*C)
350 Z(2)=ZE+Y(J+1)+1E-3*(-6+3*C*C-19*C)
360 Z(3)=ZE+Y(J)  +1E-3*(-6+3*C*C-19*C)
370 Z(4)=ZE+Y(J)  +1E-3*(+6-3*C*C-19*C)
380 FOR I=1 TO 4 :REM GARRETT(END POINTS)
390 Z=Z(I)/A
400 X=SQR((4*R)/((1+R)*(1+R)+Z*Z)):REM k
410 N=(4*R)/((1+R)*(1+R)):REM c*c
420 W(I)=FNMS(N,X)  :REM Calc Garrett function
430 NEXT I
440 M=W(1)-W(2)+W(3)-W(4)
450 S=S+M*(1-2*C*C):REM ADDS SUB TOTAL ACCOUNTING FOR SIGN OF COIL
460 NEXT C
470 T=T+S*X(J) :S=0:REM ADDS TO TOTAL FLUX, RESETS SUB TOTAL TO 0
480 NEXT J
```

/cont

```
  500 T=T*NC*BO/PHIO
  510 IF ZK=0 THEN TO=T
  511 IF ZK=0 THEN PRINT TAB(10);"TO= ";(TO*A*A*A)
  520 T=T-TO :REM ZERO NORMALISE
  530 PRINT TAB(1); ZE*1000,T*A*A*A
  540 T=0
  550 NEXT ZK
  600 STOP
 1000 REM----------FUNCTIONS----------
11495 REM-----MUTUAL INDUCTANCE--------
11500 DEF FNML(N,X)
11510 =Z*SQR((1+R)*(1+R)+Z*Z)*(FNKK(X*X)-FNEE(X*X)-
     (1-R)*(1-R)*(FNPI(N,X)-FNKK(X*X))/((1+R)*(1+R)+Z*Z))/2
11550 DEF FNMS(N,X)
11570 =Z*FNML(N,X)+2*R*SQR((1+R)*(1+R)+Z*Z)*
     (FNKK(X*X)-(2/(X*X)-1)*(FNKK(X*X)-FNEE(X*X)))/3
11800 REM-----ELLIPTIC INTEGRALS-------
11900 DEF FNKK(X)
11910 y=1-X: =1.38629436112+y*(.09666344259+y*(.03590092383+y*
     (.03742563713+y*.01451196212)))-(.5+y*(.12498593597+y*
     (.06880248576+y*(.03328355346+y*.00441787012))))*LN(y)
11920 DEF FNEE(X)
11930 y=1-X: =1+y*(.44325141463+y*(.0626060122+y*(.04757383546+y*
     .01736506451)))-(.2499836831+y*(.09200180037+y*
     (.04069697526+y*.00526449639)))*y*LN(y)
11940 DEF FNF(N,X)
11950 y=N: a=1: s=SIN(X)^2
11960 REPEAT
11970 a=a*2/(1+y):s=.5*(1+y*s-SQR((1-s)*(1-y*y*s))):y=2*SQR(y)/(1+y)
11980 UNTIL y>.999999
11990 =a*LN(TAN(.78539816339+.5*ASN(SQR(s))))
12300 DEF FNE(N,X)
12310 a=1: b=SQR(1-N*N): z=0: n=1: t=TAN(X)
12320 REPEAT
12330 t=TAN(X): t=(b/a-1)*t/(1+b*t*t/a)
12335 c=.5*(a-b): s=.5*(a+b): b=SQR(a*b): a=s: X=2*X+ATN(t)
12340 z=z+c*SIN(X): n=2*n
12350 UNTIL c<1E-8
12360 =z+X*FNEE(N*N)/(a*n*FNKK(N*N))
12400 DEF FNPI(N,X)
12405 k=FNKK(X*X): e=FNEE(X*X)
12410 IF N>=0 AND N<X*X THEN =k*(1+SQR(N/((1-N)*(X*X-N)))*
    FNz(X,ASN(SQR(N/(X*X)))))
12420 IF N>1 THEN =k-FNPI(X*X/N,X)
12430 IF X*X<N AND N<1 THEN =k+.5*PI*SQR(N/((1-N)*(N-X*X)))*
     (1-FN1(X,ASN(SQR((1-N)/(1-X*X)))))
12440 IF N<0 THEN =N*(X*X-1)*FNPI(((X*X-N)/(1-N)),X)/
     ((1-N)*(X*X-N))+X*X*k/(X*X-N)
12445 IF N=X*X THEN =e/(1-X*X)
12480 DEF FNz(N,X)=FNE(N,X)-e*FNF(N,X)/k
12490 DEF FN1(N,X)=2*(k*FNE(SQR(1-N*N),X)-(k-e)*FNF(SQR(1-N*N),X))/PI
```

Listing 2 SAMPAC

```
  1 REM     Program 'SampAC',DIH June 87
  2 REM  Uses gradiometer simulation source file "C.Grds---"
  3 REM  (x-incr.=.1 mm) to simulate a sample with Z dependent
  4 REM  susceptibility. Sample treated as 4 segments,
  5 REM  radius = ---.
  6 REM  In this case the sample is just one coil,
  7 REM  so only one segment is required.
  9
 10 MODE 4
 12 PROC INITIALISE  : REM defines function keys etc.
 15 ON ERROR GOTO 180
 20 Y1%=1060:Y2%=-16 :Y3%=0 :Y4%=1060:Y5%=1060
 22 REM  Yn's are the distances of the segment ends from the
 23 REM  coil centre when the sample comes to rest in the
 24 REM  "DOWN POSITION"    (In 0.1 mm units)
 25 X1=0:X2=8.02E-4:X3=0:X4=0 :REM in SI units
 27 REM  Xn's are the different susceptibilities of the
 28 REM  samples segments.  For a current carrying coil we
 29 REM  obtain X=ni/H (or mu0ni/B)
 40 YY$="Y1%=1060:Y2%=-16:Y3%=0 :Y4%=1060:Y5%=1060"
 45 XX$="X1=0:X2=8.02E-4:X3=0:X4=0"
 46 REM  YY$ & XX$ required for id of results on disc
 50 PRINT:PRINT:PRINT:PRINT:PRINT
 52 PRINT YY$:PRINT
 55 PRINT XX$:PRINT
 60 n%=116  :REM  n%=(x2-x1)*2,
 61 REM  the no. of points if taken at .5 mm spacing
 65 B=0.001 :REM  The magnetic field in tesla
 70 B$="B=.001"
 75 PHI0=2.07E-15 :REM Flux quantum (SI - Wb or Tm^2)
 80 CF=0.001564:REM pu coil/SQUID coupling factor
 85 CF$="CF=.001564"
 88
 90 A$="B*CF*(FNFluxTot(i%*5,Y2%,Y3%)*(-X2))/PHI0"
 92 REM   A$ defines the function which will be
 93 REM   calculated when called in PROCPLOT
110 PROC LOAD
120 PRINT F$:PRINT;" P% on file=";PF%;" P% counted in=";P%
130 DESCRIP$="DC coil 100V "+YY$+XX$+B$+CF$
131 REM  Descrip$ may be written into the program
132 REM  as a default name for any data file
133 REM  which will be saved after calculation
140 x1=0:x2=58:PRINT;"x1=";x1;" x2=";x2
142 REM  x's refer to the z-range (from the coil centre)
143 REM  over which the calculation is to be carried out.
150 PROCPLOT   :REM  This will calculate the signal over
151 REM  the specified range and display its shape and
152 REM  peak dimensions onto the screen.
155
160 PRINT "KEY 1 . . New X2 and S/pose"'"KEY 2 . . Procsave"
161 PRINT "KEY 3 . . Print Data"'"KEY 7 . . Screen Dump"
162 PRINT "KEY 9 . . List program"
170 STOP
175 END
```

/cont

```
 180 IF ERR=17 THEN PROC CLOSE
 185 REPORT:PRINT " at line ";ERL:END
 190
 200
 221 REM-------------------------------------------------------
 222 REM     THE  PROCEDURES
 230
1000 DEF PROC INITIALISE
1001 *KEY 1 PROCSUPERPOSE|M
1002 *KEY 2 PROCSAVE|M
1003 *KEY 3 PROC PrintData|M
1005 *KEY 9 MODE 3|M |NL.|M
1100 *FX6,10
1107 REM CODE FOR PRINTER
1110 DIM x(150),y(150),X(700),Y(700)
1120 REM x & y arrays contain the position and calculated flux
1121 REM X & Y arrays contain the position and value of the
1122 REM instrument function
1300 ENDPROC
1990
2000 DEF FNFluxTot(j%,Y1%,Y2%)
2010 x(i%)=X(j%)
2080 z1%=j%+Y1%:z2%=j%+Y2%
2085 IF z2%>P%-1 THEN z2%=P%-1:IF z1%>P%-1 THEN z1%=P%-1
2090 IF z1%>=0 THEN =Y(z2%)-Y(z1%)
2100 IF z1%<0 AND z2%>0 THEN =Y(z2%)+Y(-z1%)
2110 IF z2%<=0 THEN =Y(-z1%)-Y(-z2%)
2990
3070 DEFPROC CLOSE
3080 VDU1,17
3090 VDU4
3100 *FX3,0
3110 *FX5,1
3120 CLOSE£0
3130 ENDPROC
3135
3140 DEFPROC LOAD
3150 PRINTTAB(0,0) SPC(160):PRINTTAB(0,0)
3160 INPUT"Name of source file ? "SF$
3190 IN=OPENIN SF$
3200 IF IN = 0 THEN PRINT "*file name wrong* TRY
    ANOTHER FILE":GOTO 3160
3220 INPUT£IN,F$
3230 INPUT£IN,PF%
3240 J%=-1
3250 REPEAT
3260 J%=J%+1
3270 INPUT£IN,X(J%),Y(J%)
3290 UNTIL EOF£IN
3300 P%=J%+1
3310 CLOSE£IN
3320 IF J%=-1 THEN PRINT "FILE NOT LOADED":GOTO 3160
3330 ENDPROC
3335
```

/cont

```
 3340 DEFPROC PrintData
 3350 @%=&080A
 3360 PRINTTAB(0,0) SPC(160):PRINT TAB(0,0)
 3370 FOR J%=0 TO P%-1
 3380 PRINT;J%;TAB(10);x(J%);TAB(20);y(J%):NEXT
 3390 @%=10
 3400 ENDPROC
 8990
 9000 DEF PROCSAVE
 9010 INPUT "Name of new file"N$
 9020 INPUT "New description is .";DS$: IF DS$="" THEN 9040
 9030 DESCRIP$=DS$ :REM Allows overwrite of default title
 9040 PRINT "New description is ....";DESCRIP$
 9112 ST=OPENOUT N$
 9115 PRINT£ST,DESCRIP$
 9118 PRINT£ST,PS%
 9120 FOR i%=0 TO PS%-1
 9125 PRINT£ST,x(i%),y(i%)
 9130 NEXT
 9135 CLOSE£ST
 9138 ENDPROC
 9990
13000 DEF PROCPLOT
13010 clear%=TRUE
13110 y2=-1E10: y1=1E10: p=1100/(x2-x1): q%=-p*x1+100:
     dx=(x2-x1)/n%
13120 FOR i%=0 TO n%
13130 y(i%)=EVAL(A$)
13150 IF y(i%)>y2 THEN y2=y(i%)
13160 IF y(i%)<y1 THEN y1=y(i%)
13170 NEXT
13175 PS%=i%
13180 IF clear% THEN CLS: r=850/(y2-y1): s%=-r*y1+100
13182 IF s%>0 THEN MOVE 0,s%: PLOT 21,1279,s%
13184 IF q%>0 THEN MOVE q%,0: PLOT 21,q%,950
13186 MOVE p*x1+q%,r*y(0)+s%
13190 FOR i%=0 TO n%
13195 X=x1+i%*dx
13200 PLOT 5,p*X+q%,r*y(i%)+s%
13210 NEXT
13220 VDU 5: @%=&20207
13250 MOVE 1050,r*y1+s%: PRINT y1
13260 MOVE 1050,r*y2+s%: PRINT y2
13270 VDU 4: @%=2570
13280 ENDPROC
13290
13300 DEF PROCSUPERPOSE
13302 INPUT TAB(0,0) "New X2="X2
13306 INPUT "New X6="X6
13307 INPUT "New X7="X7
13310 clear%=FALSE
13320 GOTO 13120
13340 ENDPROC
```

Listing 3 TUBERS

```
  1 MODE 4
 10 REM Program 'TUBERS',DIH 16/6/86. Simulation of SQUID p/u coil
  and 4 segment 'solenoid' sample, various radii (---)mm.
 20 REM Program uses gradiometer simulation source files C.GRDS---
  eg C.Grds210 & C.Grds160, x-incr.=0.1 mm, to simulate a FOIL
  TUBE OR LB FILM sample with Z dependent susceptibility.
  Stores result on disk as S.-------
 30 N%=2:REM No. of radius codes
 32 PROC INITIALISE
 35 ON ERROR GOTO 530
 41 R%(1)=160 :REM  RADIUS CODE (RC)=1
 43 R%(2)=210 :REM  RADIUS CODE (RC)=2
 44 REM Codes give radius in units of.01mm
 45 NM=11    :REM No. of monolayers
 47 FF=.0157*NM/101  :REM Normallised Filling Factor
 50
 51 Y1%=-100  :X1=4.09E-3*FF :01%=2 :I1%=1
 52 Y2%= 100    :X2=0*FF       :02%=2 :I2%=1
 53 Y3%= -555 :X3=11E-3*FF:03%=2 :I3%=1
 54 Y4%= -545 :X4=0  :04%=0 :I4%=0
 55 Y5%= 1060 :X5=0  :05%=0 :I5%=0
 56 Y6%= 1060  :X6=0  :06%=0 :I6%=0
 57 Y7%= 1060
 80 REM Yn's are distances from coil centre -units of .1mm
 82 REM XN'S are susceptibilities (SI) x filling factor
 85 REM Om's & Im's are code nos. for outer & inner radii
  of section "m"
150 x1=0:x2=57 :REM Sample finish and end posn (mm)
155 n%=(x2-x1)*2 :REM n%=116 FOR 58 mm
170 B=0.002:B$="B=.002":REM tesla
175 PHI0=2.07E-15 :REM SI FLUX QUANTUM
180 CF=.0017: CF$="CF=.0017" :REM SQUID COUPLING FACTOR
200 DESCRIP$="11layer LBfilm -Ybot,CHI,Ytop:=-10mm,4.09E-3,10mm
  & -55.5,11E-3FF,-54.5mm"+B$+CF$
  :REM the default title put on disk
201
230 REM Below is a template for the function to be
  calculated which describes the sample of interest.
250 REM A$="B*CF*(FNFT(i%*5,Y1%,Y4%,3)*X1+FNFT(i%*5,Y2%,Y3%,3)*
  X2+FNFT(i%*5,Y4%,Y5%,3)*X4+FNFT(i%*5,Y6%,Y7%,3)*X6-
  (FNFT(i%*\5,Y1%,Y4%,1)*X1+FNFT(i%*5,Y2%,Y3%,1)*X2+
  FNFT(i%*5,Y4%,Y5%,1)*X4+FNFT(i%*5,Y6%,Y7%,1)*X6))/PHI0"
262
295 FOR r%=0 TO N% :REM Loading in (from disc) reqd "instrument
  functions"
297 IF R%(r%)=0 THEN 305
300 PROC LOAD
305 NEXT
500 PROCPLOT
505 PRINT"KEY  --- See lines 160-1300 of SAMPAC for this code
1990
```

/cont

```
 2000 DEF FNFT(j%,Y1%,Y2%,r%)
 2005 REM Get value from correct posn of appropriate
    instrument function
 2010 x(i%)=X(j%)
 2020 REM IF r%=0 THEN =0
 2080 z1%=j%+Y1%:z2%=j%+Y2%
 2085 IF z2%>P%-1 THEN z2%=P%-1
 2086 IF z1%>P%-1 THEN z1%=P%-1
 2088 IF z2%<-P%+1 THEN z2%=-P%+1
 2089 IF z1%<-P%+1 THEN z1%=-P%+1
 2090 IF z1%>=0 THEN =Y(z2%,r%)-Y(z1%,r%)
 2100 IF z1%<0 AND z2%>0 THEN =Y(z2%,r%)+Y(-z1%,r%)
 2110 IF z2%<=0 THEN =Y(-z1%,r%)-Y(-z2%,r%)
 2990
 3070 DEFPROC CLOSE  --- See SAMPAC for this procedure
 3140 DEFPROC LOAD
 3145 K$="0" REM Initialising as empty
 3150 SF$="C.GRDS"+ST!R$(R%(r%))  :REM Get correct filename
    for reqd radius
 3190 IN=OPENIN SF$
 3195 IF IN<>0 THEN 3220
 3200 IF IN=0 THEN PRINT "WANT ";SF$;'"LOAD ANOTHER DISC?"'
    "TYPE 'K' WHEN READY"
 3205 IF IN=0 THEN K$=GET$
 3210 IF IN=0 AND K$="K"THEN 3190 ELSE 3200
 3220 INPUT£IN,F$  :REM Descrition of data file being loaded
 3225 PRINT F$: PRINT SF$ :PRINT
 3230 INPUT£IN,PF%
 3240 J%=-1
 3250 REPEAT
 3260 J%=J%+1
 3270 INPUT£IN,X(J%),Y(J%,r%)
 3290 UNTIL EOF£IN
 3300 P%=J%+1
 3310 CLOSE£IN
 3320 IF J%=-1 THEN PRINT "FILE NOT LOADED, WANT ";SF$:STOP
 3330 ENDPROC
 3335
 3340 DEFPROC PrintData  --- See SAMPAC for this procedure
 9000 DEF PROCSAVE  --- see SAMPAC for this procedure
13000 DEF PROCPLOT  --- see SAMPAC for this procedure
13300 DEF PROCSUPERPOSE -- see SAMPAC for this procedure
```

Listing 4 GJDOST2

```
  0 REM Program 'GJDOst2',BHB, 7/6/86 & DIH 87:
    Solenoid-solenoid flux linkage for coil/sample/screen
    dimensions of Southampton SQUID magnetometer.
  1 MODE 4
  2 PROC INITIALISE
  5 D=.1:REM x-increment
  6 n%=500:x1=0:x2=n%*D
  7 D$="C.Sol"  :REM File title
  8 INPUT"New record number="DISK:M$=STR$(DISK)
 10 A$="FNSolFluxLink(z,A,R)"
 30 scr=9.05  :REM Screen radius in mm.
 40 A=5.185/scr:REM Pick-up coil radius.
 50 R=3.2/scr:REM Sample radius.
 55 YDIFF=FNSolOst(1,A,R)-FNSolGJD(1,A,R)
 56 PRINT;"YDIFF="YDIFF
 60 DESCRIP$="GJD(Z<=1)/Osterman(Z>1) flux calc. between
    a semi-inf. source solenoid of radius R=3.2/scr and a
    semi-inf. p/u solenoid of radius A=5.185/scr (scr=9.05mm),
    with dist. Z=z/scr between the ends.
     Units: y ("reduced SI flux"), x (mm)."
 65 REM This title is stored on results disk
 70 N$=D$+M$
100 PROCPLOT:PROCSAVE
110 VDU 14
120 STOP
190
300 DEF FNSolFluxLink(z,A,R)
310 Z=z/scr
320 IF Z<=1 THEN =FNSolGJD(Z,A,R)+YDIFF
330 IF Z>1 AND A>R THEN =FNSolOst(Z,A,R)
340 IF Z>1 AND A<R THEN =FNSolOst(Z,R,A)
420
1000 DEF PROC INITIALISE
1005 *KEY 9 MODE 7|M |NL.|M
1100 *FX6,10
1110 DIM J(15),y(500),x(500)
1120 VDU 15:VDU 28,0,31,39,29
1130 PROC CONSTANTS
1140 J(1)=3.831705970:J(2)=7.015586670
1150 J(3)=10.17346814:J(4)=13.32369194
1160 J(5)=16.47063005:J(6)=19.61585851
1170 J(7)=22.76008438:J(8)=25.90367209
1180 J(9)=29.04682853:J(10)=32.18967991
1190 J(11)=35.33230755:J(12)=38.47476623
1200 J(13)=41.61709421:J(14)=44.75931900
1210 J(15)=47.90146089
1300 ENDPROC
1990
```

/cont

```
 2000 DEF FNSolGJD(Z,A,R)
 2005 REM Uses derivation of G Daniell
 2010 P=FNLAGINT(0,2-A-R,"FNSolC(Y)")+.25*PI*R*A*Z
 2020 BETASQ=4*A*R/((A+R)*(A+R)): KSQ=BETASQ/(1+(Z/(A+R))^2):
 K=SQR(KSQ)
 2030 AK=(BETASQ/KSQ-BETASQ)/3-KSQ/BETASQ+KSQ:
  AE=1-(BETASQ+BETASQ/KSQ)/3: AP=(1-BETASQ)*(1-KSQ/BETASQ)
 2040 Q=(A+R)*(AK*FNKK(KSQ)+AE*FNEE(KSQ)-AP*FNPI(BETASQ,K))/
  (SQR(BETASQ)*K)-.25*PI*R*Z/A
 2050 =(P+Q)*2*R*A*(scr*1E-3)^3
 2060
 2070 DEF FNSolC(Y)
 2080 =(COS(Y*Z)-1)*FNI(1,Y*R)*FNK(1,Y)*FNI(1,Y*A)*
  EXP((2-A-R)*Y)/(Y*Y*FNI(1,Y))
 2090
 2100 DEF FNSolOst(Z,A,R)
 2105 REM Uses Osterman method
 2110 S=0
 2120 FOR I=1 TO 15
 2130 S=S+EXP(-J(I)*Z)*FNJ(1,J(I)*A)*FNJ(1,J(I)*R)/
  (J(I)*(J(I)*FNJ(0,J(I)))^2)
 2140 NEXT
 2150 =PI*S*2*R*A*(scr*1E-3)^3
 8990
 9111 DEF PROCSAVE
 9112 ST=OPENOUT N$
 9115 PRINT£ST,DESCRIP$
 9118 PRINT£ST,P%
 9120 FOR i%=0 TO P%-1
 9125 PRINT£ST,x(i%),y(i%)
 9130 NEXT
 9135 CLOSE£ST
 9136 DISK=DISK+1
 9137 M$=STR$(DISK)
 9138 ENDPROC
 9990
10100 DEF PROC CONSTANTS
10110 DIM glx(10),glw(10),gx(5),gw(5)
10115 REM Gauss Laguerre constants (below)
10120 glx(1)=0.137793471: glw(1)=0.308441116
10130 glx(2)=0.729454549: glw(2)=0.401119929
10140 glx(3)=1.808342900: glw(3)=0.218068288
10150 glx(4)=3.401433700: glw(4)=6.20874561E-2
10160 glx(5)=5.552496140: glw(5)=9.50151697E-3
10170 glx(6)=8.330152750: glw(6)=7.53008389E-4
10180 glx(7)=11.84378580: glw(7)=2.82592335E-5
10190 glx(8)=16.27925780: glw(8)=4.24931398E-7
10200 glx(9)=21.99658580: glw(9)=1.83956482E-9
10210 glx(10)=29.9206970: glw(10)=9.91182722E-13
10220 gx(1)=.1488743389: gw(1)=.2955242247
10230 gx(2)=.4333953941: gw(2)=.2692667193
10240 gx(3)=.6794095682: gw(3)=.2190863625
10250 gx(4)=.8650633666: gw(4)=.1494513491
10260 gx(5)=.9739065285: gw(5)=.0666713443
10270 ENDPROC
10280
```

/cont

```
10800 DEF FNLAGINT(A,K,b$)
10810 s=0
10820 FOR j%=1 TO 10
10830 Y=glx(j%)/K+A: s=s+glw(j%)*EVAL(b$)
10840 NEXT
10850 =s*EXP(-K*A)/K
13000 DEF PROCPLOT
13010 clear%=TRUE
13110 y2=-1E10: y1=1E10: p=1100/(x2-x1): q%=-p*x1+100: dx=(x2-x1)/n%
13120 FOR i%=0 TO n%
13125 X=x1+i%*dx:x(i%)=X
13130 y(i%)=EVAL(A$)
13150 IF y(i%)>y2 THEN y2=y(i%)
13160 IF y(i%)<y1 THEN y1=y(i%)
13165 PRINT "i%=";i%,"n%=";n%,"Record No.=";DISK
13166 PRINT;"x(";i%;")=";x(i%);" y(";i%;")=";y(i%)
13170 NEXT
13175 P%=i%
13180 IF clear% THEN CLS: r=850/(y2-y1): s%=-r*y1+100
13182 IF s%>0 THEN MOVE 0,s%: PLOT 21,1279,s%
13184 IF q%>0 THEN MOVE q%,0: PLOT 21,q%,950
13186 MOVE p*x1+q%,r*y(0)+s%
13190 FOR i%=0 TO n%
13195 X=x1+i%*dx
13200 PLOT 5,p*X+q%,r*y(i%)+s%
13210 NEXT
13220 VDU 5: @%=&20207
13250 MOVE 1050,r*y1+s%: PRINT y1
13260 MOVE 1050,r*y2+s%: PRINT y2
13270 VDU 4: @%=2570
13280 ENDPROC
13290
13300 DEF PROCSUPERPOSE(A$)
13310 clear%=FALSE
13320 GOTO 13120
13340 ENDPROC
13590
13595
14000 DEF FNJ(N,X)
14010 IF N>1 THEN =FNe(N,X,1)
14020 y=X*X/9: IF ABS(X)>3 THEN GOTO 14040
14030 IF N=0 THEN =1+y*(-2.2499997+y*(1.2656208+y*(-.3163866+y*
 (.0444479+y*(-.0039444+y*.00021)))))
 ELSE =X*(.5+y*(-.56249985+y*(.21093573+y*(-.03954289+y*
 (.00443319+y*(-.00031761+y*1.109E-5))))))
14040 z=ABS(X)
14050 IF N=0 THEN =FNf0(z)*COS(FNt0(z))/SQR(z) ELSE =SGN(X)*
 FNf1(z)*COS(FNt1(z))/SQR(z)
14060 DEF FNf0(X)
14070 y=3/X: =.79788456+y*(-77E-8+y*(-.0055274+y*(-.00009512+y*
 (.00137237+y*(-.00072805+y*.00014476)))))
```

/cont

```
14080 DEF FNt0(X)
14090 y=3/X: =X-.78539816+y*(-.04166397+y*(-.00003954+y*
 (.00262573+y*(-.00054125+y*(-.00029333+y*.00013558)))))
14100 DEF FNf1(X)
14110 y=3/X: =.79788456+y*(156E-8+y*(.01659667+y*(.00017105+y*
 (-.00249511+y*(.00113653-y*.00020033)))))
14120 DEF FNt1(X)
14130 y=3/X: =X-2.35619449+y*(.12499612+y*(.0000565+y*
 (-.00637879+y*(.00074348+y*(.00079824-y*.00029166)))))
14210
14220 DEF FNI(N,X)
14230 IF N>1 THEN =FNe(N,X,-1)*FNCOSH(X)
14240 y=7.11111111E-2*X*X: IF ABS(X)>3.75 THEN GOTO 14260
14250 IF N=0 THEN =1+y*(3.5156229+y*(3.0899424+y*(1.2067492+y*
 (.2659732+y*(.0360768+y*.0045813)))))
 ELSE =X*(.5+y*(.87890594+y*(.51498869+y*(.15084934+y*
 (.02658733+y*(.00301532+y*.00032411))))))
14260 y=3.75/ABS(X): IF N=0 THEN =(.39894228+y*(.01328592+y*
 (.00225319+y*(-.00157565+y*(.00916281+y*(-.02057706+y*
 (.02635537+y*(-.01647633+y*.00392377)))))))*
 EXP(ABS(X))/SQR(ABS(X))
14270 IF N=1 THEN =SGN(X)*(.39894228+y*(-.03988024+y*
 (-.00362018+y*(.00163801+y*(-.01031555+y*(.02282967+y*
 (-.02895312+y*(.01787654-y*.00420059)))))))*
 EXP(ABS(X))/SQR(ABS(X))
14275
14280 DEF FNCOSH(X): a=EXP(X): =.5*(a+1/a)
14290 DEF FNK(N,X)
14300 IF N>1 THEN GOTO 14360
14310 y=.25*X*X: IF X>2 THEN GOTO 14340
14320 IF N=0 THEN z= -.57721566+y*(.4227842+y*(.23069756+y*
 (.0348859+y*(.00262698+y*(.0001075+y*74E-7)))))
 ELSE z=(1+y*(.15443144+y*(-.67278579+y*(-.18156897+y*
 (-.01919402+y*(-.00110404-y*.00004686))))))/X
14330 =z+LN(.5*X)*FNI(N,X)*SGN(N-.5)
14340 y=2/X: IF N=0 THEN =(1.25331414+y*(-.07832358+y*
 (.02189568+y*(-.01062446+y*(.00587872+y*(-.0025154+y*
 .00053208))))))*EXP(-X)/SQR(X)
14350 IFN=1 THEN =(1.25331414+y*(.23498619+y*(-.03655620+y*
 (.01504268+y*(-.00780353+y*(.00325614-y*.00068245))))))*
 EXP(-X)/SQR(X)
14360 a=FNK(0,X): b=FNK(1,X)
14370 FOR i=1 TO N-1: c=2*i*b/X+a: a=b: b=c: NEXT: =c
14380 DEF FNe(N,X,m)
14390 IF X=0 THEN =0
14400 even%=TRUE: n=2*INT(.5*(ABS(X)+N+20)): a=0: b=1E-20: y=0
14410 FOR i=n TO 1 STEP -1
14420 IF i=N THEN z=b
14430 c=2*i*b/X-m*a: a=b: b=c
14440 IF even% THEN y=y+a
14450 even%=NOT even%
14460 NEXT
14470 y=y+y+c
14480 =z/y
```

Listing 5 SQDGRDS

```
  1 REM Program 'SQDGrdS',BHB,8/6/86 & DIH 87:
    Uses GJD/Osterman sol-sol flux calc. output
    (i.e. GJDOst2 used to generate source file
    C.Sol---, x-incr.=.1 mm) to simulate the output of the
    SQUID gradiometer. Stores result on disk in file C.GrdS---
  3 MODE 4
  4 PROC INITIALISE
  5 ON ERROR GOTO 130
  7 n%=700
  8 D$="C.GrdS"
  9 INPUT"New record number="DISK:M$=STR$(DISK)
 10 R=3.2/9.05:A=5.185/9.05:scr=9.05
 11 REM Reduced sample radius & coil radius and screen radius.
 15 A$="FNFlux(i%)"
 20 L1=-224:L2=-160:L3=-62:L4=62:L5=158:L6=226 :REM Pick-up
    coil dimension in 0.1 mm units
    (lower, central and upper sub-coil respectively).
 60 DESCRIP$="Data file produced by 'SQDGrdS'.This is the
    'Instrument Function' for the SQUID p/u coil, radii as used
    for source file C.Sol---. x-inc.=0.1 mm."
 62 REM Above is default title for file saved on disk.
 70 N$=D$+M$
 80 PROC LOAD
 85 PRINT F$:PRINT;" P% on file=";PF%;" P% counted in=";P%
 90 x1=0:x2=70:PRINT;"x1=";x1;" x2=";x2
100 PROCPLOT:PROCSAVE
110 VDU 14
120 STOP
130 IF ERR=17 THEN PROC CLOSE
140 REPORT:PRINT " at line ";ERL
150 END
190
200 DEF FNFlux(j%)
210 =-FNFluxTot(j%,L1,L2)*1.6E5/(L2-L1)+ FNFluxTot(j%,L3,L4)*
    3.2E5/(L4-L3) -FNFluxTot(j%,L5,L6)*1.6E5/(L6-L5)
211 REM Calculating the instrument function for a specific point
    (for a particular radius of sample)
990
1000 DEF PROC INITIALISE
1003 *KEY 3 PROC PrintData|M
1005 *KEY 9 MODE 7|M |NL.|M
1100 *FX6,10
1110 DIM J(15),y(700),Y(500),x(700),X(500)
1300 ENDPROC
1990
2000 DEF FNFluxTot(j%,Y1%,Y2%)
2080 z1%=j%+Y1%:z2%=j%+Y2%
2084 IF z2%>500 THEN z2%=500
2086 IF z1%>500 THEN z1%=500
2090 IF z1%>=0 THEN =-Y(z2%)+Y(z1%)
2100 IF z1%<0 AND z2%>0 THEN =-PI*R*R*A*(scr*1E-3)^3*(A-1/A)*
    X(-z1%)/9-Y(z2%)+Y(-z1%)
2110 IF z2%<=0 THEN =-PI*R*R*A*(scr*1E-3)^3*(A-1/A)*
    (X(-z1%)-X(-z2%))/9-Y(-z2%)+Y(-z1%)
```

for other procedures see SAMPAC

REFERENCES

ABRAMOVITZ M, STEGUN I (1964) Handbook of Mathematical Functions, with formulae, graphs and tables. US Government Print Office, Washington, USA

ALBRECHT O, SACKMANN E (1980) J Phy E 13,512

ARANAZ D M, LOMER T R (1969) J Phy C 2,2431

ASAOLU I A (1983) PhD Thesis, Physics Dept, Southampton University

AVIRAM A, POMERANTZ M (1982) Sol Stat Comm 41,297

AWSCHALOM D D, LEWIS G N, GREGORY S (1983) Phy Rev Lett 51,587

B.D.H. Ltd, Broom Rd, Poole, BH12 4NN

B.T.I. - Biomagnetic Technologies Inc (formerly S.H.E - Superconducting Helium Electronics) 4174 Sorrento Valley Blvd, San Diego, California CA92121

BAYREUTHER G (1983) JMMM 38,273

BEAUVILLAIN P, CHAPPERT C, RENARD J P (1985) J Phy E 18,839

BIRGENEAU R J, ALS-NIELSEN J, SHIRANE G (1977) Phy Rev B 16,280

BLEANEY B, BLEANEY B I (1976) "Electricity and Magnetism" Oxford University Press, UK

BLIGHT L, CUMPER C W M, KYTE V J (1965) J Coll Int Sci 20,393

BLODGETT K B (1935) J Amer Chem Soc 57,1007

BLODGETT K B (1938) Phy Rev 55,391

BLOEMBERGEN P, TAN K G, LEFEVRE F H J, BLEYENDAAL A H M (1970) Proc Int Conf Magn, Grenoble (J de Phys 32,supplC-1,879)

BOESCH H R, SCHMOCKER U, WALDNER F, EMERSON K, DRUMHELLER J E (1971) Phys Lett A 36,461

BOWERS R (1956) Phy Rev 102,1486

BROWN A (1981) PhD Thesis, University of Southampton

C I ELECTRONICS Ltd, Brunel Rd, Churchfields, Salisbury

CERDONIO M, MESSANA C (1975) IEEE Mag 11,728

CERDONIO M, COSMELLI C, ROMANI G L (1976) Rev Sci Instrum 47,1

CHAPPERT C, RENARD D, BEAUVILLAIN P, RENARD J P, SEIDEN J (1986) JMMM 54,795

CHARLES M W (1971) J App Phy 42,3329

CIBA GEIGY, Duxford, Cambridge CB2 4QA

CLAASEN J H (1975) J App Phy 46,2268

COLLINGS E W, HART S C (1979) Cryogenics 19,521

CUKAUSKAS E J, VINCENT D A, DEAVER B S Jr (1974) Rev Sci Instrum 45,1

DANIEL M F, LETTINGTON O C, SMALL S M (1983) Thin Sol Film 99,61

DECON LABS Ltd, Conway St, Hove, E Sussex BN3 3LY

DEJONGH L J, MIEDEMA A R (1974) Adv in Phys 23,1

DEJONGH L J, STANLEY H E (1976) Phy Rev Lett 36,817

DEJONGH L J, VAN AMSTEL W D (1970) Proc Int Conf Magn, Grenoble
J de Phy 32supplC-1,880

DIEP-THE-HUNG, MOTCHANE J L (1982) Phy stat sol(b) 111,639

DIMON P, HORN P M, SUTTON M, BIRGENEAU R J, MONCTON D E (1985)
Phy Rev B 31,437

DOMANY E, RIEDELL E K (1978) Phy Rev Lett 40,561

DONALDSON et al (1977) "Integrated Thin Film Gradiometer" at
"SQUID 76", Ed. H D Hahlbohm & H Lübbig,
W. de Gruyter, Berlin

DORAN J C, SYMKO O G (1974) IEEE Trans MAG 10,603

DUPONT CHEMICALS Ltd, Wedgewood Way, Stevanage, Herts SG1 4QM

E.I.L., Hanworth Lane, Chertsey, Surrey KT16 9LF

EDWARDS HIGH VACUUM Ltd, Manor Royal, Crawley, W Sussex, RH10 2LW

ELAHY M E, DRESSELHAUS G (1984) Phy Rev B 30,7225

EMERSON & CUMINGS (UK) Ltd, Colville Rd, London W3

ETTERS R D, HARDOUIN DUPARC O B M (1985) Phy Rev B 32,7600

FELL CLEAN Ltd, 12 New Rd, Light Ind Est, Newhaven

FENG Z X (1985) IEEE Mag 21,993

FERRIEU F, POMERANTZ M (1980) JMMM 15-18,1063

FISHER M E (1967) Rep Prog Phy 30,615

FISHER M E (1974) Rev Mod Phy 46,597

FISHER M E, JASNOW D (1971) Phy Rev B 3,895 & 907

FOTHERGILL TYGAFLOR Ltd, Summit, Littleborough, Lancashire OL15 OLT

FRÖHLICH J, LIEB E H (1977) Phy Rev Lett 38,440

GAINES G L (1966) "Insoluble Monolayers at liquid gas Interfaces"
Interscience, Wiley, NY

GAINES G L (1977) J Coll Int Sci 62,191

GAINES G L (1983) Thin Sol Film 99,ix

GALLOP J C, PETLEY B W (1976) J Phy E 9,417

GALLOP J C (1978) J Phy B 11,L96

GARRETT M W (1963) Jnl App Phy 34,2567

GIFFARD R P, WEBB R A, WHEATLEY J C (1972) J Low Temp Phy 6,533

GOODFELLOW METALS, The Science Park, Milton Rd, Cambridge CB4 4DJ

GRADMANN U, BERGHOLZ R, BERGTER E (1985) Thin Sol Film 126,107

GRAMM K, LUNDGREN L, BECKMAN O (1976) Physica Scripta 13,93

GRANT INSTRUMENTS Ltd, Barrington, Cambridge CB2 5QZ

GREGORY S (1978) Phy Rev Lett 40,723

GROVER F W (1946) "Inductance Calculations: Working formulae and tables", Dover Pub Inc, New York

GRUBE K & WACHTEL E (1976) Z. Metallk. 67,348

GRUNFELD F (1983) PhD Thesis, University College, London

GUY C N, PARK J G (1984) J Phy D 17,871

HALLIDAY D, RESNICK R (1978) "Physics" 3rd ed, John Wiley & Sons Inc, New York

HASEDA T, YAMAKAWA H, ISHIZUKA M, OKUDA Y, KUBOTA T, HATA M, AMAYA K (1977) Sol Stat Comm 24,599

HASMONAY H, VINCENT M, DUPEYRAT M (1980) Thin Sol Film 68,21

HATTA I, IKEDA H (1980) J Phy Soc Jpn 48,77

HEAD D I, DANIELL G J, BLOTT B H (1988) J Phy D 21,999

HEDGCOCK F T, LI P L (1970) Phy Rev B 2,1342

HEIKKILA D W, DREAMER D W, CORNWELL D G (1970) J Lipid Res 11,195

HEINEY P A, STEPHENS PW, MOCHRIE S G J, AKIMITSU J, BIRGENEAU R J (1983a) Surf Sci 125,539

HEINEY P A, STEPHENS PW, BIRGENEAU R J, HORN P M, MONCTON D E (1983b) Phy Rev B 28,6416

HIGHFIELD R R, THOMAS R K, CUMMINS P G, GREGORY D P, MINGINS J, HAYTER J B, SCHÄRPF P (1983) Thin Sol Film 99,165

HIRAKAWA K (1982) J App Phys 53,1893

HITCHCOCK H C (1964) Rev Mod Phys 36,61

HIZFELD M, ZIEMANN P, BUCKEL W (1984) J Phy E 17,291

HONIG E P (1973) J Coll Int Sci 43,66

HUDGENS S, KASTNER M, FRITSCHE H (1974) Phy Rev Lett 33,1552

HURD C M (1965) Rev Sci Instrum 37,515

IBRAHIM A K, ZIMMERMAN G O (1987) Phy Rev B 35,1860

IKEDA H, HUTCHINGS M T, SUZUKI M (1978) J Phy C 11,L359

ISHIZUKA M, TOHI Y (1980) Jap J App Phy 19,639

ISHIZUKA M, TOHI Y, HASEDA T (1983) J Phy Soc Jpn 52,3611

ISRAELSSON U E, GOULD C M (1984) Rev Sci Instrum 55,1143

JONES J V (1898) Proc Roy Soc (Lond) 63,192

JOSEPHSON B D (1962) Phys Lett 1,25

KESSEL R, SAPP R C (1986) Rev Sci Instrum 57,2897

KETCHEN M B, GOUBAU W, CLARKE J, DONALDSON G B (1977) IEEE MAG 13,372

KIMBERLEY CLARK, Larkfield, Maidstone, Kent

KIMISHIMA Y, FURAKAWA A, SUZUKI M, NAGANO H (1985) J Phy C 19,L43

KOSTERLITZ J M, THOULESS D J (1973) J Phy C 6,1181

KOSTERLITZ J M, SANTOS M A (1978) J Phy C 11,2835

KOSTERLITZ J M, THOULESS D J (1978) Prog in Low Temp Phys 7B (ch5), North Holland Pub Co, Amsterdam

KOSTERLITZ J M (1980) in "Phase transitions in Surface Films", Eds J G Dash & J Ruvalds, Plenum Press N.Y. p193

KUHN H MÖBIUS D (1971) Angewandte Chemie (Int Ed) 10(8),620

KUHN H, MÖBIUS D, BÜCHER H (1972) Physical Methods of Chemistry 1,577

LAKE SHORE Cryotronics Inc, 64 E. Walnut St, Westerville, Ohio 43081

LAKNER J (1977) Phys Stat Sol B 81,593

LANGMUIR I (1938) Science 87,493

LARBALESTIER D C & KING H W (1970) Cryogenics 10,410

LARBALESTIER D C & KING H W (1973) Cryogenics 13,160

LIP Ltd (Equipment & Services), 111 Dockfield Rd, Shipley, W. Yorks

LIU L L, STANLEY H E (1973) Phy Rev B 8,2279

LOUNASMAA O V (1974) "Experimental Principles and Methods below 1K" Academic Press, New York

MALLINSON J (1966) J App Phys 37,2514

MALYSHEV V A (1975) Commun Math Phy 40,75

MARX R, CHRISTOFFER B (1983) Phy Rev Lett 51,790

MATSUURA M, KOYAMA K, MURAKAMI Y (1982) abstract from "Transition to 'New type of ordered phase'", Sep 11-13, Kansai Seminar House, Kyoto, Japan

MCTAGUE J P, NIELSEN M (1976) Phy Rev Lett 37,596

MERMIN N D, WAGNER H (1966) Phy Rev Lett 17,1133

MILLIPORE (UK) Ltd, Millipore House, 11-15 Peterborough Rd, Harrow, Middlesex HA1 2YH (Tel. 01 864 5499)

MIZUNO M, MORI C, NOGUCHI H, WATANABE T (1983) Jap J App Phy 22,808

MOCHRIE S G J, BIRGENEAU R J (1984) Surf Sci 138,599

MONTGOMERY D B (1969) "Solenoid Magnet Design", Wiley Interscience, NY

MUETHING K A, EDWARDS D O, FEDER J D, GULLY W J, SCHOLZ H N (1982) Rev Sci Instrum 53,485

MUNDEN J W, BLOIS D W, SWARBRICK J (1969) J Pharm Sci 58,1308

NAGAEV E L (1986) Sov Phy Sol Stat 27,1970

NAVARRO R, DEJONGH L J (1979) Physica 98B,1

NAVE S E, HURAY P G (1980) Rev Sci Instrum 51,591

NEUMANN R D (1978) J Coll Int Sci 63,106

NEUMANN R D, SWANSON J W (1980) J Coll Int Sci 74,244

NICKLOW R M, POMERANTZ M, SEGMÜLLER A (1981) Phy Rev B 23,1081

ONSAGER L (1944) Phy Rev 65,117

OSTERMAN D P, WILLIAMSON S J (1983) Rev Sci Instrum 54,1380

OXFORD INSTRUMENTS Ltd, Eynsham, Oxford OX8 1TL

PELIZONNE M, TREYVAUD A (1981) Appl Phy 24,375

PETERSON I R, RUSSEL G J, ROBERTS G G (1983) Thin Sol Film 109,371

PETERSON I R, VEALE G, MONTGOMERY C M (1986) J Coll Int Sci 109,527

PHILO J S, FAIRBANK W M (1977) Rev Sci Instrum 48,1529

POMERANTZ M, POLLACK R A (1975) Chem Phys Lett 31,602

POMERANTZ M, AVIRAM A (1976) Sol Stat Comm 20,9

POMERANTZ M, DACOL F H, SEGMÜLLER A (1978) Phy Rev Lett 40,246

POMERANTZ M (1978) Sol Stat Comm 27,1413

POMERANTZ M, SEGMÜLLER A (1980) Thin Sol Films 68,33

POMERANTZ M (1980) in "Phase Transitions in Surface Films", Eds J G Dash & J Ruvalds, Plenum, NY & London

POMERANTZ M, AVIRAM A, TARANAKO A R (1982) JAP 53,7960

POMERANTZ M (1982) Workshop at NRL Washington DC in "Molecular Electronic Devices", Ed F L Carter (Decker)

POMERANTZ M (1983) Fifth Int. Conf. on Electronic Properties of 2-D Systems, Oxford, 5-9 Sept.

POMERANTZ M (1984) Surface Science 142,556

PRAKASH M, PENG J B, KETTERSON J B, DUTTA P (1987) Thin Sol Film 146,L15

RABINOVITZ W, ROBERTSON R F, MASON S G (1960) Can J Chem 38,1881

RAO M G, SCURLOCK R G, WU Y Y (1983) Cryogenics 23,635

REGNAULT L P, ROSSAT-MIGNOD J, HENRY J Y, DEJONGH L J (1983) JMMM 31-34,1205

ROBERTS G G (1985) Adv in Phy 34,475

ROBINSON D W (1969) Commun Math Phy 14,195

ROSE-INNES A C, RHODERICK E H (1978) "Introduction to Superconductivity", Pergamon, Oxford

ROSENBAUM E S, AUTLER S H, GOOEN K H (1964) Rev Mod Phys 36,78

RUBBER HANDBOOK C.R.C. Handbook of Chemistry and Physics C.R.C. Press Inc., West Palm Beach, Florida, USA

SAINT PIERRE M, DUPEYRAT M (1983) Thin Sol Film 99,205

SALINGER G L & WHEATLEY J C (1961) Rev Sci Instrum 32,872

SAMPLE H H, RUBIN L G (1977) Cryogenics 17,596

SARWINSKI R E (1977) Cryogenics 17,671

SEVERN J K, BATCHELDER D N (1984) J Phy E 17,113

S.H.E. - see B.T.I.

SIEMENS Ltd, 2 Hanworth Rd, Feltham, Middlesex

SIGMA CHEMICALS Ltd, Fancy Rd, Poole, BH17 7NH

SIMS B, ZOGRAFI G (1972) J Coll Int Sci 41,35

SMITH R D, BERG J C (1980) J Coll Int Sci 74,273

SMITH T I (1973) J App Phy 44,852

SNOW C (1939) Jnl Res NBS 22,239

STANLEY H E, KAPLAN T A (1966) Phy Rev Lett 17,913

STANLEY H E (1971) "Introduction to Phase Transitions & Critical Phenomena", Clarendon Press, Oxford

STEELHAMMER T J, SYMKO O G (1979) Rev Sci Instrum 50,532

STEPHENS J F (1972) J Coll Int Sci 38,557

STEPHENS P W, HEINEY P A, BIRGENEAU R J, HORN P M, STOLTENBERG J, VILCHES O E (1980) Phy Rev Lett 45,1959

STOLL E, SCHNEIDER T (1978) in "Solitons & Condensed Matter Physics", Eds A R Bishop & T Schneider, Springer Verlag, Berlin

STOLTENBERG J, VILCHES O E (1980) Phy Rev B 22,2920

SWITHENBY S J (1980) J Phy E 13,801

SZETO K Y, CHEN S T, DRESSELHAUS G (1985) Phy Rev B 32,4628

TABER M, CABRERA B (1985) Rev Sci Instrum 56,1835

TAKEDA K, KOYAMA K (1983a) Jnl Phy Soc Jpn 52,648

TAKEDA K, KOYAMA K (1983b) Jnl Phy Soc Jpn 52,656

TER BRAKE H J M, REM P C, FLOKSTRA J (1985) "SQUID 85", Eds H D Hahlbohm & H Lübig, Walter de Gruyter & Co, Berlin

TREDGOLD R H (1987) Rep Prog Phy 50,1609

VAN HARLINGEN D J, KOCH R H, CLARKE J (1982) Appl Phy Lett 41,197

VEALE G, GIRLING I R, PETERSON I R (1985) Thin Sol Film 127,293

VINNCETT P S, BARLOW W A, BOYLE F T, FINNEY J A, ROBERTS G G (1979) Thin Sol Film 60,265

VOLD R D, HATTIANGDI G S (1949) Ind Engng Chem 41,2311

VON SYDOW (1955) Acta Cryst 8,557

WALPITTA L H (1977) PhD Thesis, University College, London

WARNES L A A, KING H W (1976) Cryogenics 16,659
see also Cryogenics 16,473

WEBB W W (1972) IEEE Trans MAG 8,51

WHITE G K (1979) "Experimental Techniques in Low Temperature Physics" 3rd ed., Clarendon Press, Oxford

WILHELMY L (1863) Ann Physik 119,177

WILSON K G (1979) Scientific American 241,140

XU S, MIYANO K, ABRAHAM B M (1982) J Coll Int Sci 89,581

YAMAMATO Y, MATSUURA M, HASEDA T (1977) Jnl Phy Soc Jpn 43,1550

YOUNG A P (1980) in "Ordering in Strongly Fluctuating
Condensed Matter Systems", Ed T Riste,
NATO Advanced Study Institute Series
ZIEBA A, FONER S (1983) Rev Sci Instrum 54,137